UNIVERSITY OF SOUTHAMPTON

FACULTY OF ENGINEERING AND APPLIED SCIENCE

DEPARTMENT OF ELECTRICAL ENGINEERING

THE INFLUENCE OF ELECTROSTATIC CHARGE ON THE DEPOSITION OF THERAPEUTIC AEROSOLS AND AIRBORNE POLLUTANT PARTICLES WITHIN THE HUMAN RESPIRATORY SYSTEM

by

ADEL HASSAN HASHISH

A Thesis Submitted for the Degree
of
Doctor of Philosophy

June 1988

'... To the dear memory of my Parents ..
and to my wife Engy ..'

UNIVERSITY OF SOUTHAMPTON

ABSTRACT

FACULTY OF ENGINEERING AND APPLIED SCIENCE
ELECTRICAL ENGINEERING DEPARTMENT

Doctor of Philosophy

THE INFLUENCE OF ELECTROSTATIC CHARGE ON THE DEPOSITION OF THERAPEUTIC AEROSOLS AND AIRBORNE POLLUTANT PARTICLES WITHIN THE HUMAN RESPIRATORY SYSTEM

by Adel Hassan Hashish

Small particles present in the environment and also particles produced by clinical nebulisers and aerosol dispensers are often electrically charged. Such charge invariably plays a role in particle depositional behaviour. Studies have been carried out for two different types of nebuliser and the aerosols generated monitored under simulated breathing conditions using special apparatus. It was possible to monitor the size distribution of aerosol droplets using a laser diffraction technique. The charge carried by aerosol particles was detected using a purpose-built mobility analyser and an independent total charge monitor. During clinical trials, it was found that the charge carried by droplets generated using an ultrasonic nebuliser was important in determining the cough response.

When charge is present on aerosol particles deposition is likely to be enhanced. A predictive lung deposition model has been developed which can be executed using a personal computer. It has advantages over previously published formulations since it can deal with deposition efficiencies as high as unity with minimal computational effort. This has been achieved by using the natural definition of change in particle concentration over an airway length and by transforming the deposition surface integral into a line integral, using Green's theorem. The results are in good agreement with published experimental data for both highly-charged and naturally-occuring aerosols. If the level of charge is sufficiently high, deposition is enhanced and the regional deposition of aerosol may be influenced. The model has been used in aerosol therapy to assess the performance of clinical nebulisers with regard to total and regional deposition.

To assess properly the nature of the hazard in electrostatic crop-spraying, the lung deposition model could be used to predict the dose of toxic material deposit ed in the lung for different crop spraying scenarios. The model can also be used to assess the hazard associated with particle charge in the areas of: air pollution, health physics and industrial hygiene.

ACKNOWLEDGMENTS

I should like to thank my supervisor, Professor Adrian Bailey, for his interest, valuable advice and encouragement during this work. Dr W. Balachandran's role in initiating nebuliser research in the Electrostatics Group is also greatly appreciated.

Some aspects of the work were performed in collaboration with the Department of Medicine, Southampton General Hospital, and I am grateful to Dr R.A. Lewis and Dr C. Ellis who gave much time in helping me with the clinical measurements.

My appreciation as well is conveyed to my colleagues in the Applied Electrostatics Research Group, particularly Mr T.J. Williams for his constructive criticism and valuable discussions regarding many aspects of the work in general, Mr R.T. Jones for his interest and Mr D. White, who helped with the construction of the experimental apparatus together with Mr J. McCullen.

Thanks are also due to Professor C.P. Yu, of the Department of Mechanical and Aerospace Engineering, State University of New York at Buffalo, USA, for his communication and to Dr R.A. Coffee, of the ICI Plant Protection Division, Fernhurst, Surrey for his interest and providing data for the droplet size measurements of Electrostatic crop sprayers. I should also like to thank Dr J.H. Vincent, of the Physics Branch, Institute of Occupational Medicine, Edinburgh, for providing data for the electrical charge carried by workplace aerosols.

I am grateful to the Egyptian Government for providing my scholarship at Southampton University, and the ORS Committee for granting me the scholarship and to the Colt Foundation for supporting this work. Sincere thanks are also due to Miss D.M. Sarjeant for her effort in typing this thesis and to Dr H. Azzam and Dr M. El-Dib for helping with the graphs.

Lastly, I should like to thank my wife Engy for her help, understanding and devotion to our family during the preparation of the thesis and to my son Hassan for making everything worthwhile.

PREFACE

Electrical charge is often present on the small particles produced by various sources which contribute to air pollution and on the droplets generated by clinical nebulisers and aerosol dispensers. Invariably such charge acts to increase deposition in the human respiratory system, which is *beneficial* with regard to the delivery of therapeutic agents but *hazardous* in relation to pollutants.

This thesis is presented in three separate sections:

I. The first section describes work performed on therapeutic nebulisers. The introductory chapter describes previous work carried out on aerosol therapy, particle charging and reviews the deposition of charged particles in physical lung models, animals and humans. The purposes of this investigation are outlined and the advantages of the electrostatic charging technique, in relation to therapeutic aerosols, are highlighted.

The second chapter describes the theory and mechanisms concerned with the two types of nebuliser which were assessed, and the factors affecting the aerosols generated by them, together with the theory and techniques associated with particle charging and charge monitoring.

The third chapter deals with the experimental apparatus, associated procedures and experimental observations with regard to the measurement of droplet size and electrical charge, and nebuliser aerosol outputs.

Clinical studies have been carried out on different nebuliser types with and without electrostatic enhancement of the aerosol particles. The experimental observations with regard to the influence of charge upon the irritant effect (cough and subjective sensation) on both normal healthy subjects and asthmatic patients are presented.

II. The second part deals with a mathematical model of deposition in the human lung which accounts for the depositional effects of charge on aerosol particles.

Chapter one consists of an introduction to aerosol deposition in the respiratory tract of man and reviews the previous experimental and theoretical attempts to determine total and regional deposition of inhaled aerosols. Although much work has been performed in this area, uncertainty still exists regarding

quantitative results. Various predictive models have been developed to estimate respiratory deposition.

Using the transport approach Yu produced a time-dependent deposition theory which neglects air mixing and gives accurate prediction of total and regional deposition of inhaled aerosols. Yu's theory is only applicable to deposition efficiencies which are very small. Since, it has been necessary to deal with high deposition efficiencies in this study (which is the case with highly charged aerosols), Yu's approach had to be modified accordingly.

Chapters two and three specify the physical characteristics of the human respiratory system and breathing conditions. Chapter four reviews the factors affecting particle deposition.

In chapter five the anatomical model of the respiratory tract, adopted in this study, is presented.

Chapter six develops the predictive lung deposition model, starting with a discussion of Yu's theory. The limitations of Yu's formulation are demonstrated and an alternative method of solving the transport equation is advanced which replaces Yu's solutions with *iterative solutions* applicable at high deposition efficiency. The use of Green's theorem to transform the particle deposition expression is discussed and a computer program outlined.

Chapter seven discusses the validation of the model by comparing theoretical predictions with published experimental data for neutral and charged aerosol particles, for both total and regional deposition. The theory developed is then applied to aerosol therapy. The implications of charge carried by therapeutic aerosol particles, in relation to lung deposition, are discussed and guide-lines presented on a more efficient way of delivering therapeutic agents to different parts of the lung.

III. The third part of this thesis describes work carried out to assess the hazards of depositing electrostatically-charged particulate air pollutants in the lung.

Chapter one starts by defining an air pollutant and reviews the sources of air pollution, describing their charging mechanisms. Possible influences on the inhalation and lung deposition of airborne dusts, by living subjects, are also discussed.

In chapter two a review of electrostatic charge measurements, made in the laboratory and workplace, is presented; the predictive lung model is used to assess the associated hazards with regard to electrostatically-enhanced lung deposition.

Chapter three presents an attempt to assess the health hazards involved with electrostatic crop spraying. In chapter four, the health hazard of charged aerosols is discussed and recommendations made for future work in this area.

Finally, an overall summary of the three parts and conclusions is presented.

The appendices include a listing of the predictive lung model computer program and mathematical derivations of some of the equations used in this work.

In most of this thesis *the cgs system of units* is used since their usage is customary in this field, and certain concepts, such as aerodynamic diameter, becomes awkward in SI units. In general cgs units are easier to handle than SI units for most aerosol calculations.

PRINCIPAL NOTATION

The following notation is used throughout the text, other terms appear in less frequently used equations. Symbols used in all equations are defined where they occur.

a	radius	(cm)
A(x,t)	cross-sectional area of airway and alveoli, $[A^*(x) = A(x,0)]$.	(cm^2)
c	aerosol concentration	
C_c	slip correction factor	
d_p	particle diameter	(μm)
D	diffusion coefficient	(cm^2s^{-1})
e	electronic charge = 4.803×10^{-10} e.s.u.	
E	electric field strength	(Vcm^{-1})
f	ultrasonic frequency	(Hz)
K	number of divisions of the deposition time integral	
ℓ	airway length	(cm)
M	molecular weight of aerosol liquid	(g/mole)
P	fractional deposition during pause	
PD	fractional particle deposition	
q	particle charge	(stC)
Q	air flow rate	(cm^3s^{-1})
t,t_r	time, residence time	(s)
T	period of breathing cycle	(s)
x	penetration into lung measured from trachea	(cm)
V^*_ℓ	rest lung volume	(cm^3)
v_s	settling velocity	(cms^{-1})
V^*_x	cummulative rest volume	(cm^3)
γ	liquid surface tension	(dyne cm^{-1})
ΔA	incremental deposition area	(cm^2)
ζ	penetration parameter	
η	deposition efficiency	
λ	deposition constant	
λc	particle loss rate to the airway surface per unit length	
μ	particle mobility	($cm^2V^{-1}s^{-1}$)
ρ	particle density	(g cm^{-3})
τ	particle velocity relaxation time	(s)
τ_e	exhalation time constant = V^*_ℓ/Q_{oe}	(s)
τ_i	inhalation time constant = V^*_ℓ/Q_{oi}	(s)
τ_j	dimensionless time	

SUBSCRIPTS

e	exhalation
f	finish of airway
i	inhalation
j	jth generation
s	start of airway
o	initial value

ABBREVIATIONS

A	alveolar
FRC	function residual capacity
H	head
MMD	mass median diameter
TB	tracheobronchial
TV,v_t	tidal volume
VAS	visual analogue scale

CONTENTS

ABSTRACT i
ACKNOWLEDGEMENTS ii
PREFACE iii
PRINCIPAL NOTATION vi

PART I
A CRITICAL COMPARISON OF THE OPERATING CHARACTERISTICS OF JET AND ULTRASONIC NEBULISERS

1. INTRODUCTION AND AIMS 1

2. THEORY 4
2.1 Nebuliser Definition 4
2.1.1 Theory and mechanism of the JN 4
2.1.2 Theory and mechanism of the UN 4
2.2 Factors Affecting Nebuliser Aerosols 5
2.2.1 Particle size 5
2.2.2 Gas flow rate (jet-driven only) 6
2.2.3 Inhalation rate 6
2.2.4 Residual volume 6
2.2.5 Temperature and humidity effects 7
2.2.6 Hygroscopic growth 7
2.2.7 Electrical charge 8
2.3 Charging Mechanisms 9
2.3.1 Corona discharge 9
2.3.2 Particle charging 10
2.3.2.A Ion bombardment charging 11
2.3.2.B Ion diffusion charging 11
2.4 Electrical Mobility 12
2.5 Particle Sedimentation 13

3. MEASUREMENTS 14
3.1 Size Measurement 14
3.1.1 Introduction and Aims 14
3.1.1.A Malvern particle size analyser 14
3.1.2 Methods 16
3.1.3 Results and discussion 16
3.1.3.A Variability and Repeatability of droplet size measurement 17
3.1.3.B Effect of gas-drive flow rate on droplet size (JN) 17
3.1.3.C The effect of suction rate on droplet size 19
3.1.3.D Variation of droplet MMD with distance along the axis of the aerosol spray 19
3.1.3.E Effect of volume fill on droplet size 20
3.1.3.F Effect of temperature and humidity on droplet size 20
3.2 Electrical Charge Measurement 20

3.2.1	Introduction and Aims	20
3.2.2	Methods	21
3.2.2.A	Nebuliser modification to alter droplet charge	21
3.2.2.B	The droplet charge analyser (DCA)	22
3.2.2.C	Theory	22
3.2.3	Results and discussion	23
3.2.3.A	Charge on droplets produced by JN and UN	23
3.2.3.B	Charges on the droplets produced by the modified nebuliser	24
3.2.3.C	Effect of gas-flow rate on droplet charge and q/m ratio	24
3.3	Improved Instrumentation	25
3.3.1	Experimental	26
3.3.2	Measurements made using the improved instrumentation	27
3.3.2.1	Droplet size, results and discussion	27
3.3.2.1.A	The effect of suction rate on aerosol droplet size distribution	28
3.3.2.2	Electrical measurements, results and discussion	28
3.3.2.2.1	Ions and charged droplets generate by JN and UN	28
3.3.2.2.2	Effect of air-drive flow rate on ion production (JN only)	29
3.3.2.2.2.A	An estimate of the Maximum amount of charge available for aerosol droplets produced by JN	32
3.3.2.2.3	The effect of the addition of electrolytes to the water on ion production	32
3.4	Nebuliser Output Measurements	33
3.4.1	Introduction and Aims	33
3.4.2	Methods	33
3.4.3	Results and discussion	34
3.4.3.1	Effects of air-drive rate on output characteristics (JN only)	34
3.4.3.2	Effects of liquid volume fill	34
3.4.3.3	The effect of gas-flow rate on the temperature of solution within the nebuliser	34
3.5	Clinical Measurements	35
3.5.1	Introduction and Aims	35
3.5.2	Methods	36
3.5.2.A	Assessment of cough and irritation	36
3.5.3	Results and discussion	37
4.	SUMMARY OF RESULTS AND CONCLUSIONS OF PART I	37

PART II

PREDICTIVE LUNG AND RESPIRATORY DEPOSITION MODEL

1.	INTRODUCTION AND AIMS	40
2.	HUMAN RESPIRATORY SYSTEM	42

3. THE PHYSICS OF THE LUNGS AND BREATHING 43

4 FACTORS AFFECTING PARTICLE DEPOSITION 44

4.1 Deposition Mechanisms 45

4.1.A Inertial impaction 45
4.1.B Gravitational sedimentation 46
4.1.C Diffusion 46
4.1.D Interception 46
4.1.E Electrostatic deposition 47

4.2 Physical Properties of the Aerosol Particles 47

4.3 The Breathing Characteristics 48

4.4 The Airway Characteristics 49

5. WEIBEL'S MORPHOMETRIC MODEL 49

6. PREDICTIVE LUNG DEPOSITION MODEL 51

6.1 Yu's Theory of Lung Deposition 51

6.1.A Solution of the transport equation 53
6.1.A.1 Inhalation solution 54
6.1.A.2 Exhalation solution 56
6.1.A.3 Pause solution 58

6.2 Particle Deposition 58

6.3 Comment on Yu's Model 59

6.3.1 Definition of deposition efficiency 59
6.3.2 Limitations of Yu's solution 61

6.4 New Approach 63

6.4.1 The iterative method 64
6.4.1.A Inhalation solution 65
6.4.1.B Exhalation solution 65
6.4.1.C Pause solution 66
6.4.2 Green's theorem 67
6.4.2.A Method of partitioning the concentration solution domain 68
6.4.2.B Deposition integrals 70

6.5 To Account for Airway Diameter as a Function of Time 72

6.6 Deposition Efficiency as a Function of Time [M-factor] 73

6.7 Deposition Efficiencies 76

6.7.1 Deposition Efficiencies considered as probabilities 80
6.7.2 Deposition during the pause 81

6.8 Head Deposition 82

6.9 Critique of the Presentation of Yu's Lung Model 84

6.10 Outline of the Computer Program for Respiratory Deposition 86

7. RESULTS AND DISCUSSION 88

7.1 Respiratory Deposition of Uncharged Particles 88

7.1.A Comparison with the published data of total deposition 88

7.1.A.1 Effect of particle diameter on total deposition 89
7.1.A.2 Effect of particle mass density on total deposition 89
7.1.A.3 Effect of mean air flow rate on total deposition 90
7.1.A.4 Effect of mean residence time on total deposition 91
7.1.A.5 Effect of intersubject variation on total deposition 92
7.1.A.6 Effect of pause on total deposition 92
7.1.B Comparison with the published data of regional deposition 93

7.2 Respiratory Deposition of Charged Particles 94

7.2.1 Prediction of the effect of charge on deposition 94
7.2.2 Comparison of predicted results with published data for the effect of charge 94

7.3 Prediction of the Deposition Model as Applied to Aerosol Therapy 95

7.4 The Predictive Model : Applicability and Sensitivity 97

8. SUMMARY AND CONCLUSIONS OF PART II 98

PART III

THE EFFECT OF ENVIRONMENTAL POLLUTION ON THE HUMAN RESPIRATORY SYSTEM

1. INTRODUCTION AND AIMS 100

2. REVIEW OF ELECTROSTATIC CHARGE MEASUREMENTS ON LABORATORY AND WORKPLACE AEROSOLS 101

2.1 Electrostatic charging of aerosols in the laboratory 102

2.2 Electrostatic charging of aerosols in the workplace 104

2.3 An assessment of the hazards due to electrostatically -ehanced lung deposition 106

3. HEALTH HAZARDS ASSOCIATED WITH ELECTROSTATIC CROP SPRAYING 107

3.1 Electrostatic Crop Spraying : A brief overview 107

3.2 Droplet Evaporation 109

3.3 Theoretical Estimate of the State of Charge on Respirable Pesticide Particles 113

3.3.1 Case history of an individual evaporating droplet 114

3.4 An Assessment of the Health Hazard in Electrostatic Crop Spraying 114

4. HEALTH HAZARD OF CHARGED AEROSOL : DISCUSSION AND RECOMMENDATION FOR FUTURE WORK 115

5. SUMMARY AND CONCLUSIONS OF PART III 115

OVERALL SUMMARY AND CONCLUSIONS 117

REFERENCES 121

APPENDIX (I) : Glossary of Terms 131

APPENDIX (II-A) : The Relationships Between Airway Dimensions and the Lung Volume (Scaling Factor) 133

APPENDIX (II-B) : The deposition efficiency of charged particles during the pause 134

APPENDIX (II-C) : Listing of the computer program for the predictive lung model 136

APPENDIX (II-D) : Charging limits 142

PART

II

A CRITICAL COMPARISON OF THE OPERATING CHARACTERISTICS OF JET AND ULTRASONIC NEBULISERS

PART I

A CRITICAL COMPARISON OF THE OPERATING CHARACTERISTICS OF JET AND ULTRASONIC NEBULISERS

1. INTRODUCTION AND AIMS

The use of aerosols was one of the earliest methods by which therapeutic substances were delivered to the lung. The ancient Egyptians are known to have attached cones of burning cotton to the chests of survivors allowing them to inhale the acrid smoke produced. Since then, inhalation has been used as a route for drug administration by many cultures, Adams, 1844.

Aerosol therapy has advantages over other methods for the administration of some therapeutic agents, since the drug is delivered directly to its required site of action. The therapeutic effect is more rapid than that of an oral dose, a smaller dose may be used and there is a reduced incidence of systemic side effects, Newman, 1983.

Aerosol techniques are now widely used in medicine for: humidification of the airways; delivery of drugs to the lung; producing scans of the ventilated parts of the lung; fundamental research into mechanisms of lung disease. The use of clinical aerosols was reviewed by Brain and Valberge, 1979.

There are two fundamental methods of producing an aerosol: (1) *Condensation* of vapour molecules; (2) *Comminution* of macroscopic matter, Swift, 1980. Condensation is unsuitable for the generation of therapeutic aerosols, since the low vapour pressure of the substances used means that they are thermally degraded before sufficient condensation of vapour has occurred. The common forms of comminution are the atomization of solutions and dispersion of dry powders. The comminution of liquid requires energy to overcome viscous forces, surface tension and to disrupt liquid or large particles into vast numbers of smaller ones. For a given energy input, particle size increases with increasing viscosity or surface tension, Newman et al., 1987. The energy may be provided by compressed gas (*jet nebuliser* JN) or a piezoelectric crystal vibrating at ultrasonic frequencies (*ultrasonic nebuliser* UN), or by mixing the dry particles with flurocarbon propellants in a cannister at a pressure of around three atmospheres (*metered dose aerosol* MDA).

Aerosols produced by the mechanical disintegration of liquid surfaces are known to carry a net electrical charge; the process has been termed '*spray*

electrification', (see glossary of terms) Loeb, 1958. In the spray electrification process, charge separation takes place, whereby the net charge carried by the dispersed cloud is accompanied by a charge of opposite polarity on the spray source.

The JN is an atomizer which produces an aerosol by mechanical forces. Clinical nebulisers generate sprays of small mean droplet size, the larger droplets being removed by impaction within the device. The aerosols produced by this type of nebuliser are often polydisperse and invariably electrically charged. Charge can play a significant part in aerosol dynamic behaviour and deposition.

The influence of electrical charge on aerosol particles is rarely considered in respiratory medicine. However, there is evidence that, for a given concentration of therapeutic agent, the fraction of inhaled particles which are actually deposited in the respiratory tract will be greater for charged than for uncharged particles. Increasing the charge on an inhaled particle increases its force of attraction to the lung epithelium.

An increased deposition of charged particles in human airways was first suggested by Wilson, 1947. Since then, the role of electrical charge on the deposition of particles within the respiratory system has been studied theoretically, Chan et al., 1982, in physical lung models, and also in animals and man.

Mercer, 1975, during a *vivo* studies, noted consistently higher lung deposition when working with aerosols produced by nozzles, rather than by condensation methods. Aerosols produced by nozzles are likely to be electrically charged whereas condensation aerosols are not. Mercer suggested that electrical charge may have been responsible for the discrepancies in his findings. Fraser, 1966, showed, using rabbits, that the presence of charge (equivalent in magnitude to as many as 100 electrons per particle) brought about doubling of the total deposition in the respiratory tract.

Melandri et al., 1977 and 1983, studied the total deposition of 0.3, 0.6 and 1.0μm diameter particles that had been highly charged, using a corona discharge apparatus, from 50 to 100 electronic charges per particle. Both negative and positive charge increased deposition by 15 to 30%. Since the deposition did not increase with increased aerosol concentration, they attributed the enhanced deposition to image-force effects, rather than space charge force. Further, as the deposition was predominantly in the alveolar region, potential beneficial effects are clear.

Enhanced deposition of particles, due to their possessing charge, has also been shown using a hollow cast of the human tracheobronchial tree, Chan et al., 1978.

Particle charging and electrostatic deposition techniques have been proposed and investigated by various researchers, for example: crop spraying, Law, 1980; powder coating, Hughes, 1984; electrostatic precipitation, Inculet, 1978; pollution control, White, 1963. In crop spraying applications, charged spray can increase the deposition efficiency by up to 24 fold compared to uncharged spray. In powder coating, as the powder particles are electrically charged, deposition at the target increases resulting in efficient surface coating. Similar techniques can be employed to control the electrical charge on atomized droplets to increase deposition efficiency.

The technique of charging droplets can also be applied to therapeutic aerosols, but there will be a difference in magnitude of charge on each droplet. The nebuliser can be modified using auxiliary electrodes so that aerosol generated can be charged in a controlled manner by suitably energizing the electrodes.

The aims of this study are to assess the size and electrostatic characteristics of aerosols produced by JN and UN, and to understand the role they play in influencing the site of deposition within the human respiratory tract. It is hoped also to lay down guide-lines for the design of improved nebulisers. This assessment will be carried out in conjunction with medical researchers to determine patient response to aerosols of known size and electrical characteristics; in particular for aerosol droplets of unipolar charge.

Ultrasonically nebulised water is known to cause wheezing, coughing and subjective sensation of irritation, Cheyney and Butler, 1963. In contrast, water delivered from a JN causes significantly less subjective irritation and coughing than that from an UN, in both normal and asthmatic subjects. The difference in charge distributions, of the JN and UN, might explain the irritation caused by UN. The electrical charge itself might irritate or discharge airway receptors or bronchial smooth muscle causing coughing and wheezing not seen with the JN (Ellis, C, personal communication).

The aim of the clinical trial was to eliminate the irritation caused by the UN, by altering the charge characteristics of the aerosol, in order to establish whether it was a consequence of the particular charge distribution.

2. THEORY

2.1 Nebuliser Definition

A nebuliser is a device capable of converting a solution or a suspension of a drug into an aerosol mist. There are two methods of nebulising liquids, Steventon, 1979: (1) nebulisation by the Venturi effect of fluid passing through a Bernoulli nozzle, (JN); (2) ultrasonic nebulisation (UN).

2.1.1 Theory and mechanism of the JN

When compressed air is forced through a small hole in a nozzle (a Bernoulli nozzle), an area of reduced pressure results, where the high speed jet of gas emerges. The mass flow rate of air through the nozzle depends mainly on the diameter of the orifice and the pressure drop across it. If a tube is placed with one end in the Venturi region and the other in a reservoir of liquid, the liquid is drawn through it by the Venturi effect. The liquid comes into contact with the high-pressure air-jet which shears the liquid, dispersing droplets through the gas stream in the turbulent flow. This primary droplet size distribution is of a type described by the empirical equation of Nukyama and Tanasawa, 1939. The resultant droplets then pass through a second narrow nozzle causing further disruption (see Figure I.1).

Most nebulisers then employ an inertial impaction baffle to return large droplets to the fluid reservoir leaving the smaller droplets to pass out of the device (Figure I.2). The effectiveness of comminution is increased with increasing air velocity, Mercer, 1968.

The JN is driven by compressed air or oxygen. Compressed air is usually dry and in passing through the nebuliser becomes humidified. Thus evaporation occurs which removes a significant quantity of water from the solution, resulting in an increased concentration of drug in the remaining solution. The loss of the latent heat of evaporation leads to cooling of the remaining liquid. This cooling effect may also be enhanced by the heat loss due to adiabatic expansion of the driving gas as it leaves the nozzle.

2.1.2 Theory and mechanism of the UN

The UN uses an entirely different means of liquid comminution. In such a device, a piezoelectric transducer creates high-frequency sound waves which are

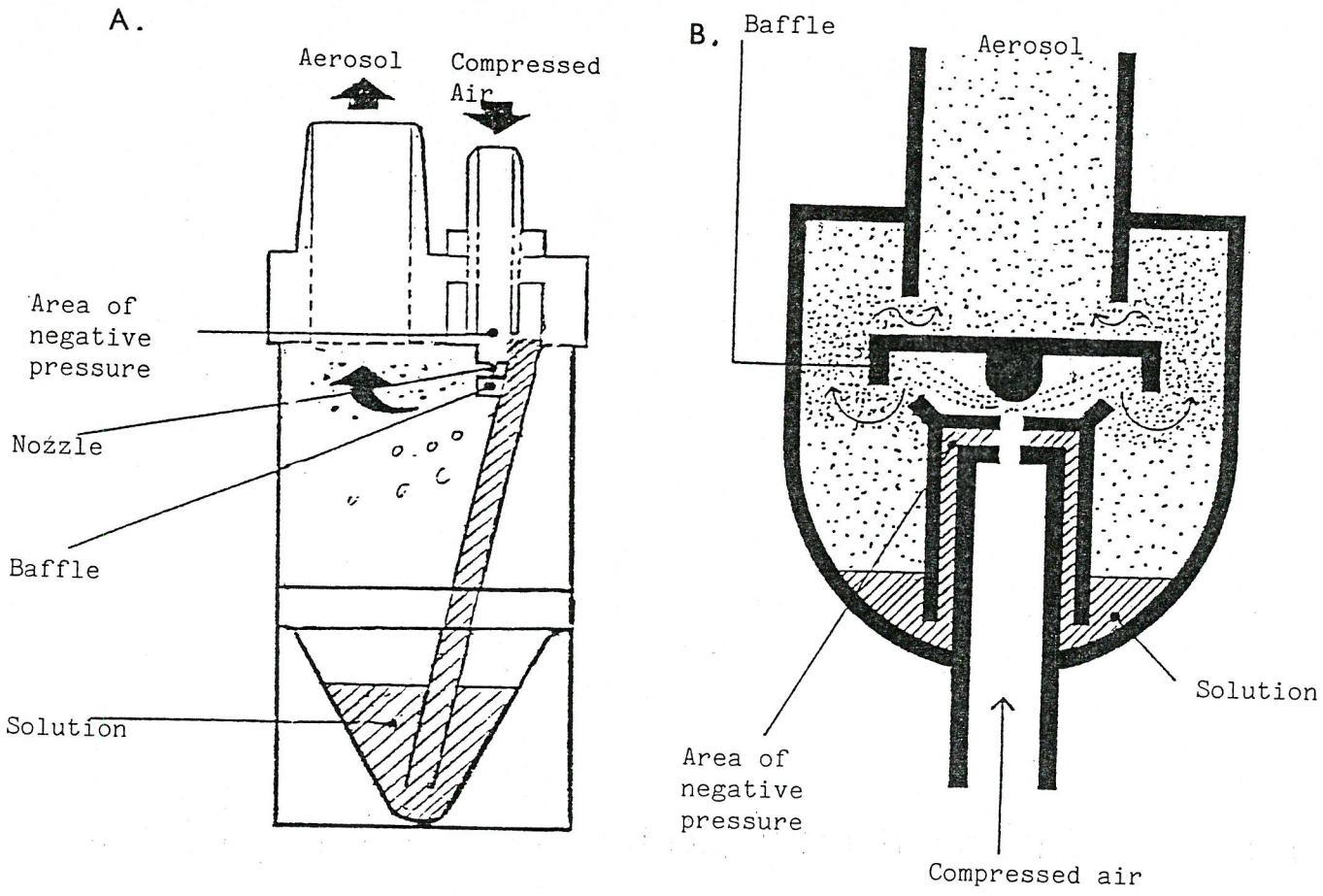

FIGURE I.1 Two type of jet nebuliser

A. Single feed tube (Inspiron Mini-Neb) B. Concentric jet (Medic-Aid 'Acorn')

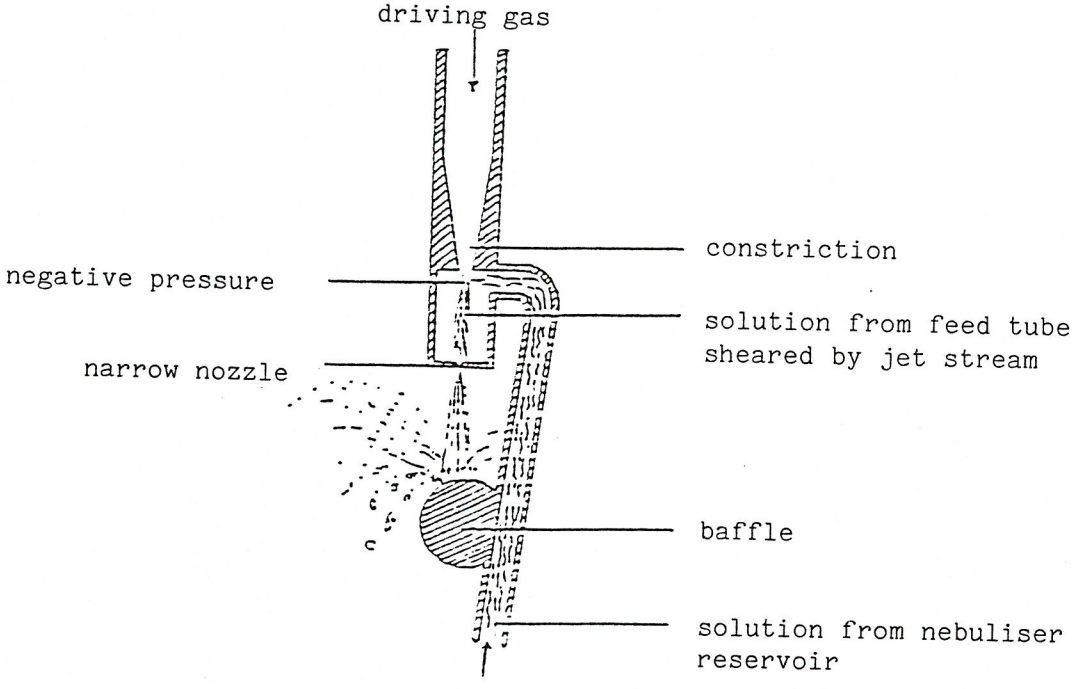

FIGURE I.2 Section from single feed tube jet nebuliser

coupled, via a fluid and diaphragm, to the liquid to be nebulised (see Figure I.3). This generates high-frequency pressure waves in the liquid, causing its surface to oscillate and producing small surface waves known as *'Faraday crispation'*.

If sufficient energy is supplied, the wave crests rupture; elongated filaments (ultrasonic geysers) form at the liquid surface and break up into droplets which escape from the liquid. The ultrasonic *'geyser'* formed, causes the formation of a small-droplets fog in a pulsating manner (a few hundred regular pulses every second), particularly from the lower zone of the fountain.

The number median diameter (NMD) of the droplets so produced correlates with the excitation sound frequency. In studies of liquid atomization at different frequencies, Lang, 1962, found that the NMD of the aerosol was given by:

$$d_{NMD} = 0.34 \left[\frac{8\pi\gamma}{\rho f^2} \right]^{1/3} \qquad (1)$$

where γ = liquid surface tension, in dyne/cm
ρ = liquid density, in g/cm^3 and
f = ultrasonic frequency, in Hz.

In the DeVilbiss Pulmasonic UN (DeVilbiss Health Care UK Ltd, Feltham, Middlesex), a piezoelectric crystal is driven by an alternating electric field at frequency of 1.35MHz (resonant frequency of system) which gives rise to an MMD of ~ 6μm for distilled water, Topp et al., 1972.

During the nebulisation process the temperature of the bulk solution rises due to the kinetic energy imported by the oscillating piezoelectric crystal.

2.2 Factors Affecting Nebuliser Aerosols

2.2.1 Particle size

The *'size'* of particles in a monodisperse aerosol is completely characterized by a single parameter, the particle diameter. Most aerosols, however, have polydisperse size distributions. It is necessary to accurately characterize these size distributions by statistical means. The 'mass median diameter (MMD)' of an aerosol is defined as the diameter above which 50% of the total aerosol particle mass resides. The MMD may be used as an index to characterize the behaviour

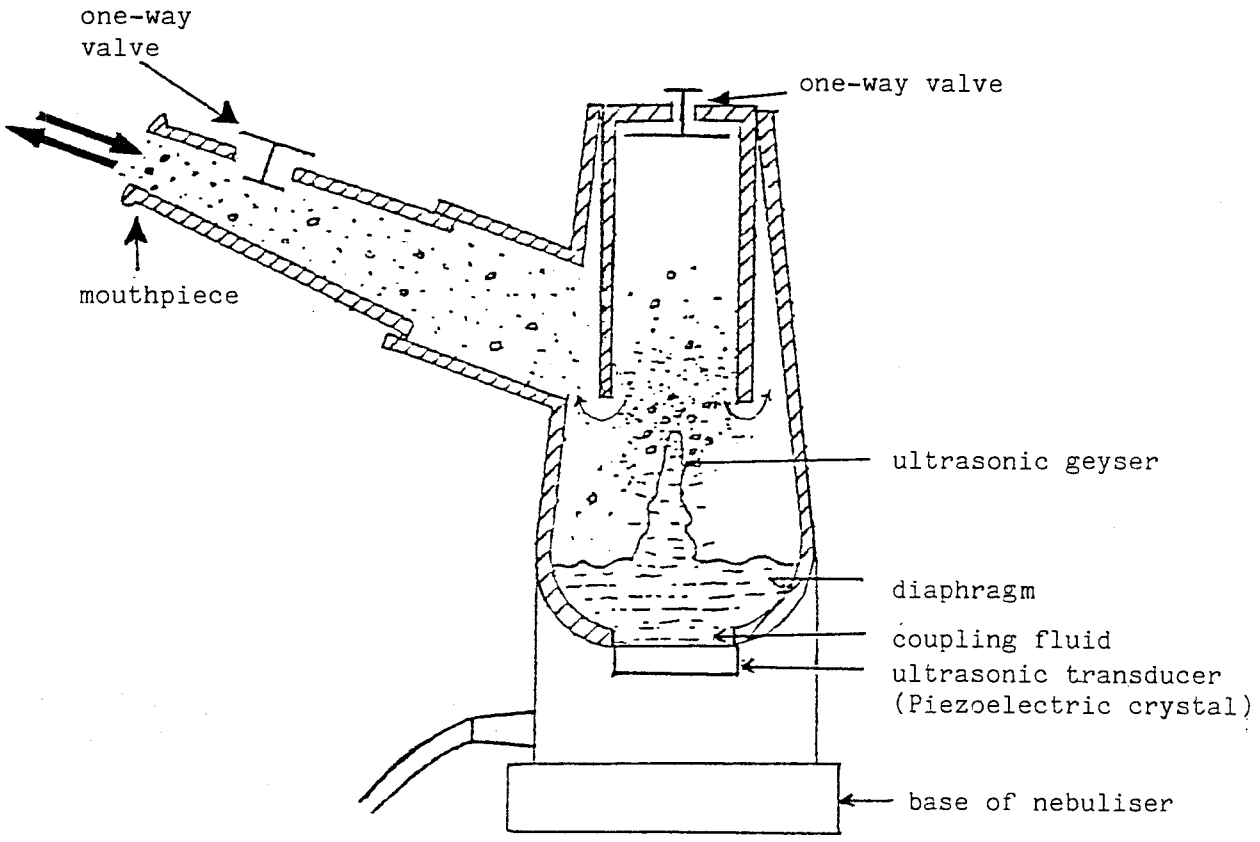

FIGURE I.3 De Vilbiss Pulmasonic (UN)

of the entire size distribution of an aerosol, Task Group on Lung Dynamics, 1966.

In order to be clinically viable, an aerosol must contain enough fine particles to reach the smaller airways of the lung (see part II). If the aerosol has an MMD $> 8\mu m$, a significant amount of drug can be wasted by deposition in the mouth, Lippmann, 1977. Further the site of drug deposition within the lung is dependent on the size of the particles being inhaled, see Figure I.4.

It is quite clear, therefore, that the therapeutic effect of a nebulised drug is highly dependent on particle size and that the majority of droplets should be of diameter $< 5\mu m$ to allow adequate penetration into the airways.

2.2.2 Gas flow rate (jet-driven nebuliser only)

The MMD of aerosols produced using a JN is dependent on the flow rate of the driven-gas, since this determines the energy with which the particles are comminuted. The fall in MMD with increasing drive rate is due to the increasing force with which the liquid is disrupted. It would appear, therefore, that the maximum percentage of respirable particles ($< 5\mu m$ diameter) is produced when the nebuliser is driven at as high a flow rate as possible.

2.2.3 Inhalation rate

During the administration of an aerosol, a patient applies suction (by inhaling) to the nebuliser mouthpiece; air plus the aerosol delivered from the nebuliser is delivered to the patient's lungs. The main air flow, up to 60ℓ/min during heavy breathing, is not drawn through the nebuliser body but rather through a by-pass valve, eg as shown in Figure I.3. However, suction does cause a pressure reduction in the nebuliser output and may well influence the size distribution of droplets in inhaled aerosol.

At rapid inhalation rates, larger particles (which would normally fall back into the nebuliser by gravitational forces) may be drawn up into the inspired aerosol, increasing its MMD. Figure I.5 shows the results of previous work performed in this Department into the relationship between inhalation rate and MMD for the Inspiron Mini-neb JN. The principle is the same for the UN.

2.2.4 Residual volume

The residual volume (*dead volume*) of a nebuliser, is the volume of

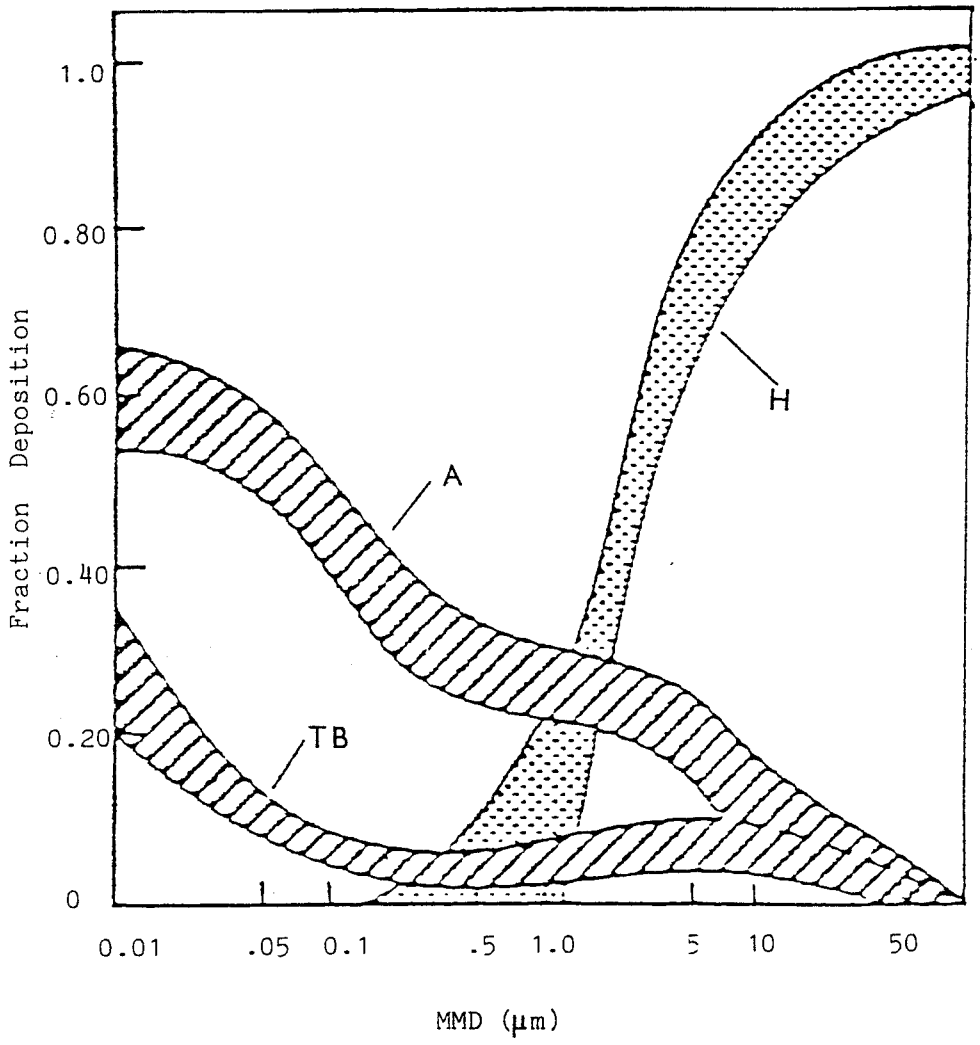

FIGURE I.4 Regional deposition based on model proposed by Task Group on Lung Dynamics, 1966

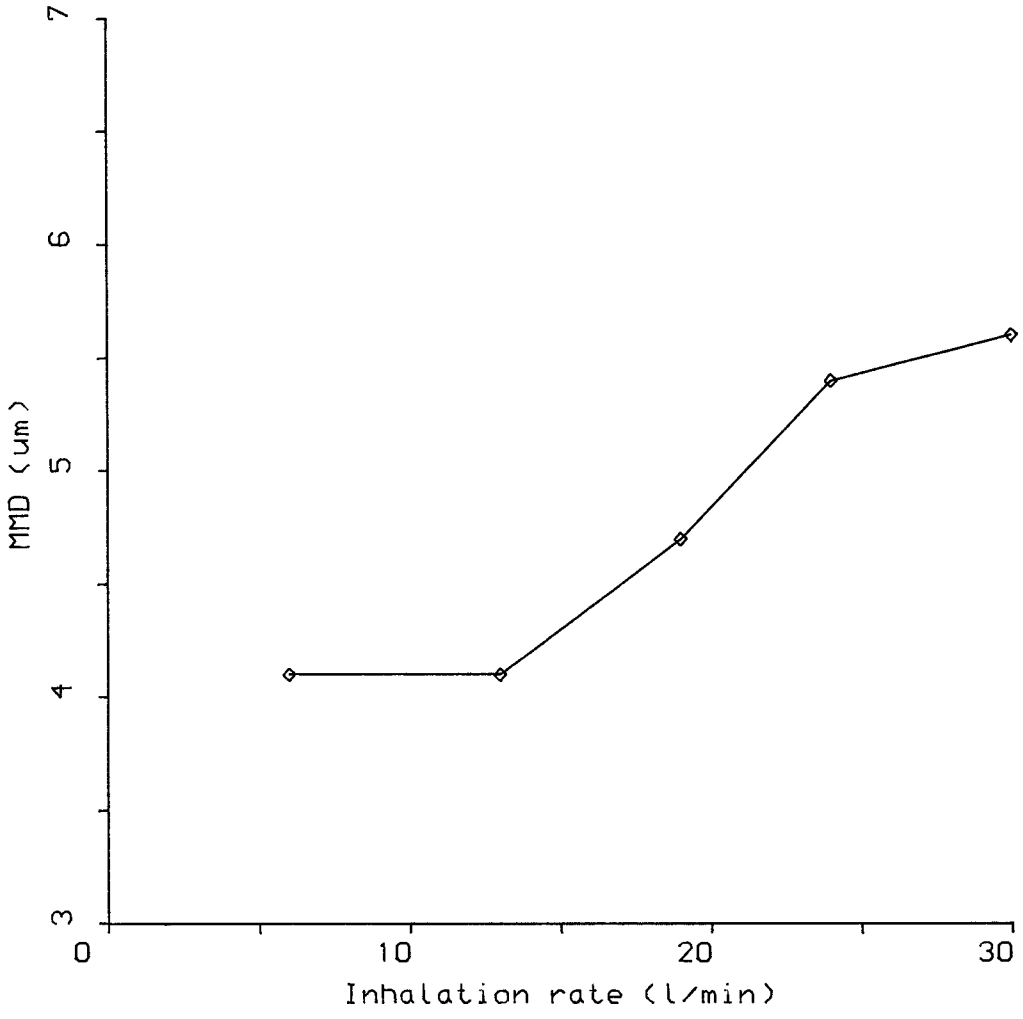

FIG.(I.5): Graph of inhalation rate versus MMD using Inspiron Mini-Neb JN, drived at 8l/min (the principle is the same for UN).
(Data produced by Balachandra and R.lewis)

liquid remaining after the nebuliser solution has run *'dry'*. Such liquid may be deposited on the walls of the nebuliser and tubing, or in a pool below the feed tube in the case of the JN. The residual volume depends on how vigorously the nebuliser is agitated in order to displace droplets from the walls.

The fact that some solution is left in the nebuliser makes the volume of diluent important; the more diluent used the greater the amount of drug delivered by the nebuliser.

Air flow over these droplets will very slowly evaporate them, whether it be due to jet-drive or inhalation *'suction'* of the UN, but a true aerosol cannot be maintained.

2.2.5 Temperature and humidity effects

Aerosol evaporation leads to an increasing concentration of drug within the residual solution. This, in turn, causes an increase in concentration of drug in the aerosol produced. Evaporation leads to cooling of the solution within the nebuliser due to the loss of the latent heat of vaporisation. The rate of cooling depends on the size of the heat sink, that is the volume of liquid within the nebuliser.

At higher ambient temperatures, the water-holding capacity of air is greater, more evaporation can take place, and the aerosol output from the nebuliser increases. In addition, particle size reduces due to an increase in evaporation rate at the elevated temperature. Particle size is also influenced by the humidity of the auxiliary air drawn into the nebuliser, through the non-return valve, during inspiration (see previous data, Figures I.6 a and b). When the humidity of the inspired air is unsaturated, evaporation may readily take place leading to a rapid reduction in particle size.

However, particles which have initially been reduced in size by evaporation can rapidly increase in size by hygroscopic growth in the saturated environment of the airways.

2.2.6 Hygroscopic growth

Many types of particle will undergo hygroscopic growth at high relative humidities, especially in the water-saturated environment of the lungs. The effect of hygroscopicity varies with the solubility and molecular weight of the compound

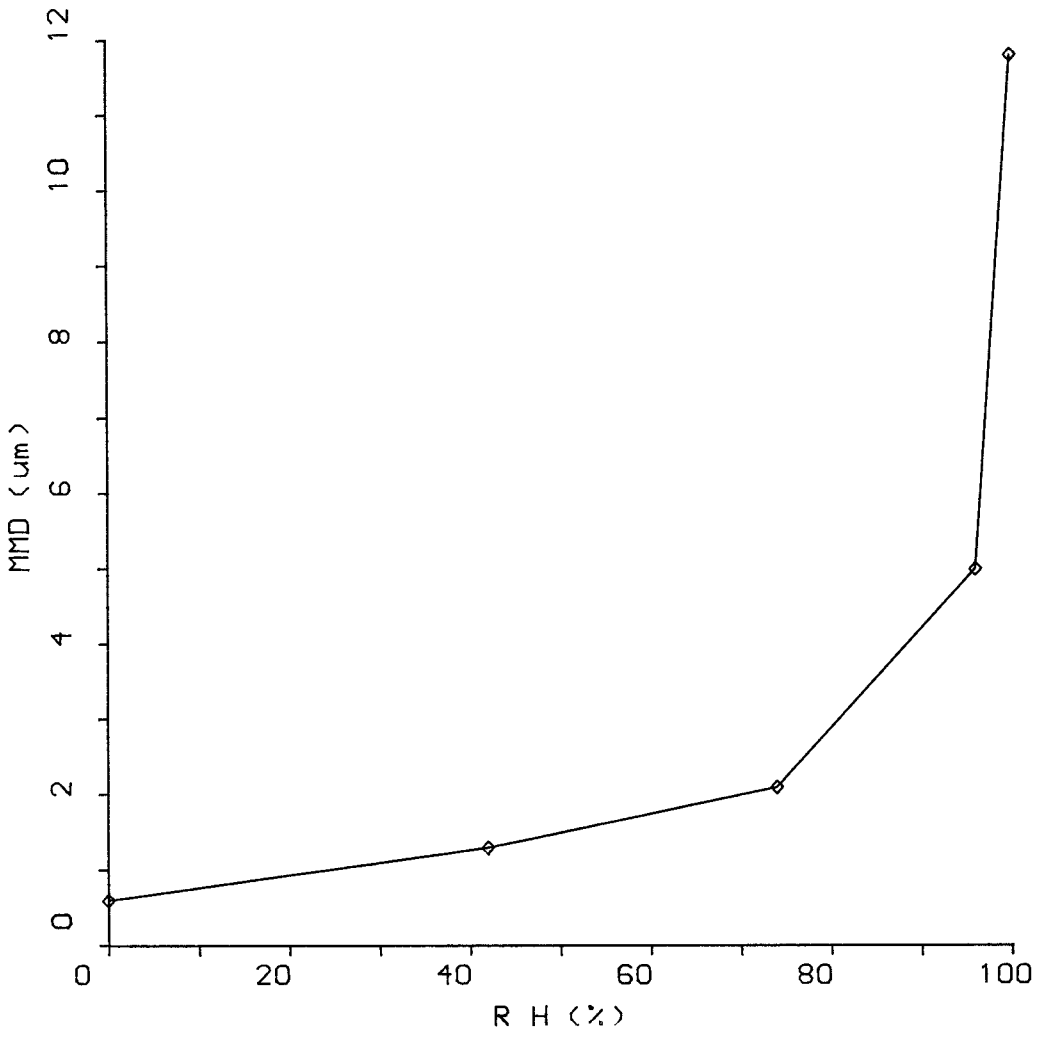

FIG.(I.6a): Effect of relative humidity on the MMD of JN showing a large rise in particle size as the humidity approaches 100%.
(Data produced by Balachandra and R.Lewis)

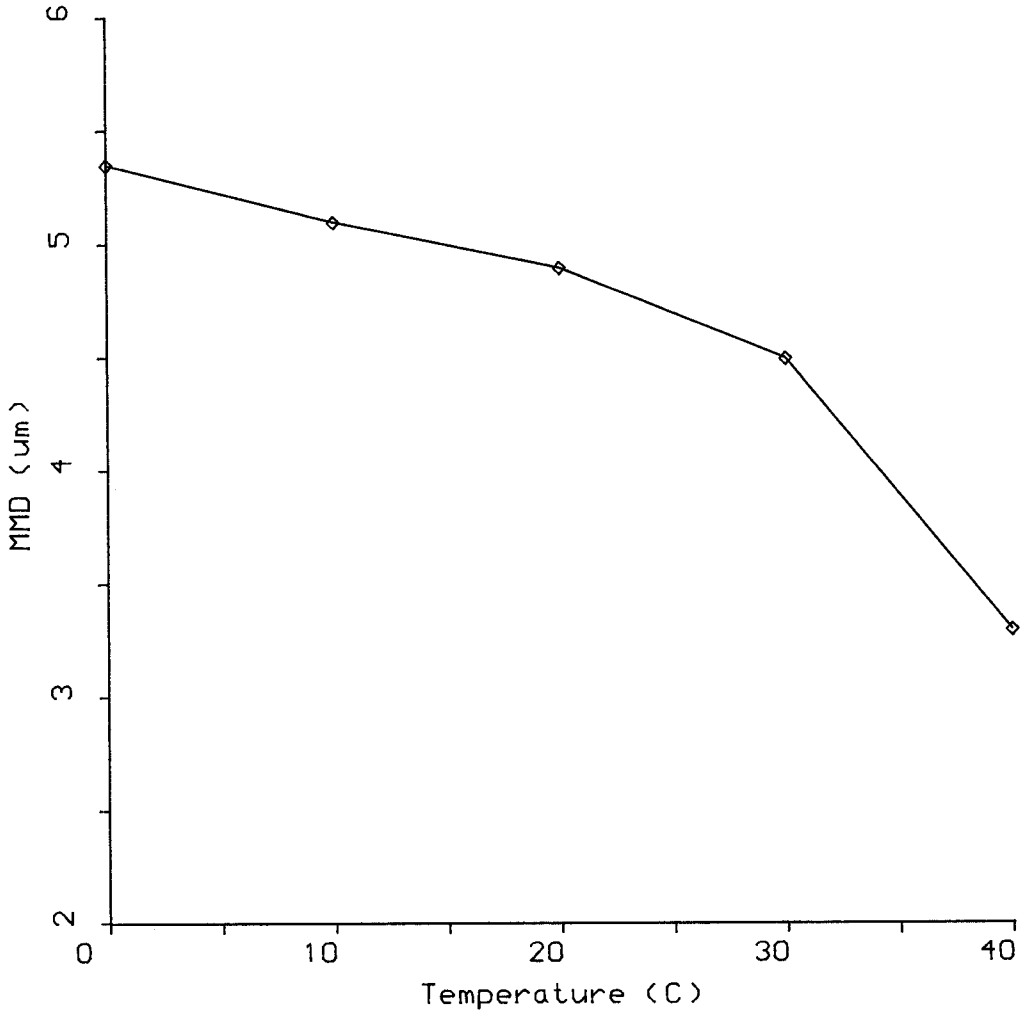

FIG.(I.6b): Effect of water bath temperature on the particle size from Mini-Neb JN, driven at a gas flow rate of 8l/min.
(Data produced by Balachandra and R.lewis)

of which the particle is composed. Its significance depends on the degree to which accretion of water by a particle alters depositional probabiity and site of deposition in relation to a similar insoluble particle, Mercer, 1973.

The influence of hygroscopic growth, in relation to particle generation and deposition, needs to be assessed for the majority of the therapeutic agents used. Up to now, there is little information available in the literature relating to this subject.

2.2.7 Electrical charge

According to Vincent et al., 1983, all natural and generated aerosol particles are electrically charged. It follows that the droplets in therapeutic aerosols are charged. Aerosol particles may acquire charge either in the process of their formation or from the environment after formation. Such charge may play a significant part in aerosol dynamic behaviour and deposition. When aerosol droplets acquire a unipolar charge, they display certain physical characteristics and biological effects which are summarized in Table I.1.

TABLE I.1 "Effect of Unipolar Electric Charges on Aerosol Droplets"*

Physical effects	Physiological effects	
.Fewer collisions .Less evaporation .Better homogenity .Better stability .Reduced concentration .Better deposition in respiratory tract. .Smaller droplets	Local effects on physiology & biochemistry of cells and tissues: .Ciliary activity .Mucus flow .Smooth muscle tone .Permeability of cell membrane .Enzyme activity .Cell metabolism	Central effects on physiology & biochemistry of the body: .Physical activity .Performance .Blood pressure, heart rate. .Hormone levels ... etc.

*Source: Wehner, 1969.

2.3 Charging Mechanisms

Although droplets generated by a nebuliser are inherently charged, it may be possible to manipulate the level of charge on droplets in several ways. The most common charging mechanisms, Hinds, 1982a, are: (i) *corona discharge*, and (ii) *static electrification* (which includes electrolytic charging, spray electrification and contact charging). In this study, the corona discharge technique is used for charging droplets.

2.3.1 Corona discharge

Corona arises due to the ionization of a gas near a sharp electrode and occurs at a voltage less than the spark breakdown value. In air, the corona discharge is a highly active glowing region, bluish white or possibly reddish in colour, extending into the gas a short distance beyond the discharge electrode surface.

Initiation of the corona discharge requires the availability of free electrons in the gas in the region of the intense electric field surrounding the discharge electrode. Such electrons can be produced by cosmic rays interaction with air molecules in the atmosphere.

The mechanisms of corona formation are summarized as follows, (Struss, 1971):

- In the case of a negative discharge electrode

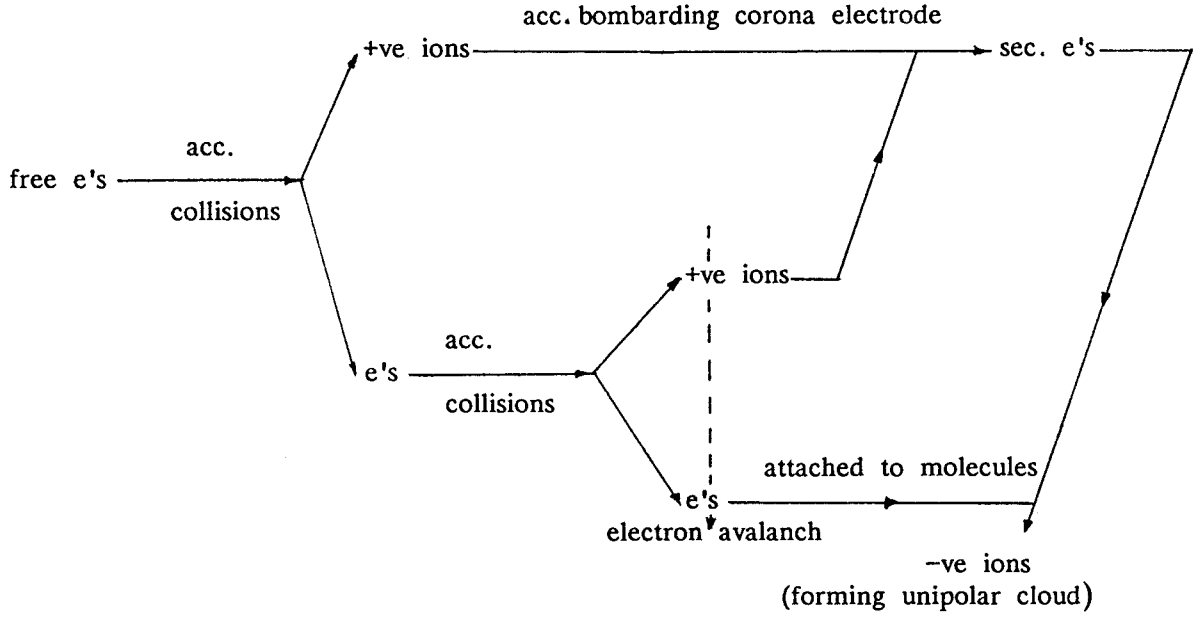

– In the case of a positive discharge electrode

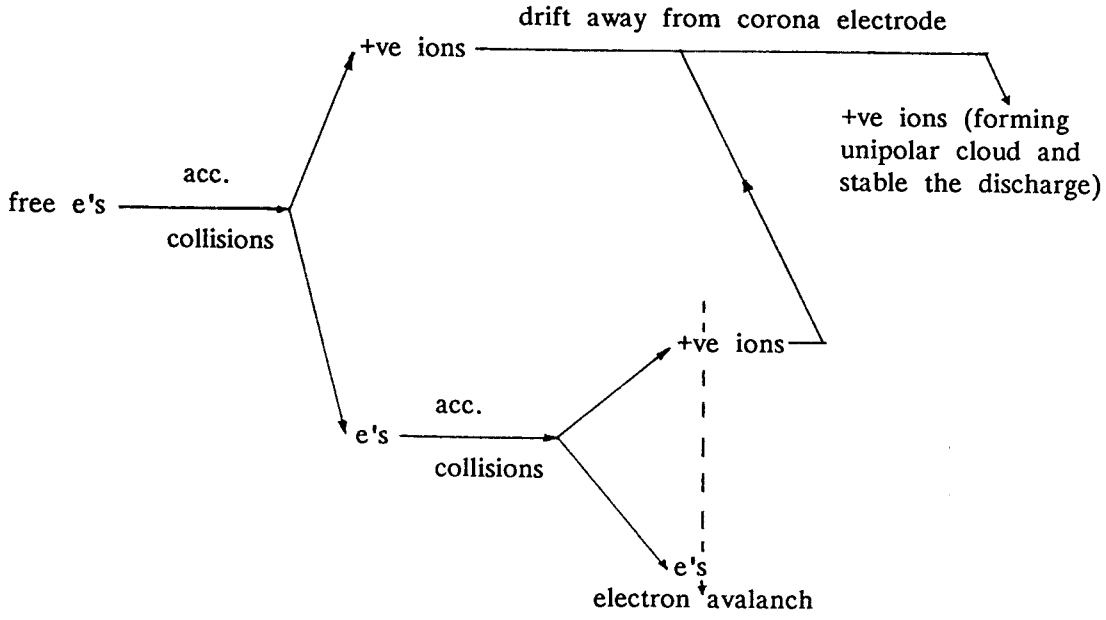

Both types of corona are maintained by the sporadic appearance of free electrons from random processes associated with the discharge. Possible processes are photo ionisation by ultraviolet radiation from the discharge or the recombination of electrons and positive ions in the corona region which can give rise to high–energy photons, and in the case of negative corona, the release of electrons at the cathode by positive–ion impact.

2.3.2 Particle charging

Particles in the gas stream are charged by impinging ions produced in the corona discharge. There are two mechanisms by which charging may occur. These are referred to as ion bombardment (or *field charging*) and ion diffusion (or *thermal charging*). Figure I.7 illustrates the above mentioned droplet charging processes.

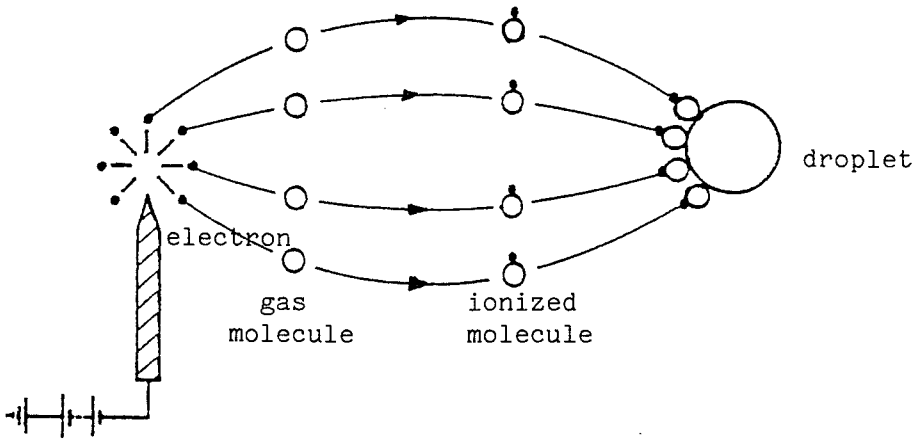

Figure I.7: Process of charging the droplet

2.3.2.A Ion bombardment charging

Field charging occurs when unipolar or bipolar ions attach to a particle in the presence of a strong electric field. Ions present in the electric field, travel along the field lines and collide with the particle where the lines intersect its surface. In the unipolar theory of particle charging by ion bombardment, as stated by Pauthenier and Moreau-Hanot, 1932, the charge deposited on a particle is given by:

$$q = \left[\frac{3\epsilon}{\epsilon + 2} \right] \left[\frac{Ed_p^2}{4} \right] \left[\frac{\pi e \mu_i N_i t}{1+\pi e \mu_i N_i t} \right] \qquad (2)$$

where cgs units are used and:

q = particle charge
N_i = ion number concentration
ϵ = dielectric constant of the particle
E = electric field strength at particle position
d_p = particle diameter
t = time
μ_i = mobility of the ions (~ 450 $cm^2/stV.s$)

The limiting form of this expression as $t \rightarrow \infty$ is:

$$q_\infty = \left[\frac{3\epsilon}{\epsilon + 2} \right] \frac{Ed_p^2}{4} \qquad (3)$$

2.3.2.B Ion diffusion charging

In diffusion charging, particles acquire charge by random collisions with ions. The process results from the Brownian motion of the ions and particles and has been studied quantitatively by White, 1963, who gives the following expression for theoretical charge of a spherical particle.

$$q = \frac{d_p kT}{2e} \ell n \left[1 + \frac{\pi d_p \bar{c}_i e^2 N_i t}{2kT} \right] \qquad (4)$$

where cgs units are used and

q = particle charge

d_p = particle diameter

k = Boltzmann's constant (1.38×10^{-16} erg K^{-1})

T = absolute temperature

e = electron charge (4.803×10^{-10} esu)

c = RMS value of ion thermal velocity (2.4×10^{4}cm s^{-1})

N_i = number of ion per unit volume

t = time

A number of workers have attempted to formulate a complete theory of particle charging, taking into account the effect of ion bombardment and ion diffusion simultaneously, Lui and Kapadia, 1978.

2.4 Electrical Mobility

Electrical mobility is a property of a charged particle which is subjected to an electric field in a fluid medium. By definition, it is the particle speed per unit electric field. Electrical mobility can be measured using a mobility analyser. In a cylindrical tube/coaxial rod mobility analyser, ions are deflected and precipitated through a laminar air stream. The analyser collects all ions of mobility greater than or equal to a particular value which is related to the geometry of the analyser and the applied voltage.

To calculate the minimum mobility of ions collected, assume that the flow velocity inside the tube represented by the mean velocity $\bar{U} = Q/A$, where Q is the air flow rate and A is the cross-sectional area of the tube.

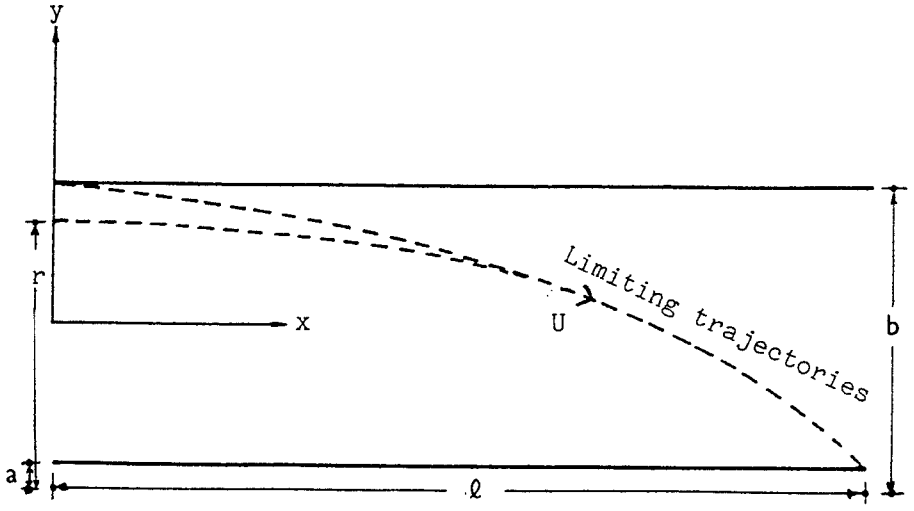

Limiting trajectory of charged particles in mobility analyser

The axial distance travelled by the ion in moving from radius "b" to radius "a" (see diagram) will be:

$$\ell = \int \bar{U}\, dt = \int_r^a \bar{U} \left[\frac{dt}{dr} \right] dr \qquad (5)$$

Now, $dr/dt = -\mu E$ is the radial velocity of the ion passing through the radial electric field of the cylinder, μ being the electrical mobility of the particle. The minimum rod length required to collect the ion is:

$$\ell = \int_a^r \frac{\bar{U}}{\mu E} dr \qquad (6)$$

Now, $\bar{U} = Q/\pi(b^2-a^2)$ and $E = V/r\ \ell n\ (b/a)$

where V = the potential difference between the electrodes,

a,b = the radius of the inner and outer electrodes respectively.

$$\therefore \quad \ell = \int_a^r \frac{rQ\ell n(b/a)}{\pi(b^2-a^2)\mu V} dr = \frac{Q\ell n(b/a)}{\pi(b^2-a^2)\mu V} \left[\frac{r^2-a^2}{2} \right] \qquad (7)$$

Consider the collection of ions from radius r = b

$$\ell = \frac{Q\ell n\ (b/a)}{2\pi\ \mu\ V} \qquad (8)$$

The ion mobility analyser will therefore collect all ions of mobility greater than or equal to:

$$\mu = \frac{\ell n\ (b/a)}{2\ \pi\ \ell} \cdot \frac{Q}{V} \qquad (9)$$

2.5 Particle Sedimentation

The sedimentation of particles from a gas in laminar flow, in a horizontal, circular tube, has been considered by Fuchs, 1964. Using an equation

due to Natansen, Fuchs gives the following expression for particle deposition efficiency:

$$\eta_S = \frac{2}{\pi}\left[(\sqrt{1-\epsilon^{2/3}})\ (2\epsilon-\epsilon^{1/3}) + \sin^{-1}\epsilon^{1/3} \right] \qquad (10)$$

where $\epsilon = \frac{3\ v_s L}{4\ \bar{v}\ a}$ is a dimensionless parameter

and:
- v_s = particle settling velocity
- $\bar{v}$ = mean velocity of fluid passing through the tube
- L = tube length
- a = tube diameter

The same expression can be used to calculate the sedimentation of particles flowing in a human airway. However, a factor of $\pi/4$ is introduced into the definition of ϵ, Heyder, 1975, to account approximately for the orientation effect of the airways, i.e.

$$\epsilon = \frac{3\pi v_s L}{16\ \bar{v}\ a}$$

3. MEASUREMENT

3.1 Size Measurement

3.1.1 Introduction and aims

The therapeutic effect of a nebulised drug is highly dependent on particle size. The size distribution of an aerosol may be assessed by different techniques, Bailey, 1974. The requirements for particle size analysis, in this study, were that the technique should be able to measure particle size in real time, at a position equivalent to the mouthpiece of the nebuliser, and that sampling problems should be avoided. An item of equipment which fulfilled these requirements was the Malvern Particle Size Analyser, based on the technique developed by Swithenbank et al., 1977.

3.1.1.A Malvern Particle Size Analyser

The Malvern Particle Size Analyser can be used to measure the size distribution of particle or droplet ensembles having diameters ranging from about 1μm to 1000μm. The technique is based on the Fraunhofer diffraction principle.

A 2mW He/Ne laser beam (6mm in diameter) is used as a coherent light source. A particle in the measuring volume (see foot note)** diffracts the laser radiation by an amount which depends on particle size but which is independent of particle speed.

A spherical particle diffracts maximum energy at an angle inversely proportional to its diameter (see Figure I.7a). A Fourier transform lens (receiving lens) is used to focus the diffracted light pattern onto a photo-detector consisting of 30 concentric rings (Figure I.7b).

The size range may be varied by changing the focal lens of the Fourier transform lens; however, there is a lower limit of ~ 1μ in diameter for He/Ne laser light. This is due to the fact that the required diffraction pattern is only formed when the particle diameter is greater than the wavelength of the laser radiation (λ = 0.6328μm). The output of the photo-detector is processed by a micro-computer which is controlled by a keyboard. The measured energy distribution is compared with a calculated energy distribution based on known models of particle size distribution (eg. normal, log normal and Rosin-Rammler distributions or model independent) and a *'best fit'* to the model obtained by the method of least squares. Calculation of the particle size distribution is performed using model independent or two-parameters software.

The apparatus is calibrated by the manufacturers (Malvern Instruments Ltd., Malvern, Worcestershire) and the computed mean diameter has an accuracy of ±4% when the total size distribution lies within the measuring range of the equipment. Automatic compensation for background particles counts is incorporated into the procedure after an initial background reading has been taken. The sampling time may be varied from a minimum of 30msec to 50sec, the time chosen being sufficiently long to obtain a representative sample.

The Malvern Particle Size Analyser was used to assess the effect on aerosol droplet sizes of: (1) nebuliser type, (2) drive gas flow rate (JN only), (3) suction rate, (4) distance from the mouthpiece, (5) volume of solution placed in the nebuliser, and (6) temperature and humidity.

** The measuring volume is the space in the laser beam from the front of the Fourier transform lens to a distance away from it equal to the focal length of the lens. This is to ensure that all the diffracted light is collected by the Fourier transform lens and hence multi-ring detectors.

(a) Principle of operation

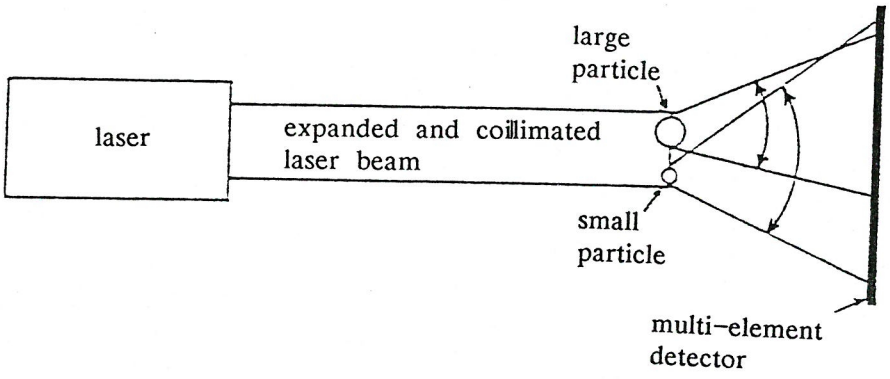

(b) Diagram of Malvern particle sizer

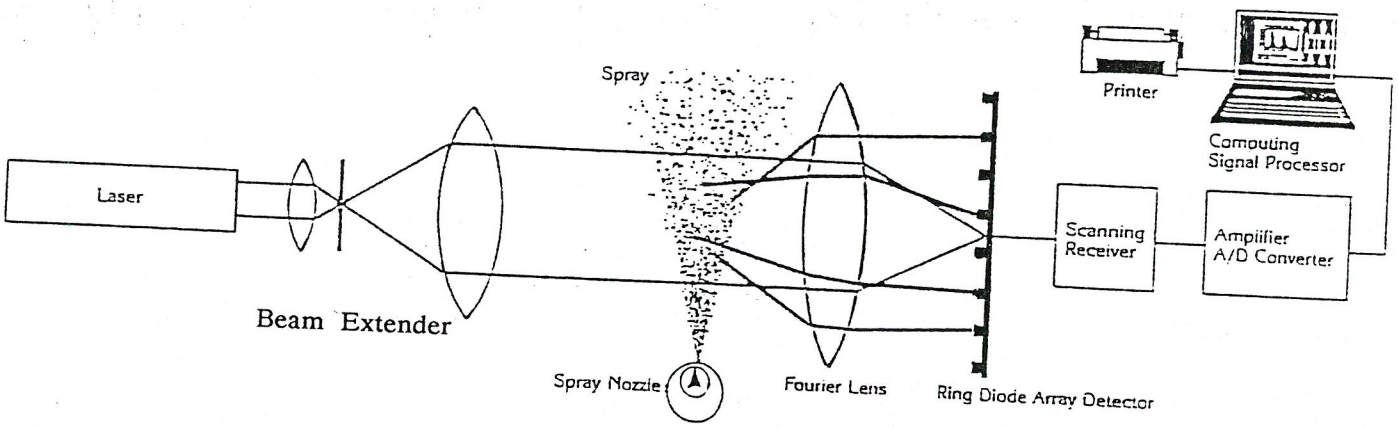

FIGURE I.7 MALVERN PARTICLE AND DROPLET SIZE ANALYSER

3.1.2 Methods

A Malvern Particle Size Analyser (Model 2600HSD), fitted with a 63mm focal length lens, was used to measure aerosol droplet size distributions. The aerosol MMD and percentage mass of droplets of diameter $<5\mu m$ (within the respirable range) were then calculated from the distributions. The experimental sampling time was typically 1 sec and the resultant data were recorded on magnetic disc for subsequent analysis, using model independent or two-parameter software.

The arrangement shown in Figure I.8 was used when testing a nebuliser. Clamping the nebuliser in a vertical position enabled the aerosol, released from the mouthpiece, to cross the laser beam between the lens and its outer focal plane (the focal plane region is the most sensitive area for detecting drops of different sizes, Swithenbank et al., 1977). The nebuliser was driven by compressed air, from a cylinder, and the flow rate regulated using a reducing valve and monitored by rotameter. Air pressure was measured using a pressure gauge. The nebuliser side arm was left open to enable auxiliary air to be drawn into the aerosol, from the atmosphere, as occurs when a subject inhales through a mouthpiece. The aerosol was conducted, via the usual nebuliser mouthpiece tubing, into the laser beam, at a point corresponding to the mouth of the subject.

For some measurements, the aerosol was not allowed to issue freely into the atmosphere at this point, but instead was drawn, at a controlled suction rate, through a sealed optical chamber (*supplied by the Respiratory Dept., Southampton General Hospital*) which was penetrated by the laser beam. The chamber was mounted so that its windows were perpendicular to the laser beam. The aerosol was sucked through the chamber by a variable-flow vacuum pump, a rotameter being used to measure the flow rate. Periodically, it was necessary to clean the glass windows of the optical chamber since droplets deposited on them. Distilled water was used; as the nebuliser solution, in all of the experiments. Unless otherwise specified, all measurements were made under ambient conditions of temperature and humidity which were both monitored during each experiment.

In the case of the UN, it was necessary to transport the aerosol to the measurement zone using an auxiliary air flow.

3.1.3 Results and discussion

The aerosols measured were all found to have polydisperse size distributions. The use of model independent software, to represent such

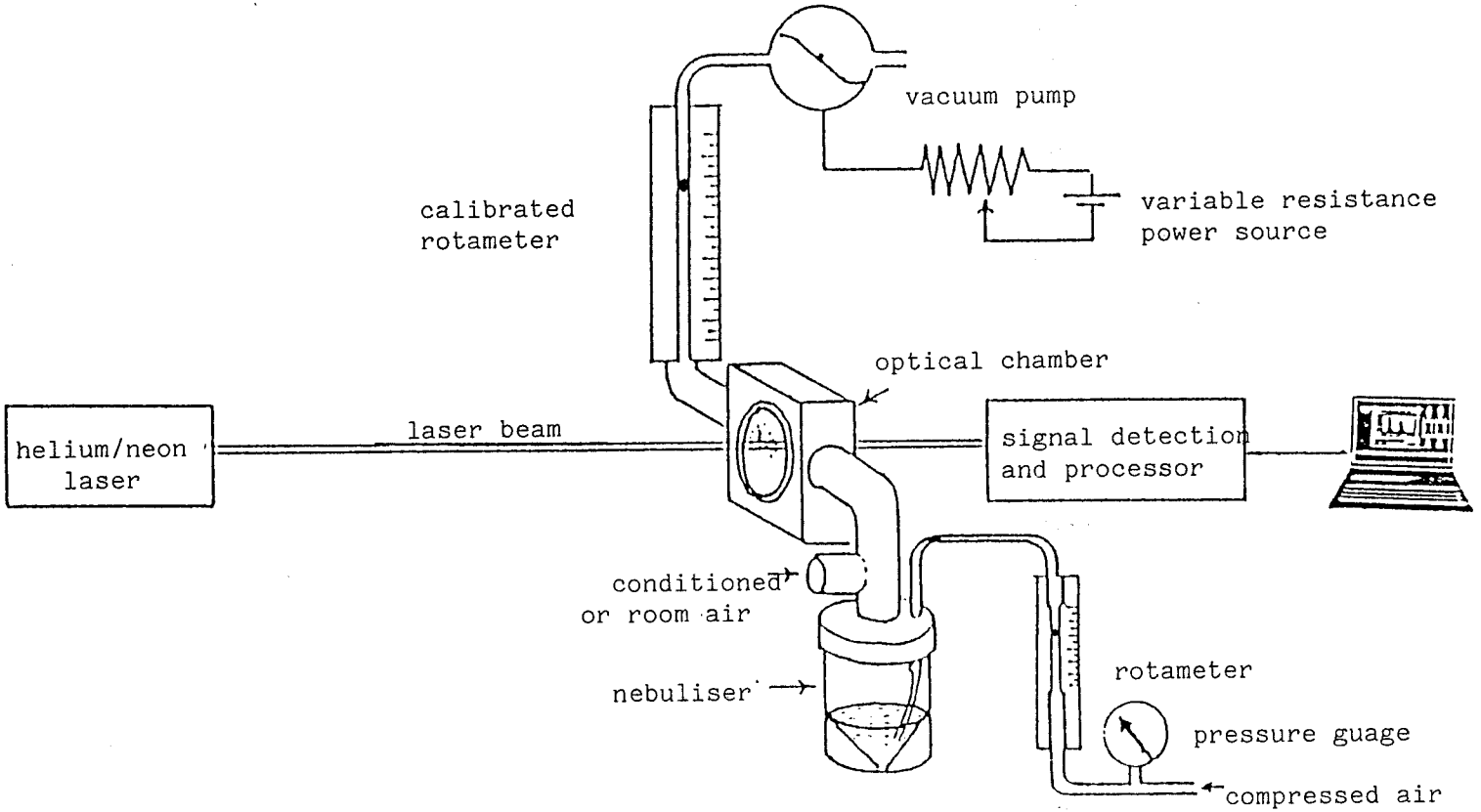

FIGURE I.8 Apparatus for nebuliser generated particle size analysis

distributions, is appropriate since no analytical model for the weight distribution of the sample is assumed. Instead, the software considers a set of 15 weight bands, chosen according to focal length of the receiver lens used in the measurement. Using the least squares technique, the sizer optimises 15 independent parameters and can accommodate any type of size distribution.

3.1.3.A A variability and repeatability of droplet size measurements

The aims of these experiments were: to investigate the repeatability of nebuliser performance, using the same nebuliser under identical conditions of nebulisation; to investigate the variation in nebuliser performance, when using different nebulisers in a similar manner.

Three nebulisers were assessed: two JN's the Inspiron Mini-neb JN (Bird Ltd., Sunderland) and Unicorn (Medic-Aid Ltd., Chichester), and one UN, the DeVilbiss Pulmasonic UN. For both the JN's and the UN, one of each nebuliser type was tested 6 times under identical conditions, and for the JN's, 6 nebulisers were tested twice (with the mean value given) under the same conditions.

The data are summarized in Tables I.2 and I.3, and the six size distributions, obtained for the Inspiron JN, are shown in Figure I.9. There was uniformity of droplet size, particularly for the Inspiron Mini-neb JN. This is the most frequently used nebuliser in UK hospitals, Stainforth et al., 1983.

NB After using the nebuliser for some time, a noticeable increase in MMD was observed. This indicates that any JN has a fixed lifetime, after which the size distribution changes resulting in larger MMD. This may be due, perhaps, to wear in the orifice or baffle, or possibly ageing or conditioning of the surface material.

3.1.3.B Effect of gas-drive flow rate on droplet size (JN)

Three JN's, the Inspiron Mini-neb, Unicorn and Acorn, were driven at flow rates of 4 to 12ℓ/min. It was not possible to drive the Acorn at flow rates exceeding 11ℓ/min and the Inspiron Mini-neb could not be driven at flow rates greater than 12ℓ/min. At higher flow rates, the tubing, supplying the drive gas, tended to become disconnected from the nebuliser.

TABLE I.2 Repeatability: a series of tests on a single nebuliser enables its repeatability of output to be determined.

Test No	JN		UN
	Inspiron Mini-neb	Unicorn	DeVilbiss Pulmasonic
	8ℓ/min drive 18 ~ suck H_2O 5mℓ fill	8ℓ/min drive 18 ~ suck H_2O 5mℓ fill	18ℓ/min suck H_2O 10mℓ fill
	MMD (μm)	MMD (μm)	MMD (μm)
1	4.50	3.60	4.45
2	4.55	3.60	4.50
3	4.45	3.80	4.40
4	4.55	3.65	4.40
5	4.40	3.65	4.30
6	4.45	3.65	4.40
Mean MMD	4.48	3.66	4.41
SD	0.06	0.07	0.06

TABLE I.3 Variability: a series of tests on different nebulisers enables its variability of output to be determined.

Test No.	Inspiron Mini-neb JN	Unicorn JN
	8ℓ/min drive 10 ~ suck H_2O 5mℓ fill	8ℓ/min drive 10 ~ suck H_2O 5mℓ fill
	MMD (μm)	MMD (μm)
1	4.16	6.8
2	4.16	6.9
3	4.16	7.7
4	4.16	6.0
5	4.30	6.1
6	4.16	7.5
Mean MMD	4.18	6.83
S.D	0.05	0.64

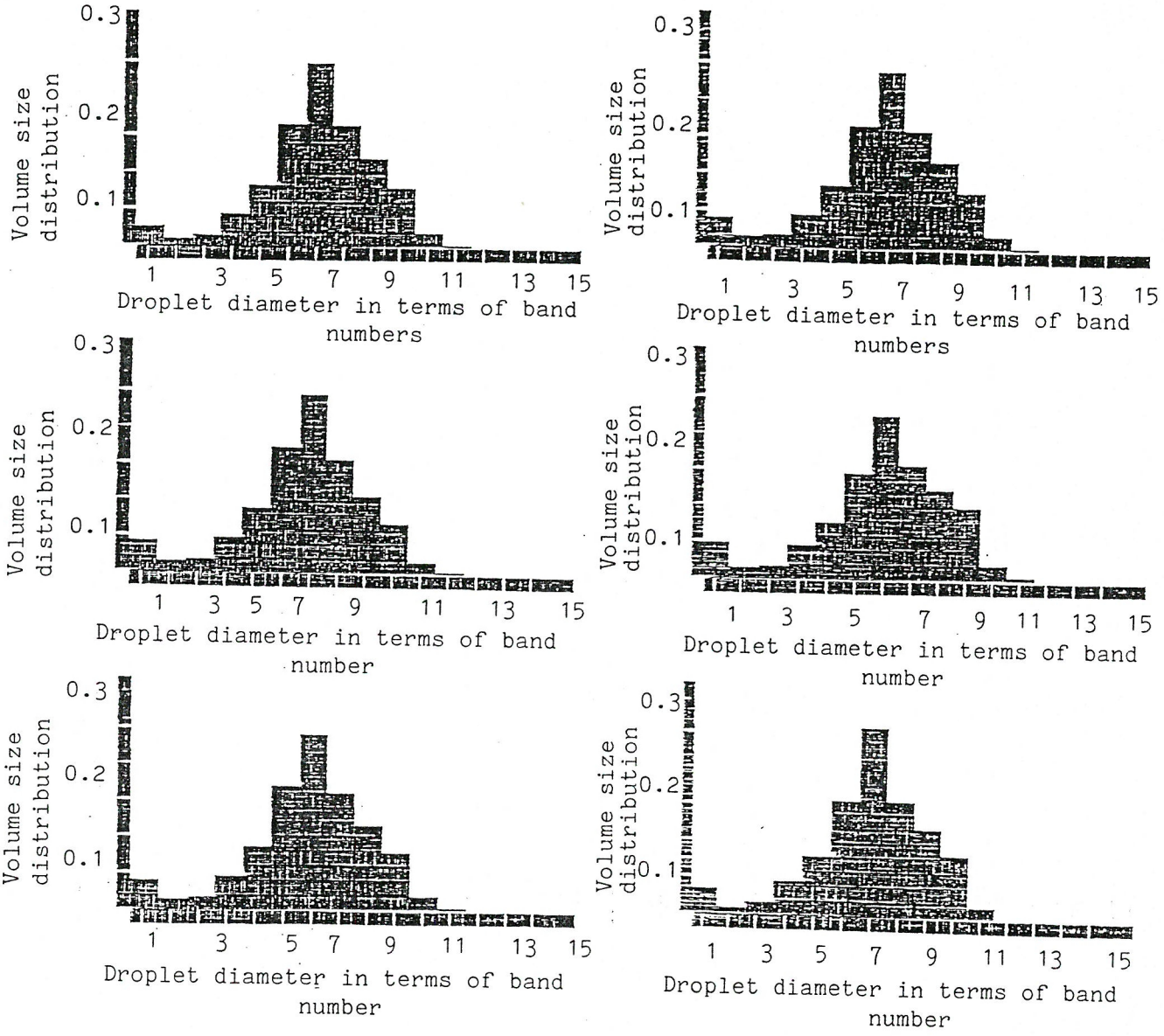

Nebuliser Type : Inspiron Mini-Neb JN
Air-Drive Flow Rate = 8ℓ/min
Suction Rate = 30 ℓ/min
Volume Fill = 10mℓ

FIGURE I.9 Size distribution to show the repeatability of aerosol produced by JN

band no.	size range (μm)
1.	1.2 - 1.5
2.	1.5 - 1.9
3.	1.9 - 2.4
4.	2.4 - 3.0
5.	3.0 - 3.9
6.	3.9 - 5.0
7.	5.0 - 6.4
8.	6.4 - 8.2
9.	8.2 - 10.5
10.	10.5 - 13.6
11.	13.6 - 17.7
12.	17.7 - 23.7
13.	23.7 - 33.7
14.	33.7 - 54.9
15.	54.9 -118.4

The MMD's of the aerosols generated by the three jet nebulisers were strongly influenced by the driving flow rate, see Figure I.10a. An overall 25–36% reduction in MMD could be achieved by increasing the flow rate from 4 to 10ℓ/min.

The percentage of droplets < 5μm in Figure I.10b shows an increase with increasing drive rate up to 52.7% at 10ℓ/min for the Unicorn, 47.4% at 8ℓ/min for the Acorn and 44.4% at 12ℓ/min for the Mini-neb. Since for any given rate the pressure is constant, pressure may be substituted for flow as shown in Figures I.10a and I.10b.

For UN, the auxiliary air flow rates used to transport the spray to the sampling area does not have any effect on droplet size.

3.1.3.C The effect of suction rate on droplet size

To assess the effect of inhalation rate on particle size, one UN and two JN's were studied. The two JN's were driven at an air flow rate of 8ℓ/min by air which was sucked through the nebulisers at a constant flow rate (5, 10, 15, 20, 25, and 30ℓ/min).

At suction rates exceeding 10ℓ/min, experimental difficulties arose and meaningless results were obtained. Apparently, the design of the optical chamber was unsuitable for high suction rates. As a result of turbulant motion, droplets deposited, to an unacceptable extent, on the glass windows of the optical chamber. It was necessary, therefore, to redesign the chamber to overcome this problem.

As the suction rate was increased to 10ℓ/min, the MMD was found to increase whereas the percentage of respirable droplets (< 5μm in diameter) decreased.

3.1.3.D Variation of droplet MMD with distance along the axis of the aerosol spray

In moving the nebuliser away from the laser beam (i.e. increasing the distance of the laser beam from the nebuliser along the axis of the aerosol spray) the MMD would be expected to decrease, due to the effects of evaporation and sedimentation.

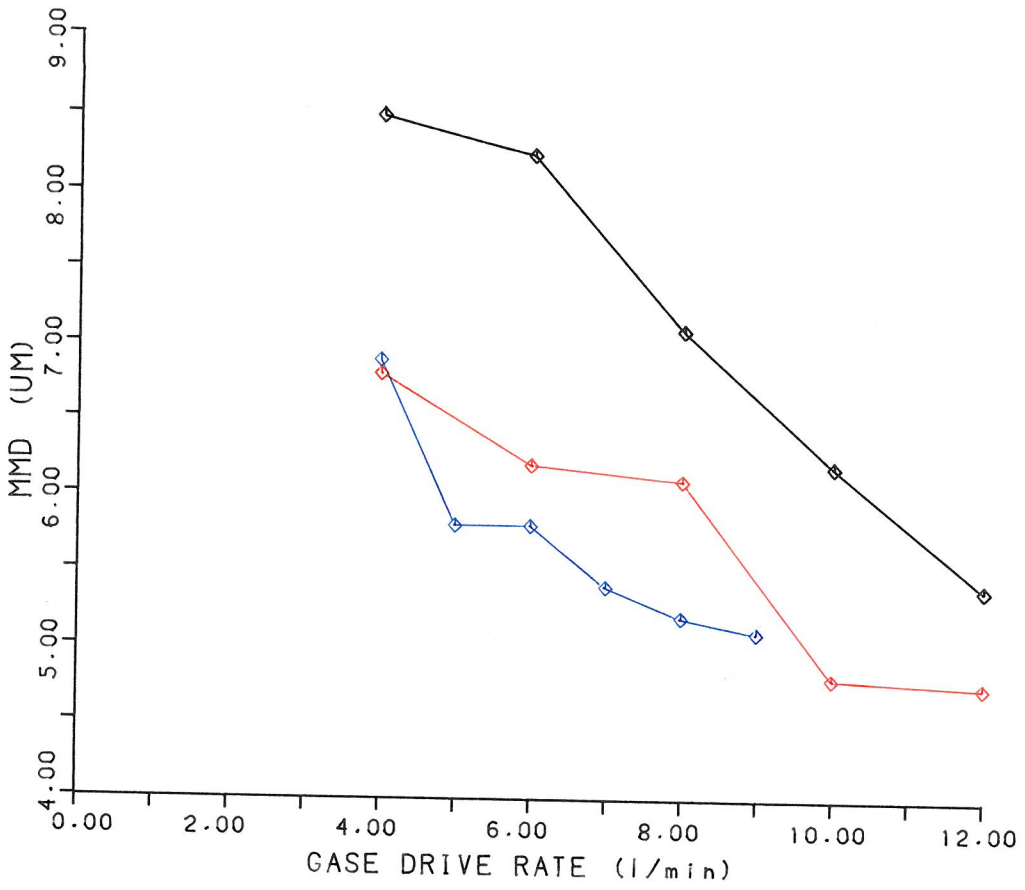

FIG (I.10a): EFFECT OF GASE DRIVE RATE UPON AEROSOL DROPLET SIZE OF JN'S WITH NO SUCTION INTO ATMOSPHERE.

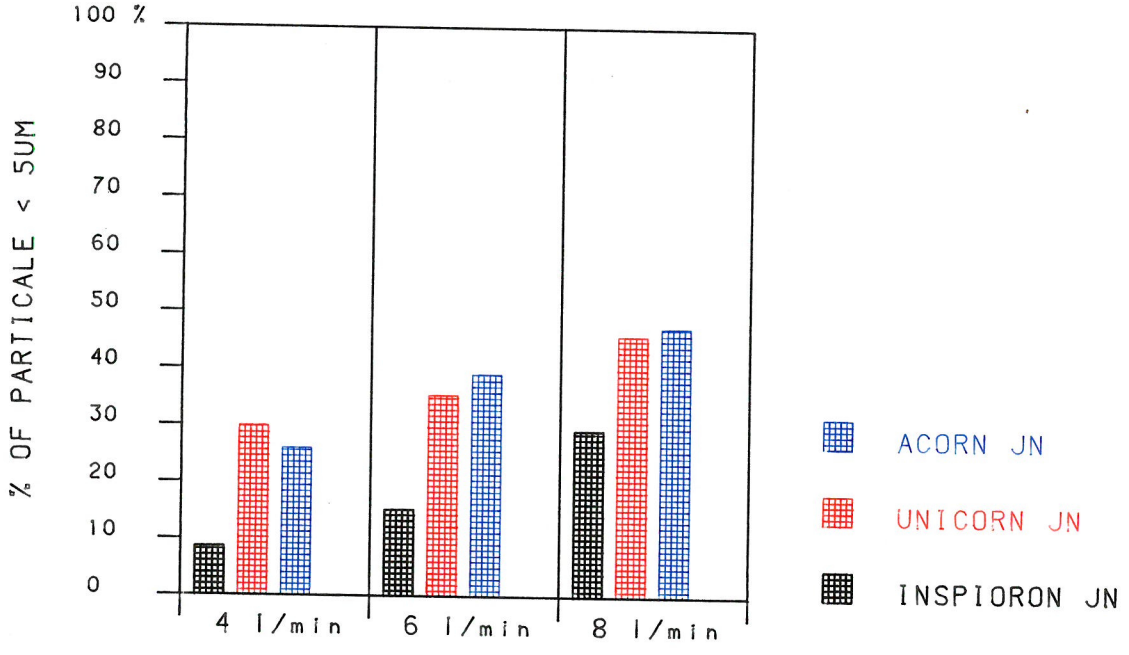

FIG. (I.10b): EFFECT OF DRIVE RATE UPON PERCENTAGE OF DROPLETS OF DIAMETER < 5 UM FOR JN'S.

The experimental results for JN's, however, showed that the MMD increased (Figure I.11a) which could possibly be attributed to bi-polar charging of the forming aerosol droplets and coalescence effects. The percentage of droplets of diameter $< 5\mu m$ decreased (only for Unicorn JN) with increasing distance from the laser beam to the nebuliser (Figure I.11b). This may have been due to the smaller droplets having insufficient inertia to travel the greater distance.

The MMD of aerosol droplets generated using the UN was found to be about $6.5\mu m$. The experimental results indicated that there was effectively no change in MMD or the percentage of respirable droplets (see Figures I.11a and I.11b).

3.1.3.E Effect of volume fill on droplet size

The MMD and the percentage of respirable droplets, produced using both the JN's and UN, were found to be largely independent of the volume of liquid within the nebuliser. Figures I.12a and I.12b show how they are affected by liquid level for the various nebulisers.

3.1.3.F Effect of temperature and humidity on droplet size

The MMD was found to increase with increasing humidity. This was because droplet rate decreased with increasing relative humidity. An increase in evaporation rate was responsible for the decrease in droplet size with increasing temperature.

The effects of R.H. and temperature on the MMD of aerosol droplets, for the Inspiron Mini-neb JN, are shown in Figures I.6a and 1.6b in Section 2.2.5

3.2 Electrical Charge Measurement

3.2.1 Introduction and aims

Many types of clinical nebuliser are presently in use. However, there is little information available regarding nebuliser output characteristics, especially in relation to the magnitude and nature of any electrostatic charge that might be present upon the aerosol droplets.

Whenever aerosols are generated, aerosol droplets are electrostatically charged. Whether an aerosol consists of droplets all having the same polarity of

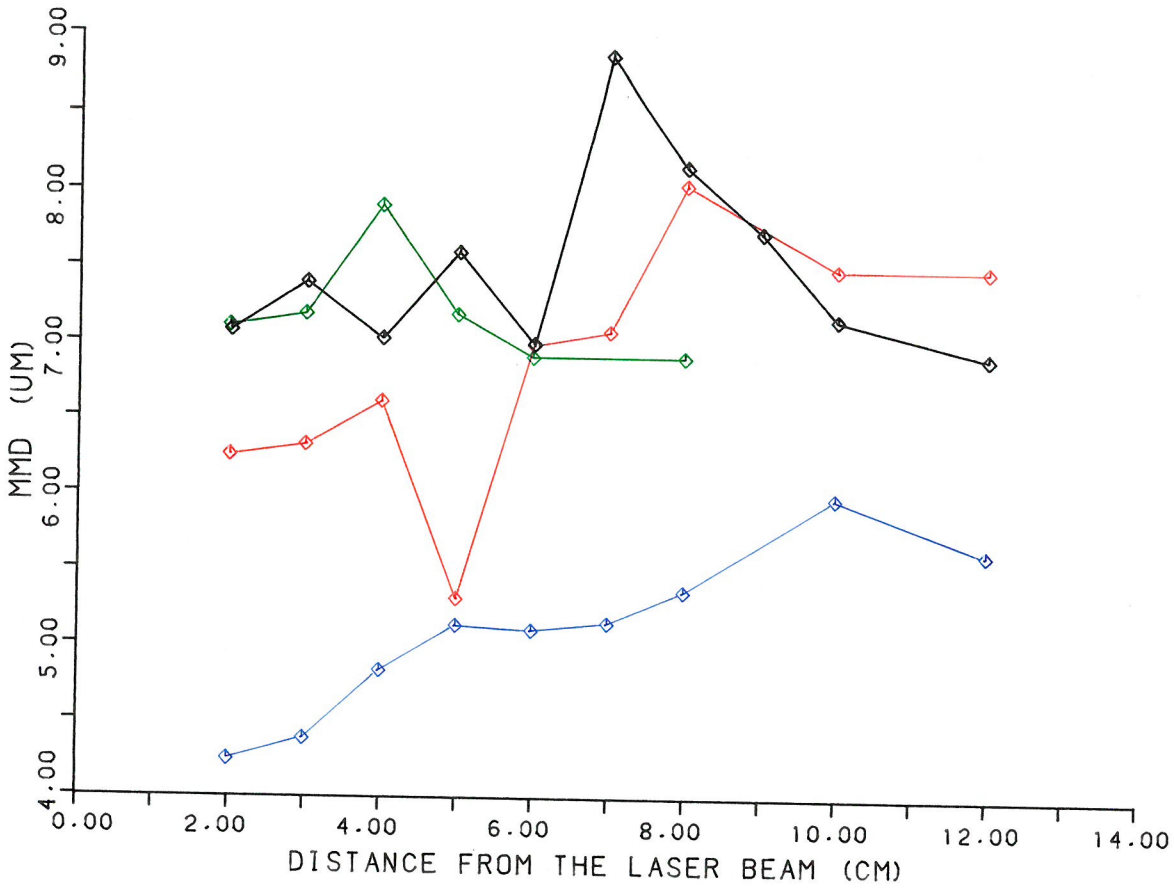

FIG (I.11a): EFFECT OF THE DISTANCE FROM THE LASER BEAM UPON THE DROPLET SIZE MEASURED FOR UN AND JN'S WITH NO SUCTION.

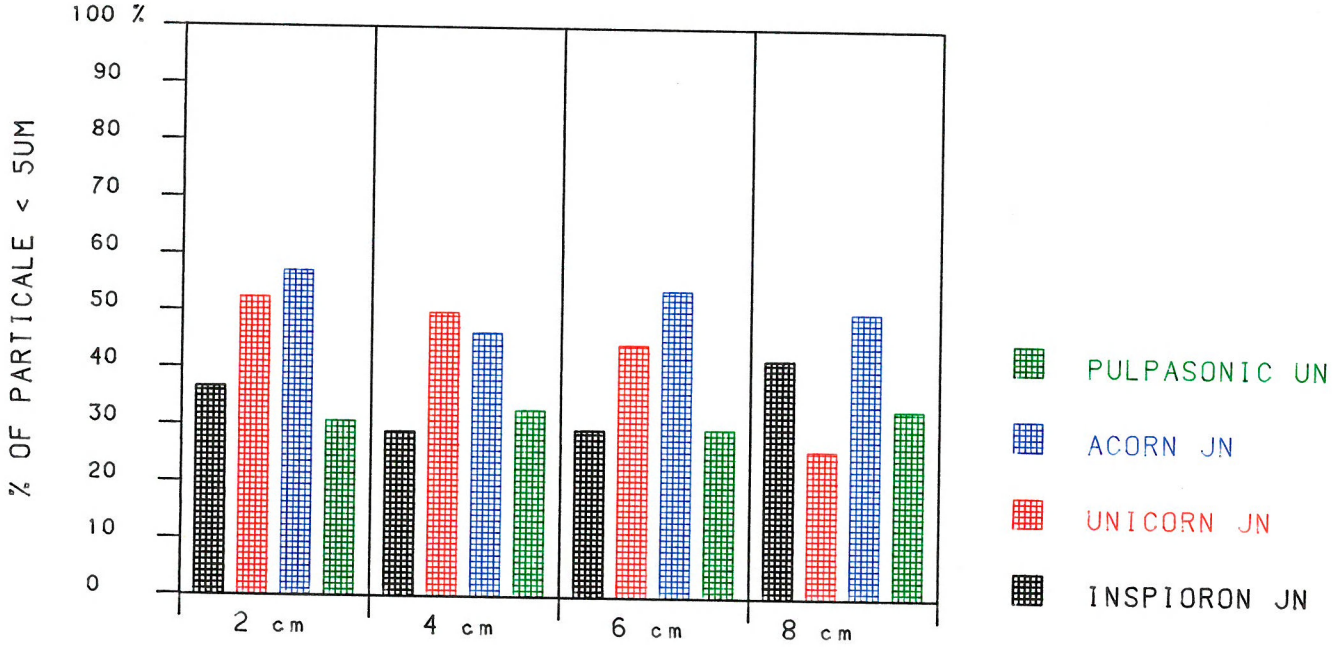

FIG. (I.11b): EFFECT OF THE DISTANCE FROM THE LASER BEAM PERCENTAGE OF DROPLETS OF DIAMETER < 5 UM FOR UN AND JN'S.

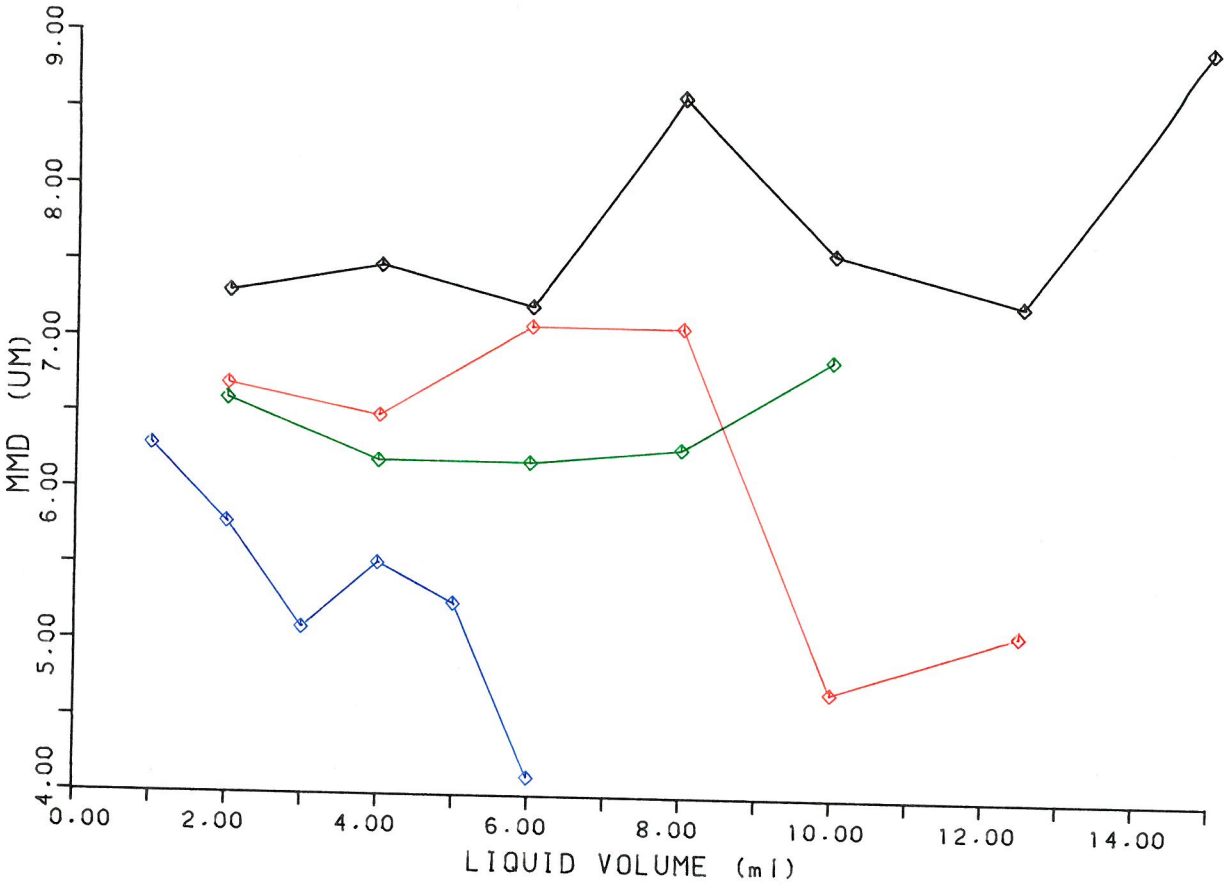

FIG (I.12a): EFFECT OF VOLUME FILL UPON AEROSOL DROPLET SIZE FOR UN AND JN'S (DRIVE RATE= 8 l/min) WITH NO SUCTION.

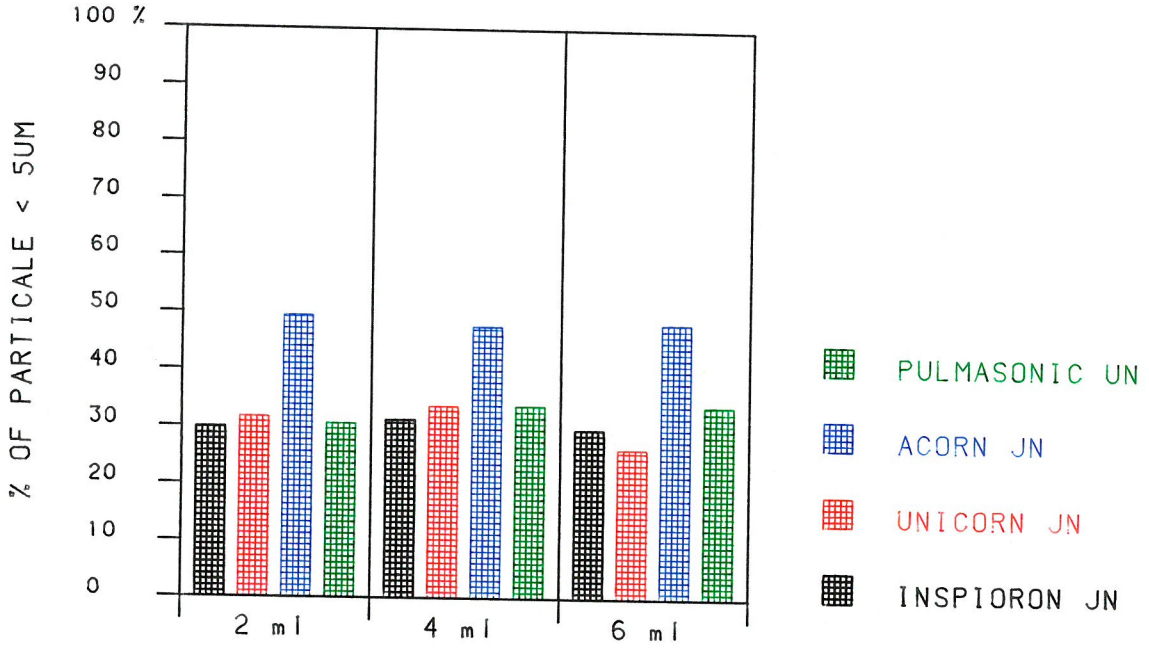

FIG. (I.12b): EFFECT OF THE VOLUME FILL UPON PERCENTAGE OF DROPLETS OF DIAMETER < 5 UM FOR UN AND JN'S.

charge or both polarities depends upon the aerosol generation device. Many aerosols are bi-polar in nature, i.e., both positively and negatively charged droplets are present. The droplet charging mechanisms that occur during atomization are not fully understood. Many aerosols are found to consist of approximately equal numbers of positively and negatively charged droplets having a Gaussian charge distribution. The level of charge on such aerosol droplets is unlikely to play a significant part in their deposition within the respiratory tract, since the corresponding image forces are negligible (see Part II).

It is necessary, therefore, to resort to charging the aerosol by some external means (eg. corona charging) to increase electrostatic particle deposition in the respiratory system.

In practice, many atomization processes produced charged spray with varying charge levels on the droplets. Often, the level of charge is found to increase considerably as the energy of the atomization process is increased. Very fine droplets are required for therapeutic aerosols and so fairly energetic atomisation processes are used for this purpose.

The aims of this study are to assess and compare the electrostatic characteristics of aerosols produced using JN's and UN. Most types of nebuliser can be modified to incorporate electrodes which allow the generated aerosol to be charged in a controlled manner (by application of a suitable electrical excitation voltage to the electrodes).

The effect of (1) electrode potential, and (2) air drive flow rate on droplet charge (q) and charge to mass ratio (q/m) were also studied.

3.2.2 Methods

3.2.2.A Nebuliser modification to alter droplet charge

The nebulisers were modified using a sharp pointed electrode which was placed in the mouthpiece and went into corona when a suitable voltage was applied. The electrode was fixed centrally at the end of a tube in line with the axis of the tube (see Figure I.13). Secondary air was driven through the tube to prevent the electrode from being wetted by the spray and to carry the ions towards the incoming droplets. This air also assisted the transport of charged droplets to the target. The corona discharge created an ionic current, part of which charged the droplets, the remainder of which was collected by the earthed

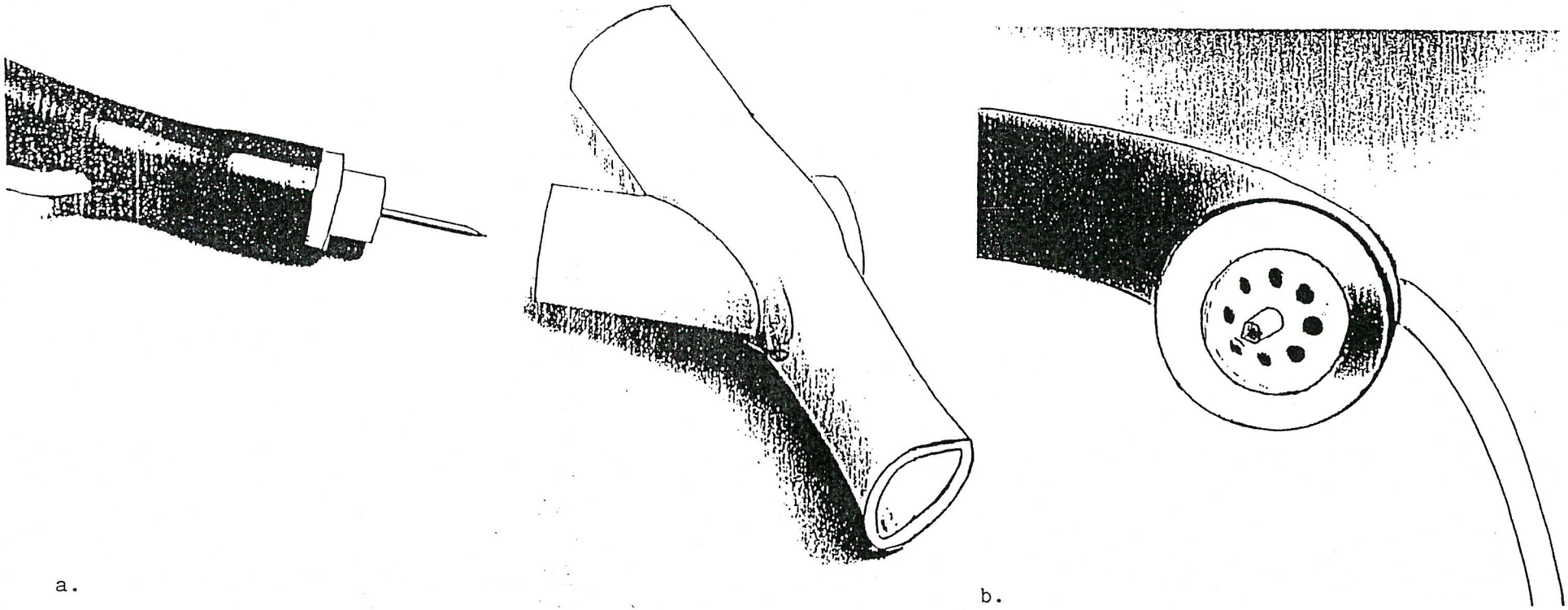

a.

b.

FIGURE I.13 "a" Corona point which inserts into the underside of a modified nebuliser mouthpiece. The power supply lead (white) may be seen passing into the airline (black)

"b" End-on view of the corona point showing 8 air vents for the passage of a 6l/min air current to keep the corona point dry.

walls of the mouthpiece.

3.2.2.B The droplet charge analyser (DCA)

The DCA consists of two opposed circular nickel plates, of diameter 7cm and thickness 1cm, situated parallel to one another, each fixed to an insulated base, see Figure I.14. To create an electric field between the plates, one was connected to a high-voltage supply (Brandenburg power supply, model 807R), and the other was earthed via an electrometer (Keithly, model 602). The electrometer output was connected to a chart recorder (J.J recorder, model CR522), to enable electrode current to be monitored as a function of time. Charged droplets within the aerosol spray were deflected by the high electrostatic field and caused to deposit on the electrodes. Positive droplets deposited on one electrode and negative ones on the other. The total amount of charge, corresponding to the deposition of charged droplets, could thus be calculated.

In order to determine the mass of liquid that was deposited on the electrodes, a sodium fluorescence tracer technique was used. Distilled water, which was used for most of the testing, was doped with 0.15% by volume sodium fluorescence. After a test, usually of measured duration, the two electrodes were separately washed with a known quantity of distilled water which was then transferred to a calibrated fluorometer (Terner, model 110). The fluorescence of the sample when irradiated with ultra-violet light was monitored, and quantified.

In this way the mass of spray deposited onto each electrode could be determined quite accurately. A knowledge of the recorded charge, which corresponded to deposited mass, enabled the average charge-to-mass ratio of the captured droplets to be determined.

It was important to determine the average amount of liquid nebulised per unit time. To do this, the quantity of liquid in the nebuliser reservoir was weighed before and after a test and the mass difference divided by the test duration.

3.2.2.C Theory

It is important to assess the effectiveness of the electrostatic field system in capturing charged aerosol droplets. Although the spray is polydisperse and there is clearly a considerable spread in the electrical mobilities of the charged particle population, it is convenient first of all to consider particles of a fixed size and

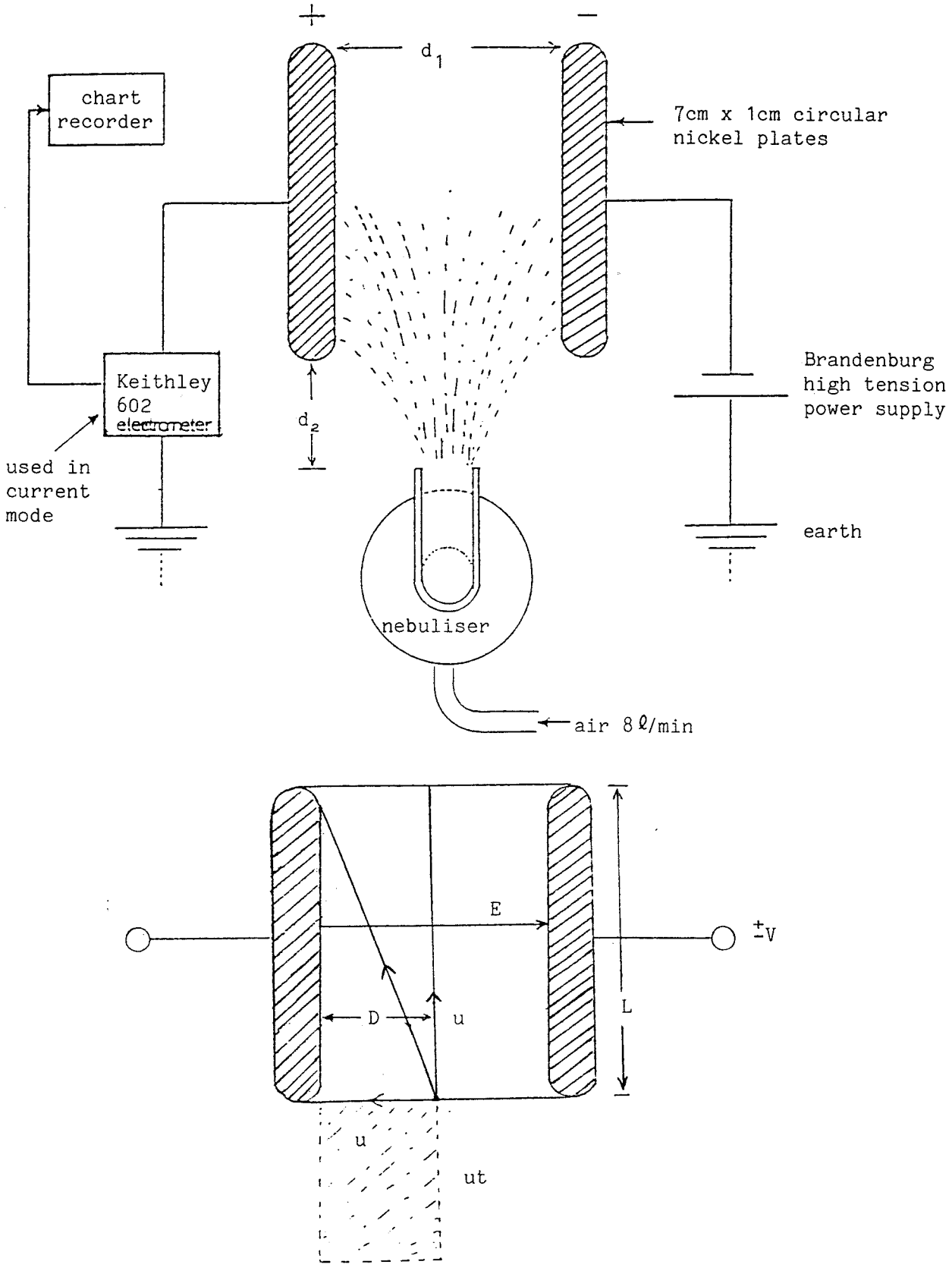

FIGURE I.14 Schematic diagram of droplet charge analyser (DCA)

charge. Consider the parallel plate system shown schematically in Figure I.14. The electrostatic field between the plates is assumed to be uniform. If the electric field between the plates is E, the drift velocity of charged droplets of diameter d_p and charge q is given by:

$$U = \frac{q\,E}{3\pi\eta d_p}$$

where η is the bulk viscosity of air.
For a plate separation d_1 the electric field $E = V/d_1$, where V is the potential difference between the two plates. A charged drop is considered to enter the plate system with velocity u as shown in Figure I.14. If the path length between the plates is L, the transit time of droplets is simply given by: $t = L/u$. During this time droplets are deflected towards one or other of the plates, depending on droplet charge polarity.

The droplet capture distance D is defined in Figure I.14. It can be seen that:

$$D = Ut = \frac{q\,E}{3\pi\eta d_p} \cdot \frac{L}{u} = \frac{EL}{3\pi\eta u}\left[\frac{q}{d_p}\right]$$

where η is the viscosity of air

In general, we have:

$$D_n = \frac{EL}{3\pi\eta u}\left[\frac{q}{d_p}\right]_n .$$

As the mechanism of droplet charging during atomisation is not fully understood, it is necessary to propose some mathematical relationship which describes the manner in which electrical charge is distributed over droplets in the size range produced. A model proposed for some atomisers is that droplet charge is directly proportional to the surface area of the droplet, i.e. $q = Ad^2$.

3.2.3 Results and discussion

3.2.3.A Charge on droplets produced by JN and UN

The aerosols generated using both JN's and the UN were invariably charged. It was found that the level of electrostatic charge on droplets generated

by the UN was significantly less than that produced by the jet unit. The results confirmed the presence of charge of both polarities in each case, but more negative charge was produced with the Inspiron JN than with the Pulmasonic UN, see Figures I.15 and I.16.

No reprodi cable current could be measured for aerosols generated using the UN. The only currents measured were of random nature, fluctuating between net negative and net positive polarity.

3.2.3.B Charges on the droplets produced by the modified nebulisers (*Effect of corona electrode potential on droplet charge for JN and UN*)

Unipolar gaseous ions, created in the corona discharge, were driven by the electric field and auxiliary air flow so as to impinge upon droplets in free flight within the nebuliser mouthpiece. The charged droplets produced using the modified nebulisers were detected by the DCA. Typical chart recorder current traces are shown in Figures I.17a and I.17b. It can be seen from these figures that the droplet current increased as the air flow rate increased and with the application of voltage to the corona electrode. When the potential applied to the corona electrode was increased, the level of charge on the aerosol droplets was found to increase, as expected. This effect is shown in Figures I.18 and I.19 for both types of nebulisers. Figure I.20 compares the effects of positive and negative corona in charging droplets generated by the UN. The higher values which the current obtained with positive corona might be explained by assuming more ionization in the case of positive than negative corona.

Aerosols generated by the UN acquired more corona charge (relative to those produced without corona charging) than those produced by the JN, as shown in Figures I.19 and I.21; with the UN the charge level increased by two orders of magnitude whereas with the JN only one order of magnitude was observed. The lower acquisition of corona charge by aerosol droplets in the case of the JN may be due to a higher level of bi-polar charging.

3.2.3.C Effect of a flow rate on droplet charge and q/m ratio

While applying - ve corona, droplet charge was observed to increase with increasing gas drive flow rate for the JN, see Figure I.22. This may be due to a decrease in MMD of the droplets, making them more mobile.

Figures I.23 and I.24, illustrate the effect of gas flow rate on the

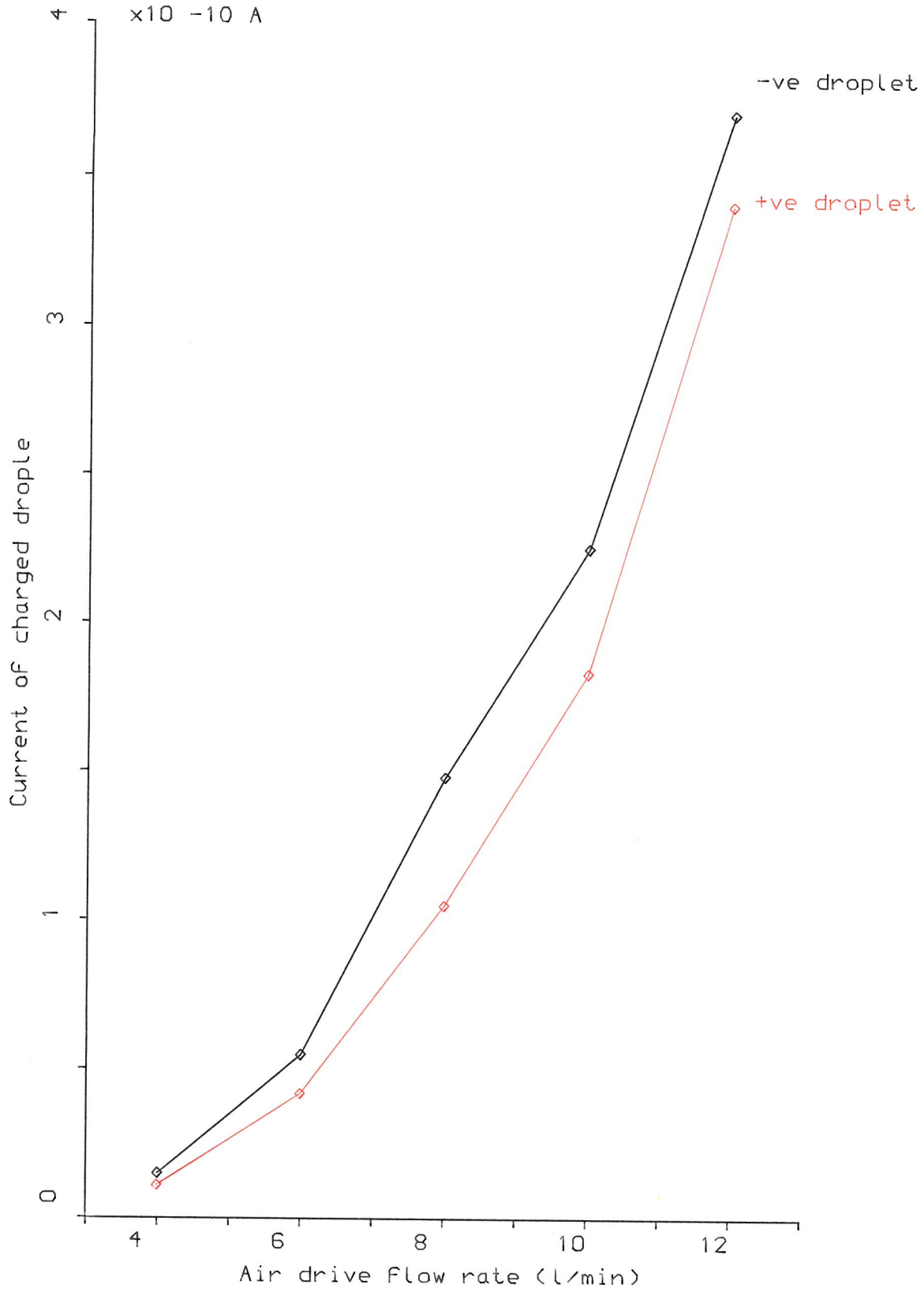

FIG.(I.15): Effect of air drive flow rate on droplet charge produced by Inspiron Mini-Neb JN.
(liquid level=10ml, Temp.=18C, RH=47%, DCA:V=10kV, d1=5cm, d2=3.5cm)

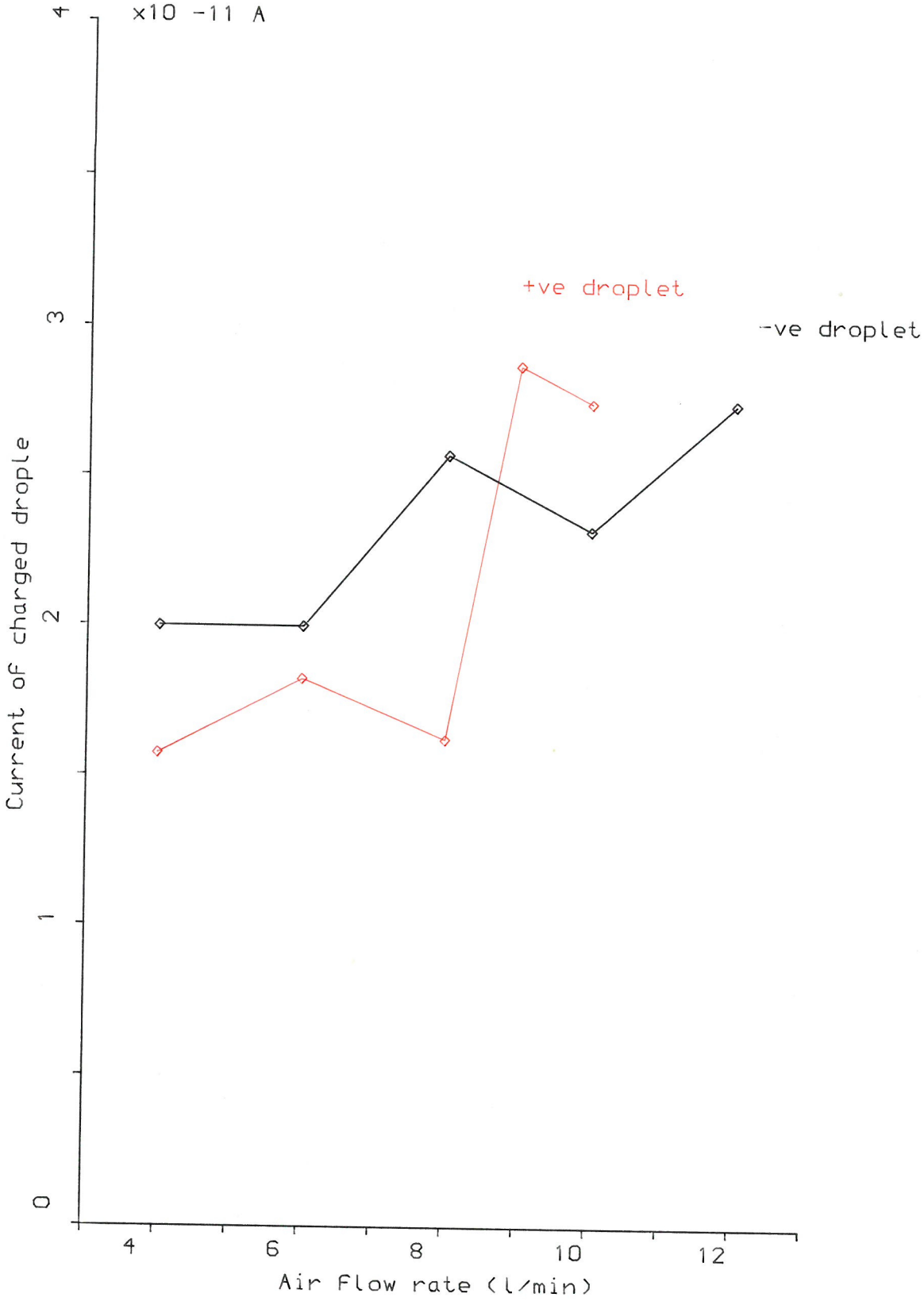

FIG.(I.16): Effect of air (used to blow up the droplets) on aerosol droplet charge produced by Pulmasonic UN.
(liquid level=10ml, Temp.=21C, RH=35%, DCA: V=10kV, d1=5cm, d2=7cm)

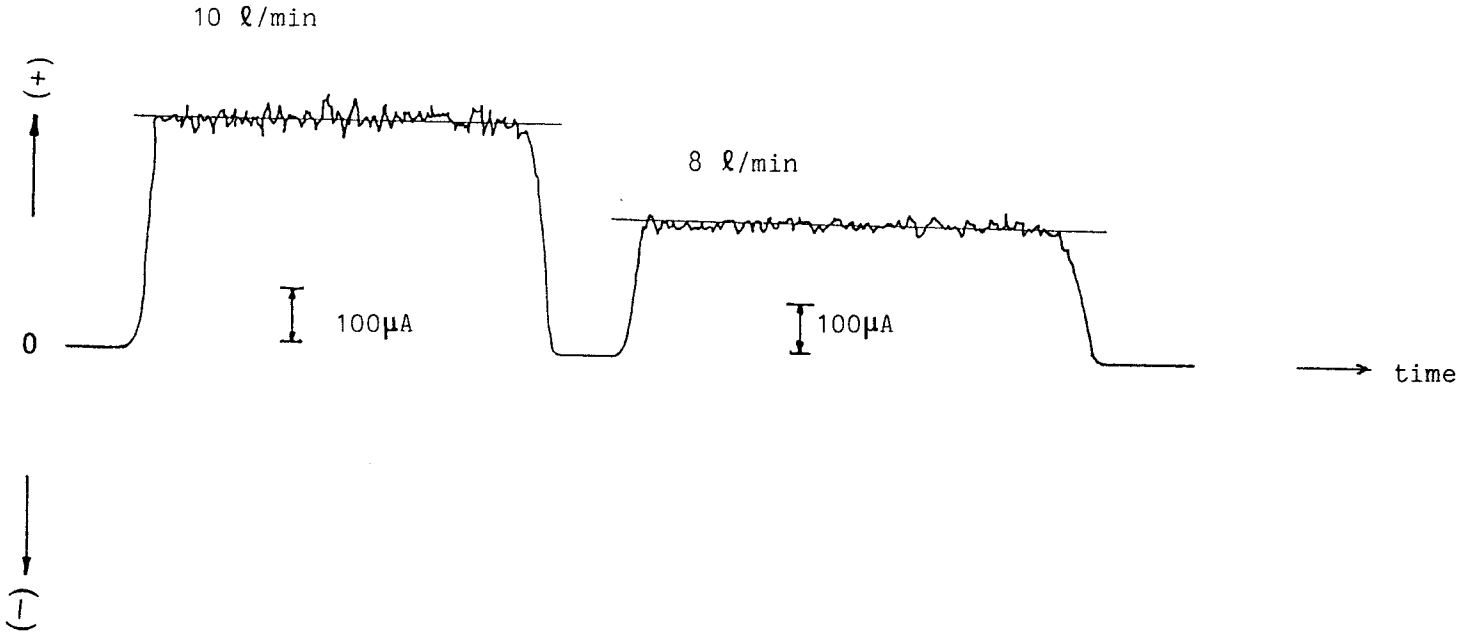

FIGURE I.17A Traces of electrical current from Inspiron Mini-Neb JN at flow rates 8 and 10 ℓ/min

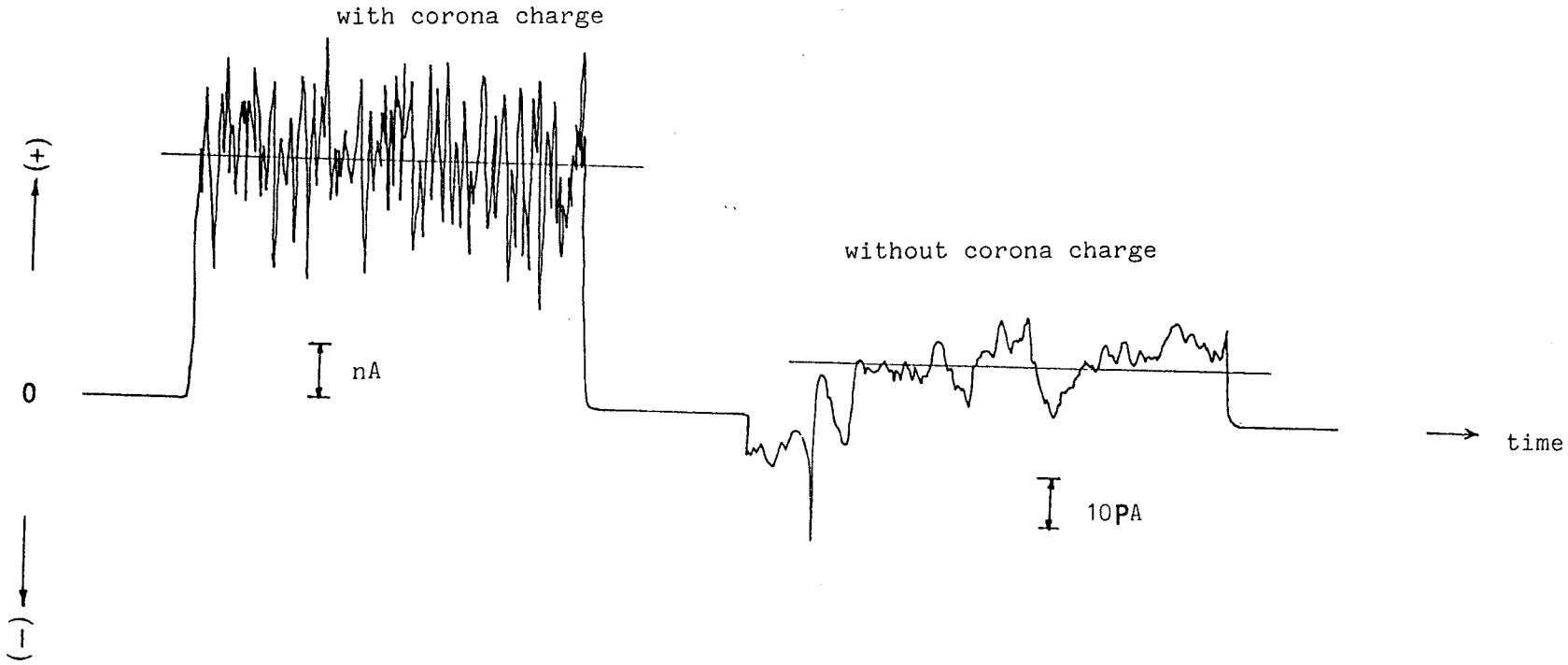

FIGURE I.17B Traces of electrical current from Pulmasonic UN with the without corona charge (+5kV)

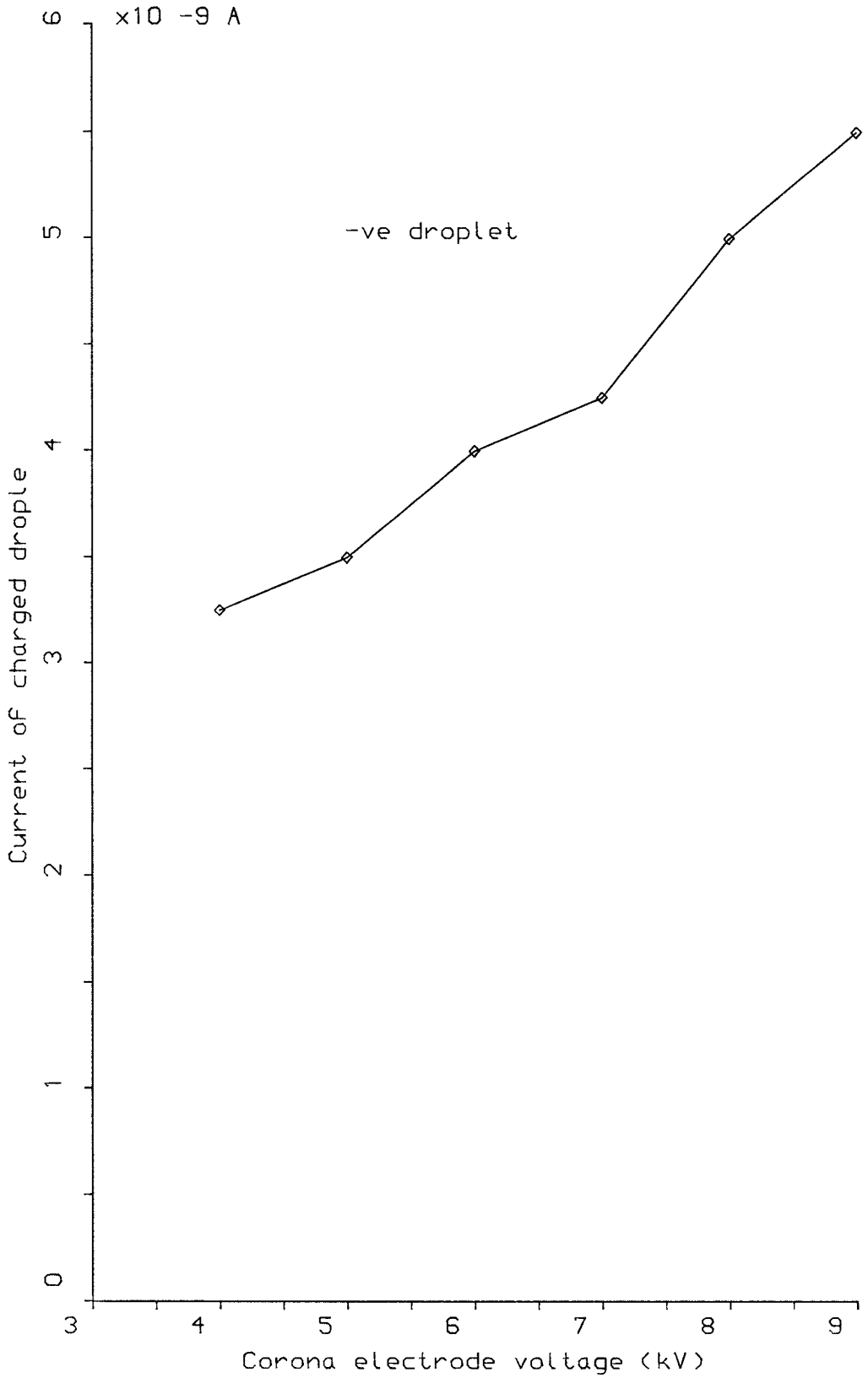

FIG.(I.18): Effect of corona electrode potential on aerosol droplet charge produced by Inspiron Mini-Ne
(liquid level=10ml, Temp.=21C, RH=26%, DCA:V=10kV, d1=5cm, d2=3.5cm)

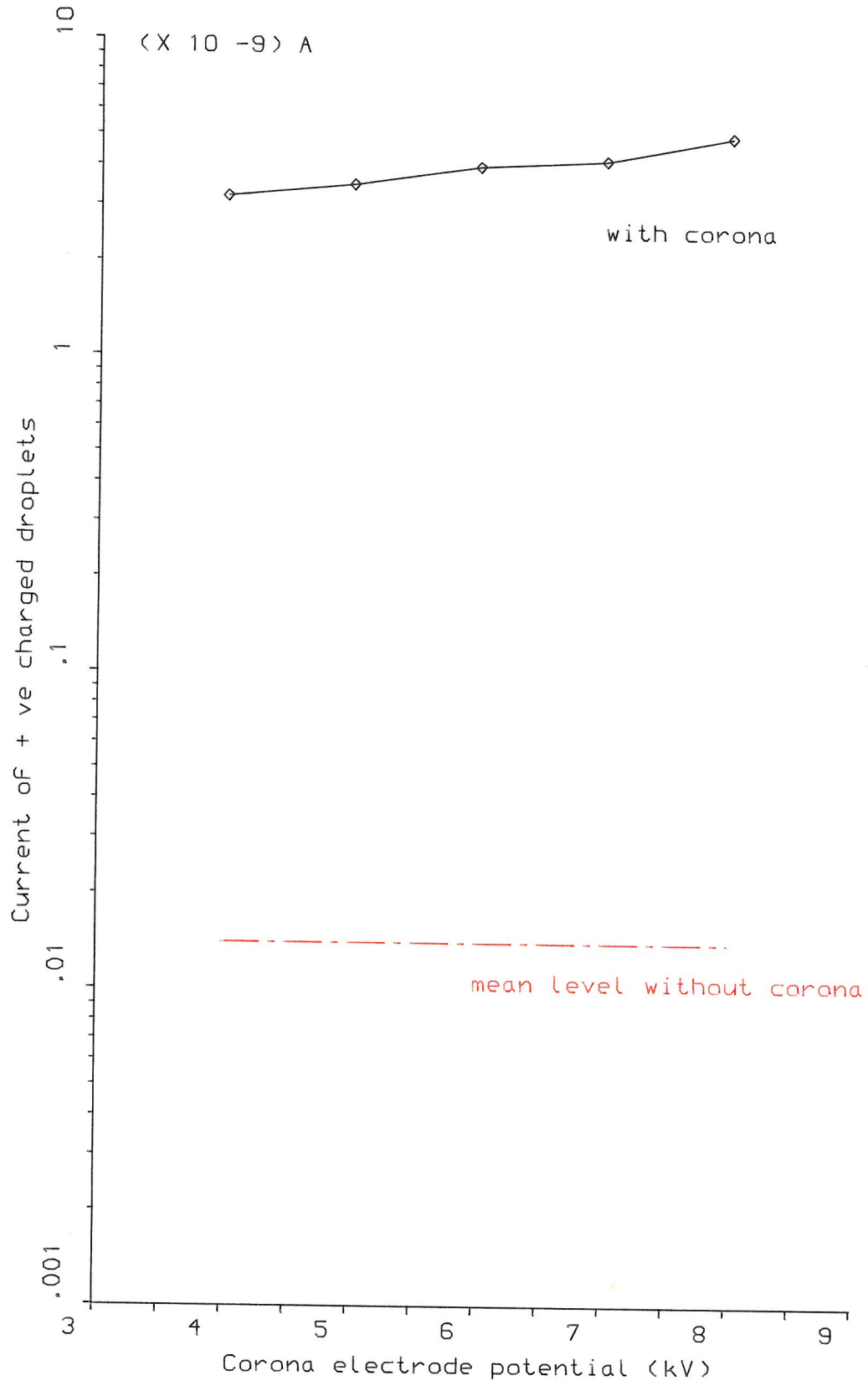

FIG.(I.19): Effect of corona electrode potential on aerosol droplet charge produced by the modified UN (liquid level=10cc ,temp.=17C RH=40%, air flow rate=8 l/min, DCA: V=10kV ,d1=5cm ,d2=3.5cm)

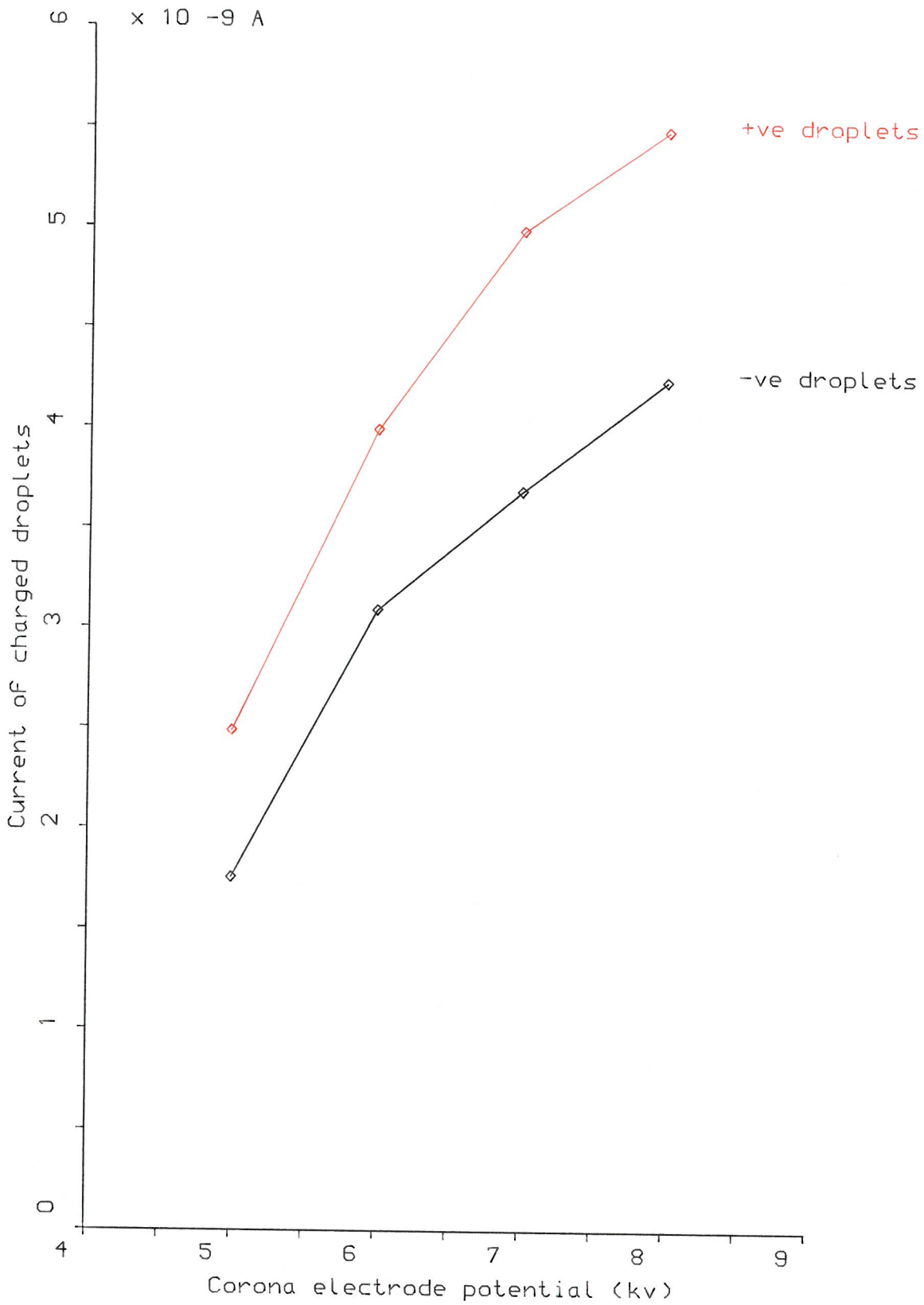

FIG.(I.20): Effect of corona electrode potential and polarity on aerosol particle charge produced by the modified Pulmasonic UN. (liquid level=10cc, temp.=21c, RH=38%, DCA: V=10kv, d1=5cm, d2=7cm)

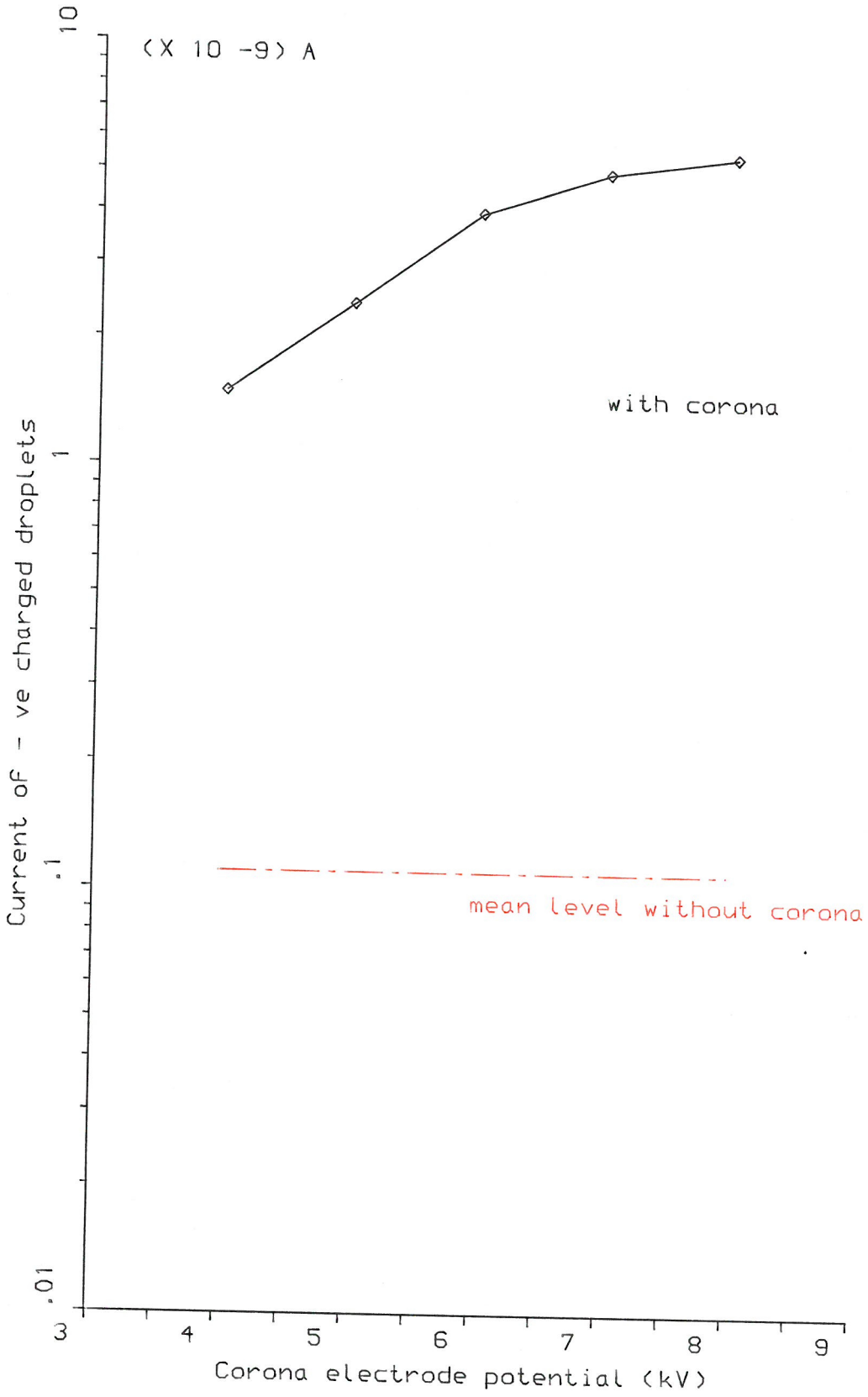

FIG.(I.21): Effect of corona electrode potential on aerosol droplet charge produced by JN (liquid level=10cc ,temp.=21c ,RH=26% , air drive flow rate=8 l/min, DCA: V=10kV ,d1=5cm ,d2=3.5cm)

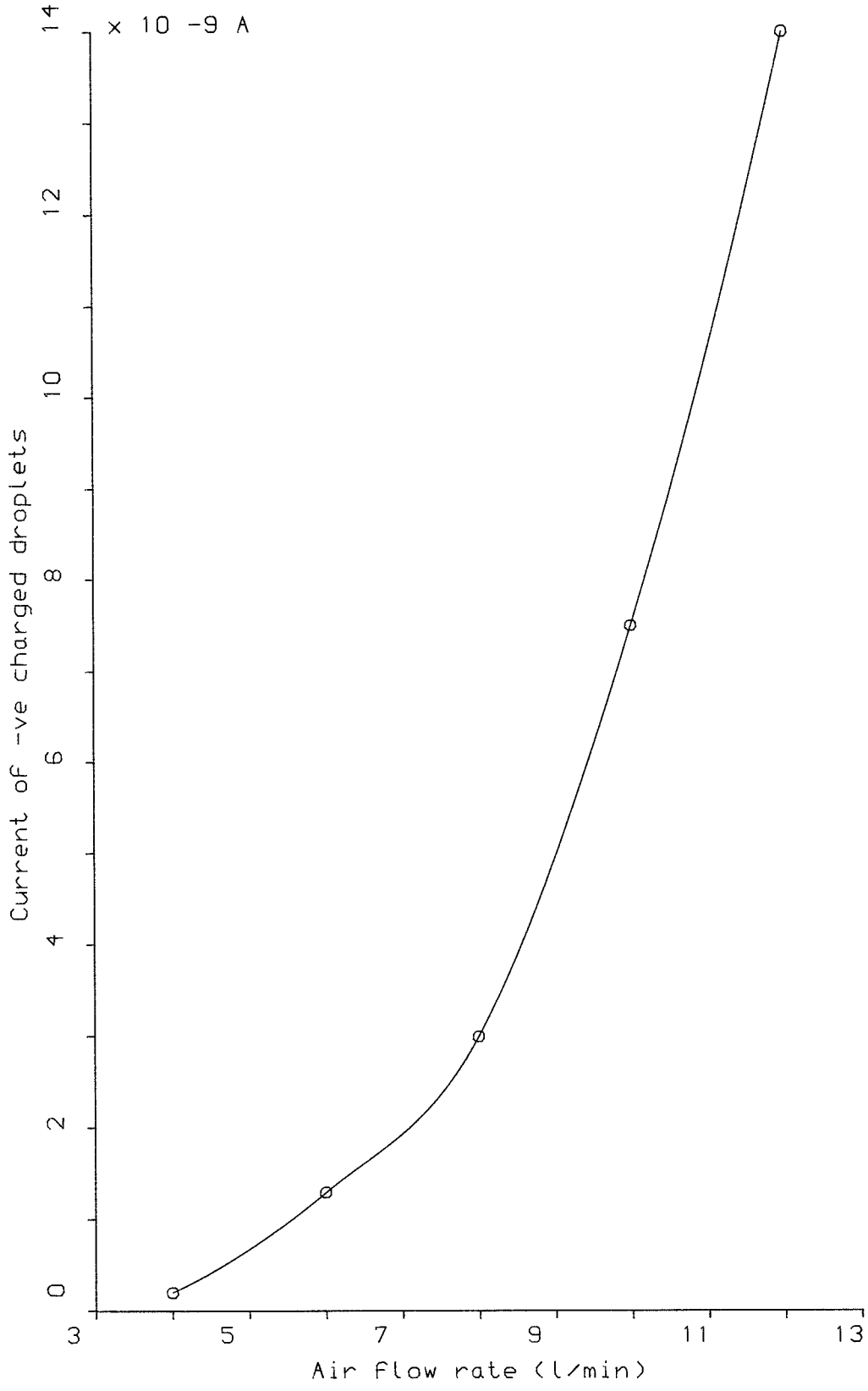

FIG.(I.22): Effect of air drive flow rate on aerosol droplet charge produced by modified JN with corona charging(V=-10kv,sec.air=4l/min) (liquid level=10cc,temp.=25c,RH=26%,DCA: V=10kv,d1=5cm,d2=3.5cm)

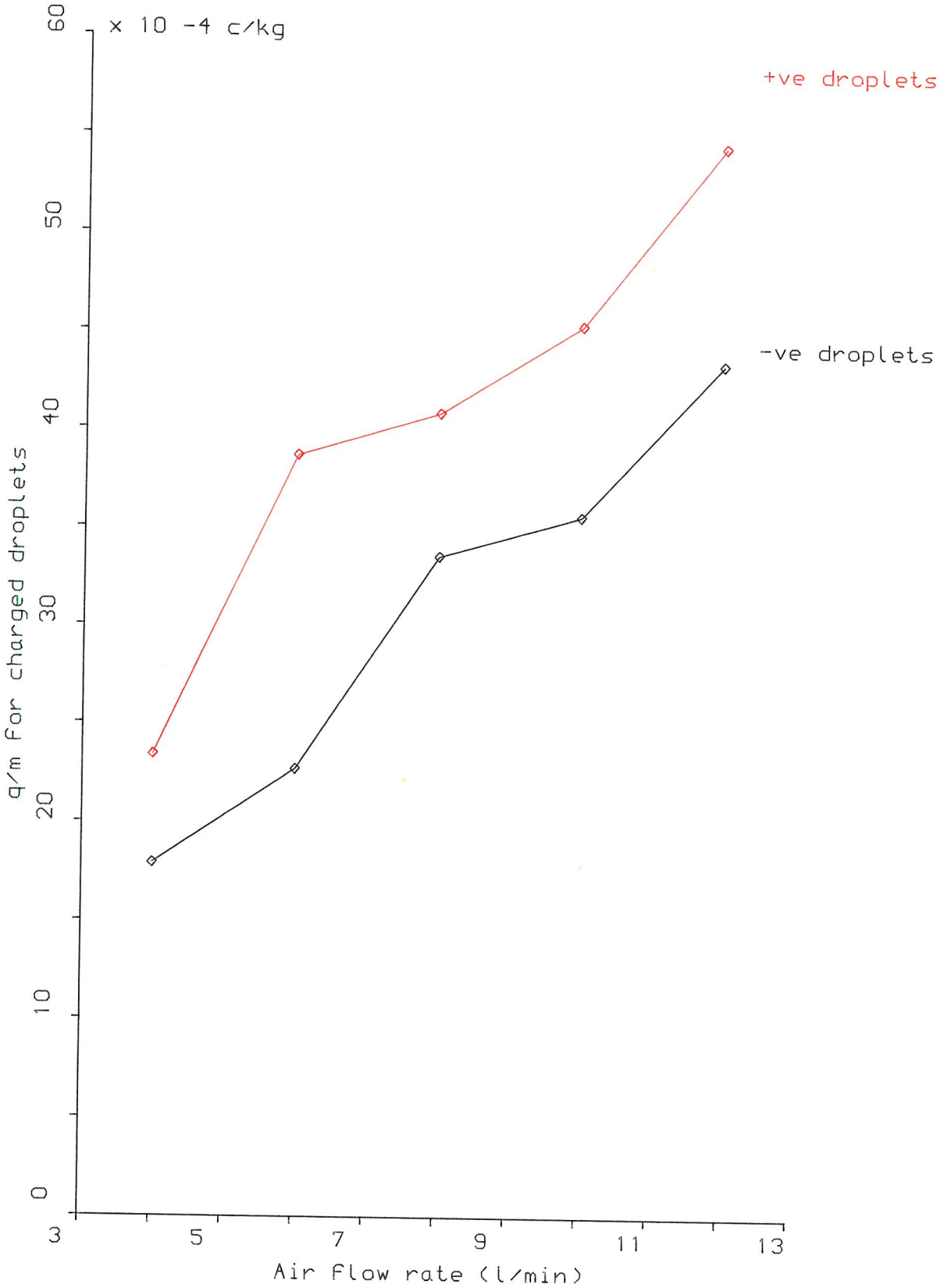

FIG.(I.23): Effect of air drive rate on charge-to-ass ratio of aerosol droplets produced by JN.
(liquid level=12cc, temp.=21C, RH=60%, DCA: V=10kv, d1=5cm, d2=3cm)
0.15% Sodium Fluorescence in distilled water, (60 sec.)

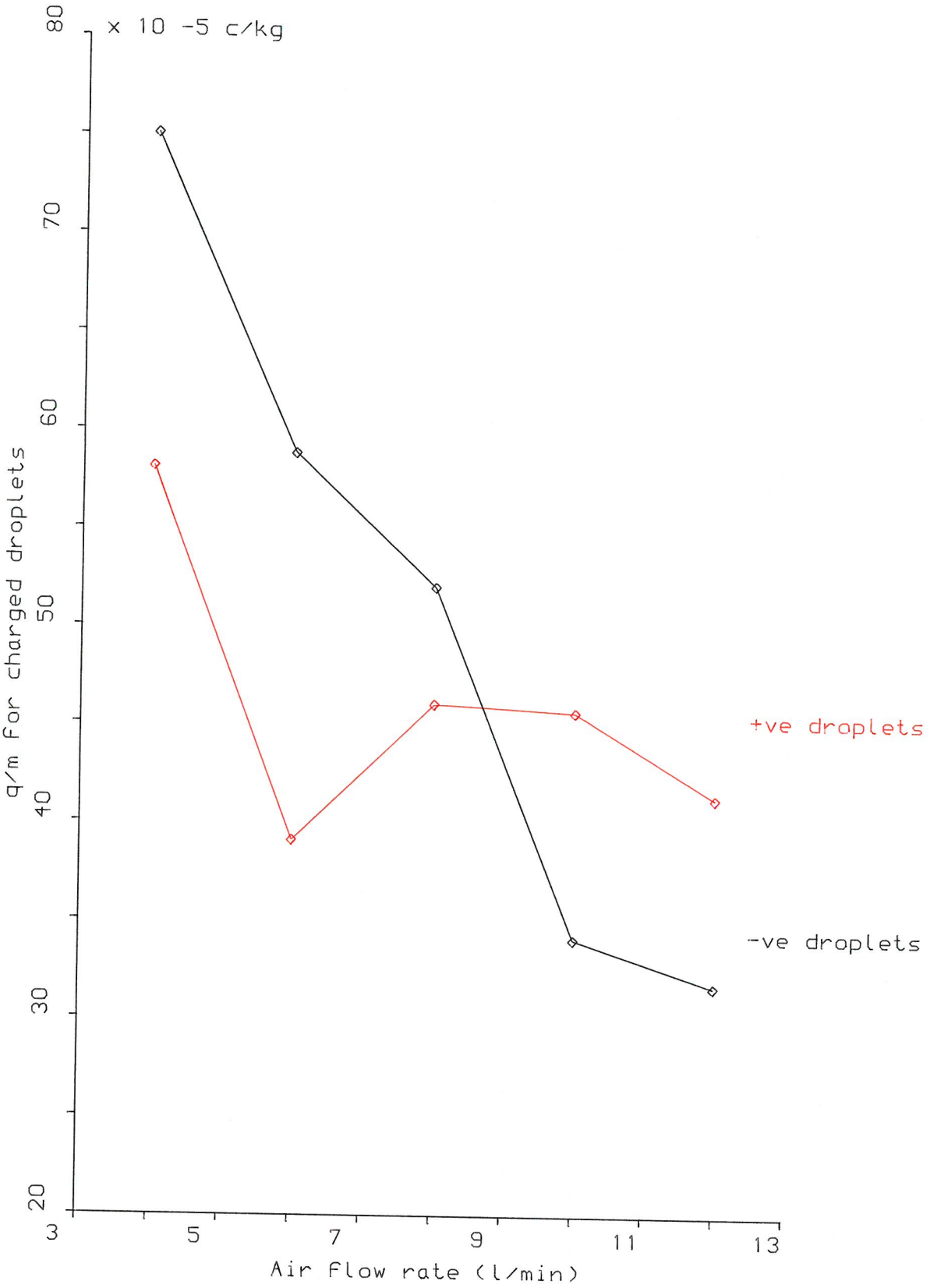

FIG.(I.24): Effect of air flow rate (to blow up the droplets) on charge-to-mass ratio aerosol droplets produced by UN.
(liquid level=10cc, temp.=22c, RH=53%, DCA: V=10 kv, d1=5 cm, d2=3 cm)
0.15% Sodium Fluorescence in distilled water, (60 sec.)

charge-to-mass ratio (q/m) of positively and negatively charged aerosol droplets, produced by JN and UN. The (q/m) was determined by dividing the mean droplet current by the mean mass flow rate of liquid. For the JN, (q/m) increased with gas flow rate, probably due to an increase in aerosol droplet charge resulting from the increased energy of liquid shearing. For the UN, (q/m) varied, as expected, because of the random nature of aerosol droplet charging.

Notes: During a spray test, the mass of aerosol deposited on each electrode was measured, as was the total mass of liquid lost from the nebuliser reservoir. The difference between these two masses was the amount of neutral and low mobility droplets not deposited on the electrodes. If the size distribution of the deposited and undeposited droplets are assumed to be identical, the number of droplets deposited on the electrode, in each size band, can be calculated. The charge distribution for each size band, is possibly Gaussian which would account for some of the undeposited neutral droplets. One unknown is the standard deviation of the charge distribution.

3.3 Improved Instrumentation

When a liquid surface is disrupted by nebulisation, electric charge is separated which may be in the form of charged droplets or free ions. Little work has been reported on the electrostatic characteristics of aerosols generated by clinical nebulisers. The possibility that nebulised aerosol droplets are charged has been considered, though this is not the case for *free ions*, to the author's knowledge.

The objective of improving the instrumentation was to examine the charge generated by nebulisation of a liquid, with particular emphasis on determining the polarity of charge associated with ions and droplets of different size. It was also necessary to improve the design of the optical chamber in order to study the effect of inhalation on droplet size distribution, for both types of nebuliser.

Essentially, the improved instrumentation comprised a Malvern particle and droplet size analyser, and a purpose-built charge analyser. A conventional cylindrical tube/coaxial rod ion mobility analyser was used in the charge analyser, in order to measure ion concentration. Experimental difficulties detailed below limited the range of this instrument to mobilities $\geq 0.004 cm^2 V^{-1} s^{-1}$. With the old instrumentation, the suction flow rate was limited to 10ℓ/min for laminar flow

whereas for the new instrumentation the suction flow rate could be increased up to 50ℓ/min. (Under turbulent flow conditions there was a tendency for aerosol droplets to deposit on the glass windows of the optical chamber which made it impossible to obtain size distribution information). Another disadvantage of the old instrumentation was that parallel plate electrodes were used and consequently some aerosol remained undeposited. This was not a problem with the new instrumentation because a radial electrode arrangement was used through which all the aerosol passed. Measurements of ion concentration for mobilities $<0.004 cm^2 V^{-1} s^{-1}$ were required in order to determine whether ionic charge was conserved, as opposed to total ionic and droplet charge being conserved. As the range of the ion mobility analyser could not be extended, it was decided to draw a sample of air (comparable to that passing through the ion mobility analyser) through a wire mesh and to measure its rate of charging. This part of the apparatus was termed the *total-air charge monitor*.

A comparison between the integrated average of the total-air charge monitor currents and the sum of positive and negative ionic currents (measured during independent experiments), using the ion mobility analyser, allowed the overall charge on droplets and ions of mobility $<0.004 cm^2 V^{-1} s^{-1}$ (corresponding to droplets of diameter $<50 \mu m$) to be established.

3.3.1 Experimental

In order to test the nebuliser, it was set up using the experimental arrangement shown in Figure I.25 and Plate 1a. The main test chamber consisted of a cylindrical glass reservoir arranged vertically. The nebuliser and air feed tubes could be mounted in the upper spray chamber or externally to spray into this region. The aerosol output from the nebuliser was arranged so as to be in line with a pair of optical windows, one on either side of the test chamber. The He/Ne laser beam of the Malvern particle size analyser could pass through these windows, enabling droplet size distribution to be measured.

Suction, simulating inhalation, was applied to the main chamber via two side arms. These were connected via pipework to a suction pump. The suction rate could be controlled using a valve in the pipe network.

One of the side arms contained the Ion Mobility Analyser. By appropriately biasing the voltage of the central electrode, with respect to the outer earthed cylindrical tube, any ions flowing along the analyser could be deflected towards (by means of the resultant radial electric field) and intercepted by the

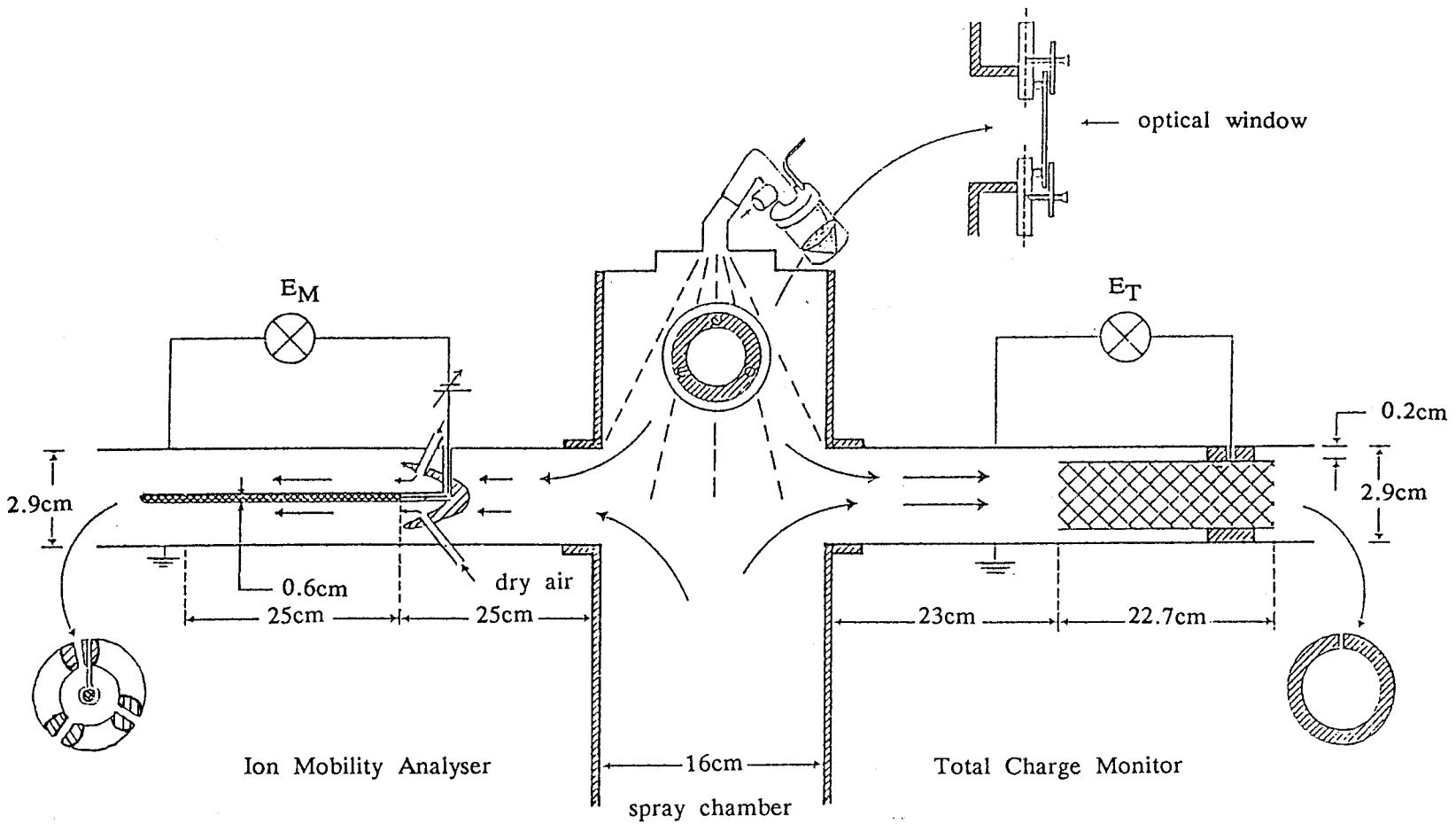

FIGURE 1.25 SCHEMATIC DIAGRAM FOR THE EXPERIMENTAL SET UP

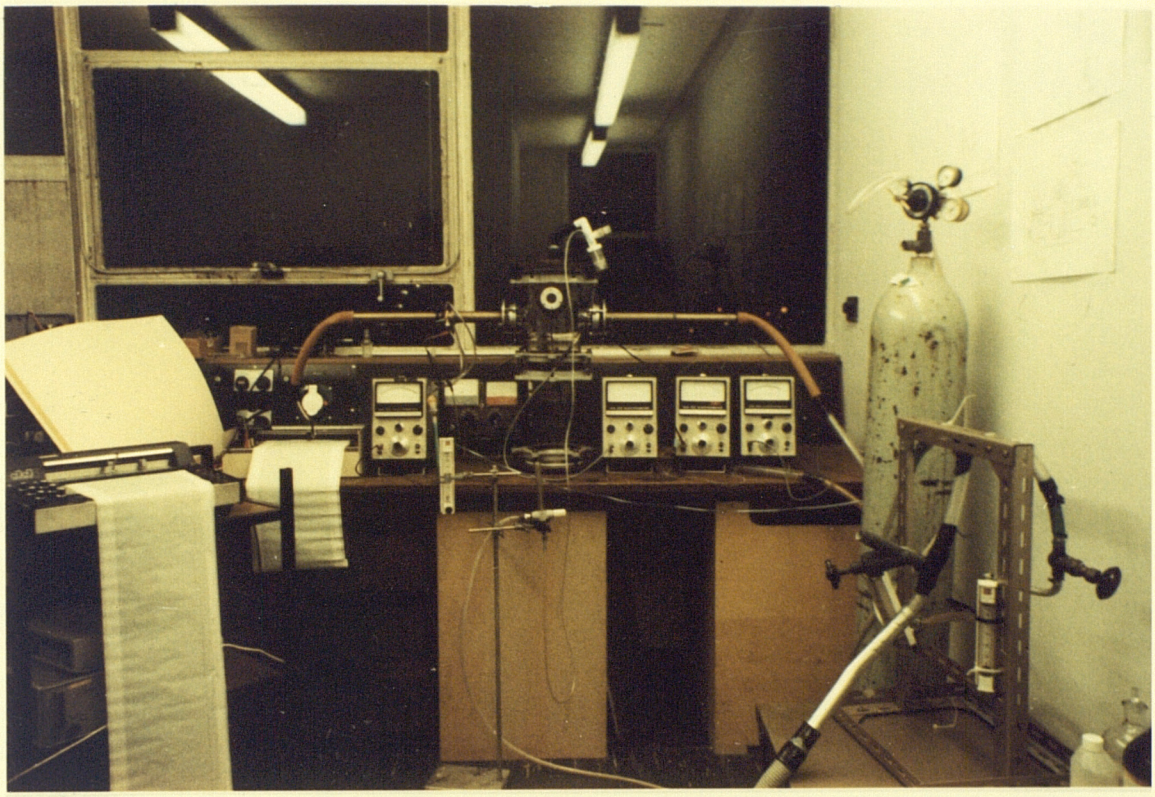

Plate 1a: Experimental set up

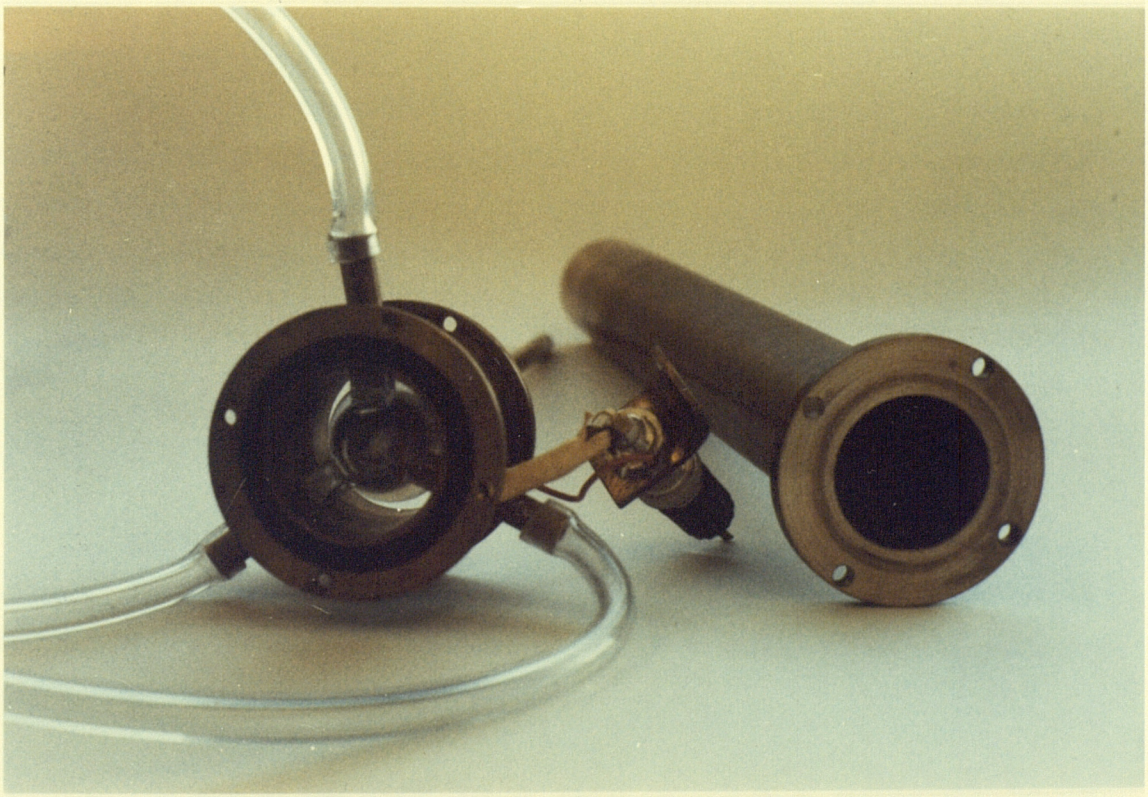

Plate 1b: Ion mobility analyser showing dry air inlets

central electrode. A dry air sheath was applied adjacent to the central electrode, to keep the aerosol stream away from the central electrode (see Plate 1b). The current flowing to the central electrode was a measure of the charge carried by intercepted ions.

For the particular mobility analyser used in these experiments, b = 2.9cm, a = 0.6cm and L = 25cm. If mobility μ is expressed in units of $cm^2V^{-1}s^{-1}$, it follows that (see equation 9, Section 2.4):

$$\mu = 0.167 \frac{Q}{V}$$

where Q is in ℓ/min and V is in volts. For typical operating conditions, ie. an air flow rate of 15ℓ/min through the analyser and an applied voltage of 100V, ions with mobilities down to $0.0251 cm^2V^{-1}s^{-1}$ were collected.

The other suction arm contained a conducting mesh which was used to collect charged droplets and ions, ie. this arrangement constituted a *total air-charge monitor*. The pre tube connecting it to the main measurement reservoir was 23cm long and 3.4cm in diameter. Using the Natansin equation (10), with an air flow of 15ℓ/min, it can be shown (see Figure I.26) that only droplets of diameter $>50\mu m$ are deposited in the pre tube, and therefore that the total charge will be monitored for all droplets and ions of size $\leq 50\mu m$.

For each measurement, the net charge of aerosol droplets was determined by subtracting the ionic current from the total-charge monitor current. In order to estimate the charge on the large droplets, a circular metal tray was mounted a few centimeters up from the bottom of the spray chamber. It was shielded, insulated and connected to ground via an electrometer.

3.3.2 Measurements made using the improved instrumentation

3.3.2.1 Droplet size, results and discussion

Making use of the experimental set-up shown in Figure I.25, with the nebuliser mounted inside the spray chamber, the size distributions of aerosols generated by the JN and UN, operating at controlled suction rates, were measured using a laser particle size analyser.

The aim of this study was to assess the effect of suction rate on the size of aerosol droplets.

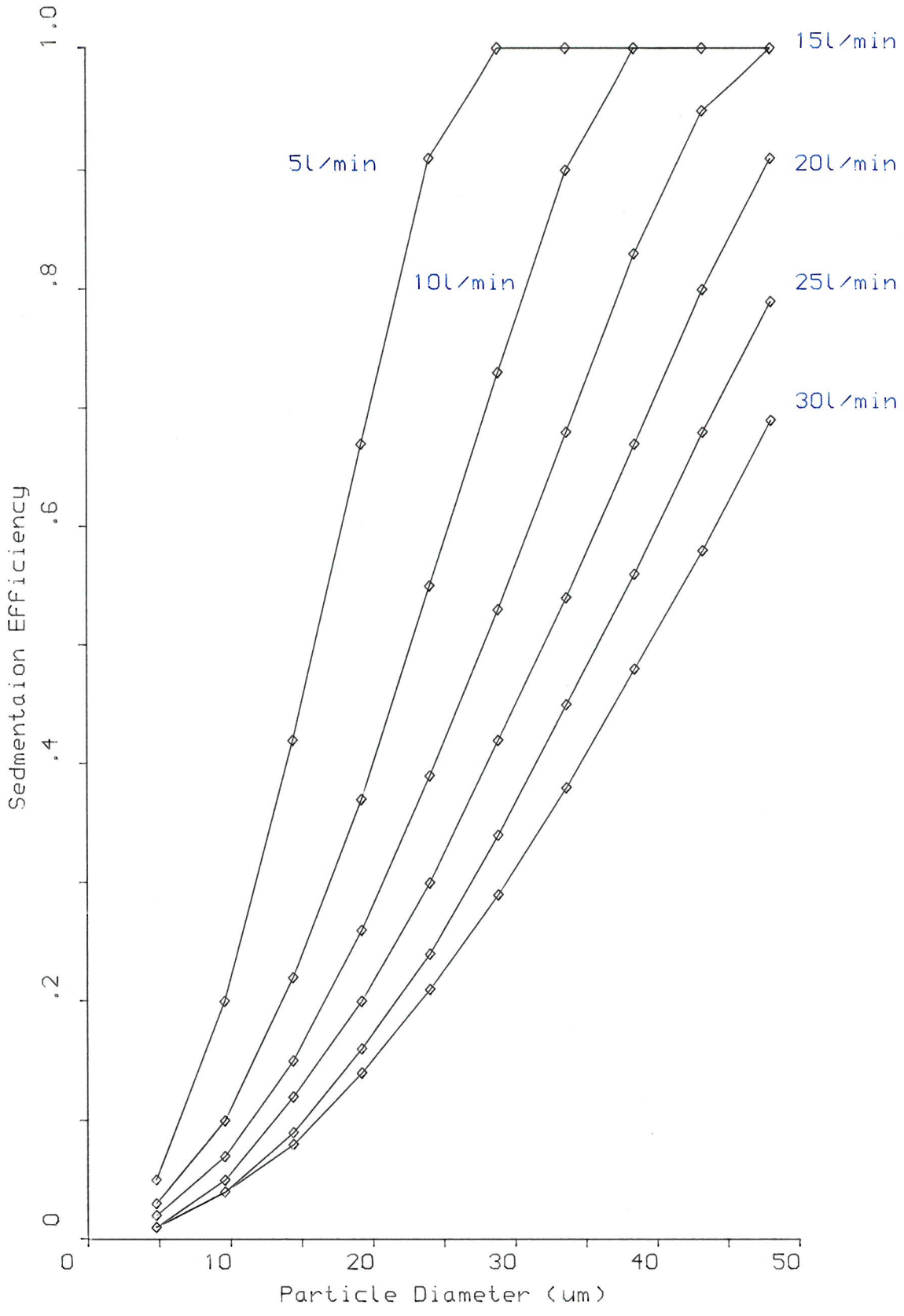

FIG.(I.26): Sedimentation calculation for the pre tube(*) of the Total Charge Monitor,TCM, (tube diameter= 3.4cm , length= 23cm)
(*)Pre-tube is the sedimental tube before the TCM arrangment.

3.3.2.1A The effect of suction rate on aerosol droplet size distribution

Two JN's, the Inspiron Mini-neb and Unicorn, both driven at flow rates of 8ℓ/min, and the Pulmasonic UN were studied. Figures I.27a and I.27b show the results for the effect of suction rate on aerosol droplet MMD and the percentage of respirable droplets produced by these nebulisers.

The size distribution, at high suction rates (>30ℓ/min), was found to be bimodal with one peak corresponding to small droplets and the other to very large droplets (e.g. see Figures I.28 and I.29 for the results with the Unicorn JN and the UN). The results need to be interpreted with caution however. It appears that at higher suction rates, a number of large droplets are pulled up into the aerosol cloud which would have fallen back into the nebuliser reservoir at lower suction rates. In comparing Figures I.28a and b, and I.29a and b, it can be seen that the composition of the fine part of the aerosol cloud remains unaltered, whereas a second peak, corresponding to large droplets, appears at high suction rates. Since the mass of a droplet is proportional to the cube of its diameter, the small number of very large droplets may contain a relatively large mass, that of the original aerosol cloud being insignificant in comparison. Such large droplets would be expected to deposit in the head and not enter the lung (see Part II).

The results of this study indicate that, during inhalation, not only fine but even coarse droplets may be drawn into the patient's lungs.

3.3.2.2 Electrical measurement, results and discussion

Wide ranging experiments were performed to examine the effects of varying nebuliser parameters with respect to the aerosol charge generated by both JN and UN types.

3.3.2.2.1 Ions and charged droplets generated by JN and UN

When a water surface is disrupted by nebulisation, electric charge is separated, (by a little understood mechanism) which may be in the form of charged droplets and free ions. It is possible to investigate the level of charge carried by aerosol droplets and ions, of mobility less than the maximum value which can be detected by an ion mobility analyser, by performing two consecutive experiments under identical conditions. The second run is performed after

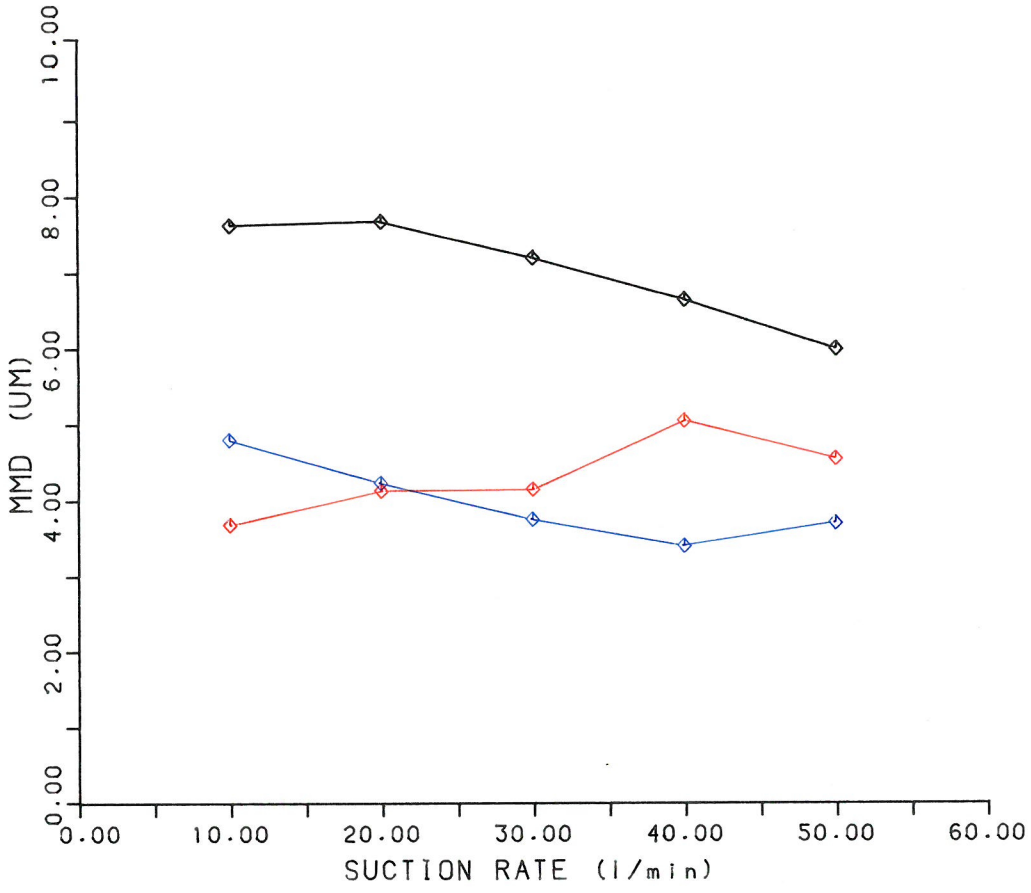

FIG (I.27a): EFFECT OF SUCTION RATE UPON AEROSOL DROPLET SIZE OF UN AND JN'S (DRIVEN AT 8 l/min)

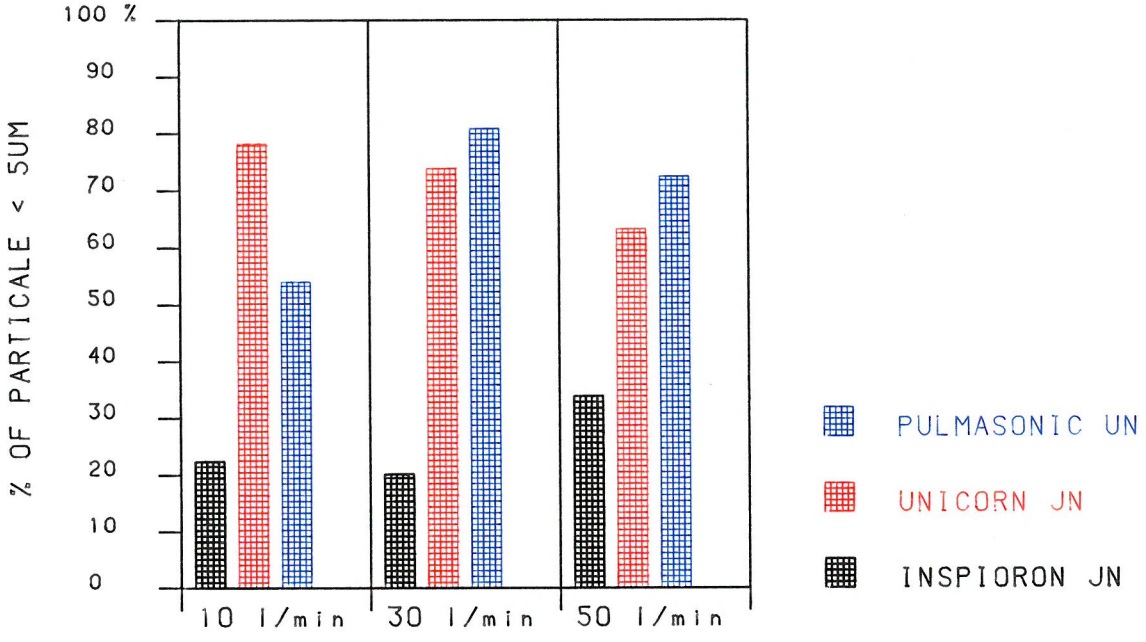

FIG. (I.27b): EFFECT OF SUCTION RATE UPON PERCENTAGE OF DROPLETS OF DIAMETER < 5 UM FOR UN AND JN'S.

a)

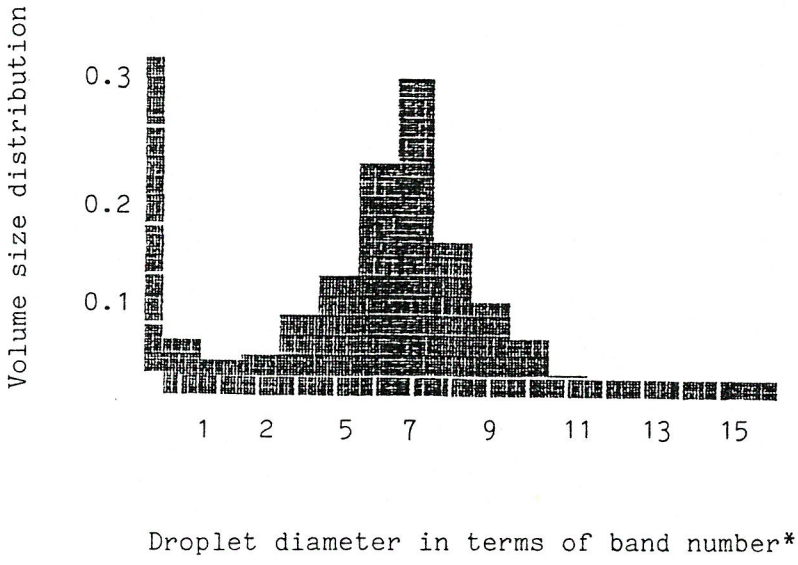

b)

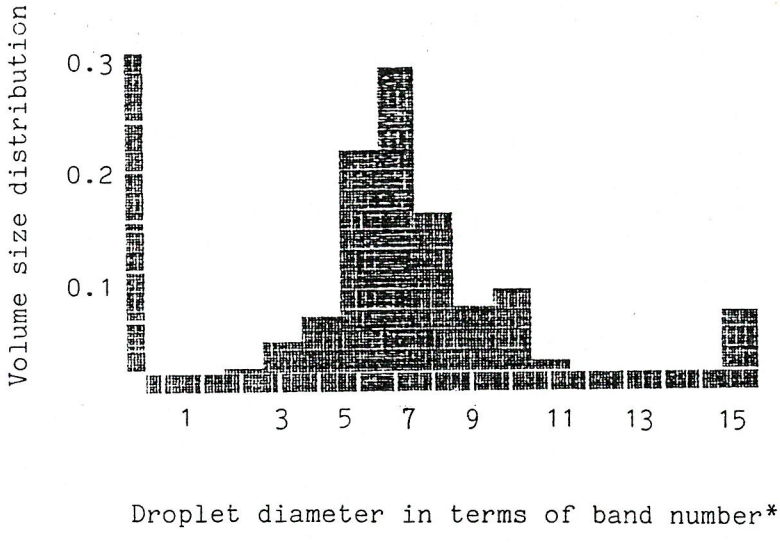

FIGURE I.28 Output size distribution of Unicorn JN derived at 8l/min and sucked at:

(a) 20ℓ/min (b) 50ℓ/min

*(see Figure I.9 for the size bands table)

a)

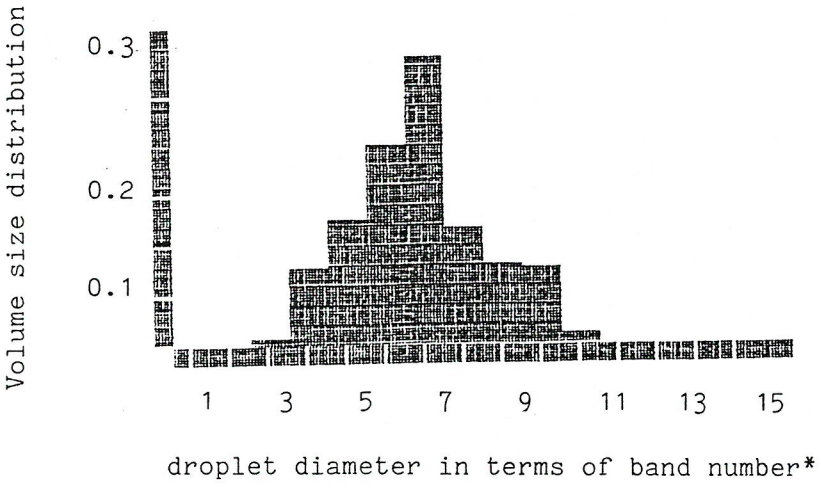

b)

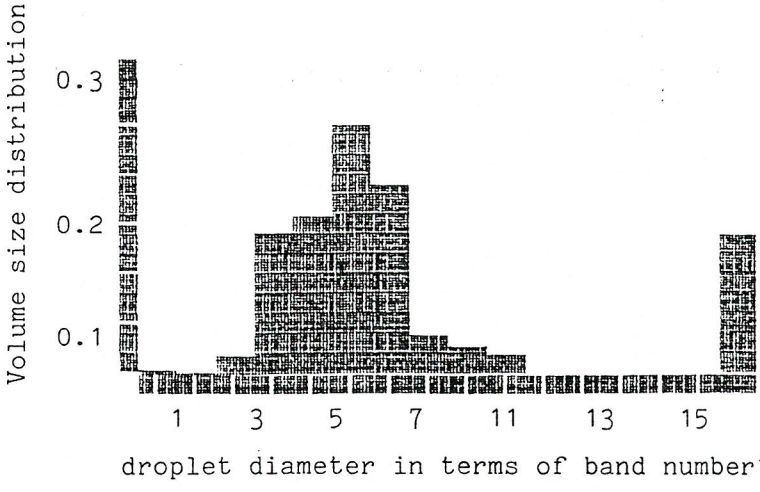

FIGURE I.29 Output size distribution of Pulmasonic UN sucked at (a) 20 ℓ/min (b) 50ℓ/min

*(see Figure I.9 for the size bands table)

changing polarity of the ion mobility analyser electrode, to enable the ionic currents corresponding to both positive and negative polarity to be measured. The object is to compare the sum of the positive and negative ionic currents to the current measured using the total-air-charge monitor. If they are the same, to all intents and purposes, it can be deduced that the net charge carried by the aerosol droplets and low mobility ions is zero, otherwise they will carry net charge.

Tables I.4 and I.5 show data obtained simultaneously for the total-air-charge monitor and the ion mobility analyser, for ions and charged droplets produced by JN and UN.

In Table I.4, the currents are the same, implying a net charge of zero for the JN. This is compatible with the droplets and low mobility ions satisfying one of the following three requirements:

1. all droplets are neutral;
2. all droplets are charged, there are equal amounts of positive and negative polarity;
3. some are neutral and some are positive and negative with equal amounts of charge.

In Table I.5, the currents are different, implying that the droplets and low mobility ion carry a net charge. Some of the droplets possibly are neutral.

3.3.2.2.2 Effect of air-drive flow rate on ion production (JN only)

Table I.6, shows data obtained simultaneously, using the ion mobility analyser and the total-air-charge monitor, for a number of different nebulising conditions. The current due to charge carried by the large droplets sedimenting into the tray at the bottom of the spray chamber was measured. Typical results are given in column 7 along with the rate at which the liquid reservoir was charging. In Table I.6, the air flow rate through both the ion mobility analyser and the total-air-charge monitor was 15ℓ/min and the mobility of ions collected $\geq 0.0251 cm^2V^{-1}s^{-1}$ (corresponding to size diameter ~0.008μm, assume that the ions carried unit charge, Testone, 1986).

TABLE I.4

Charge on droplets of diameter $\leq 50\mu m$

Nebuliser type: Inspiron Mini-neb JN
Nebuliser air-drive flow rate 8ℓ/min
Ion mobility analyser flow rate 15ℓ/min
Total-air-charge monitor flow rate 15ℓ/min

Applied Voltage (V)	Mobility of ions collected $cm^2V^{-1}s^{-1}$	ionic current -ve (PA)	ionic current +ve (PA)	ionic current ratio -/+	net ionic current (PA)	Total -air charge monitor current (PA)
10	$\geq$ 0.2505	16.3	12.8	1.27	-3.5	-5.8
20	$\geq$ 0.1253	21.0	34.8	0.60	+13.8	+33.3
50	$\geq$ 0.0501	55.0	67.5	0.81	+12.5	+15.4
60	$\geq$ 0.0418	62.5	67.5	0.93	+5.0	+4.3
80	$\geq$ 0.0313	77.5	82.5	0.84	+5.0	+4.8
100	$\geq$ 0.0251	90.0	75.0	1.20	-15.0	-13.8

TABLE I.5

Charge on droplets of diameter $\leq 50\mu m$

Nebuliser type: Pulmasonic UN

Ion mobility analyser flow rate 15ℓ/min
Total-air-charge monitor flow rate 15ℓ/min

Applied Voltage (V)	Mobility of ions collected $cm^2V^{-1}s^{-1}$	ionic current -ve (PA)	ionic current +ve (PA)	ionic current ratio -/+	net ionic current (PA)	Total-air charge monitored (PA)
10	$\geq$0.2505	110	180	0.61	+70	-34.2
20	$\geq$0.1253	475	165	2.88	-310	-27.4
30	$\geq$0.0835	1630	1630	1.00	-	-45.3
40	$\geq$0.0626	2050	2680	0.76	+630	-52.5
50	$\geq$0.0501	2500	2830	0.88	+330	-55.0
60	$\geq$0.0418	2700	2980	0.91	+280	-42.5
80	$\geq$0.0313	2230	4380	0.51	+215	-42.5
100	$\geq$0.0251	7500	4500	1.67	-300	-46.3

TABLE I.6

Aerosol and Ion Charge data for Inspiron JN

Air-drive flow rate ℓ/min	ionic current -ve (PA)	ionic current +ve (PA)	ionic current ratio -/+	net ionic current (PA)	total -air charge monitor (PA)	large droplets current (PA)	liquid reservior current (PA)
4	12.8	5.3	2.42	-7.5	-5.9	-1.1	+40
6	29.5	13.0	2.27	-16.5	-14.9	-4.8	+150
8	47.0	30.0	1.57	-17	-19.3	-13.8	+250
10	100.0	90.0	1.11	-10	-4.9	-16.5	+310
12	390.0	415	0.94	+25	+30.0	-7.5	-115

It was found that ion production rate increased with increasing air-drive flow rate, but that the ratio of concentration of negative to positive ions decreased. These results indicate that the ratio of ion concentrations produced is a function of the violence with which the liquid is disrupted. This is in agreement with the results obtained by Byrne, 1977, for his water spraying experiments.

As the total-air-charge monitor currents were equal within the limits of experimental error, to the sum of the positive and negative ionic currents, measured using the mobility analyser in consecutive experiments, it can be deduced that the ions and aerosol droplets of mobility $<0.0251 cm^2 V^{-1} s^{-1}$ (i.e. low mobility ions and virtually all the aerosol droplets) carried equal amounts of positive and negative charge.

3.3.2.2.2A An estimate of the maximum amount of charge available for aerosol droplets produced by JN

An estimate of the maximum amount of charge available for aerosol droplets can be obtained by dividing the reservoir current by the liquid volume-flow rate. This is a maximum estimate since some of the charge is likely to be in the form of ions and neutralization processes will occur. Assuming charge to be distributed amongst the droplets in direct proportion to droplet surface area, the amount of charge for the different droplet size fractions, measured using the Malvern particle sizer, can be calculated. This assumes that each band consists of mono-disperse aerosol droplets of size represented by the midpoint values.

The results are summarized in Tables I.7 and I.8. In Table I.4, it is assumed that $q = Ad^2$ and that constant A is defined by

$$A = \frac{\text{charge held by droplet of MMD}}{(\text{MMD})^2}$$

This approach overestimates the value of the constant A (and hence q), since the total surface area of all aerosol droplets will be much greater than the equivalent value obtained using the MMD approach. The justification for using the MMD approach is that it is simpler and the same conclusion can be obtained since droplet charge is overestimated and even the overestimated charge is insignificant.

Table I.7, gives various values of the constant A for different values of air-drive flow rate in the Inspiron JN. The value of A, corresponding to an air-drive flow rate of 8ℓ/min is used in Table I.8, which shows that the natural level of aerosol charging (which is overestimated) in a JN is negligible (see Part II).

3.3.2.2.3 The effect of the addition of electrolytes to the water on ion production

Experiments were carried out to examine the effect which the addition of electrolyte had on the ion production for aerosol produced using the JN. Ion mobility curves were plotted for four different solutions (mobility analyser electrode voltage varying in magnitude from 10-100 volts) and these are shown in Figures (I.30, a to d).

The purest solution corresponded to distilled, deionized water and the others were obtained by the addition of 0.45%, 0.9% and 5% by volume of sodium chloride, respectively. It can be seen from Figures (I.30, a to d) that the purest water gave the largest proportion of high mobility ions. Therefore, the

TABLE I.7

Parameters used in the calculation of the constant A (used in Table 5 for air-drive flow rate of 8ℓ/min):

Air-drive flow rate	Liquid-volume flow rate		Liquid reservoir current	Mean charge-to-mass ratio for unit density liquid	MMD	Volume of one droplet of diameter MMD	Charge held by droplet of diameter =MMD (elementary unit e)	Value of constant A
(ℓ/min)	(mℓ/min)	($\times 10^{-9} m^3 s^{-1}$)	(PA)	(C/m^3)	(μm)	($\times 10^{-16} m^3$)		($\times 10^{-7} C/m^2$)
4	0.08	1.33	40	0.030	11.8	8.603	161	1.85
6	0.16	2.67	150	0.056	10.6	6.236	219	3.12
8	0.22	3.67	250	0.068	9.1	3.946	168	3.25
10	0.27	4.50	310	0.069	7.6	2.299	99	2.74
12	0.31	5.17	115	0.022	6.8	1.646	23	0.79

TABLE I.8

An estimate of the maximum charge distribution on aerosol droplets measured using the Malvern Particle sizer

Type of nebuliser: Inspiron Mini-neb JN
(nebuliser air-drive flow rate 8ℓ/min, suction rate 30 ℓ/min)
For the prevailing conditions A = $3.25 \times 10^{-7} Cm^{-2}$
Liquid-volume flow rate = 0.22 mℓ/min

Size band			Volume of droplet having diameter = mid point value $\times 10^{-6}$ m³	% volume in band	number of droplets in band	Number of elementary charge on each droplet
Upper band (μm)	Mid-point (μm)	Lower band (μm)				
1.2	0.6	assumed 0	1.13×10^{-13}	1.2	5.8×10^{8}	1
1.5	1.35	1.2	1.29×10^{-12}	0.2	4.3×10^{6}	4
1.9	1.70	1.5	2.57 ~	0.3	3.2 ~	6
2.4	2.15	1.9	5.20 ~	0.7	3.7 ~	9
3.0	2.70	2.4	1.97×10^{-11}	1.2	1.7 ~	15
3.9	3.45	3.0	2.15 ~	4.1	5.2 ~	24
5.0	4.45	3.9	4.16 ~	13.9	9.2 ~	40
6.4	5.70	5.0	9.70 ~	19.4	5.5 ~	66
8.2	7.30	6.4	2.04×10^{-10}	26.0	3.5 ~	108
10.2	9.35	8.2	4.28 ~	22.4	1.4 ~	177
13.6	12.05	10.2	9.16 ~	7.8	2.3 ~	295
17.7	15.65	13.6	1.97×10^{-9}	2.8	3.9×10^{4}	497
23.7	20.70	17.7	4.64 ~	0.6	3.6×10^{3}	869

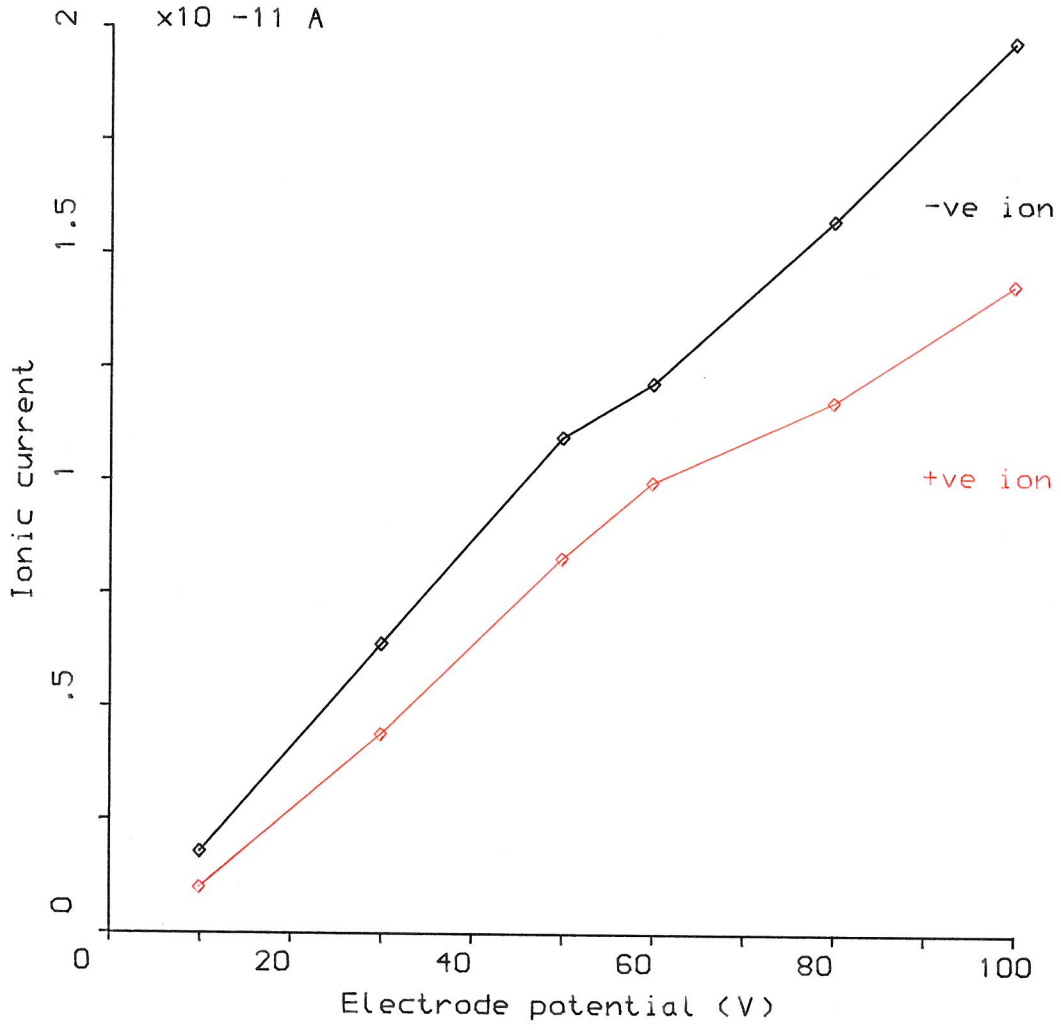

FIG.(I.30a): Ion mobility curves for Distilled water.

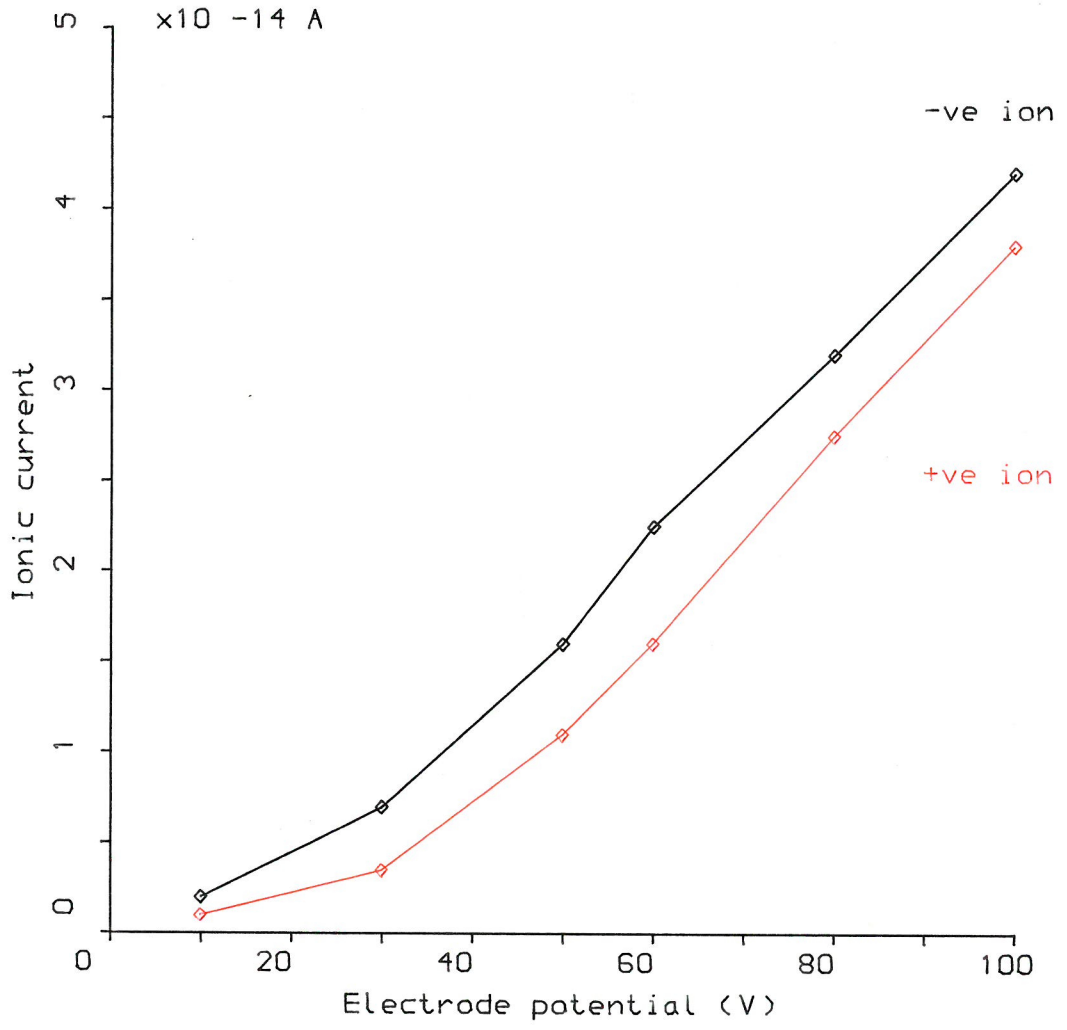

FIG.(I.30b): Ion mobility curves for Hypotonic solution.
(0.45% by volume Saline in distilled water)

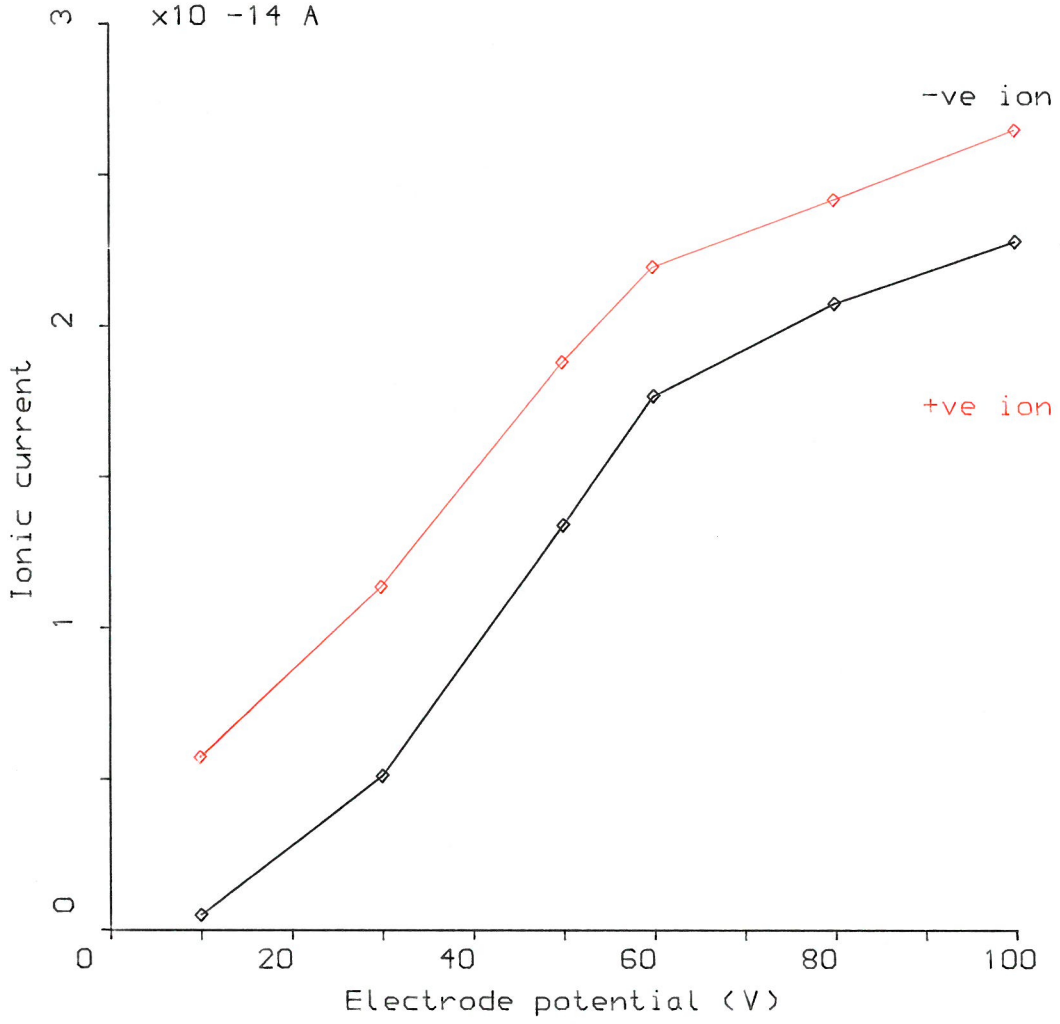

FIG.(I.30c): Ion mobility curves for Hypertonic solution.
(0.9% by volume Saline in distilled water)

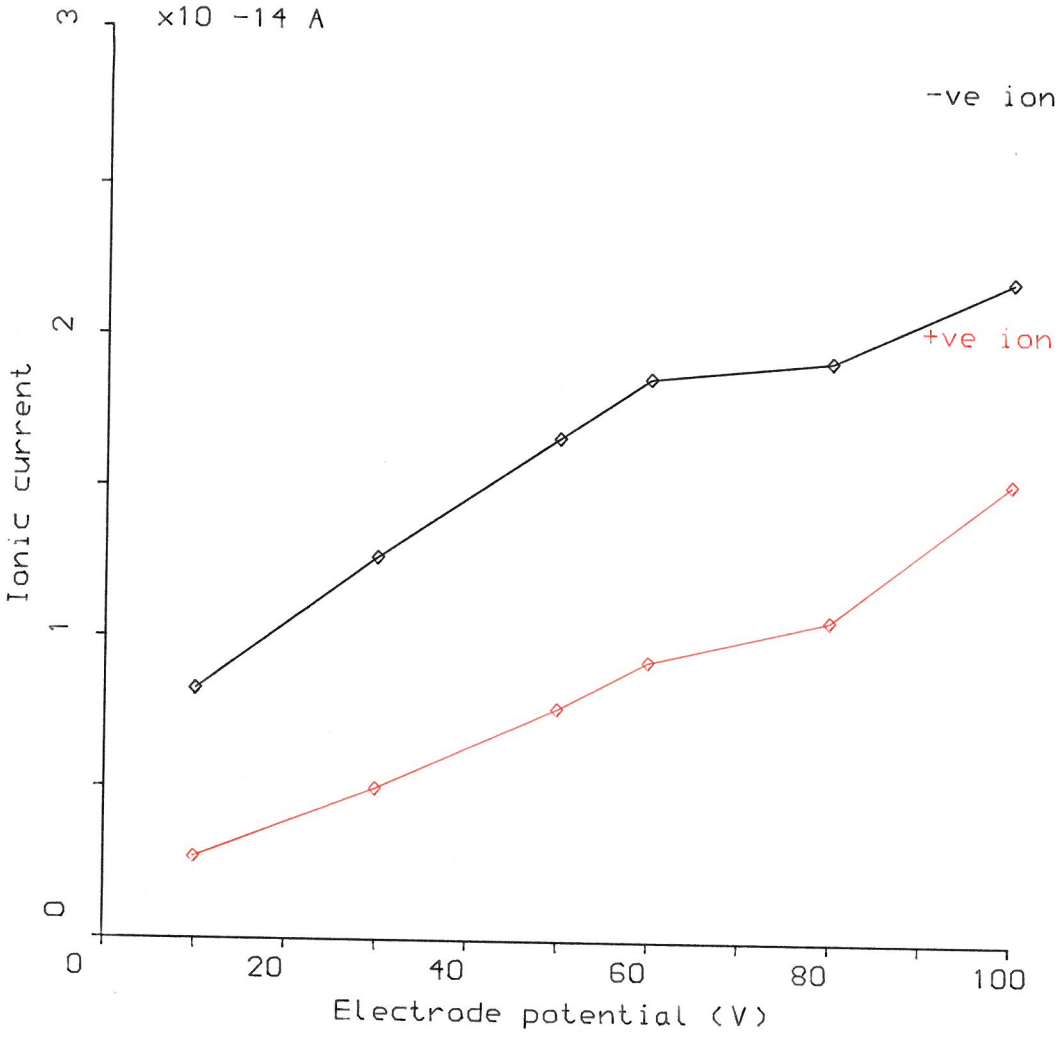

FIG.(I.30d): Ion mobility curves for isotonic solution
(5% by volume Saline in distilled water)

addition of electrolyte reduces the concentration of ions produced and hence the charge on the aerosol droplets.

The salient feature of the curves is the vast drop in magnitude (~3–orders) of ionic current on the addition of small quantities of electrolyte. This suggests that solution conductivity (which increase with electrolyte concentration) may play an important part in ion production.

3.4 Nebuliser Output Measurements

3.4.1 Introduction and aims

The use of nebuliser therapy in respiratory diseases is now established. Unfortunately, little information is available about the nebuliser output characteristics under various conditions. The ultimate measure of therapeutic efficiency is the patient response. Two major factors determine the effectiveness of treatment: (1) the appropriate particle size, and (2) the correct therapeutic dosage. To achieve this, the volume output must be known.

The aims of this study were to assess the effect on nebuliser output and temperature of the solution of (1) air drive flow rate, and (2) liquid volume within the nebuliser.

3.4.2. Methods

Nebulisers were driven by a controlled flow of compressed air that was monitored by a rotameter. Distilled water was used in all experiments. The volume of aerosol released could be determined by measuring the difference in weight of the device before and after the nebulisation. At low liquid volumes the flow of aerosol becomes interrupted. This interruption of flow may occur while there is still liquid left in the nebuliser deposited around the walls of the apparatus. The fluid is displaced from the walls of the apparatus by tapping so that it falls back into the reservoir. The *'dead volume'* is dependent upon the amount of tapping done during nebulisation.

Four parameters were measured for each nebuliser:

(1) the output liquid volume: the difference between the volume of respirator solution placed in the nebuliser and that remaining after nebulisation, determined by the weight loss of the device.

(2) the output liquid flow rate: (Volume/time), the nebulisers were weighed periodically every minute throughout nebulisation to determine the volume released during the previous minute.

(3) the temperature: a thermocouple was inserted into the reservoir and read every minute during the nebulisation.

(4) the duration time: the time taken to complete nebulisation was measured by stop-watch.

The volume released as aerosol, the dead volume and nebulisation duration were then calculated from these parameters.

3.4.3 Results and discussion

3.4.3.1 Effect of air-drive flow rate on output characteristics (JN only)

As the air drive flow rate is increased, the amount of liquid leaving the nebuliser per minute increases as expected. The total 'operational time' for a nebuliser before refilling is required, therefore, decreases with increasing of air drive flow rate. The results of these tests are shown in Figure I.31.

3.4.3.2 Effect of liquid-volume fill

Figure I.32 shows the effect of liquid volume within the nebuliser on mass output characteristics of JN and UN. The rate of aerosol formation by the nebulisers varied during the process of nebulisation. During the first few minutes the output rate and the temperature of the liquid fell. The drop in temperature of the solution results in a rise in the surface tension and the viscosity of the reservoir solution which may in turn have caused the observed fall in mass output rate (see Figures I.33 and I.34).

The final fall in mass output rate occurred when the volume remaining in the JN was not available to the feed tube of the device.

3.4.3.3 The effect of gas-flow rate on the temperature of solution within the nebuliser

A rapid fall in temperature occurs within a JN. This fall increases with increasing gas-flow rate. An increase in the driving gas-flow rate causes an increase in output from JN which increases evaporation, therefore a transfer of

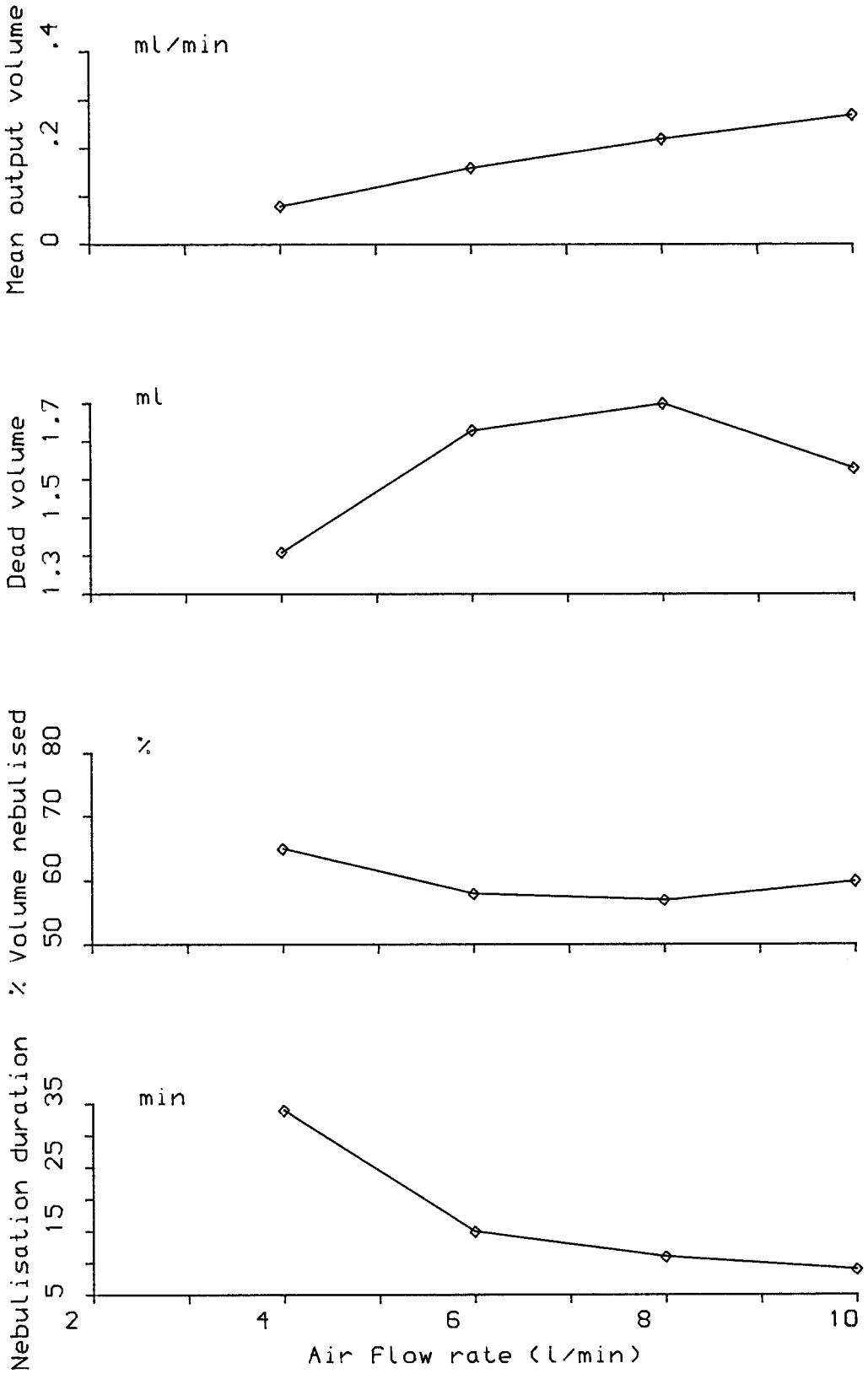

FIG(I.31): Effect of air drive flow rate on duration of nebulisation ,percentage of volume nebulised,dead volume and mean output volume for Inspiron JN (liquid volume=4cc,temp.=22C,RH=30%,No suction)

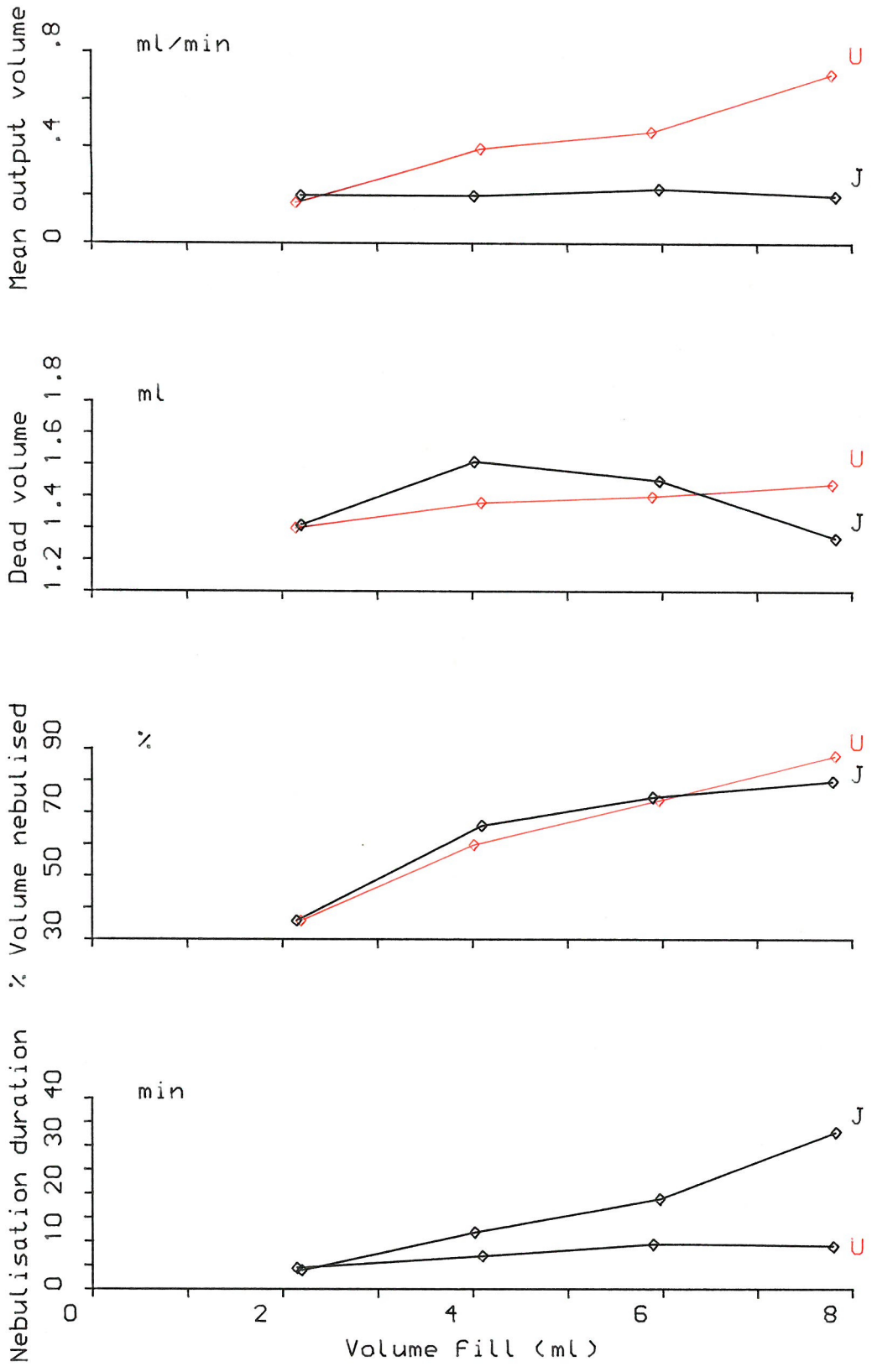

FIG(I.32): Effect of liquid volume fill on duration of nebulisation ,percentage of volume nebulised,dead volume and mean output volume for JN and UN (liquid volume=4cc,temp.=22C,RH=30%,No suction)

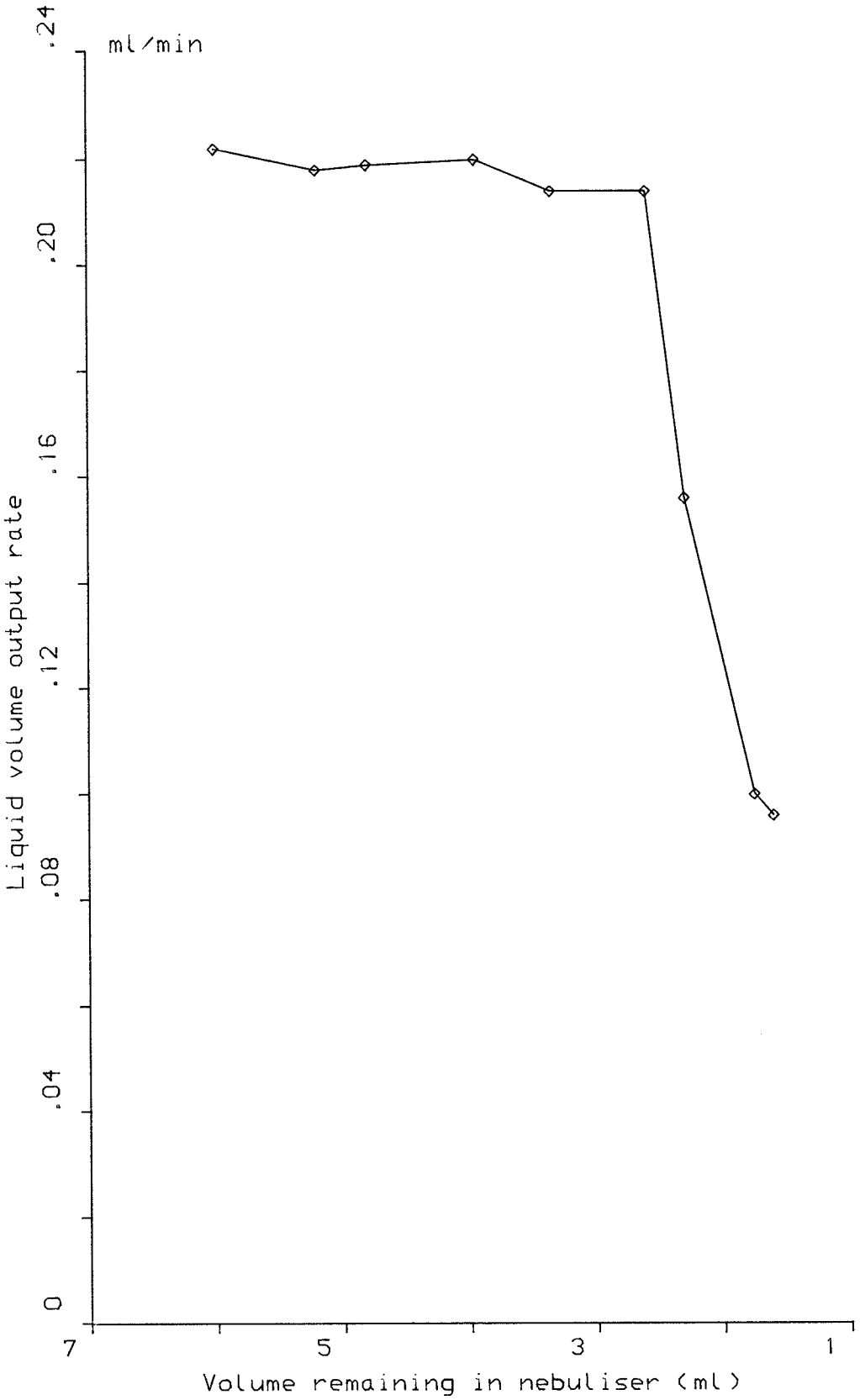

FIG.(I.33): Liquid volume output rate as a function of the volume remaining in the Inspiron Mini-neb JN.
(liquid level=6ml, air drive flow rate=8 l/min,No suction)

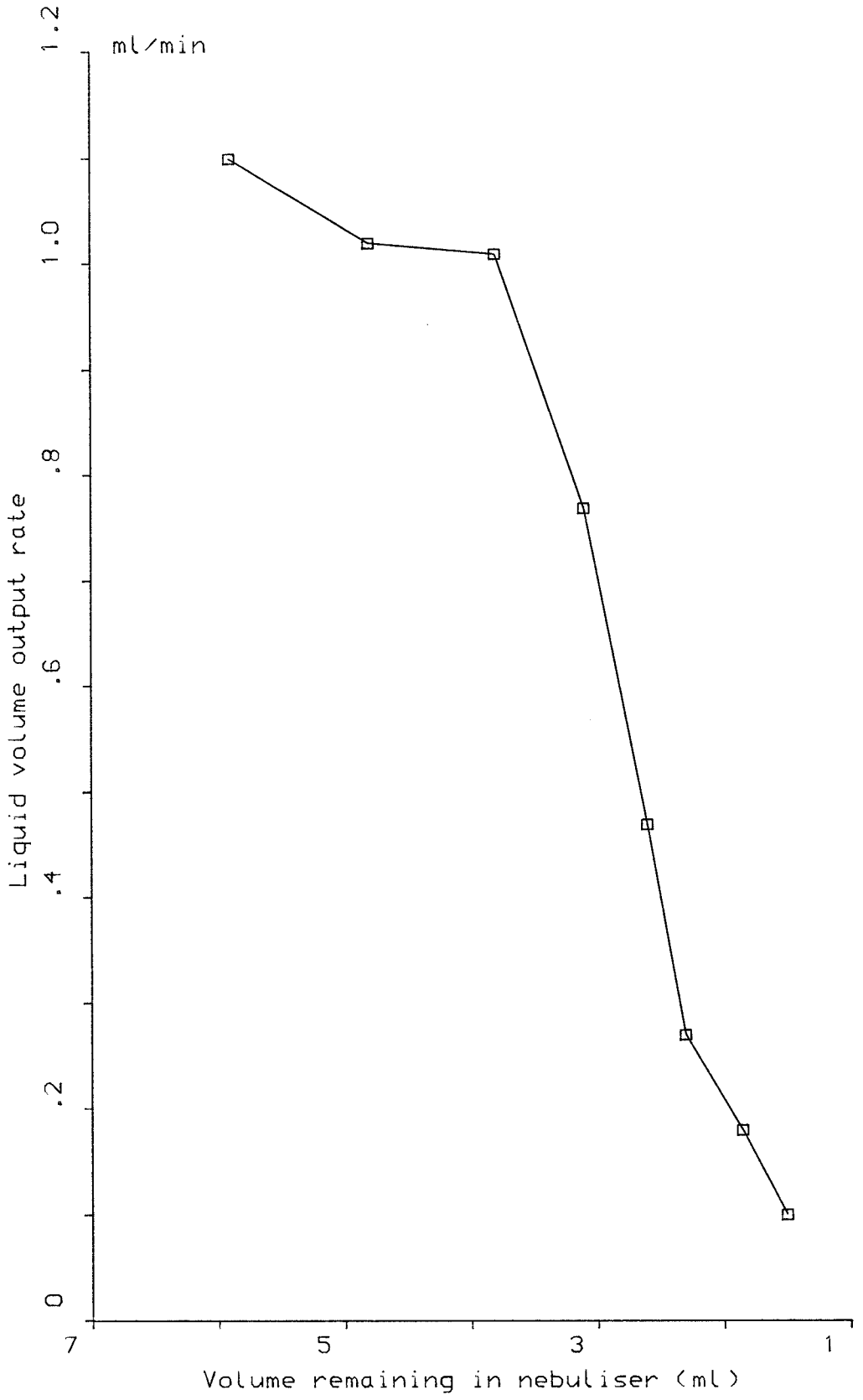

FIG.(I.34): Liquid volume output rate as a function of the volume remaining in the Pulmasonic UN.
(liquid level=6ml, air flow rate=8 l/min,No suction)

energy within the nebuliser to latent heat of evaporation and the new droplet surface area occurs. Also, the cooling caused by heat loss due to adiabatic expansion of the air jet increases with increasing gas-flow rate. Figures I.35 and I.36 show the effect for the Inspiron Mini-neb and Acorn JN's. At a gas-drive flow rate of 8ℓ/min, typically the temperature fell by a maximum of 12.5°C from the ambient temperature after 8.5 minutes for Mini-neb JN, while it fell by a maximum of 13.8°C for Acorn JN after the same time.

The rate of cooling is dependent on the size of the heat sink, ie, the volume of liquid within the nebuliser as shown in Figures I.37 and I.38.

For UN, air flow was used to blow out the droplets from the device. There was more fluctuation in temperature than for the JN. There was a rise in temperature with more liquid-volume fill and drop in temperature with less volume fill and higher air flow rates. This was probably due to a balance between the increase in temperature of the solution due to transfer of kinetic energy of the oscillating droplets and transducers into heat energy and fall in temperature due to loss of latent heat of evaporation and adiabatic expansion of the air set. Figures I.39 and I.40 show the results for Pulmasonic UN.

3.5 Clinical Measurements

3.5.1 Introduction and aims

Cough and irritation in both normal and asthmatic subjects following inhalation of distilled water and saline solution was found if solutions were generated from an UN but not a JN. This could not be explained by differences in output, temperature or size of the droplets from the two devices. The different charge patterns of JN and UN might explain the irritation caused by UN, Lewis et al., 1985.

The aims of this study (*which were done in the Respiratory Dept., Medicine I, Southampton General Hospital*) were to assess whether or not the fluctuation of electrical charge of droplets from an UN was responsible for the increased irritation when inhaling water. By the addition of constant negative or positive charge to the droplets generated from Pulmasonic UN sufficient to overcome the fluctuating charge recorded for the UN, it would be possible to assess the contribution of electrical charge to airway response.

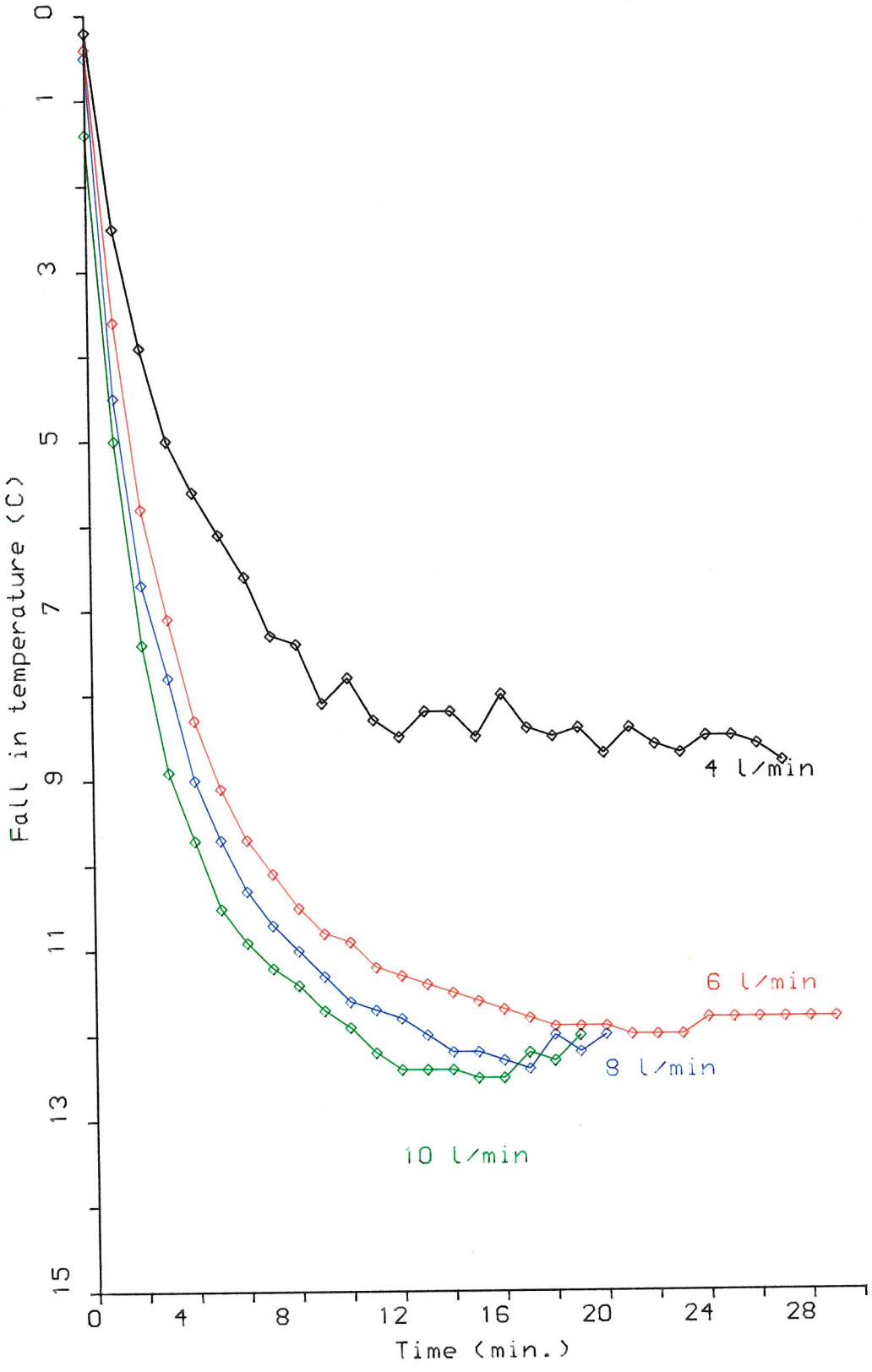

FIG.(I.35): Effect of driving gas flow rate on temperature drop of the solution within the Inspiron Mini-Neb JN.
(liquid level= 4ml , RH= 24% , No suction into atmosphere)

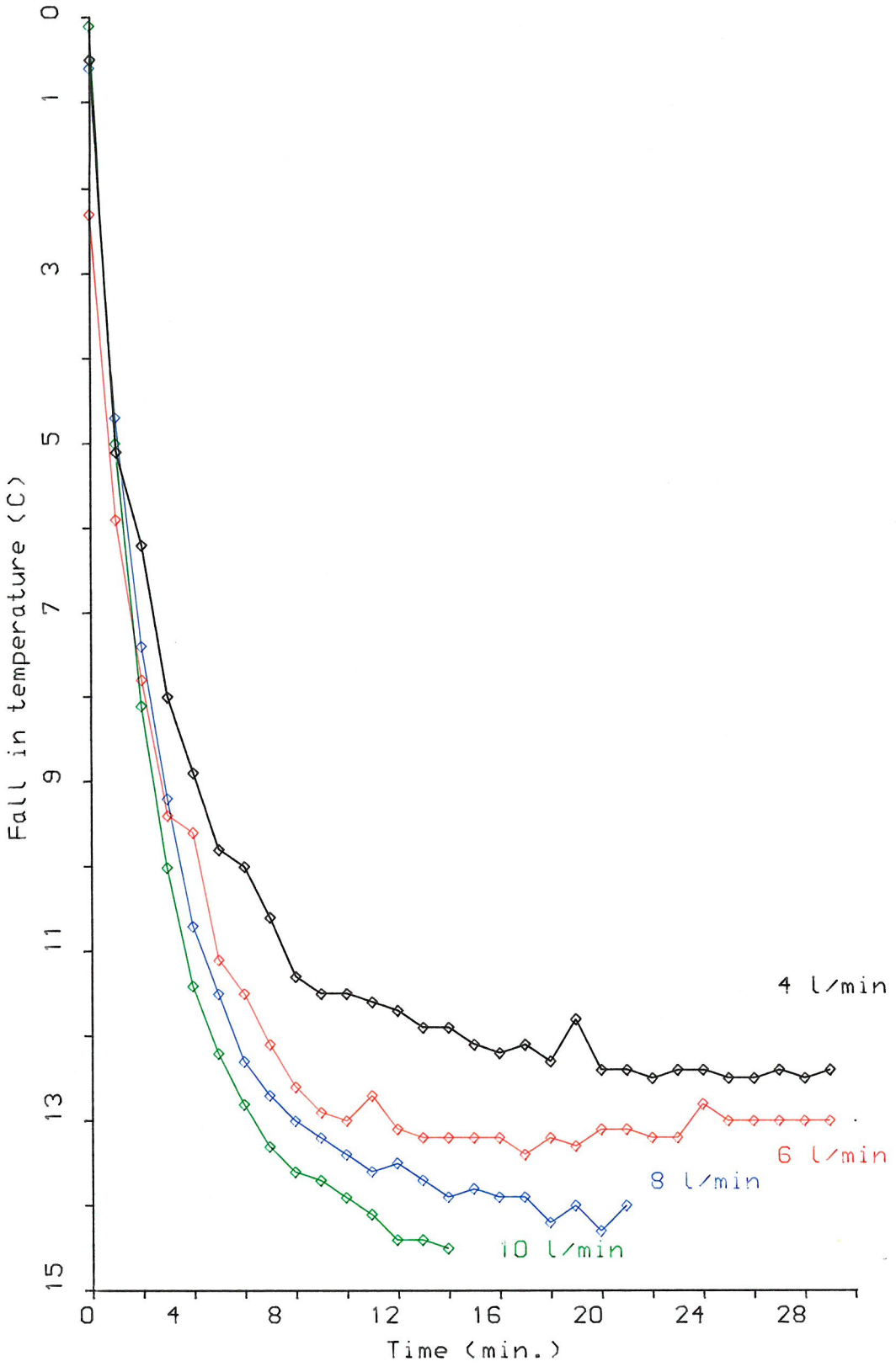

FIG.(I.36): Effect of driving gas flow rate on temperature drop of the solution within the Medic-Aid Acorn JN (liquid level= 4ml , RH= 24% , No suction into atmosphere)

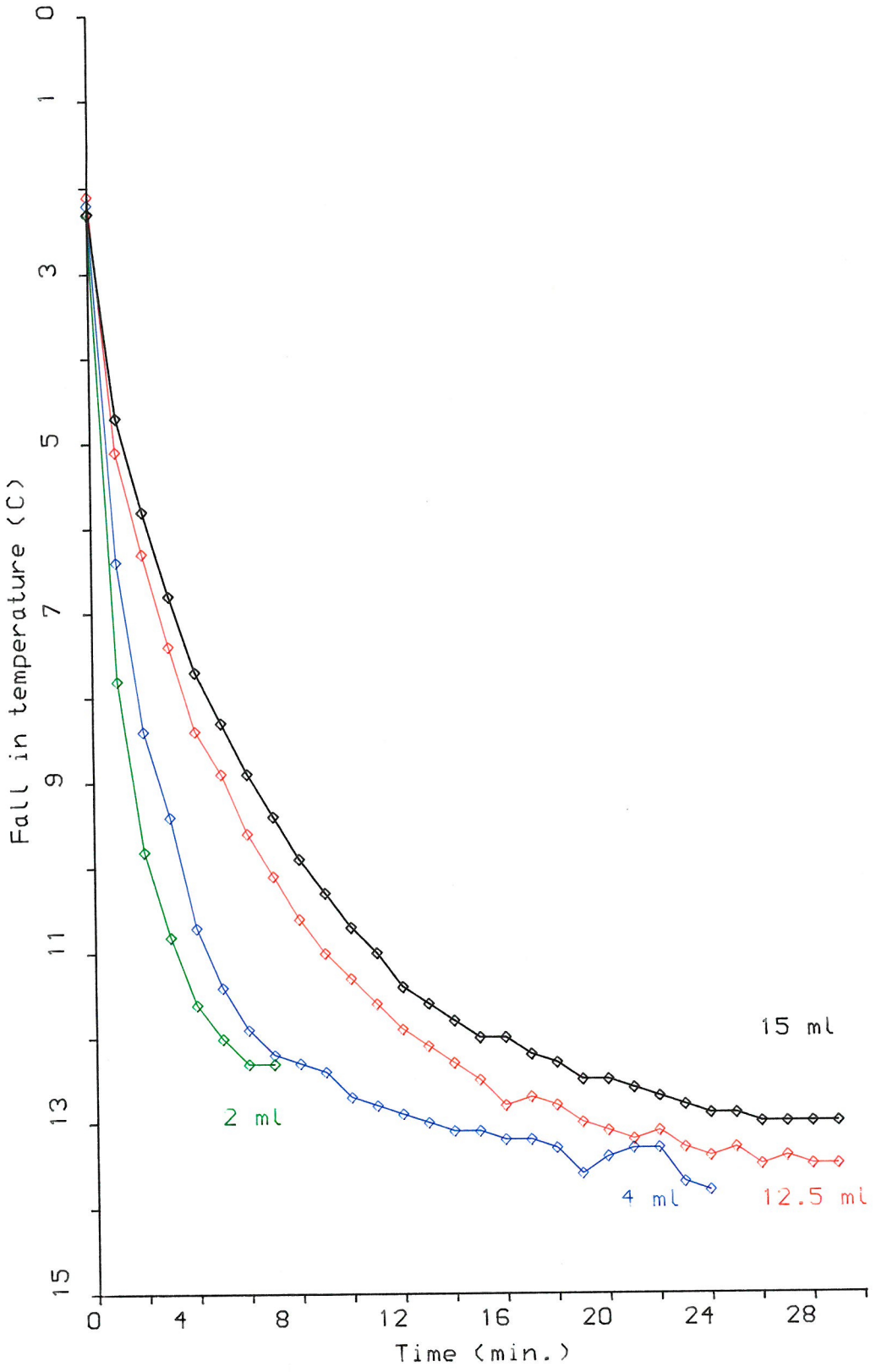

FIG.(I.37): Effect of the liquid volume fill on the drop in temperature for Inspiron Mini-Neb JN.
(air drive flow rate=8 l/min, RH= 29% , No suction into atmosphere)

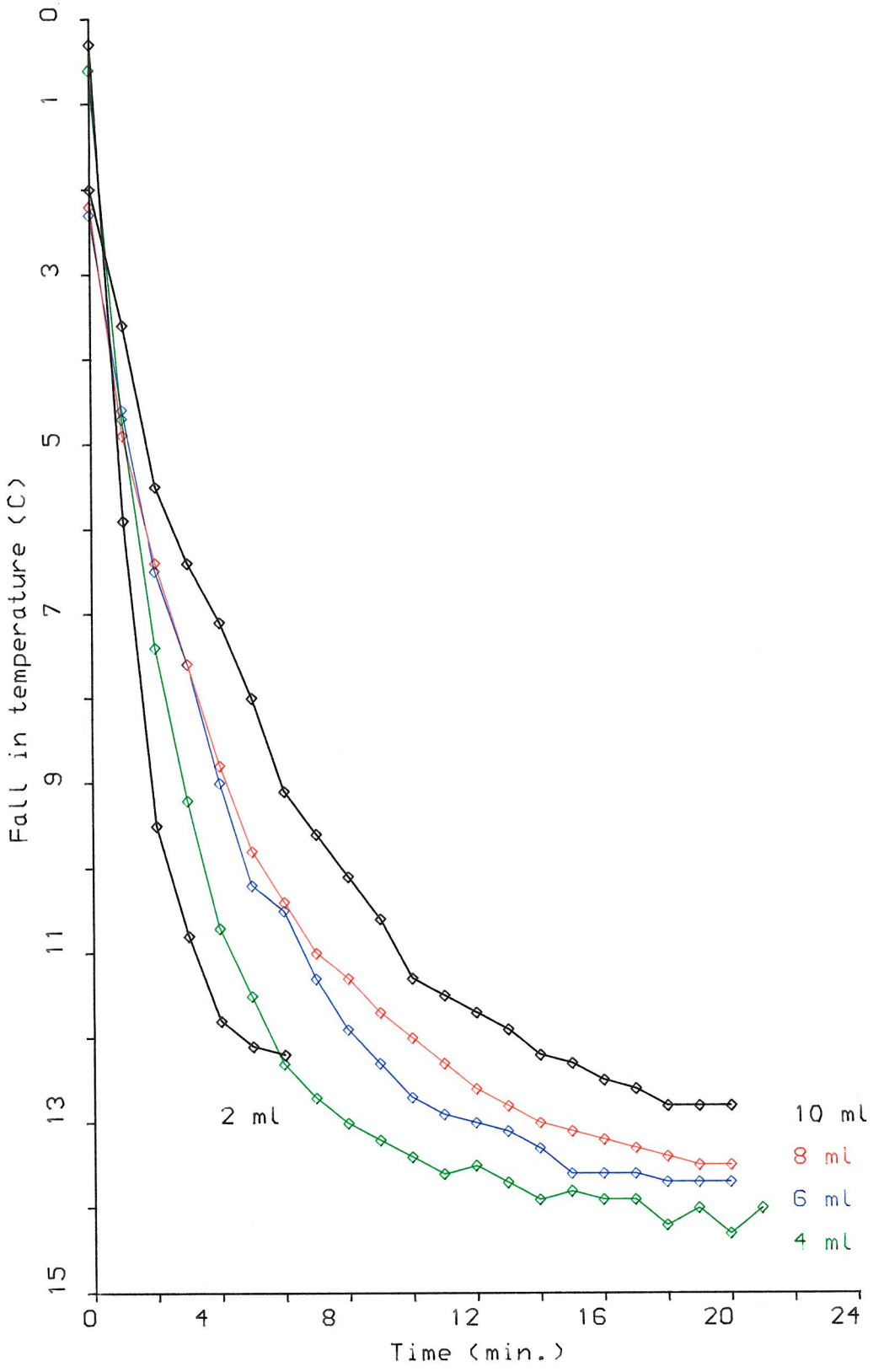

FIG.(I.38): Effect of the liquid volume fill on the drop in temperature for Medic-Aid Acorn JN.
(air drive flow rate=8 l/min, RH= 29% , No suction into atmosphere)

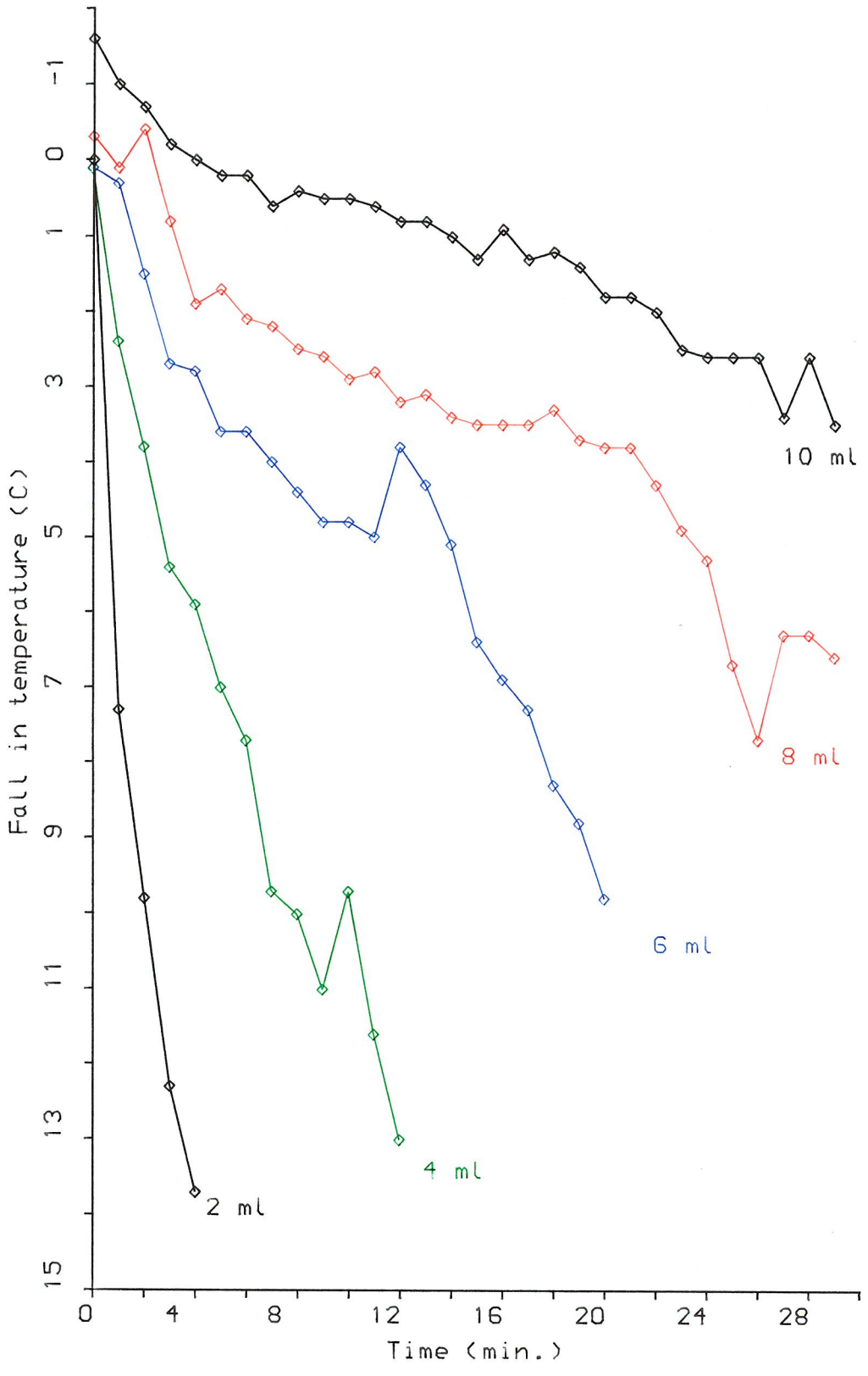

FIG.(I.39): Effect of the liquid volume fill on the drop in temperature for Pulmasonic UN.
(air flow rate=8 l/min, RH= 18% , No suction into atmosphere)

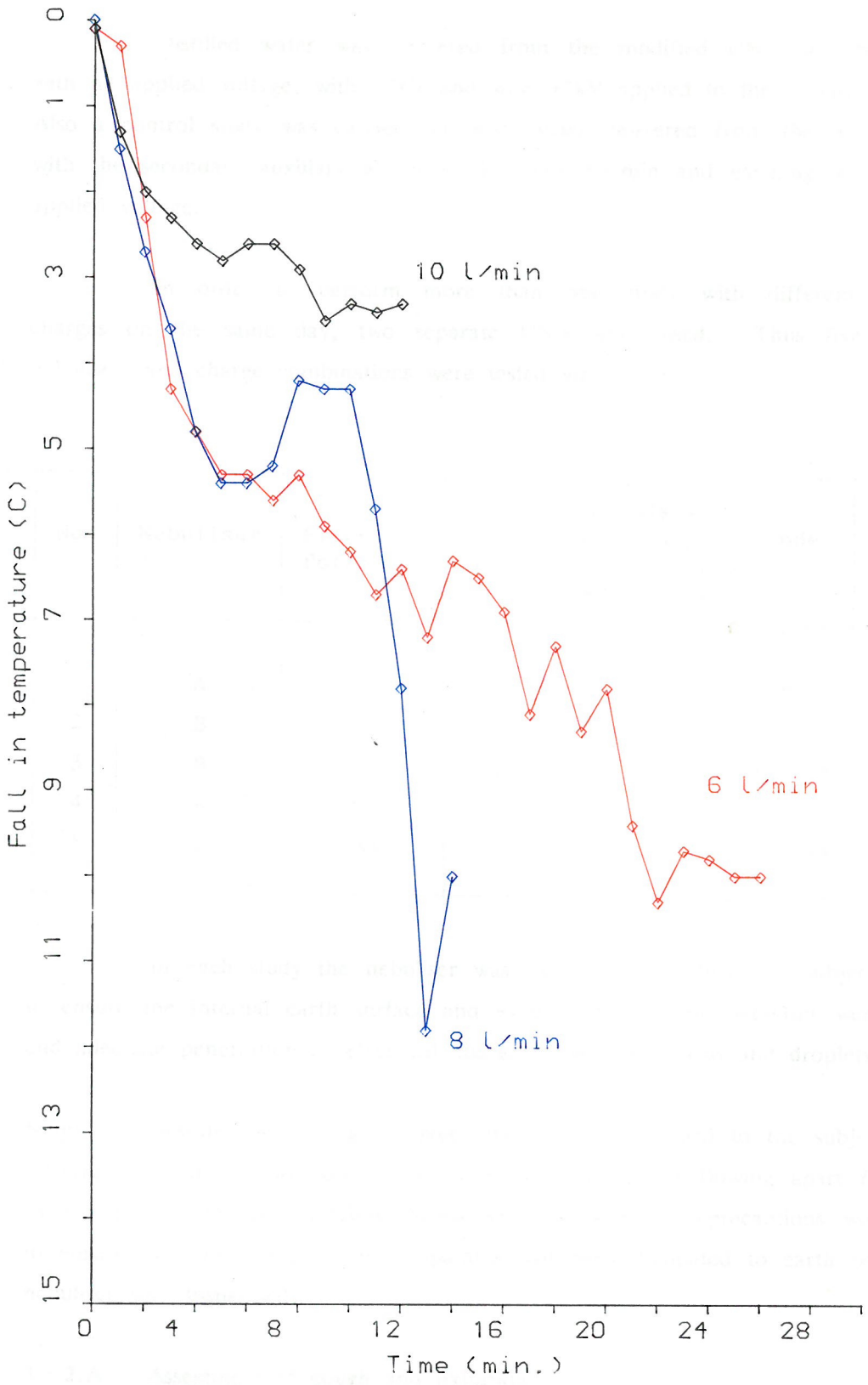

FIG.(I.40): Effect of air flow rate (used to blow the droplets out into the atmosphere) on the drop in temperature for Pulmasonic UN. (liquid volume fill=6 ml , RH= 18% , No suction into atmosphere)

3.5.2 Methods

Distilled water was delivered from the modified UN, see Figure I.41, with no applied voltage, with −7kV and with +7kV applied to the corona electrode. Also a control study was carried out with water delivered from the modified UN with the secondary auxiliary air-drive flow rate 6ℓ/min and earthing lead, but no applied voltage.

In order to perform more than one study with different electrical charges on the same day, two separate UN's were used. Thus five different nebulisers and charge combinations were tested viz:

No.	Nebuliser	Electrode Potential	Earth	Secondary auxiliary air in the mouthpiece	Code
1	A	0	0	0	A_o
2	B	0	0	0	B_o
3	B	0	✓	✓	B_o.e.a
4	B	-7kV	✓	✓	B -7kV
5	B	+7kV	✓	✓	B +7kV

In each study the nebuliser was run for 10sec before a subject inhaled to ensure the internal earth surface and excess tubes of the nebuliser were wetted and adequate penetration of electrical charge to both apparatus and droplets.

Note: Despite such a high voltage, there was no hazard to the subjects when inhaling from the mouthpiece, since there was no current flowing apart from that carried by the charged droplets themselves. Nevertheless, precautions were taken to ensure that the charge of the apparatus had been dissipated to earth before the nebuliser was dismantled.

3.5.2.A Assessment of cough and irritation

Cough frequency may be measured by listening and counting, by tape-recording or by using a pneumotachograph. A diagram of the apparatus used is shown in Figure 1.42. Cough frequency was assessed by counting the number of characteristic cough peaks at time intervals throughout the period of inhalation.

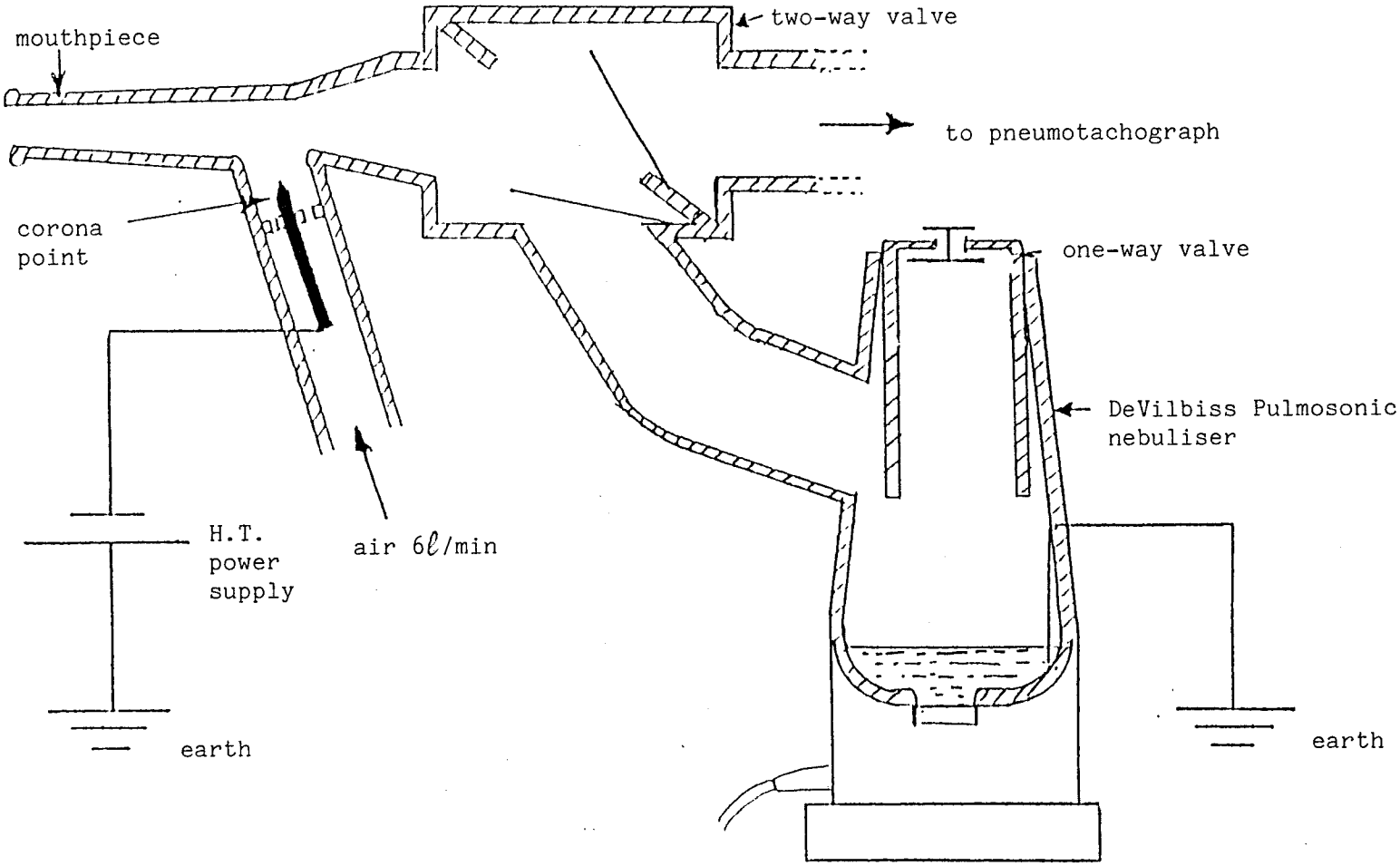

FIGURE I.41 Modification of ultrasonic nebuliser to alter particle charge

Figure I.44 shows a typical flow trace.

A subject assessment of the degree of irritation of the inhaled solution was made using a Visual Analogue Scale (VAS). This was a 10cm long straight line, marked on one end as *'no irritation'* and on the other end as *'extremely irritant'*. The subject was asked to score the line at a point corresponding to the sensation of irritance. The mark made, was then measured in mm from the 'no irritation' end of the line, see Figure I.43.

3.5.3 Results and discussion

Eight normal and eight asthmatic subjects inhaled water from two unmodified UN's, and an UN modified so that droplets were charged from a corona discharge delivery, either +5nA with +7kV, or −4nA with −7kV. Subjects also inhaled from the modified apparatus without the addition of electrical charge.

Despite considerable individual variation in cough response, the addition of both negative and positive charge significantly reduced the number of coughs induced by ultrasonically nebulised water in normal and asthmatic subjects, see results in Figures I.45 and I.46. Subjective irritation as assessed on a VAS correlated with coughs in the majority of both normal and asthmatic subjects, see Figures I.46 and I.47.

It thus appears that the irritant effect (cough and subjective sensation) induced by ultrasonically nebulised water is related to the fluctuation of electrical charge carried by the droplets.

4. SUMMARY OF RESULTS AND CONCLUSIONS OF PART I

1.(a) The spray produced by the JN's has a polydisperse size distribution. The MMD is strongly dependent on gas-drive flow rate, typically for 8ℓ/min air-flow rate the MMD for an Inspiron Mini-neb ~ 7μm, Medic-Aid unicorn ~ 6μm and Acorn ~ 5μm.

(b) The aerosol generated by the Pulmasonic UN has a MMD of ~ 6.5μm at an operating frequency of 1.35MHz.

(c) For the two types JN and UN the droplet size was influenced much more by the inhalation rate with large droplets being pulled up into the

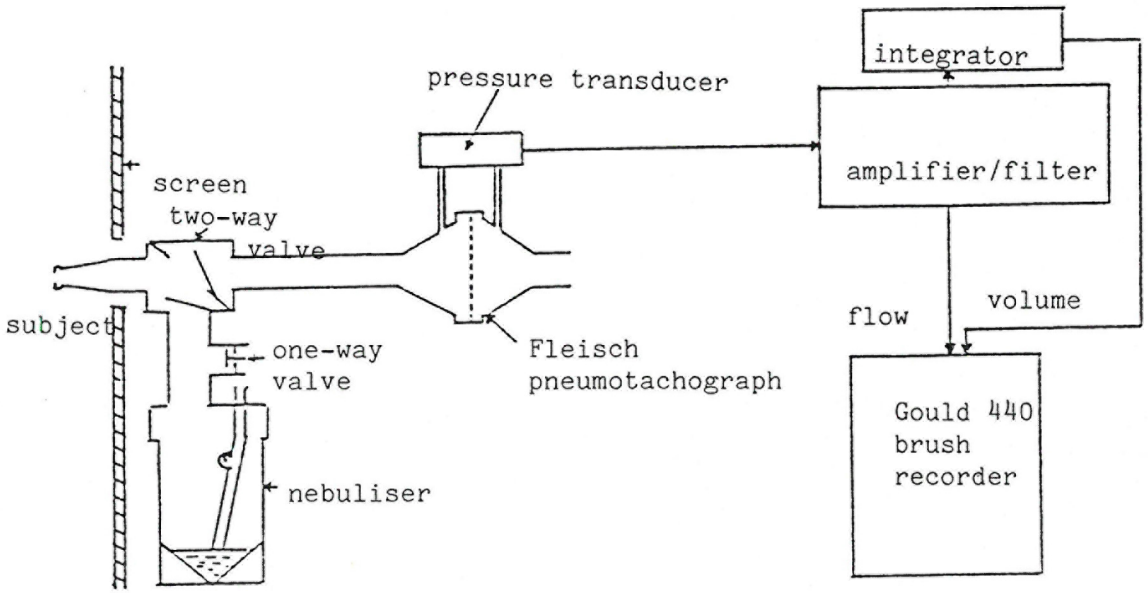

FIGURE I.42 Apparatus for measurement of cough

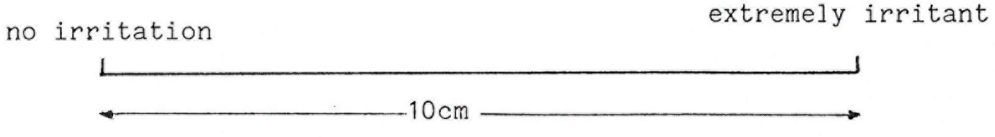

FIGURE I.43 Visual analogue scale

FIGURE I.44

Flow and Volume Traces, Actual Size

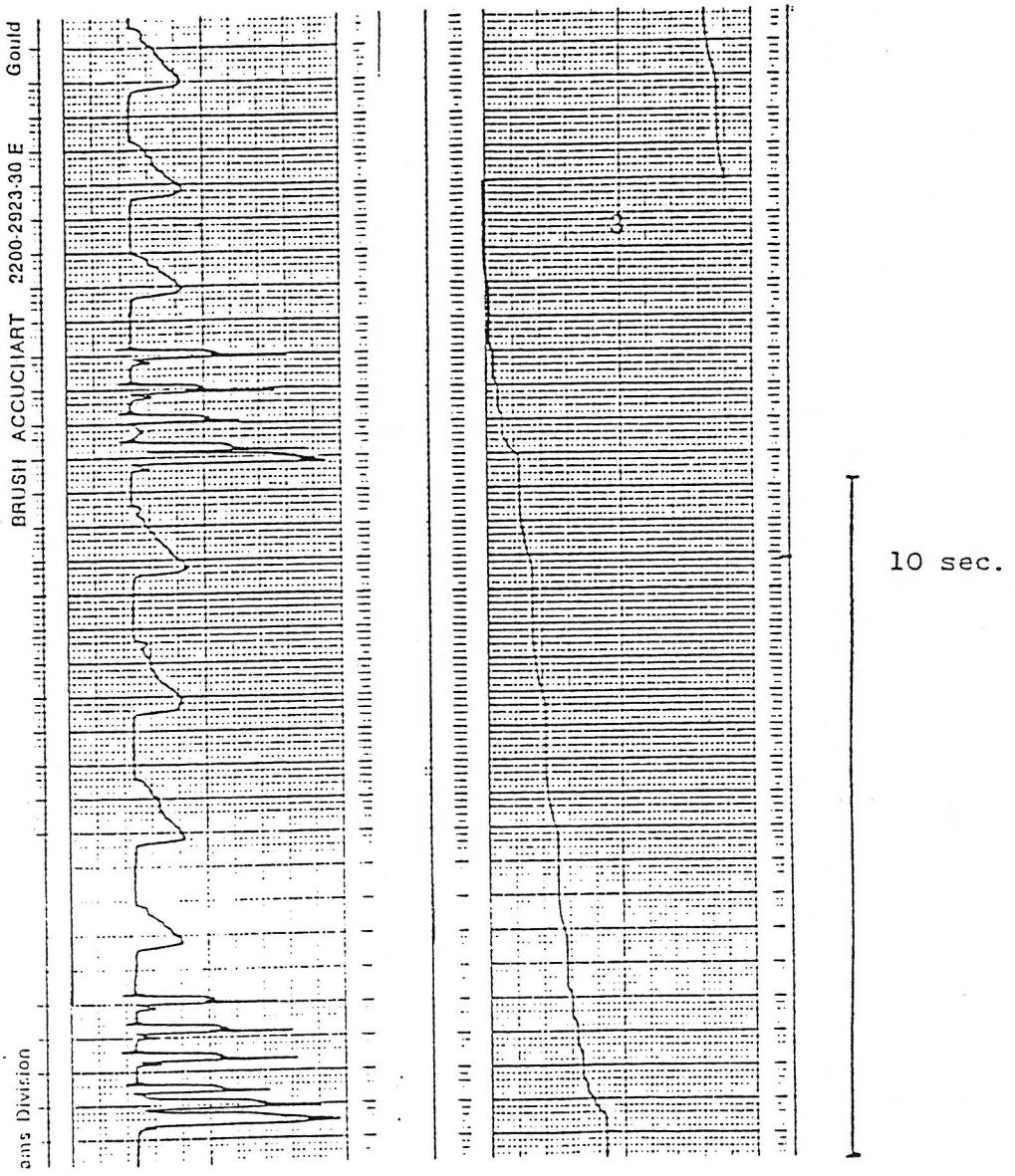

Flow

X axis, Air flow exhaled

Volume

X axis, Volume exhaled

The flow traces shows regular tidal breathing, interspersed with high peaks representing the coughs. These coughs can be seen to be individually distinct with a characteristic shape.

The corresponding volume trace is also shown. The tidal breathing and cough volumes being recorded in an accumulative manner.

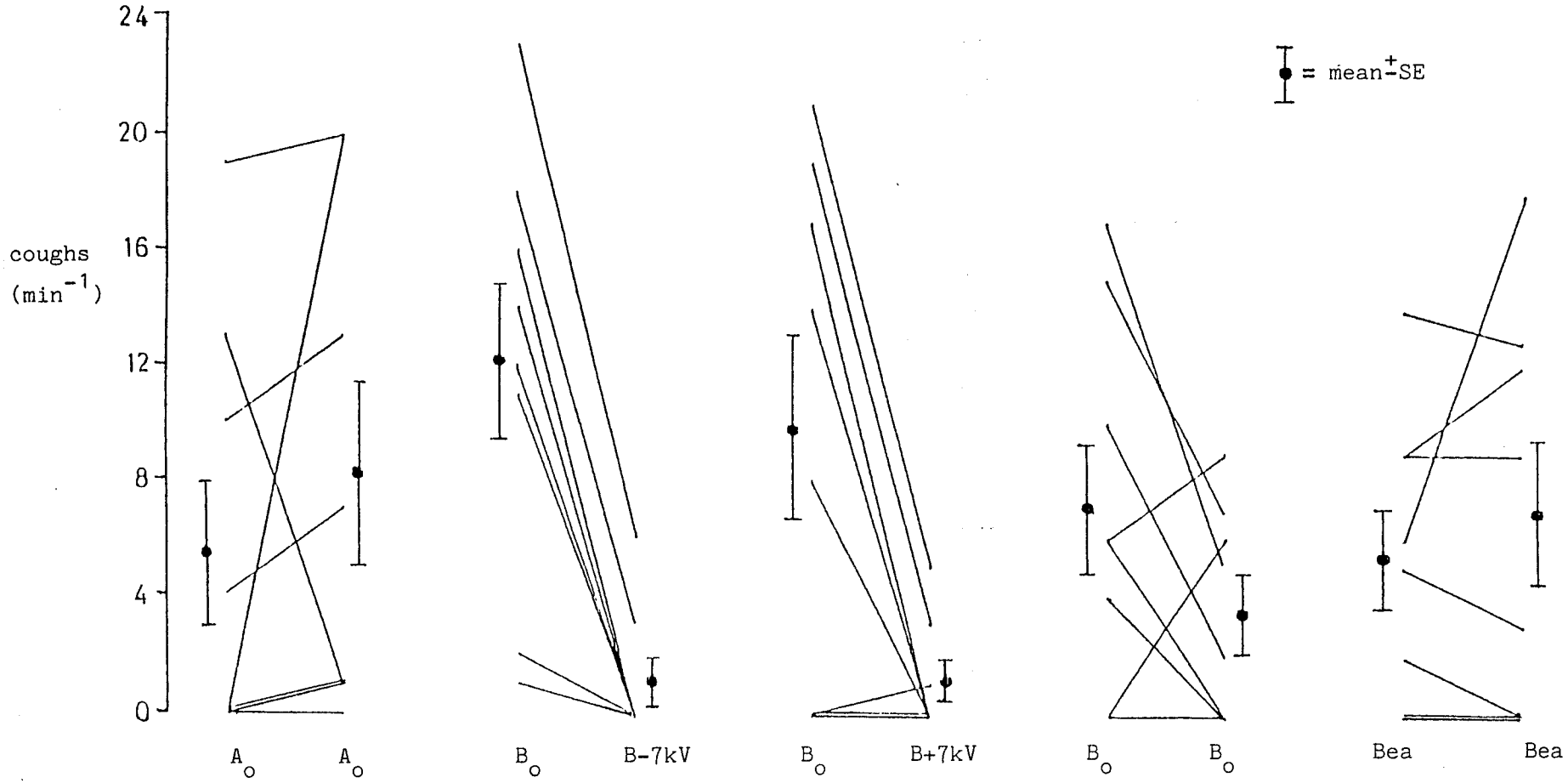

Showing 5 pairs of studies carried out on separate days in normal subjects

FIGURE I.45 Effect of electrical charge on cough induced by ultrasonically nebulised water

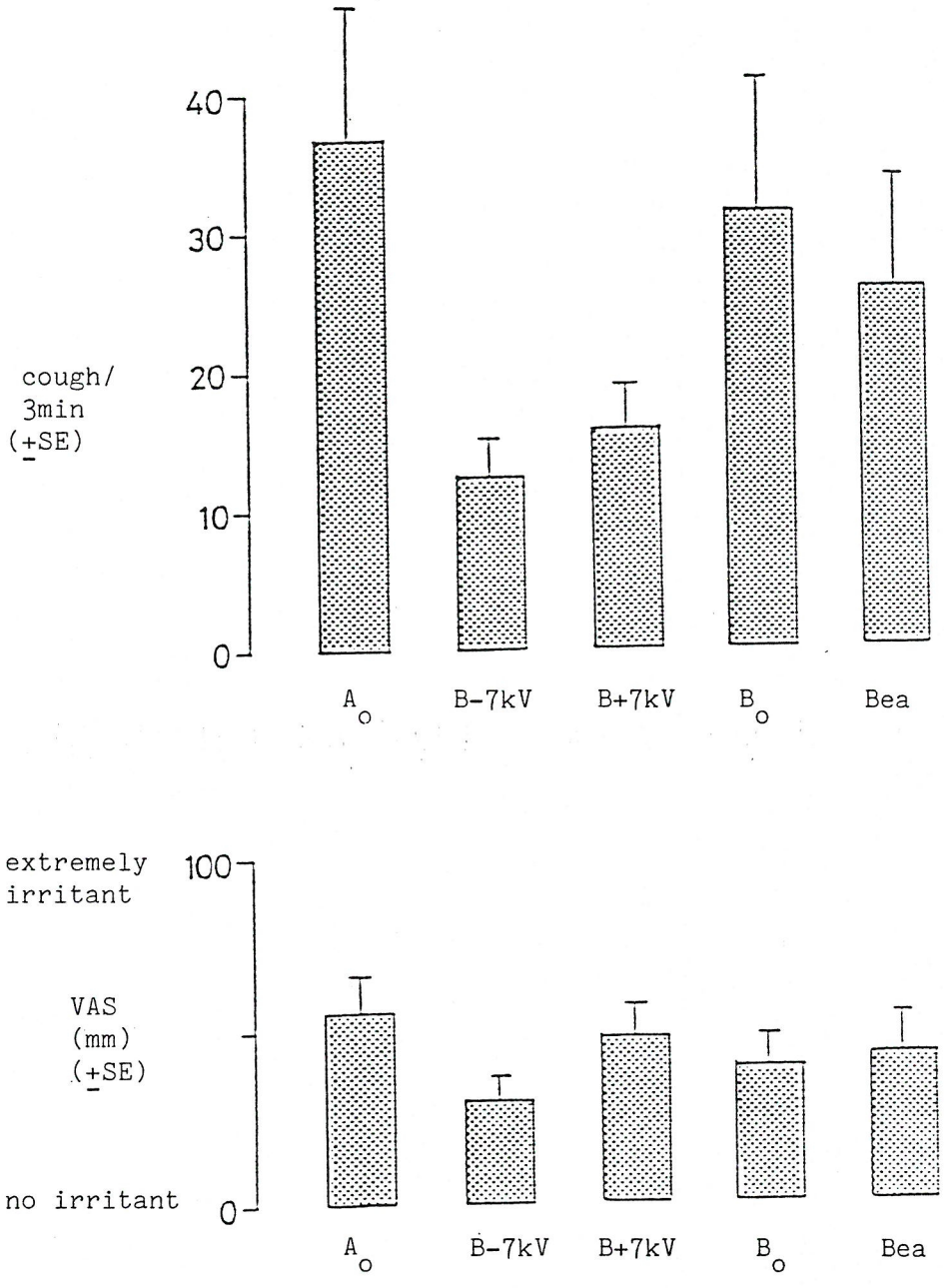

FIGURE I.46 Effect of electrical charge on airway response to ultrasonically nebulised water : asthmatic subjects

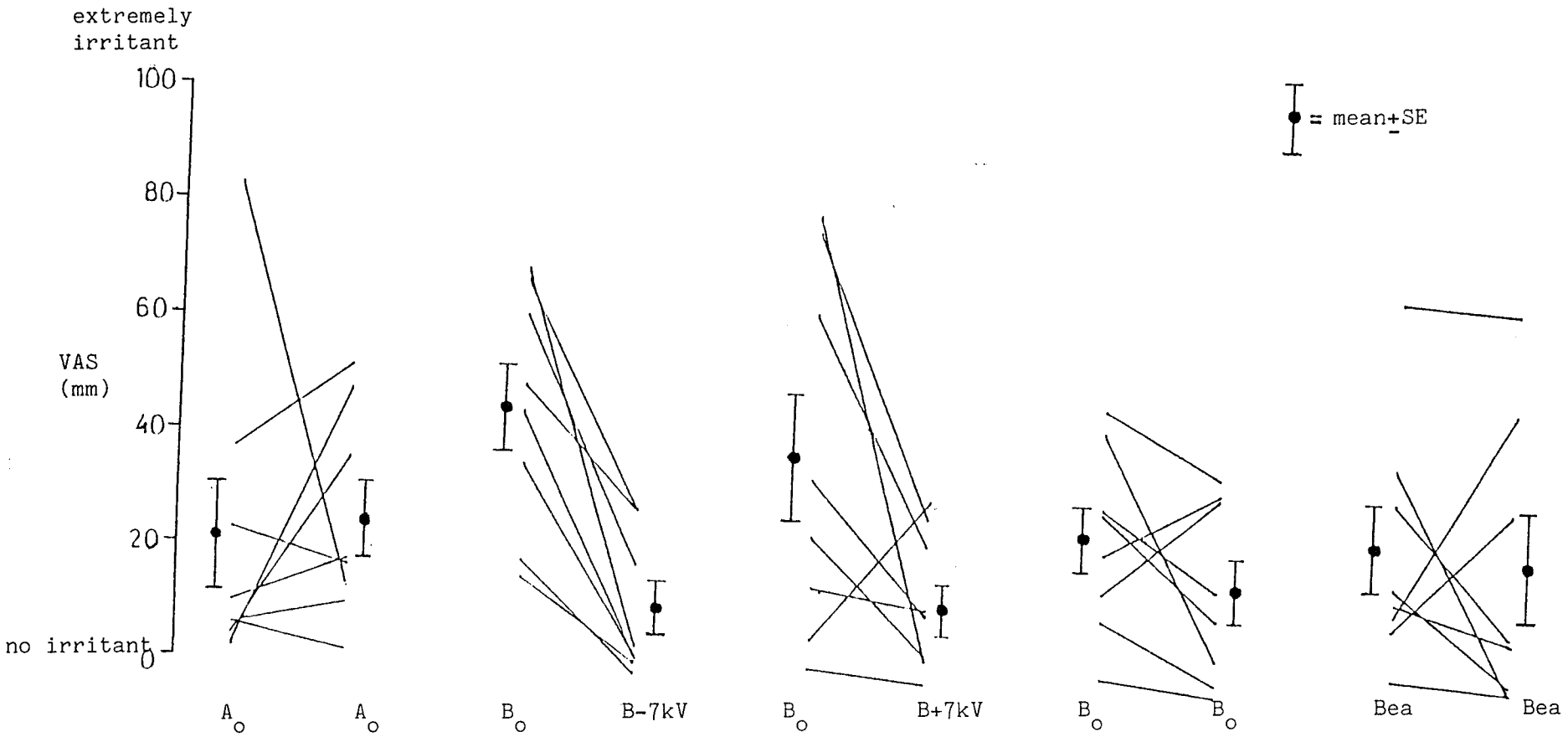

Showing 5 pairs of studies carried out on separate days in normal subjects

FIGURE I.47 Effect of electrical charge on irritation induced by ultrasonically nebulised water; normal subjects

aerosol cloud at high suction rates.

Thus to maximum the number of respirable droplets a JN should be driven at as high air-drive flow rate as possible and subjects should inhale at low inspiratory flow rates.

(d) Volume of solution placed within the nebuliser has no effect on aerosol MMD.

(e) MMD from a JN decreased with decreasing humidity and increasing temperature of the solution.

2.(a) Neutral droplets, charged droplets and free ions are present in the output aerosol from JN and UN.

(b) For JN's, the ion production rate increased with increasing air-drive flow rate, but the ratio of negative to positive ionic charge decreased. The ratio of ionic charge was found to be a function of the violence with which the liquid was disrupted.

(c) Ions and droplets of mobility $<0.004 cm^2 V^{-1} s^{-1}$ were found to have net zero charge, in the case of JN.

(d) The addition of electrolyte reduced the concentration of charged ions (about 3-orders of magnitude on addition of the initial small amount of electrolyte to the pure solution).

(e) No reproduc i ble current could be measured using aerosols generated by UN.

(f) The JN as well as the UN can be modified using an auxiliary corona electrode to manipulate the level of charge on droplets.

(g) The level of charge that can be imparted to the droplets generated by UN was found to be 2-orders of magnitude greater than the level of inherent charge. With JN, 1-order of magnitude difference was observed.

(h) For JN the charge-to-mass ratio increased with the drive-flow rate. For UN, charge-to-mass ratio varied in a random way.

3.(a) As the air-drive flow rate increased the mass output rate increased and the total '*operated time*' decreased.

(b) A rapid fall in temperature occurs within a JN. This fall increases with increasing gas-flow rate. The cooling is caused by heat loss due to latent heat evaporation, the new droplets surface area and to adiabatic expansion of air jet.

(c) The rate of cooling is dependent on the volume of the liquid within the nebuliser.

4. The irritant effects (cough and subjective sensation) of ultrasonically nebulised distilled water can be significantly reduced when the same aerosol is unipolarly charged. It was found that the irritant effects are related to the fluctuating electrical charge carried by the droplets.

PART

III

PREDICTIVE LUNG AND RESPIRATORY DEPOSITION MODEL

PART II

PREDICTIVE LUNG AND RESPIRATORY DEPOSITION MODEL

1. INTRODUCTION AND AIMS

The study of aerosol deposition and the distribution of deposition sites in the lung is important in the following: the evaluation of airborne health hazards, the administration of therapeutic drugs by inhalation, and the diagnosis of obstructive pulmonary disease.

Respiratory deposition occurs in a system of complex geometry, in which the air flow changes with time and direction (*inhalation* or *exhalation*). This complexity means that it is impracticable to predict deposition from basic theory and that empirically derived equations are needed.

Although numerous experimental and theoretical attempts have been made to determine the total and regional deposition (see glossary of terms) of inhaled aerosols in the human respiratory tract, uncertainty still exists regarding quantitative results. The experimental data in the literature shows a large amount of scatter, due not only to the usual difficulties experienced with aerosol experiments but also to the different experimental conditions and intersubject variation. A mathematical formulation for the calculation of aerosol deposition is called a "*deposition model*". Predictive models have been developed to estimate respiratory deposition; a recent review classifying these models was published by Heyder et al., 1984. Theoretical estimates of deposition require an idealised model of lung anatomy and air flow patterns. Calculations of this type have been performed by Findeisen, 1935, Landahl, 1950 and further by Beeckmans, 1960. The theory of Findeisen, Landahl and Beeckmans is steady-state in nature, and can only be used to predict particle deposition for a steady-state breathing cycle consisting of constant velocity of inhalation and exhalation.

In order to estimate the probability of removal of any particles from the air stream, it is necessary to establish a morphometric model for the structure of the respiratory tract. To this end, Weibel's symmetric lung model A, 1963, is used. The 1966, International Commission on Radiological Protection, Task Group on Lung Dynamics, defined the regions of the respiratory system, and using what has come to be referred to as the Task Group Model, concluded that deposition within the respiratory tract, for a wide range of particle sizes, could be estimated using a single aerosol parameter. That parameter is *the Median Mass Diameter* (MMD), illustrated previously in Figure I.4, Part I. There are, however,

discrepancies between the model developed by this Task Group and in *vivo* experimental measurements of Lippmann, 1977, Mercer, 1975, and Chain et al., 1980.

In 1975, Taulbee and Yu developed a time-dependent deposition theory based on a transport approach. Their theory gives more physical insight about air mixing and particle deposition in the lung. The governing equation in this theory has been solved numerically and applied to Weibel's lung model A. The theoretical predictions compare reasonably well with the experimental results for many arbitrary breathing conditions. Air mixing effects were initially considered but subsequently omitted because of experimental evidence, provided by Davies et al., 1972, that the influence of air mixing on aerosol deposition is negligible. In 1978, Yu produced an exact analytical solution for the transport equation which neglects air mixing. Yu's analysis gives a reasonably accurate prediction of total and regional deposition of inhaled aerosols in the lung, during steady breathing (Yu and Diu, 1983). Unfortunately Yu's theory is only applicable to deposition efficiencies which are very small, (Yu, 1987).

Electrification occurs naturally in most aerosol generating processes. It has been observed that most airborne dust particles in the industrial workplace (Vincent et al., 1983) and most therapeutic aerosols (Wehner, 1969; Hashish and Bailey, 1987) are electrically charged to levels above Boltzmann equilibrium. The charge carried by these particles may influence their deposition in the lung.

In *vivo* experiments in humans (Melandri et al., 1977, Tarroni et al., 1980, Melandri et al., 1983) and animals, (Fraser, 1966, Vincent et al., 1981, Ferin et al., 1983) have all shown a significant increase in lung deposition due to particle charge. Also, the electrostatic potential of an animal may have a strong influence on its reaction to an environmental aerosol in either natural or experimental situations, Longley, 1960. Theoretical studies (Yu, 1977, Yu and Chandra, 1978, Pich, 1978, Ingham, 1981, Chan et al., 1981, Luke et al., 1985, and Yu, 1985) support this finding and indicate that the main reason for this electrostatic enhancement is the image force which acts on charged particles situated near the walls of conducting airways.

When charge is present on an aerosol particle, its deposition efficiency is increased. Since, it has been necessary to deal with high deposition efficiencies in this study, Yu's approach had to be modified accordingly. Consequently, a lung deposition model, based on Yu's theory (1978, 1983) has been developed which can be implemented using a personal computer. It has advantages over Yu's original

treatment, since deposition efficiencies as high as unity can be considered with minimal computational effort.

The approach used has been to develop a model which will: (1) account for the depositional effect of charge on aerosol particles, (2) agree with experimental data, (3) be applicable to air pollution (health effects), health physics, aerosol therapy and industrial hygiene, and (4) be easily modifiable to incorporate differing requirements (eg. non spherical particles, alternative deposition efficiency expressions, different human and mammalian lung morphologies ...etc).

The aims of Part II are to develop and validate the deposition model so that it can be applied to observed data and used to predict the amount and site of deposition in the human respiratory tract under various breathing conditions.

Upper particle charge limits corresponding to: half the Rayleigh limit (Rayleigh, 1882) atomization charging (Smoluchowski, 1912) and corona charging (Pauthenier, 1932) are used in some of the calculations. These limits are used in a consideration of the *worst-case* conditions which might be encountered in an occupational environment involving freshly generated aerosols, in so far as air pollution is concerned. For therapeutic applications, which generaly require maximum deposition, these limits should be regarded as *best-case* conditions.

In order to proceed, it is first necessary to specify the physical characteristics of the human respiratory system and the breathing conditions.

2. HUMAN RESPIRATORY SYSTEM

From the standpoint of respiratory deposition, the human respiratory system can be divided into three regions, each covering one or more anatomical zones. These regions differ markedly in structure, size, airflow pattern; function and sensitivity to deposited particles.

The first is the *head region* (H), or extrathoracic region, which includes nose; mouth; pharynx and larynx. Inhaled air is warmed and humidified in this region. The second is the *tracheobronchial region* (TB), or conductive airways, which includes the airways from the larynx to the terminal bronchiales. This region resembles an inverted tree with a single trunk, the trachea, which subdivides into smaller and smaller airways. The third is the *alveolar region* (A), or pulmonary region, which includes the alveoli where gas exchange takes place.

Since no gas exchange across membranes takes place in the H and TB regions, these regions are often referred to as respiratory dead space. Figure II.1 shows the features of the human respiratory system.

Inhaled air and particles follow a flow path that passes through a sequence of 23 branches as it travels from the trachea to the alveolar sacs as shown in Figure II.2. The first 16 branches occur in the TB–region and the remainder in the A–region. Once deposited, particles are retained in the lung for varying times depending on their chemical properties, their location within the lung, and the clearance mechanism involved, Hinds, 1982b.

The airway surfaces of the first two respiratory regions are covered with a layer of mucus that is slowly propelled by ciliary action to the pharynx where particles which were deposited on the wall of the dead space airways are swallowed; sneezed away or spat out in a matter of hours. The A–region does not have this protective mucous layer because of its gas–exchange function. Insoluble particles deposited in the A–region are cleared very slowly over a period of months. Soluble particles pass through the thin alveolar membrane into the blood–stream.

3. THE PHYSICS OF THE LUNG AND BREATHING

The respiratory system of a normal adult processes 10–20m^3 (12–24kg) of air per day. The gas–exchange area of the lungs is about 80m^2 and is perfused with over 2000km of capillaries, Cameron et al., 1978. The volume of air breathed in and out in a single quiet respiration is abut 500mℓ, this being termed "*the resting tidal volume* (TV)". A violent inspiratory effort can take into the lungs about 2500mℓ measured from the resting respiratory level (R.R.L.) which by convention is taken as the end of normal expiration (see Figure II.3). This is called "*the inspiratory capacity*", it includes the resting tidal volume and "*the inspiratory reserve volume*".

After quiet expiration (500mℓ), it is possible by a violent expiratory effort to blow out approximately 1300mℓ of air, this is "*the expiratory reserve volume* (ERV)". Even after the deepest possible expiration the lungs and respiratory passage still contain about 1600mℓ of air, this is "*the residual volume*". At the end of quiet expiration, the lung contains "*the expiratory reserve volume* (ERV)" and the residual volume which together are called "*the function residual capacity* (FRC)" ~ 3000mℓ. This large volume prevents rapid change in the

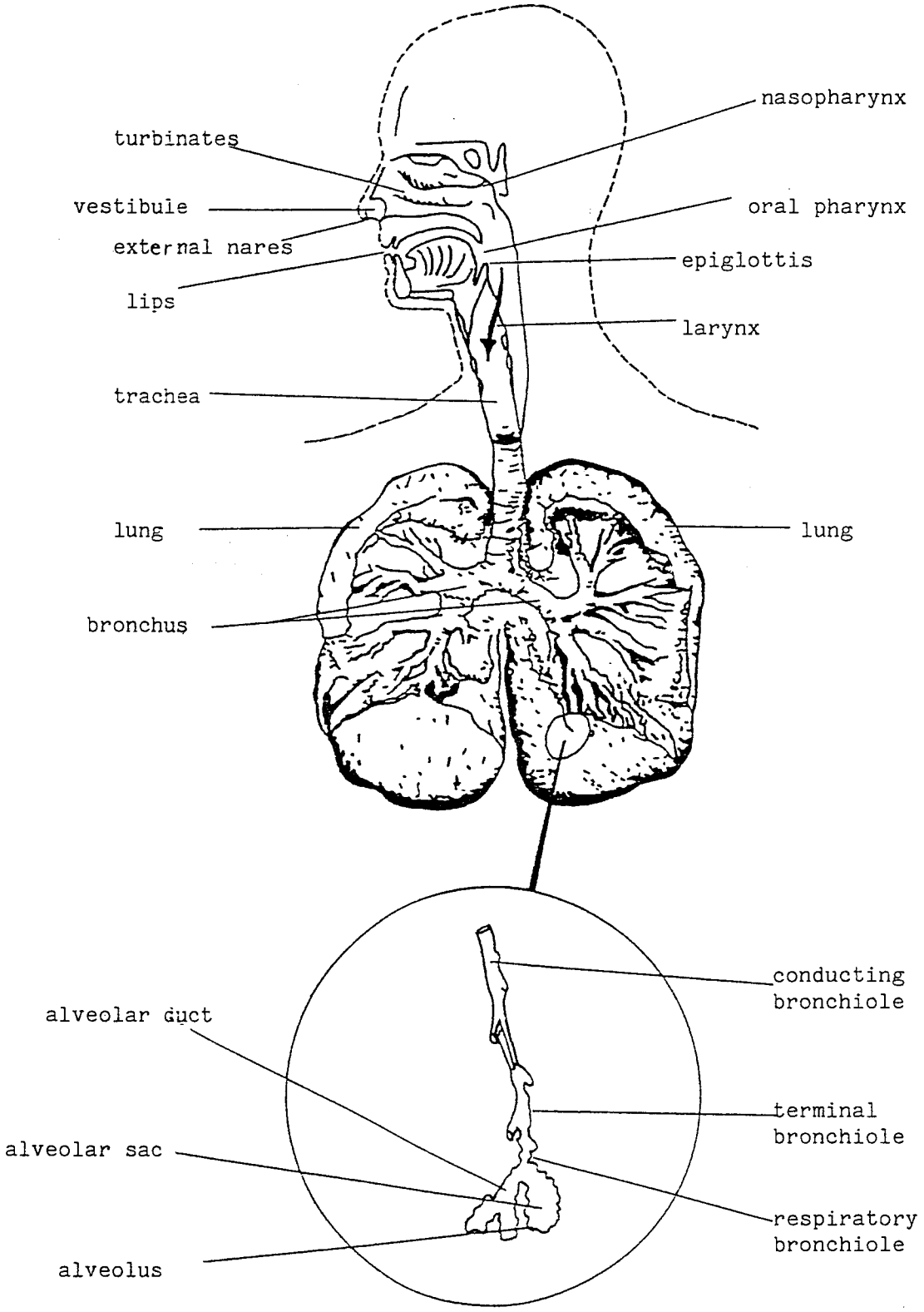

FIGURE II.1 The respiratory system [adapted from the Handbook of Air Pollution USPHS - 999 - AP - (1968)]

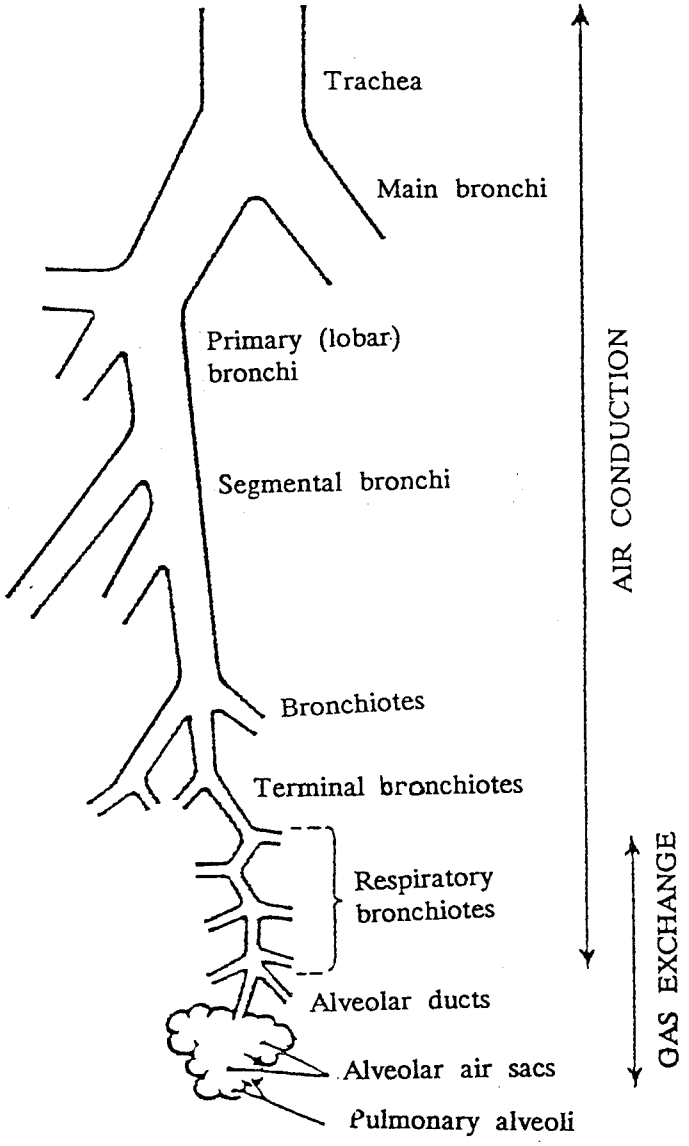

FIGURE II.2 THE AIR PASSAGES

There are approximately 23 orders of branching between the bifurcation of the trachea and the alveolar sacs.

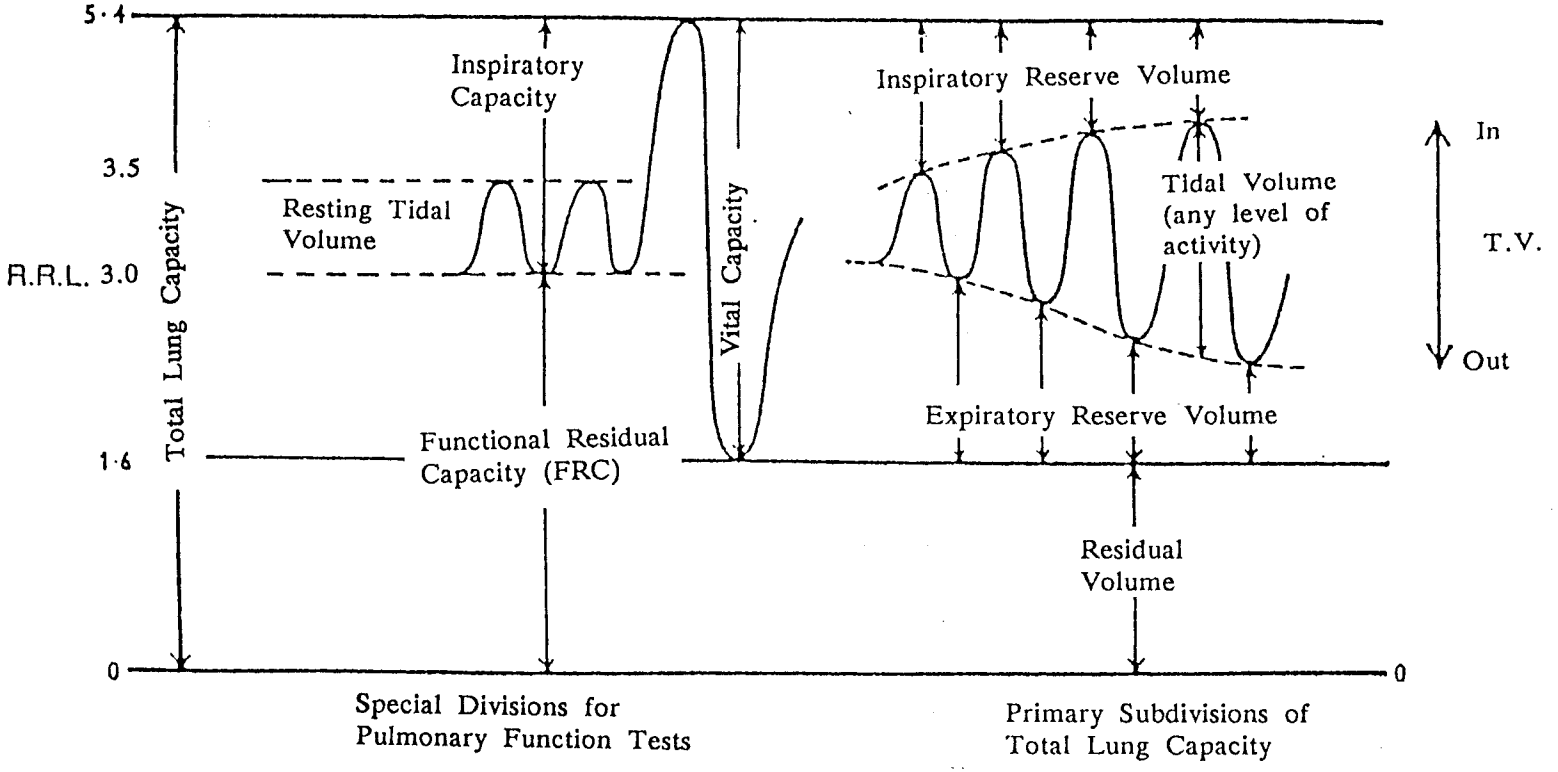

FIGURE II.3 ILLUSTRATION OF THE SUBDIVISIONS OF THE LUNG CAPACITY

composition of the alveolar air and the collapse of the alveoli after deep expiration, Guyton, 1986.

A resting adult breathes about 12–15 times a minute and this rate triples during heavy work. The amount of air breathed in per minute is called "*the respiratory minute volume*", since the respiratory rate at rest is about 12 per minute and the tidal volume of 500mℓ, the minute volume is about 6 litres. In exercises it may go up to 100 litres.

In normal breathing, fresh air pushes the residual air ahead of it so that the fresh air travels only as far as the alveolar ducts. Nevertheless, gas exchange takes place rapidly by diffusion of O_2 and CO_2 over the very short terminal distances (<1mm).

The airway size in the external nares, and probably parts of the nasal pharynx as well, contracts at high air flow rates; thus these areas of the respiratory system serve as flow-limiting regions, Hinds (1980). Mouth breathing by-passes this flow-limiting region and permits greater inspiratory flow rates. As shown in Table II.1, during steady inhalation of 1ℓ/s, the velocity of air penetrating the first few airways increases because the diameter of the airways decrease from generation to generation. Subsequently, however, the velocity of the air decreases distally because the total cross-sectional area of the airways increase due to increasing number of tubes. In the trachea and the main bronchi, air flow is turbulent at the peak inspiration and expiration flow rates for the normal breathing cycle. The remaining air flow is laminar (smooth) under all conditions but, because the airway lengths are very short compared to their diameters, the flow of gases in these smaller airways is not fully developed laminar flow. This complicates mathematical analysis and modelling.

Note: The air velocities given in Table II.1 are based on steady flow rates, whereas during actual breathing the flow is cyclical, reversing several times per minute.

4. FACTORS AFFECTING PARTICLE DEPOSITION

Particles are deposited in the various regions of the respiratory tract by a variety of physical mechanisms. Deposition efficiency in each region depends on: (1) physical properties of the aerosol particles; (2) the breathing characteristics; and (3) the airway characteristics.

4.1 Deposition Mechanisms

There are five mechanisms by which significant particle deposition can occur within the respiratory tract: impaction; sedimentation; diffusion; interception and electrostatic deposition. The particles will deposit by a combination of all of these mechanisms. Figure II.4 illustrates the different deposition mechanisms.

4.1.A Inertial impaction

During inhalation, the incoming air must negotiate a series of direction changes as it flows from the nose or mouth down through the branching airway system. Each time the air changes direction, the momentum of particles tends to keep them on their pre-established trajectories, which can cause them to impact on airway surfaces. The net result is the deposition of some of the particles near the airway surfaces which is termed "*inertial impaction*".

The maximum distance a particle will continue along its original trajectory is its *stopping distance*, ds,

$$d_s = v\,\tau$$

where, v is the air velocity and τ is the relaxation time. Table II.2, provides the ratios of particle stopping distance to airway dimensions at velocities associated with a steady inhalation of 1ℓ/s at selected regions of the lung. The probability of deposition by impaction depends on this ratio and is highest in the TB-region, i.e. impaction is of primary concern in the large airways.

It is also dependent on the location of the particles within the airways. For example, in a bifurcation airway, deposition probability on inhalation is much higher for a particle travelling along the centre line of the parent tube than for particles moving nearer to the walls, and the most likely deposition sites are at or near the carina of the bifurcation. The maximum deposition by impaction occurs at the throat, the first airway bifurcation and to a lesser degree at other bifurcations, Brain et al., 1979. This is because the air streamline bends most sharply in these areas and passes close to the bifurcation. It is known that inertial impaction depends upon aerodynamic diameter and air flow rate, Heyder et al., 1980. No adequate mathematical model exists for impaction deposition in the bronchial tree, Lippmann, 1977.

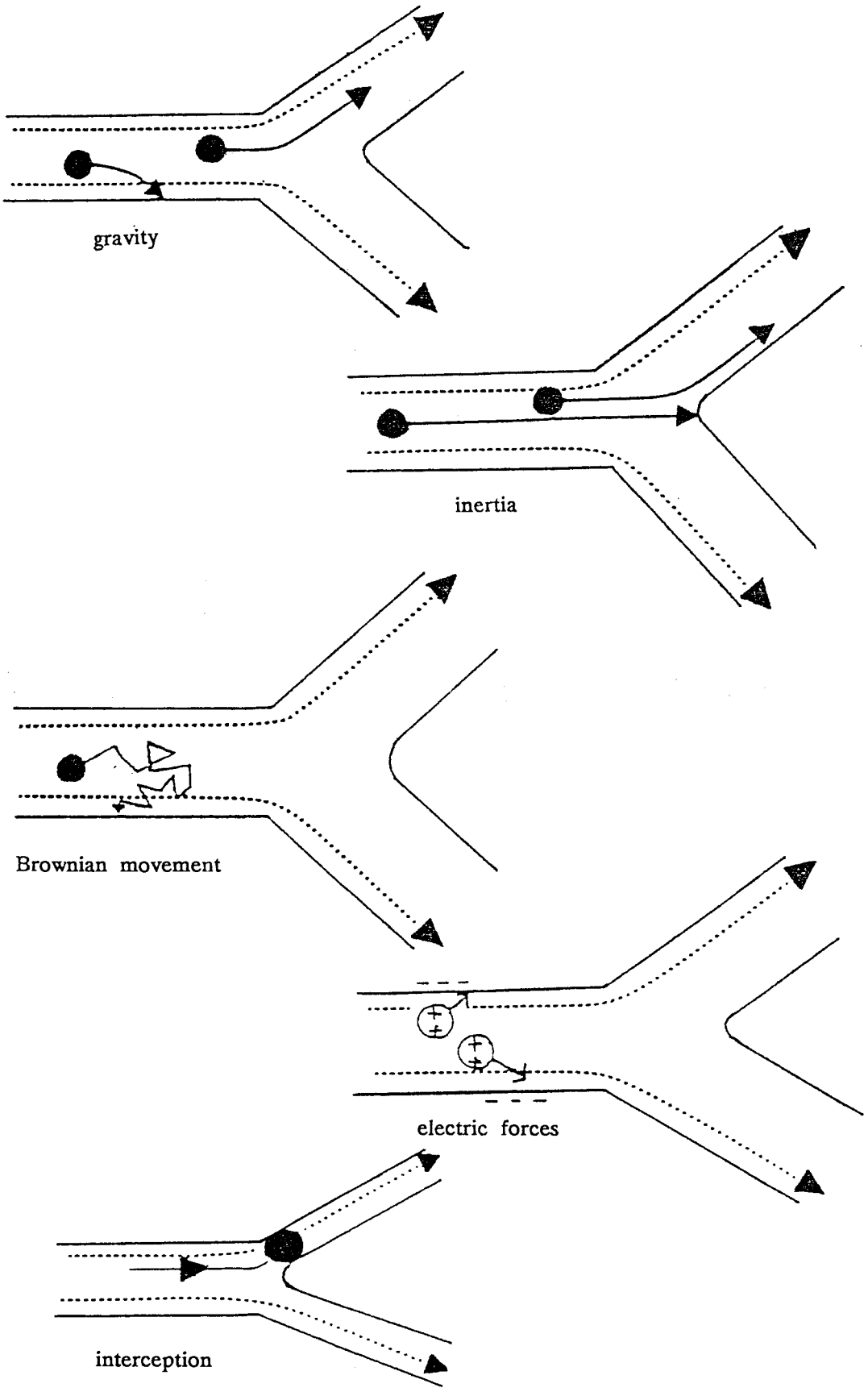

FIGURE II.4 MECHANISMS OF DEPOSITION IN THE RESPIRATORY TRACT

TABLE II.1

Architecture of the human lung based on Weibel's Model A : Average adult lung with volume 4800cm³ at about three-fourths maximal inflation

Airway	Generation	Number Per Gen.	Diameter, mm	Length, mm	Cum. Length, mm	Total Cross Section, cm²	Volume, cm³	Cum. Volume, cm³	At flow rate = 1.0 ℓ/s		
									Velocity cm/s	Residence Time, ms	Reynolds Number
Trachea	0	1	18.0	120.0	120.0	2.54	30.5	30.5	393	30.5	4350
Main bronchus	1	2	12.2	47.6	167.6	2.33	11.3	41.8	427	11.1	3210
Lobar bronchus	2	4	8.3	19.0	186.6	2.13	4.0	45.8	462	4.11	2390
	3	8	5.6	7.6	194.2	2.00	1.5	47.2	507	1.50	1720
Segmental bronchus	4	16	4.5	12.7	206.9	2.48	3.5	50.7	392	3.23	1110
Bronchi with cartilage in wall	5	32	3.5	10.7	217.6	3.11	3.3	54.0	325	3.29	690
	6	64	2.8	9.0	226.6	3.96	3.5	57.5	254	3.55	434
	7	128	2.3	7.6	234.2	5.10	3.9	61.4	188	4.04	277
	8	256	1.86	6.4	240.6	6.95	4.5	65.8	144	4.45	164
	9	512	1.54	5.4	246.0	9.56	5.2	71.0	105	5.15	99
	10	1.02 K	1.30	4.6	250.6	13.4	6.2	77.2	73.6	6.25	60
Terminal bronchus	11	2.05 K	1.09	3.9	254.5	19.6	7.6	84.8	52.3	7.45	34
Bronchioles with muscle in wall	12	4.10 K	0.95	3.3	257.8	28.8	9.8	94.6	34.4	9.58	20
	13	8.19 K	0.82	2.7	260.5	44.5	12.5	106	23.1	11.7	11
	14	16.4 K	0.74	2.3	262.8	69.4	16.4	123	14.1	16.2	6.5
	15	32.8 K	0.66	2.0	264.8	113	21.7	145	8.92	22.4	3.6
Terminal bronchiole	16	65.5 K	0.60	1.65	266.5	180	29.7	175	5.40	30.6	2.0
Respiratory bronchiole	17	131 K	0.54	1.41	267.9	300	41.8	217	3.33	42.3	1.1
Respiratory bronchiole	18	262 K	0.50	1.17	269.0	534	61.1	278	1.94	60.2	0.57
Respiratory bronchiole	19	524 K	0.47	0.99	270.0	944	93.2	371	1.10	90.0	0.31
Alveolar duct	20	1.05 M	0.45	0.83	270.9	1.60 K	140	510	0.60	138	0.17
Alveolar duct	21	2.10 M	0.43	0.70	271.6	3.22 K	224	735	0.32	213	0.08
Alveolar duct	22	4.19 M	0.41	0.59	272.1	5.88 K	350	1085	0.18	326	0.04
Alveolar sac	23	8.39 M	0.41	0.50	272.6	11.8 K	591	1675	0.09	553	
Alveoli, 21 per duct		300 M	0.28	0.23	272.9		3200	4875			

TABLE II.2

Relative importance of Impaction, sedimentation and diffusion mechanisms for deposition of unit-density particles at selected regions of the lung (at steady flow of 1 ℓ/s).

Airway	Inertial Impaction Stopping distance[1] / Airway Diameter			Gravity Settled Distance[2] / Airway Diameter			Brownian motion RMS Displacement[3] / Airway Diameter		
	0.1μm	1.0μm	10.0μm	0.1μm	1.0μm	10.0μm	0.1μm	1.0μm	10.0μm
Trachea	~0	0.0008	0.068	~0	~0	0.0052	0.0004	0.0001	~0
Main bronchus	~0	0.0013	0.109	~0	~0	0.0041	0.0003	0.0001	~0
Segmental bronchus	~0	0.0031	0.272	~0	~0	0.0022	0.0005	0.0001	~0
Terminal bronchus	~0	0.0017	0.149	~0	0.0002	0.021	0.0029	0.0006	0.0002
Terminal bronchiole	~0	0.0003	0.028	~0	0.0018	0.156	0.011	0.0022	0.0006
Alveolar duct	~0	~0	0.0023	0.0004	0.017	1.52	0.0039	0.0079	0.0023
Alveolar sac	~0	~0	0.0007	0.0012	0.047	4.13	0.067	0.013	0.004

(1) Stopping distance = air velocity × relaxation time

(2) Settled distance = settling velocity × residence time in each airway

(3) RMS displacement = SQR (diffusion coefficient × residence time)

4.1.B Gravitational sedimentation

All particles having density greater than that of air experience a downward force due to gravity. Such particles accelerate, under the force of gravity, to their settling velocities at which time the gravitational force is balanced by air resistance. Sedimentation is an important contribution to deposition in the smaller airways and in the A-region, where flow velocities are low and airway dimensions are small. Processes of sedimentation have a maximum effect in those airways that are oriented horizontally, Hinds, 1980.

Table II.2 includes the ratio of *settling distance* (terminal settling velocity × residence time in each airway at a steady flow of 1ℓ/s) to airway diameter. As can be seen this ratio and this mechanism are most important in the distal (farthest from trachea) airways.

4.1.C Diffusion

Submicron particles in air undergo a random motion (Brownian motion) caused by collisions with gas molecules. The expected degree of displacement of a particle as a result of Brownian motion increases as particle size decreases and is independent of particle density. Table II.2 includes the ratio of *the root mean square displacement* during residence in each generation to airway diameter of that generation, and this determines the probability of deposition by diffusion. Diffusional deposition is important in the small airways and alveoli and at airway bifurcations for particle sizes below ~ 0.5μm in diameter and is governed by geometric rather than aerodynamic size.

The same airway and flow conditions that favour sedimentation also favour diffusion (that is, long residence time and small airway diameter).

4.1.D Interception

Interception is the process by which a particle, although it does not deviate from its gas streamline, contacts the airway surfaces because of its physical size such as when a particle moves into an airway narrower in size than the particle diameter.

The chance of deposition by interception depends on the proximity of the gas streamline to the airway surface and on the ratio of particle size to airway diameter, which is usually small even in the smallest airways. Interception,

generally is less important than the other deposition mechanisms and is usually significant only for fibrous particles.

4.1.E Electrostatic deposition

The electric charge on an aerosol particle affects its behaviour in three ways: (1) in the absence of other forces, a charged particle will move along an electric field line; (2) droplet evaporation, condensation and coagulation are altered; (3) particles are attracted to neutral surfaces by the image charge induced.

Since negligible electric fields exist within the air spaces of the respiratory system, which will act as a Faraday cage, Longley, 1960, the first consideration does not apply. Except for the collection of water, the second factor is of primary importance in altering the aerosol characteristics while it is still outside the respiratory tract. Therefore, once inhaled, the only electrical force of importance to deposition is the attraction between the charge on the particle and its image on the collecting surface, which is uncharged and electrically conducting.

In general, particles with high electric mobility can have an enhanced respiratory tract deposition even though no external field is applied across the chest. The electrostatic enhancement of particle deposition, when it does occur, takes place predominantly in the A–region, Yu (1985). In practice, most ambient aerosols have reached charge equilibrium and have relatively low charge levels. Thus the deposition due to charge is usually small compared to deposition by the mechanical mechanisms. It is possible, however, that some industrial processes could produce very highly charged aerosols, for example, in milling and grinding of materials, powder handling operations generally and also during electrostatic spraying of paints and pesticides, leading to significant enhancement of lung deposition (see Part III).

Figure II.5, summarises the main physical mechanisms for the deposition of inhaled aerosol particles in the different regions of the respiratory system.

4.2 Physical properties of the aerosol particles

The most important aerosol properties governing where in the respiratory tract deposition may occur are particle size, shape, density and charge. Particle size can be expressed as the geometrical size of the particle or described in terms of some type of "*equivalent size*". The aerodynamic diameter standardizes all particles for both shape and density by expressing the size of the particle as the

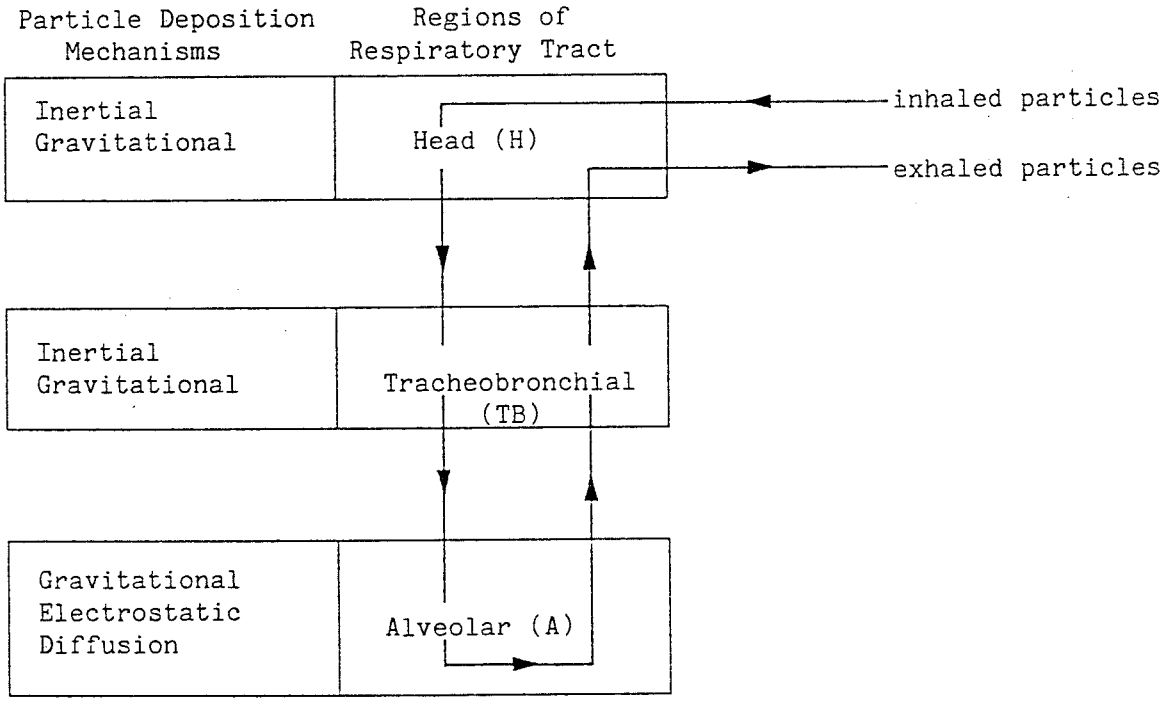

FIGURE II.5 Schematic diagram of the regions of the respiratory tract, indicating the main mechanisms for deposition of inhaled particles

diameter of a unit density sphere with the same aerodynamic characteristics (eg. settling velocity) as the particle in question.

Aerodynamic diameter is the most appropriate parameter in terms of particle deposition by impaction and sedimentation which usually accounts for most of the deposition by mass in the head and lungs. On the other hand, diffusional transport, which is the dominant mechanism for particles $< 0.5\mu m$ in diameter, depends only on particle size and not on density or shape.

The growth kinetics and the change in size that may take place within the respiratory tract depend on the hygroscopicity of the particles which, for aqueous droplets depends on the concentration of water soluble compounds in the droplet, Lippmann (1977). Electrostatic charges on particles may significantly enhance their deposition as discussed before.

4.3 The Breathing Characteristics

Inhaled particles will deposit along the air passages between the point of entry at the lips or nose and larynx. The amount of particles entering the lung depends upon the mode and the route of entry in the head. Normally, the nasal route collects more particles than the oral, because it has nasal hairs and a more complex air passage. Inhalation through the mouth is usual, because airway resistance is lower there than in the nasal passage.

One of the important respiratory characteristics affecting deposition is the air velocity. Increasing velocity increases impaction deposition, but decreases sedimentation and diffusion by decreasing residence time. During exhalation, the flow profiles within the airways differ from those during inhalation and will affect particle deposition probabilities, especially for the impaction mechanism. The flow is cyclical and reverses many times per minute. At its peak, it may be turbulent in the trachea, but the Reynolds number decreases with increasing lung depth, so that in the smaller conducting airways it is always laminar, and in the alveolar region it is always viscous (ie. inertial forces will be negligible).

The tidal volume is an important respiratory parameter. The air inhaled at the start of each breath goes deeper into the lung and remains there longer than the air inhaled later in the breath. It follows that the deeper the air goes and the longer it stays, the greater is the deposition of inhaled particles.

4.4 The Airway Characteristics

Individual variations in airway anatomy affect particle deposition in several ways: (1) the *diameter* of the airway determines the displacement required by the particle before it contacts the airway surface, and (2) the *cross-section area* of the airway determine the flow velocity for a given volumetric flow rate. Velocity affects particle deposition as discussed earlier, (Section 4.1).

The effects of airway diameter and length, for a particular lung, on deposition probability depend on the deposition mechanisms as well as the particle and respiratory parameters. Airway radius has the greatest effect on impaction and diffusion, since air velocity and diffusion rate vary as the inverse square of the radius, Lippmann (1977), the radius has less effect on sedimentation. Airway length has no direct effect on impaction, which takes place because of changes in direction. Sedimentation and diffusion vary with residence time in the airway which in turn is directly proportional to length.

5. WEIBEL'S MORPHOMETRIC MODEL

It is well recognised that the deposition of inhaled particles in the human respiratory tract depends upon the anatomic structure and physical dimensions of the airways. The anatomical model of the respiratory tract used in our calculations is based on Weibel's symmetric lung model "A" (1963). Weibel's model has been widely used in the literature for studying gas diffusion and particle deposition because of its simplicity and it gives a median deposition among all existing models, Yu et al. (1982).

The morphometric measurements made by Weibel, see Table II.1, correspond to excised lungs at three-quarters maximum inflation. When breathing at the normal FRC, Weibel's data of airway dimensions should be scaled down, see Tables (II.3 A and B).

Since detailed measurements of airway dimensions at different levels of lung inflation are not yet available, an assumption has been made that the airway diameters and lengths are proportional to the one-third power of the lung volume. These relationships between airway dimensions with the lung volume were suggested by Hughes et al. (1972), from the measured data of dog lungs. See Appendix II.A for more details.

TABLE II.3.A

"Lung Model of Weibel Adjusted to 3000cm³ Lung Volume"

Generation Number	Number of Airways	Length ℓ(cm)	Diameter d(cm)	Airways Volume (cm^3)	acc. lung Volume (cm^3)*
0	1	10.260	1.539	19.06	19.06
1	2	4.070	1.043	6.57	25.63
2	4	1.624	.710	3.00	28.63
3	8	.650	.479	.87	29.50
4	16	1.086	.385	2.19	31.69
5	32	.915	.299	2.06	33.75
6	64	.769	.239	2.19	35.94
7	128	.650	.197	2.44	38.38
8	256	.547	.159	2.75	41.13
9	512	.462	.132	3.25	44.38
10	1024	.393	.111	3.87	48.25
11	2048	.333	.093	4.75	53.00
12	4096	.282	.081	6.13	59.13
13	8192	.231	.070	7.12	66.25
14	16384	.197	.063	10.88	77.13
15	32768	.171	.056	13.56	90.69
16	65536	.141	.051	18.56	109.25
17	131072	.121	.046	26.36	139.31
18	262144	.100	.043	38.07	190.60
19	524288	.085	.040	56.00	288.16
20	1048578	.071	.038	84.43	512.04
21	2097152	.060	.037	135.29	925.04
22	4194304	.050	.035	201.77	1694.16
23	8388608	.043	.035	347.04	3000.00

* Including Alveolar Volume

TABLE II.3.B

Alveolar Volume and Number of Alveoli for Weibel's Model Adjusted to 3000cm^3 Lung Volume

Generation Number	No. of Alveoli per		Total Alveoli Volume (cm^3)	Volume of one* alveolus (cm^3)
	duct	generation		
17	5	655360	3.70	5.64575×10^{-6}
18	8	2097152	13.22	6.30378×10^{-6}
19	12	6291456	41.56	6.60578×10^{-6}
20	20	20971520	140.35	6.69240×10^{-6}
21	20	41943040	276.81	6.59966×10^{-6}
22	20	83886080	567.35	6.76333×10^{-6}
23	17	1.42606×10^8	958.80	6.72341×10^{-6}

* Total alveoli volume = 2001.79cm^3
Total number of alveoli = 2.9845×10^8
$\therefore$ Average volume of one alveolus = 6.70728×10^{-6}cm^3

6. PREDICTIVE LUNG DEPOSITION MODEL

In order to establish a starting position, the model according to Yu (1978, 1983) is presented and later modified to account for high deposition efficiencies.

6.1 Yu's Theory of Lung Deposition

The anatomical model of the respiratory tract adopted in this study is *trumpet shaped*, as proposed by Scherer et al. (1972). Each airway generation is represented by a cylinder whose length decreases and diameter increases with penetration into the lung. The cross-sectional area of each cylinder is representative of all the airways associated with a particular generation and is quantified in Weibel's model A. In the final seven generations, the alveolar region, additional volume is present accounting for the alveoli (see Figure II.6).

Let the average concentration at a given airway depth x and time t be

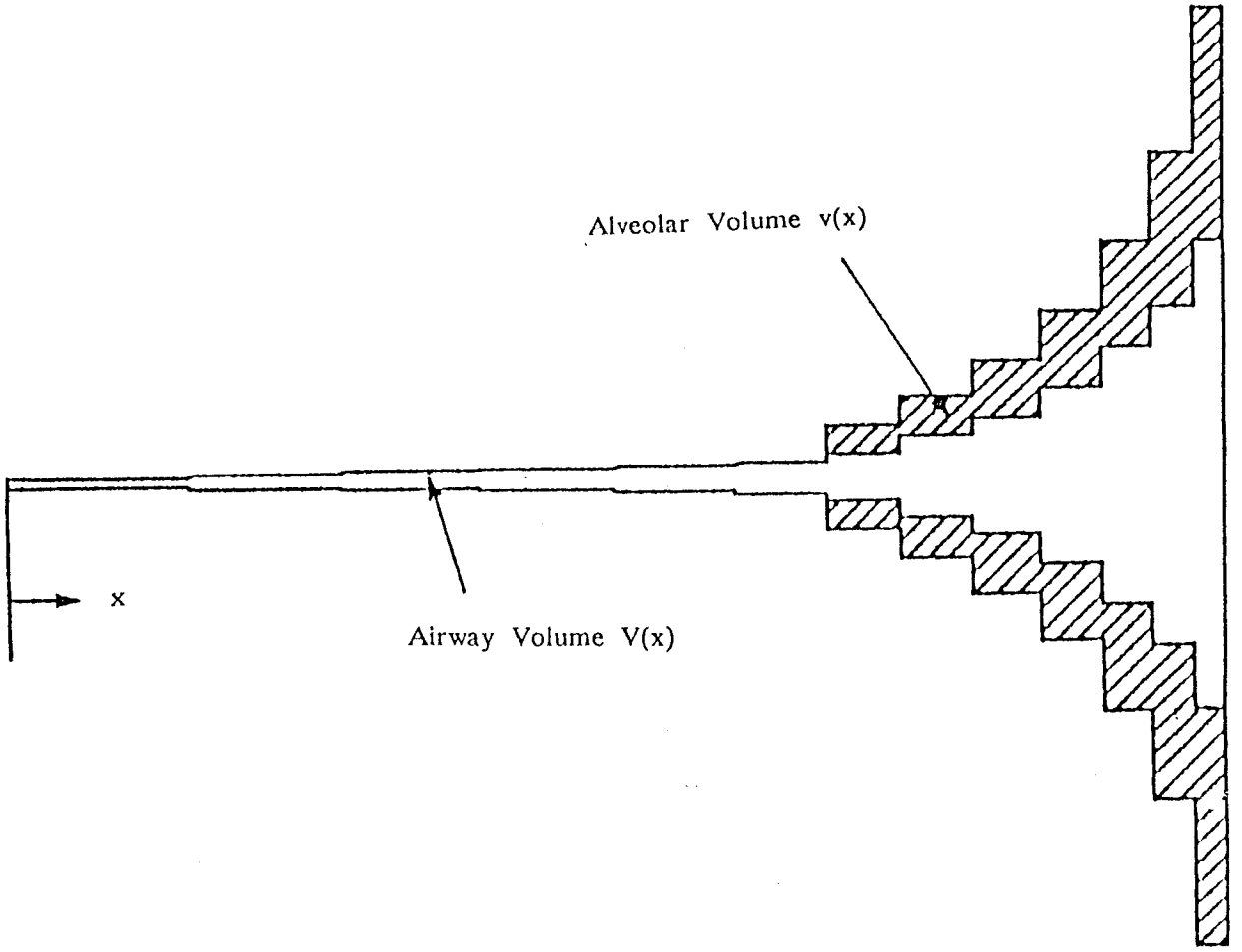

FIGURE II.6 SCHEMATIC OF HUMAN LUNG AIRWAYS
(Trumpet Model)

c. Then during the breathing cycle, which includes inhalation, pause and exhalation, the equation of particle conservation (*transport equation*) has the form:

$$\frac{\partial}{\partial t}(Ac) + \frac{\partial}{\partial x}(Qc) = -\lambda c \qquad (1)$$

where: A = cross-sectional area of the airway and alveoli at depth x and time t.

λc = particle loss to the airway surfaces per unit length per unit time.

Q = air flow rate ($Q > 0$ for inhalation, $Q = 0$ for pause and $Q < 0$ for exhalation)

As the lung expands and contracts, the flow rate Q varies with x. The conservation of air mass requires:

$$\frac{\partial A}{\partial t} + \frac{\partial Q}{\partial x} = 0 \qquad (2)$$

which is the continuity equation.

Yu et al. (1979), assumed the expansion and contraction to be uniform over the entire lung inhalation and exhalation, so that:

$$\frac{\partial A}{\partial t} = A^* Q_o / V_\ell^* \qquad (3)$$

where: A^* = cross-sectional area of airway and alveoli at the start of inhalation A(x,o)

V_ℓ^* = total rest lung volume

Q_o = flow rate at the beginning of the trachea (x = 0)

Assuming Q to be time independent, equation (2) can be integrated with respect to x, and using equation (3) gives:

$$Q(x) = Q_o \left[1 - \frac{V_x^*}{V_\ell^*} \right] \qquad (4)$$

where: V_x^* = the cumulative rest lung volume from 0 to x.

From equation (3) it follows that:

$$A = A^* \left[1 + \frac{v_t}{V_\ell^*} \right] \tag{5}$$

where: v_t = tidal volume

$$v(t) = \int_0^t Q_o \, dt = Q_o t \qquad \text{for inhalation} \tag{6}$$

and

$$v(t) = \int_t^T Q_o \, dt = Q_o(T-t) \qquad \text{for exhalation} \tag{7}$$

where: T = period of a breathing cycle.

Using equations (2) and (3), equation (1) reduces to:

$$A^* \left[1 + \frac{v_t}{V_\ell^*} \right] \frac{\partial c}{\partial t} + Q \frac{\partial c}{\partial x} = -\lambda c \tag{8}$$

During the pause, since Q = 0, equation (1) takes the form:

$$A^* \left[1 + \frac{v_{t_1}}{v_\ell^*} \right] \frac{\partial c}{\partial t} = -\lambda c \tag{9}$$

where: t_1 = time at the end of inhalation

v_{t_1} = tidal volume at the end of inhalation

λc = the particle loss per unit time during the pause (deposition mechanisms are different from inhalation and exhalation cases)

6.1.A Solution of the transport equation

Consider a respiratory cycle consisting of:

(i) inhalation with constant flow rate $Q_o = Q_{oi}$ from t = 0 to t_1,

(ii) a pause from t_1 to t_2, and

(iii) exhalation with constant flow rate $Q_o = - Q_{oe}$ from t_2 to T.

6.1.A.1 Inhalation solution

Equation (8) may be rewritten as:

$$A^* \left[1 + \frac{t}{\tau_i} \right] \frac{\partial c}{\partial t} + Q \frac{\partial c}{\partial x} = -\lambda c \qquad (10)$$

where: $\tau_i = V^*_\ell / Q_{oi}$

The characteristic equations of equation (10) are:

$$\frac{\tau_i \, dt}{(\tau_i + t)} = \frac{A^* \, dx}{Q} = \frac{-A^* \, dc}{\lambda c} \qquad (11)$$

which can be integrated as follows:

$$\int_{c_o}^{c} \frac{dc}{c} = \int_{o}^{x} -\frac{\lambda}{Q} \, dx$$

where:

$c = c_o$ at $x = 0$ for $0 \leq t \leq t_1$

$$\therefore \quad c = c_o \exp \int_{o}^{x} \frac{-\lambda}{Q} \, dx \qquad (12)$$

Equation (12) is valid for $x \leq x'$ where x' is the position of the aerosol front obtained by integrating the first equality of equation (11).

$$\tau_i \, \ell n \left[1 + \frac{t}{\tau_i} \right] = \int_{o}^{x'} \frac{A^*}{Q} \, dx \qquad (13)$$

Using equation (4) and the definition $dV^*_x = A^* dx$, equation (13) becomes:

$$\ell n \left[1 + \frac{t}{\tau_i} \right] = \int_{o}^{x'} \frac{A^*}{\left[V^*_\ell - V^*_x \right]} \, dx = \int_{o}^{V^*_{x'}} \frac{dV^*_x}{\left[V^*_\ell - V^*_x \right]}$$

$$\ell n\left[1 + \frac{t}{\tau_i} \right] = \ell n \left[\frac{V_\ell^*}{V_\ell^* - V_x^*} \right]$$

$$\therefore \quad \frac{V_{x'}^*}{V_\ell^*} = \frac{t}{t + \tau_i} \tag{14}$$

It is conventional to discretize the integral in equation (12) and to use *deposition efficiency* η_i (see Section 6.6) instead of *deposition constant* λ_i (Yu and Diu, 1983) as follows:

For small deposition efficiencies:

$$\eta_i = \frac{\lambda_i \ \ell_i}{Q_i} \tag{15}$$

If the individual airways are considered, equation (12) becomes:

$$c_n = c_o \exp \left[- \sum_{i=1}^{n} \int_{x_{i-1}}^{x_i} \frac{\lambda_i}{Q_i} \, dx \right] \tag{16}$$

If λ and Q are assumed to be constant in any airway:

$$c_n = c_o \exp \left[- \sum_{i=1}^{n} \frac{\lambda_i}{Q_i} \int_{x_{i-1}}^{x_i} dx \right]$$

$$\therefore \quad c_n = c_o \exp \left[- \sum_{i=1}^{n} \frac{\lambda_i \ \ell_i}{Q_i} \right] \tag{17}$$

Using equation (15), equation (17) becomes:

$$c_n = c_o \exp \left[- \sum_{i=1}^{n} \eta_i \right]$$

$$\therefore \quad c_n = c_o \prod_{i=1}^{n} \exp\left[-\eta_i \right] \tag{18}$$

Using the definition of η_i (specified in section 6.7), the aerosol concentration can be determined.

6.1.A.2 Exhalation solution

For exhalation, the transport equation has the form:

$$A^* \left[1 + \frac{T-t}{\tau_e} \right] \frac{\partial c}{\partial t} + Q \frac{\partial c}{\partial x} = -\lambda c \tag{19}$$

where:

$$\tau_e = V_\ell^*/Q_{oe}$$

The characteristic equations of equation (19) are:

$$\frac{\tau_e dt}{[\tau_e+T-t]} = \frac{A^* dx}{Q} = \frac{-A^* dc}{\lambda c} \tag{20}$$

For the exhalation solution, let (x,t) be the general co-ordinate in the exhalation domain and consider the point (ζ,t_2) on the boundary between pause and exhalation (see Figure II.7, for schematic representation of the solution domain). Equation (20) can be integrated using equation (4) to obtain:

$$\int_{t_2}^{t} \frac{\tau_e dt}{[\tau_e+T-t]} = \int_{\zeta}^{x} \frac{A^*}{Q} dx = \int_{V_\zeta^*}^{V_x^*} \frac{-dV_x^*}{Q_{oe}(1-V_x^*/V_\ell^*)} \tag{21}$$

This simplifies to give the following characteristic curves:

$$\frac{\tau_e + T - t}{\tau_e + T - t_2} = \frac{V_\ell^* - V_\zeta^*}{V_\ell^* - V_x^*} \qquad (22)$$

The concentration during exhalation, can be found from equation (20) by integrating in a similar way to the inhalation case, the result being:

$$c(x,t) = c(\zeta,t_2) \exp\left[- \int_\zeta^x \frac{\lambda}{Q} \, dx \right] \qquad (23)$$

where ζ is a function of x and t determine from equation (22).

In effect, the integration in equation (21) is performed along a characteristic curve from the point (ζ,t_2), on the initial exhalation boundary, to the general point (x,t) in the exhalation solution domain (see Figure II.7). Similarly, the position of the aerosol front x', may be determined from equation (20) to give:

$$\frac{V_{x'}^*}{V_\ell^*} = \frac{T - t}{\tau_e + T - t} \qquad (24)$$

In a similar way to before, equation (23) implies:

$$\int_x^\zeta \frac{\lambda}{Q} \, dx = \sum_{i=n}^{m} \int_{x_{i-1}}^{x_i} \frac{\lambda}{Q} \, dx = \sum_{i=n}^{m} \frac{\lambda_i}{Q_i} \int_{x_{i-1}}^{x_i} dx$$

$$= \sum_{i=n}^{m} \frac{\lambda_i \ell_i}{Q_i} = - \sum_{i=n}^{m} \eta_i$$

The *sign* reversal occurs because exhalation is being considered. Hence, equation (23) becomes:

$$c(x,t) = c(\zeta,t_2) \exp\left[- \sum_{i=n}^{m} \eta_i \right] \qquad (25)$$

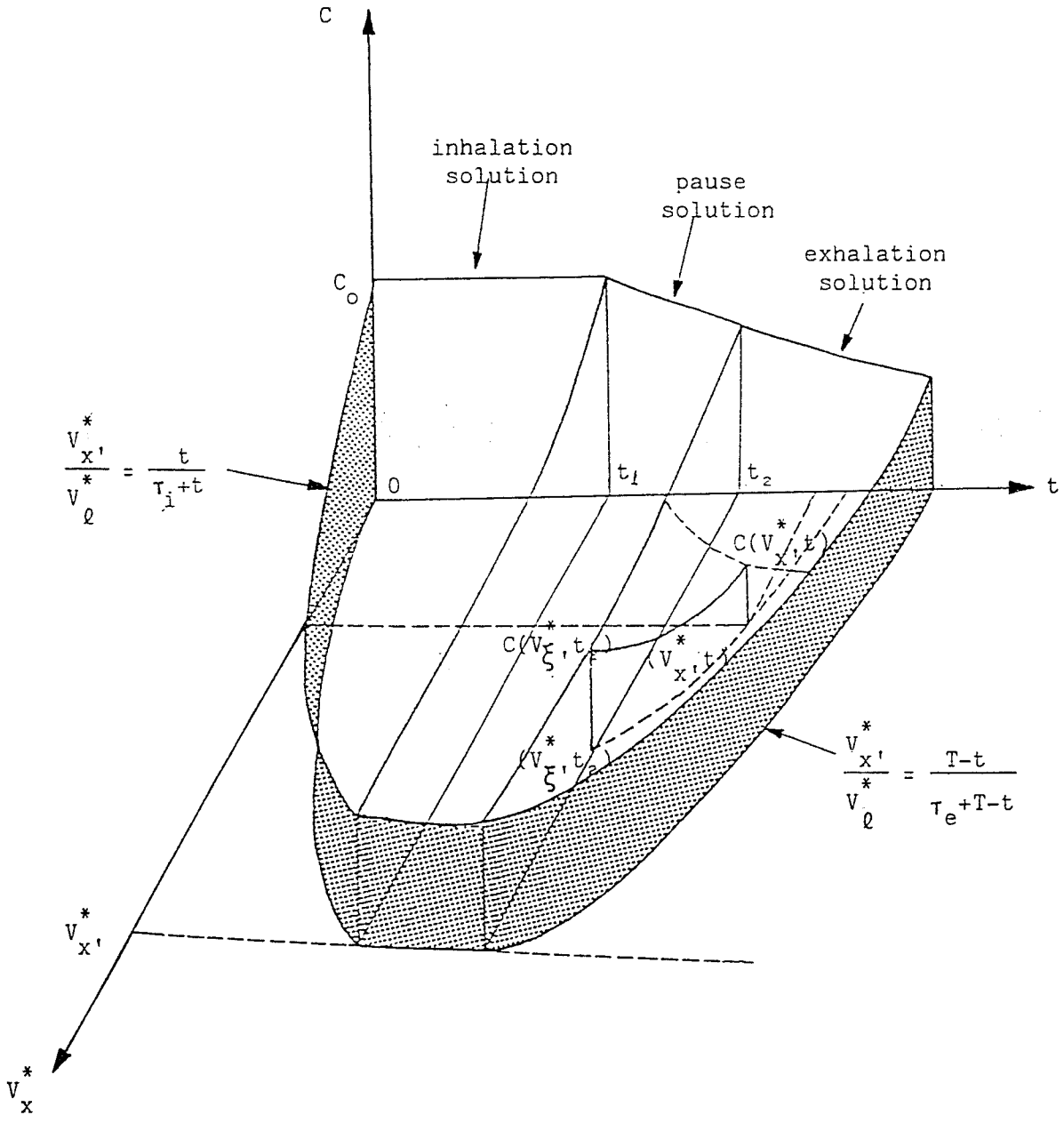

FIGURE II.7 Schematic representation of the solution domain

$$\therefore \quad c(x,t) = c(\zeta,t_2) \prod_{i=n}^{m} \exp\left[-\eta_i \right] \qquad (26)$$

6.1.A.3 Pause solution

The transport equation (9), during the pause has the solution:

$$c(x,t) = c(x,t_1) \exp\left[\frac{-\int_{t_1}^{t} \lambda \, dt}{A^*(1+v_t/V_\ell^*)} \right]$$

$$= c(x,t_1)\ (1-P) \qquad (27)$$

where: P = the fractional loss of aerosol to the airway from time t_1 to t (see Section 6.7.2)

Using the expression for P, defined in Section 6.7.2, the aerosol concentration c can be determined.

6.2 Particle Deposition

Particle deposition is a function of aerosol concentration, as discussed in the previous section. Figure II.7, is a schematic representation of the concentration solutions for inhalation, exhalation and pause which helps to visualise the deposition process.

The fractional deposition of particles during a respiratory cycle is obtained by integrating the particle loss over the entire airway length and time dividing by the amount of particles inhaled ($Q_o c_o t_1$). The fractional deposition in the j^{th} generation can be shown to be:

$$PD_j = \frac{1}{Q_o c_o t_1} \int_{t_{\alpha_j}}^{t_{\beta_j}} \int_{x_{s_j}}^{x_{f_j}} \lambda(x) c(x,t) \, dx dt \qquad (28)$$

where: x_{s_j}, x_{f_j} = start and end of the j^{th} generation airway

$(t_{\beta_j} - t_{\alpha_j})$ = the aerosol residence time in j^{th} generation airway

Assuming λ and c to be constant for $x_{s_j} \leq x \leq x_{f_j}$, and subdividing the time integral into K parts gives:

$$PD_j = \frac{1}{Q_o c_o t_1} \lambda_i \sum_{k=1}^{K} c_{jk} \int_{t_{\alpha_{jk}}}^{t_{\beta_{jk}}} \int_{x_{s_j}}^{x_{f_j}} dx dt \qquad (29)$$

By definition:

$$\Delta A_{jk} = \int_{t_{\alpha_{jk}}}^{t_{\beta_{jk}}} \int_{x_{s_i}}^{x_{f_j}} dx\, dt \qquad (30)$$

The term ΔA_{jk} is the *incremental* deposition area, which can have any shape, allowing it to be defined in terms of the natural boundary curves (characteristic curves). Using (15), equation (29) becomes:

$$PD_j = \frac{1}{Q_o c_o t_1} \sum_{k=1}^{K} c_{jk} \eta_j Q_j \left[\frac{\Delta A_{jk}}{\ell_j} \right] \qquad (31)$$

This expression is general since it applies to inhalation, exhalation and pause. In the pause case, however, the term $Q_j(\Delta A_j / \ell_j)_k$ must be replaced by the airway volume. The fractional particle deposition in the TB- and A-regions during a respiratory cycle are respectively:

$$TB = \sum_{j=1}^{16} PD_j \quad \text{and} \quad A = \sum_{j=17}^{23} PD_j \qquad (32)$$

6.3 Comment on Yu's Model

6.3.1 Definition of deposition efficiency η

Deposition efficiency is *never* explicitly stated in any of Yu's papers, but the following form has been assumed:

$$\eta = \frac{\int_{t_s}^{t_s+\Delta t}\int_{x_s}^{x_s+\Delta x} \lambda(x,t)c(x,t)\,dx\,dt}{\int_{t_s}^{t_s+\Delta t} Q(x_s,t)c(x,t_s)\,dt} \qquad (33)$$

In equation (33) the numerator is the number of particles deposited in an airway of length Δx in time Δt, and the denominator is the number entering the airway in time Δt. It was assume that λ, Q and c do not vary over the airway length Δx and in the time interval Δt, then:

$$\eta = \frac{\lambda c(x_s,t_s)\Delta x \Delta t}{Q(x_s,t_s)c(x_s,t_s)\Delta t}$$

which gives:

$$\eta = \frac{\lambda\ \Delta x}{Q(x_s,t_s)} \qquad (34)$$

Using this definition of η, the concentration in the next generation is zero if $\eta = 1$ (i.e. no particles leave the airway since all of them are deposited in the previous generation).

Yu's expression, equation (18), is:

$$c_n = c_o \exp\left[-\sum_{j=0}^{n} \eta_j\right]$$

This does not yield $C_n = 0$ in subsequent generations when

$$\sum_{j=0}^{n} \eta_j = 1$$

Accordingly, the basic spatial discretization used by Yu (i.e. 23 generations) is inadequate for high deposition efficiencies, because the concentration changes significantly over the airway length used. To validate this, a demonstration for the limitations of Yu's solution will follow.

6.3.2 Limitation of Yu's solution

Consider the conventional 23-bit discretization of the lung and assume the concentration to be constant over the length of each airway. Further, assume that the outlet of an airway belongs to the inlet of the next airway (dotted line in the diagram below).

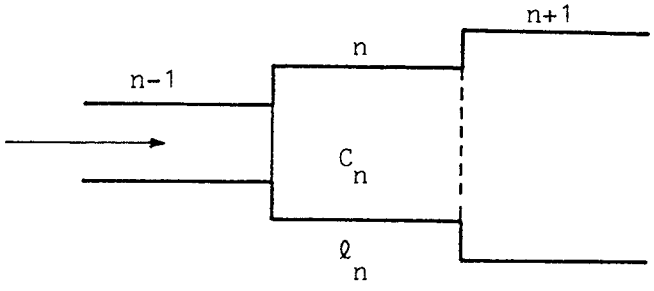

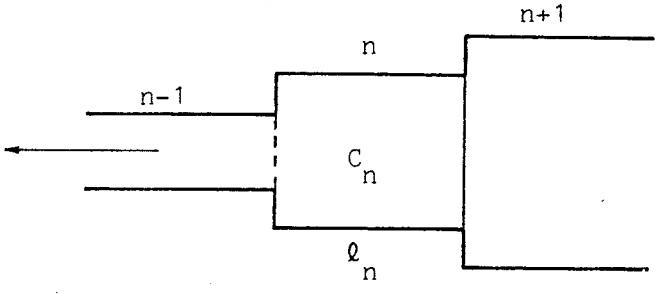

For inhalation, equation (18) gives:

$$c_{n+1} = c_o \exp\left[-\sum_{j=1}^{n} \eta_j\right] = c_o \prod_{j=1}^{n} \exp\left[-\eta_j\right] \quad (35)$$

where: $c_1 = c_o$

For exhalation, equation (25) gives:

$$c_{n-1}(t) = c_m(t_2) \exp\left[-\sum_{j=n}^{m} \eta_j\right] = c_m(t_2) \prod_{j=m}^{m} \left[-\eta_j\right] \quad (36)$$

Iterative relationships can be derived from (35) and (36), though care must be taken with the exhalation case, to ensure that the same parametric curve given by equation (22), is used for all iterated values (this maintains the value of m but requires the time value to change accordingly). Thus for the exhalation solution, the iteration is valid along the parametric curve given by equation (22) with ζ kept constant. For inhalation:

$$\left.\begin{aligned} c_{n+1} &= c_o \prod_{j=0}^{n} \exp(-\eta_j) \\ c_n &= c_o \prod_{j=0}^{n-1} \exp(-\eta_j) \end{aligned}\right\} \qquad (37)$$

Equation (37) implies:

$$\frac{c_{n+1}}{c_n} = \exp(-\eta_n)$$

$$\therefore \quad c_{n+1} = c_n \exp(-\eta_n) \qquad (38)$$

where

$$c_1 = c_o \quad \text{and} \quad 1 \leqslant n \leqslant 22$$

For exhalation:

$$\left.\begin{aligned} c_{n-1} &= c_m(t_2) \prod_{j=n}^{m} \exp(-\eta_j) \\ c_n &= c_m(t_2) \prod_{j=n+1}^{m} \exp(-\eta_j) \end{aligned}\right\} \qquad (39)$$

Equation (39) implies:

$$\frac{c_{n-1}}{c_n} = \exp(-\eta_n) \qquad (40)$$

$$\therefore \quad c_{n-1} = c_n \exp(-\eta_n) \qquad (41)$$

where $c_n = c_n(\zeta, t_\zeta)$ and $1 \leq n \leq m$, $1 \leq m \leq 23$.

Equations (38) and (41) are basically the same iteration.

The deposition efficiency can be defined as *the change in concentration from start to end of an airway, divided by the concentration at the entrance.* This leads to the following expression:

$$\eta_n = \frac{c_n - c_{n+1}}{c_n} \qquad (42)$$

Equations (42) can be re-arranged as follows to give an iterative expression for concentration:

$$c_{n+1} = c_n(1-\eta_n) \qquad (43)$$

Now, compare equation (38), considering the inhalation case without loss of generality, with equation (43). The two expressions become similar for small values of deposition efficiency η_n since:

$$\exp(-\eta_n) \approx 1-\eta_n \quad \text{for } \eta_n \ll 1 \qquad (44)$$

Consequently, if Yu's analytical expressions are to be used (equations 18 and 25) η_n *must* be much less than unity. To deal with higher deposition efficiencies the discretization of the system must be refined, that is, the number of generations considered must be increased. This has the effect of lowering the deposition efficiency, since deposition efficiency decreases as airway length decreases. Unfortunately the programming complexity and time required to obtain a solution increase.

6.4 New Approach

In Yu's approach small values of η are always considered which allows the transport equation to be solved using the exponential approach described above. As high deposition efficiencies are of interest in this study (which is the case for charged aerosols) it is more appropriate to use the natural definition of change in concentration along an airway, which has been termed "*the iterative approach*". The two approaches should be equivalent for small η, as described in Section 6.3.2.

6.4.1 The iterative method

An alternative method of solving the transport equation is proposed which dispenses with Yu's exponential solutions and replaces them with iterative solutions. In the following formulation, it should be noted that λ, the combined deposition constant, is different for inhalation, exhalation and pause solutions.

The transport and continuity equations are:

$$\frac{\partial}{\partial t}(Ac) + \frac{\partial}{\partial x}(Qc) = -\lambda c \qquad (45)$$

$$\frac{\partial A}{\partial t} + \frac{\partial Q}{\partial x} = 0 \qquad (46)$$

Equations (45) and (46) imply:

$$A\frac{\partial c}{\partial t} + Q\frac{\partial c}{\partial x} = -\lambda c \qquad (47)$$

To solve (47), A and Q must be known functions of x and t. Yu (1978), assumed Q to be a function of x only and A to be a linear function of t (see Table II.4 for definitions of constants)

$$Q(x) = Q_o\,(1 - V_x^*/V_\ell^*) \qquad (48)$$

$$A(x,t) = A^*(x)\,(1 + \alpha t + \beta) \qquad (49)$$

TABLE II.4

Solution Type	α	β	Q_o	t_n
Inhalation	$1/\tau_i$	0	Q_{oi}	t_1
Exhalation	$-1/\tau_e$	T/τ_e	Q_{oe}	t_2

Equation (47) can now be solved, by the method of characteristics, using the natural definition of deposition efficiency shown below.

$$\eta = \int_{x_s}^{x_f} \lambda\, c(x,t)dx/(Q_s c_s) \qquad (50)$$

The characteristic equations of (47) are as follows:

$$\frac{dt}{A} = \frac{dx}{Q} = \frac{-dc}{\lambda c} \qquad (51)$$

Considering aerosol concentration c to be a *continuous variable over the airway length*, the second equality in equation (51) can be integrated, yielding the following result:

$$\int_{c_s}^{c_f} dc = -\int_{x_s}^{x_f} \frac{\lambda c(x)}{Q}\, dx \qquad (52)$$

In the model, flow rate is considered to be a constant Q_s over the airway length. Equations (50) and (52) lead to the following results:

$$c_f = c_s\,(1 - \eta) \qquad (53)$$

6.4.1.A Inhalation solution

For inhalation, equation (53) can be presented in the following iterative form (where $c_1 = c_o$ and $1 \leq n \leq 22$)

$$c_{n+1} = c_n\,(1-\eta_n) \qquad (54)$$

This iteration is valid for any path in the inhalation solution domain, since the concentration c(x,t) there is *independent of time* (because the concentration entering the lung c(0,t) is constant).

6.4.1.B Exhalation solution

For exhalation, however, it is appropriate to consider a different iterative expression (where $c_n = c(\zeta,t_\zeta)$ and $1 \leq n \leq m$, $1 \leq m \leq 23$. The point (ζ,t_ζ) is a parametric co-ordinate in the exhalation domain and m is defined below).

$$c_{n-1} = c_n (1-\eta_n) \tag{55}$$

Since the exhalation solution is *time dependent*, this iteration must be applied to a path corresponding to a characteristic curve. By way of defining m above, the characteristic curve of interest intersects the line $t = t_2$ (exhalation boundary) at the end of m^{th} generation. The characteristic curve can be found by integrating the first equality of equation (51), as follows. In order to do this, it is necessary to change the variable from x to V_x^* which are related by the expression.

$$dV_x^* = A^*(x)\, dx \tag{56}$$

proceeding with the integration gives:

$$\int_{t_n}^{t} \frac{dt}{A^*(1+\alpha t+\beta)} = \int_{\zeta}^{x} \frac{dx}{Q_o(1-V_x^*/V_\ell^*)} \tag{57}$$

$$\frac{1 + \alpha t + \beta}{1 + \alpha t_n + \beta} = \frac{V_\ell^* - V_\zeta^*}{V_\ell^* - V_x^*} \tag{58}$$

Equation (57) is the characteristic curve for both inhalation and exhalation (Table II.4 should be consulted for the appropriate values of α, β, Q_o and t_n).

6.4.1.C Pause solution

For the pause solution, the transport equation must be rewritten in the following form (since Q = 0):

$$A(x,t_1) \frac{\partial c}{\partial t} = -\lambda c \tag{59}$$

Equation (58) can be integrated to give the pause solution

$$c(x,t) = c(x,t_1) \exp \left\{ \frac{-1}{A(x,t_1)} \int_{t_1}^{t} \lambda \, dt \right\}$$

$$c(x,t) = c(x,t_1)\ (1 - P) \qquad (60)$$

where P is the fractional loss of aerosol in the interval t_1 to t.

Equations (54) and (55) can be used to deal with deposition efficiencies as high as unity. If the deposition efficiency for an airway exceeds this value (i.e. $\eta_j > 1$) then the airway should be subdivided (refining the discretization) sufficienctly to obtain deposition efficiencies $\eta_j \leq 1$. This situation has not arisen yet.

A good test of the iterative equations (54) and (55) is that a value of $\eta_n = 1$ reduces the concentration in the next generation to zero, as it should. Having found the concentration during inhalation and exhalation, it is then necessary to calculate the deposition.

For computational purposes, Green's theorem has been used to transform the deposition double integral (equation 28) into a line integral, so that the aerosol concentration c only needs to be evalutaed at the airway entrances and exits.

6.4.2 Green's theorem

Let D be a normal region, with respect to the x and y axes, bounded by the closed path Γ. Suppose that P_1 and P_2 have partial derivatives $\partial P_1/\partial x$ and $\partial P_2/\partial y$ and that P_1, P_2, $\partial P_1/\partial x$ and $\partial P_2/\partial y$ are continuous in D, and that $\hat{n} = (n_1, n_2)$ is a unit vector in the direction of the outward-drawn normal, at an arbitrary point of Γ (Ledermann, 1966), then:

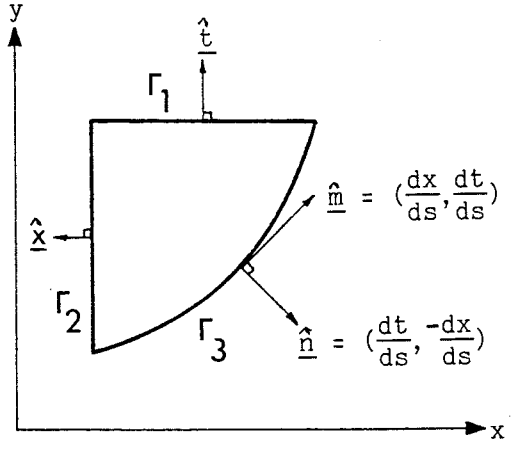

$$\int_{\Gamma} (P_1 n_1 + P_2 n_2) ds = \iint_D \left[\frac{\partial P_1}{\partial x} + \frac{\partial P_2}{\partial x} \right] dxdy \qquad (61)$$

where $\Gamma \equiv$ boundary of domain D

$D \equiv$ domain of integration in x–y plane

Applying Green's theorem to the transport equation (47) with x=x, t=y, P_1=Ac and P_2=Qc.

The discontinuities in A and Q, associated with the mathematical model, are dealt with as described in the *footnote**. Green's theorem implies:

$$\iint_D \lambda \, c \, dxdt = -\int_{\Gamma} (Qcdt - Acdx) \qquad (62)$$

= number of aerosol particles deposited within Γ.

6.4.2.A Method of partitioning the concentration solution domain

The model is most easily understood in terms of (x,t) or equivalently (V_x^*,t) space shown schematically in Figure II.8. It shows:

(i) the three solution domains inhalation, exhalation and pause.

(ii) the aerosol front position at different times.

(iii) the curves corresponding to the characteristics solutions.

---

* Mathematical discontinuities in the functions A and Q can be avoided by assuming a smooth transition in A between one generation and the next. This amounts to rounding off the corners of the step function, allowing finite gradients as shown in the transition regions of the above diagram. The function Q is ultimately determined by the function A; if A is continuous so will be Q.

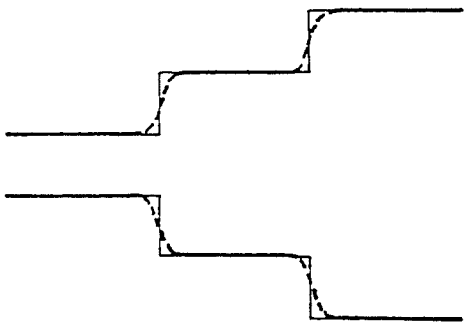

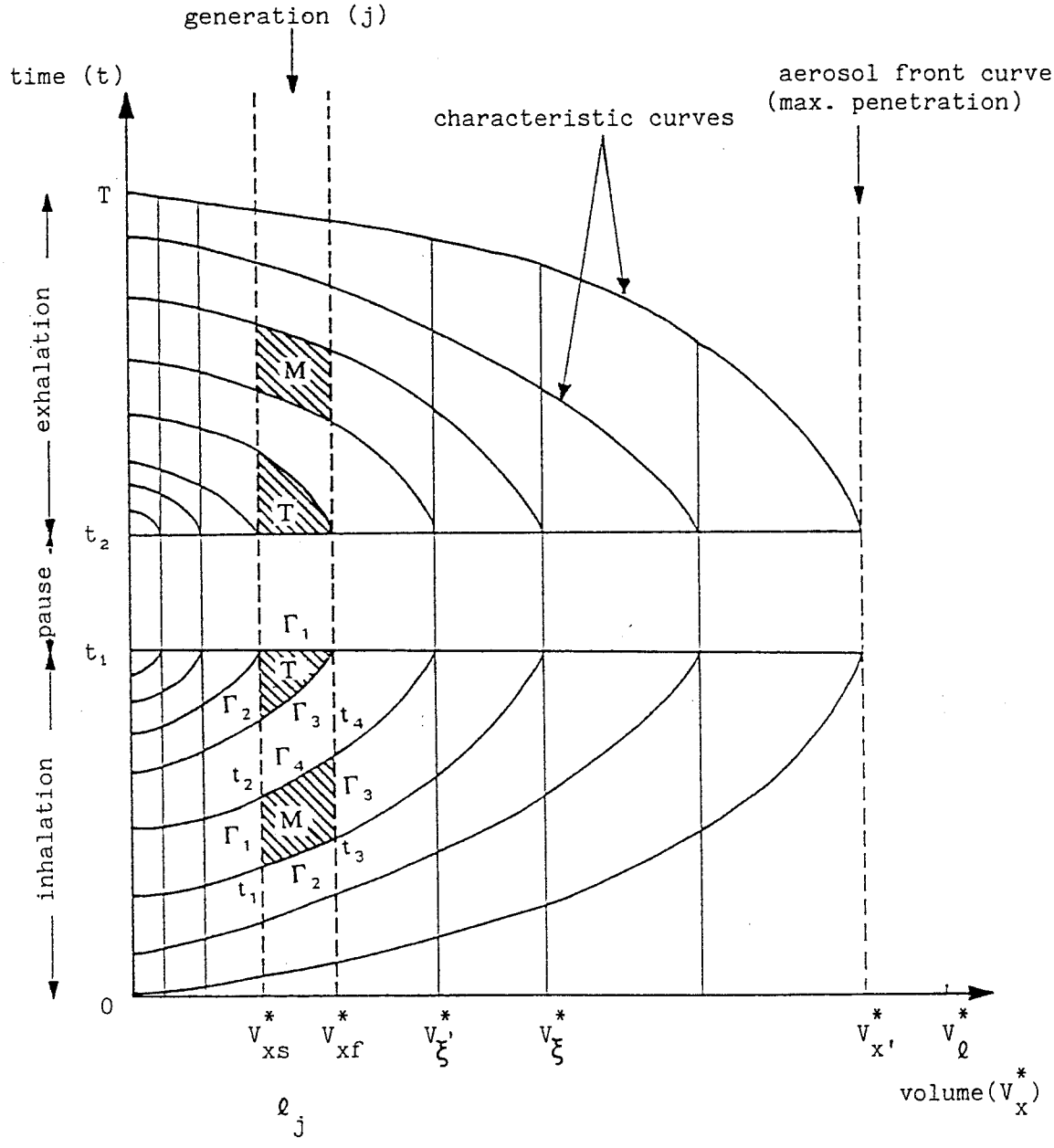

FIGURE II.8 Possible method of partitioning the domain of the concentration solution

It is convenient to use the characteristic curves, equation (58), to partition the solution domain, since there is no aerosol flux across them (see below). The intersection of these curves with the generation boundary lines forms a net of diamond- and triangle-shaped regions for the inhalation and exhalation domains and rectangular regions for the pause.

Considering the line integral, with respect to:

(1) Triangular-shaped regions [(T) shown in the diagram]

$$D = -\int_{\Gamma} c(Qn_1 + An_2)ds \tag{63}$$

Γ_1: $\hat{n} = (0,1)$, Γ_2: $\hat{n} = (-1,0)$ and Γ_3: $\hat{n} = \left[\frac{dt}{ds} , \frac{-dx}{ds} \right]$

$$D = -\int_{\Gamma_1} Acdx + \int_{\Gamma_2} Qcdt - \int_{\Gamma_3} c\left[Q\frac{dt}{ds} - A\frac{dx}{ds}\right]ds \tag{64}$$

Now, the characteristic equations of (47) are:

$$\frac{dt}{A} = \frac{dx}{Q} = \frac{-dc}{\lambda c} \tag{65}$$

The first equality in equations (65) implies: Qdt = Adx, hence

$$\int_{\Gamma_3} c\left[Q\frac{dt}{ds} - A\frac{dx}{ds}\right]ds = \int_{\Gamma_3} c(Qdt - Adx) = 0 \tag{66}$$

This means that integrals along characteristic curves are zero (basically there is no flow across them). Equation (64) therefore reduces to:

$$D = \int_{t_1}^{t_2} Qcdt - \int_{x_s}^{x_f} Acdx \tag{67}$$

where: D ≡ number of aerosol particles deposited in airway (over T)

$\int_{t_1}^{t_2} Qcdt \equiv$ number of aerosol particles entering an airway.

$\int_{x_s}^{x_f} Acdx \equiv$ number of undeposited aerosol particles in an airway.

(2) Diamond-shaped regions [(M) shown in the diagram]

$$D = -\int c(Qn_1 + An_2)ds \qquad (68)$$

Since Γ_2 and Γ_4 are characteristic curves:

$$\therefore \quad \int_{\Gamma_2} c(Qn_1 + An_2)ds = 0, \quad \int_{\Gamma_4} c(Qn_1 + An_2)ds = 0$$

$$\therefore \quad D = -\int_{\Gamma_1 + \Gamma_3} c(Qn_1 + An_2)ds \qquad (69)$$

where Γ_1 : $\hat{\underline{n}} = (-1,0)$ and Γ_3: $\hat{\underline{n}} = (1,0)$

For the diamond-shaped region, the particle deposition is therefore:

$$D = \int_{t_1}^{t_2} c(x_s,t)Q(x_s)dt - \int_{t_3}^{t_4} c(x_f,t)Q(x_f)dt \qquad (70)$$

6.4.2.B Deposition integrals

For Figure II.8, the deposition can be obtained in terms of a line integral as follows:

The total domain can be partitioned into 3-regions (see Figure II.9): inhalation, exhalation and pause.

FIGURE II.9

Deposition integrals

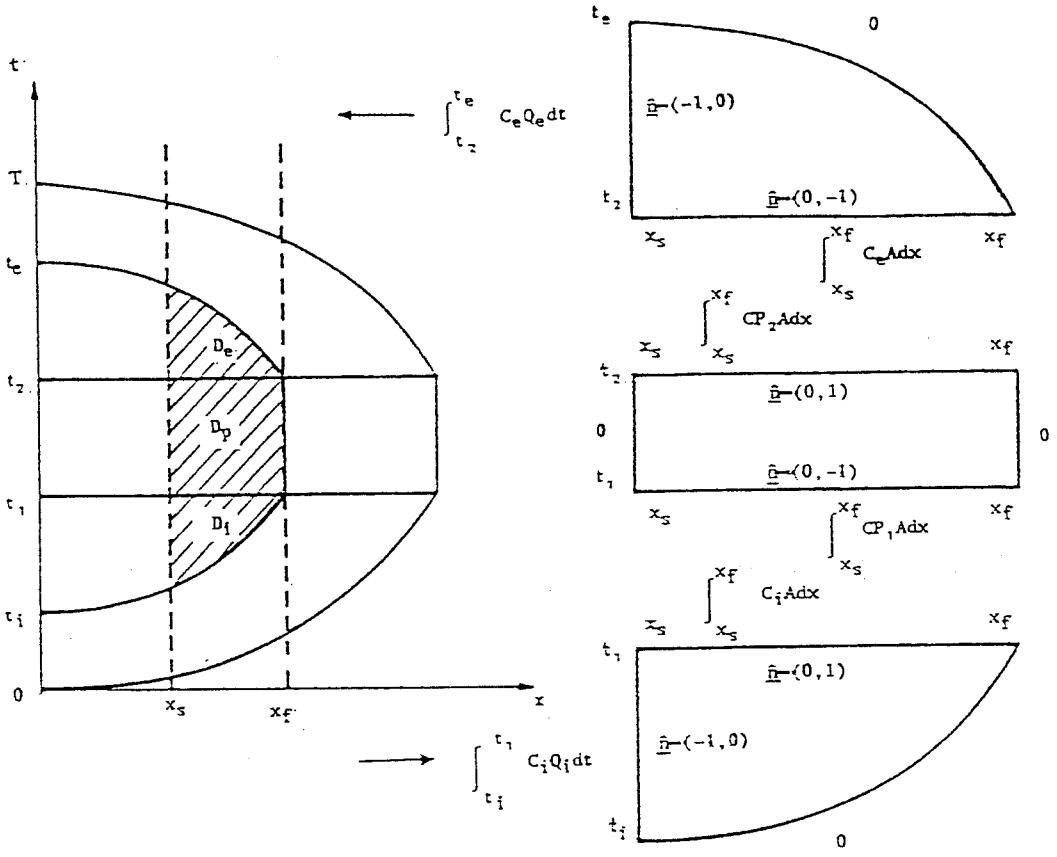

Particle deposition corresponding to inhalation (D_i) can be performed in the following way:

$$D_i = \int_{t_i}^{t_1} c_iQ_i dt - \int_{x_s}^{x_f} c_i A dx \qquad (71)$$

The deposition corresponding to the pause (D_p) is:

$$D_p = \int_{x_s}^{x_f} c_{P_1} A dx - \int_{x_s}^{x_f} c_{P_2} A dx = \int_{x_s}^{x_f} (c_{P_1} - c_{P_2}) A dx \qquad (72)$$

in which $c_i = c_{P_1}$ and $c_e = c_{P_2}$

The deposition corresponding to the exhalation (D_e) is:

$$D_e = \int_{t_2}^{t_e} c_e Q_e dt + \int_{x_s}^{x_f} c_e A dx \qquad (73)$$

The line integral components along common boundaries cancel when considering the three domains as a whole, so that the total deposition (D_t) is given by:

$$D_t = D_i + D_p + D_e$$

$$D_t = \int_{t_i}^{t_1} c_i Q_i dt - \int_{t_2}^{t_e} c_e Q_e dt \qquad (74)$$

The *sign* changes as Q_e is negative.

6.5 To Account for Airway Diameter as a Function of Time

In Yu's model (1978), he used *global* averaging for the airway dimension, based on a half-tidal volume inflation. The cross-sectional area, in general, is given by equation (5) which is re-written below.

$$A = A^* \left[1 + \frac{v_t}{V_\ell^*} \right] \qquad (75)$$

see previous definitions.

The global time-averaged value of A is:

$$\bar{A} = A^* \left[1 + \frac{v_t}{2V_\ell^*} \right] \qquad (76)$$

where: v_t = tidal volume at the end of inhalation

$$\therefore \quad \frac{\bar{A}}{A^*} = \left[1 + \frac{v_t}{2V_\ell^*} \right] \qquad (77)$$

Since $\bar{A} = \Pi(\bar{d})^2$ and $A^* = \Pi(d^*)^2$ it follows that:

$$\frac{\bar{A}}{A^*} = \frac{(\bar{d})^2}{(d^*)^2} \tag{78}$$

Equations (77) and (78) imply:

$$\frac{\bar{d}}{d^*} = \left[1 + \frac{v_t}{2V_\ell^*} \right]^{\frac{1}{2}} \tag{79}$$

which is the diameter correction factor according to Yu. A *local* time average was considered but better agreement with the experimental data was obtained using the global approach.

6.6 Deposition Efficiency as a Function of Time [M-Factor]

Deposition efficiency can be defined as:

$$\eta(x,t) = \frac{\int_{x_s}^{x_f} \lambda(x,t)c(x,t)dx}{Q(x_s)c(x_s,t_s)} \tag{80}$$

This is equivalent to the previous definition of η (equation 33) applicable to the steady-state condition, which is not time dependent. For small deposition efficiencies ($\eta \ll 1$), aerosol concentration is assumed to be constant over the airway length ℓ, so that η may take the form:

$$\eta = \frac{\lambda \ell}{Q} \tag{81}$$

This expression for deposition efficiency is used in Yu's deposition calculations.

Since the airway diameters change as a function of time, it is necessary to consider deposition efficiency as a function of time. In order to solve the characteristic equations, it is necessary to have an appropriate definition of $\lambda(x,t)$, which can be obtained from equation (80) by letting $x_f \rightarrow x_s$

$$\frac{\partial \eta(x,t)}{\partial x} = \frac{\lambda(x,t)c(x,t)}{Q(x_s)c(x_s,t_{x_s})} \tag{82}$$

Now, the characteristic equations are:

$$\frac{dt}{A^*(t)} = \frac{dx}{Q(x)} = \frac{-dc}{\lambda(x,t)c(x,t)} \tag{83}$$

The first equality in equation (83) can be integrated to obtain the functional relationship between x and t (i.e. a characteristic curve).

The second equality gives:

$$\frac{\lambda(x,t)c(x,t)}{Q(x)}\, dx = -dc \tag{84}$$

Using (82) in equation (84) gives:

$$c(x_s,t(x_s))\, \frac{Q(x_s)}{Q(x)}\, \frac{\partial \eta(x,t)}{\partial x}\, dx = -dc \tag{85}$$

Assuming the functional relationship between x and t be t = t(x) along a characteristic curve, equation (85) implies:

$$c(x_s,t(x_s))\, \frac{Q(x_s)}{Q(x)}\, \frac{\partial \eta(x,t(x))}{\partial x}\, dx = -dc$$

Integration yields:

$$c(x_s,t(x_s)) \int_{x_s}^{x_f} \frac{Q(x_s)}{Q(x)}\, \frac{\partial \eta(x,t(x))}{\partial x}\, dx$$

$$= c(x_s,t(x_s)) - c(x_f,t(x_f))$$

$$c(x,t(x)) = c(x_s,t(x_s)) \left[1 - \int_{x_s}^{x_f} \frac{Q(x_s)}{Q(x)} \frac{\partial \eta(x,t(x))}{\partial x} dx \right] \quad (86)$$

[To obtain $\partial\eta(x,t(x))/\partial x$ in equation (86), differentiate η partially with respect to x then subtitue t = t(x)].

This degenerates to the conventional expression, equation (53), when airway diameter is constant in time, since $Q(x) = Q(x_s)$ and $\eta = \eta(x)$, as shown below

$$c(x,t(x)) = c(x_s,t(x_s)) \left[1 - \int_{x_s}^{x_f} \frac{\partial \eta(x)}{\partial x} dx \right]$$

$$= c(x_s,t(x_s)) \left[1 - \int_{\eta(x_s)}^{\eta(x_f)} d\eta \right]$$

$$= c(x_s,t(x_s)) \; [\; 1 - (\eta(x_f) - \eta(x_s))]$$

Now $\eta(x_s) = 0$ and $\eta(x_f) = \eta$ thus:

$$c(x,t(x)) = c(x_s,t(x_s)) \; (1 - \eta) \quad (87)$$

If Q_{av} is taken as the average flow rate over the airway length, the integral in equation (86) can be approximated by:

$$I = \frac{Q(x_s)}{Q_{av}} \int_{x_s}^{x_f} \left[\frac{\partial \eta(x,t)}{\partial x} \right]_{t=t(x)} dx \quad (88)$$

The integral can further be approximated by using an average value of η over the length of airway, so that:

$$I = \frac{Q(x_s)}{Q_{av}} \qquad \eta_{av} = M\,\eta_{av} \tag{89}$$

The so-called *M-Factor* arises in the iterative expressions for deposition to account for the effect of change in airway area as a function of time.

Numerically, M takes a value between 1 and 2 if the final generation (twenty-third) does not take part in the calculation, as is usual. This may seem unimportant, however, the inhalation model depends on the accuracy of the concentration calculation. For example, the concentration of aerosol exhaled into the atmosphere, at the end of exhalation, is dependent on all intermediate values of concentration and so any errors involved will accumulate.

6.7 Deposition Efficiencies

The adopted expressions for η and P have been derived by various authors (see below). For a given airway generation, the deposition efficiency components are as follows:

1. Inertial Impaction

The expression for η_{Ij} is an empirical relation derived from the experimental data of Schlesinger et al. (1969, 1977) and given by Yu (1982) as:

$$\eta_{Ij} = 0.768\ (St_j)\ \theta_j \tag{90}$$

where

$$St_j = \frac{\rho d_p^2 U_j}{9\mu d_j} \quad \text{and} \quad \theta_j = \frac{L_j}{4d_j}$$

in which:

ρ = particle mass density
d_p = particle diameter
L_j = length of j^{th} generation airway
d_j = diameter of j^{th} generation airway
U_j = air velocity in the j^{th} generation airway
μ = air viscosity (~ 1.89×10^{-4}g/cm.s at body temperature 37°C)
θ_j = bend angle of the j^{th} generation airway

2. Gravitational sedimentation

The expression of η_{sj}, given by Pich (1972), for deposition by settling in a parabolic flow is adopted. The result is:

$$\eta_{sj} = \frac{2}{\pi}\left[\left[1 - \epsilon_j^{2/3}\right]^{\frac{1}{2}}\left[2\epsilon_j - \epsilon_j^{1/3}\right] + \sin^{-1}\epsilon_j^{1/3}\right] \quad (91)$$

where:

$$\epsilon_j = \frac{3\,U_g L_j}{4U_j d_j} \qquad \sin\varphi = \frac{3\pi U_g L_j}{16 U_j d_j}$$

in which:

U_g = settling velocity of the particle

φ = angle of inclination of the airway to the vertical.

In the present calculation:

I. The angle of inclination of the airway to the vertical, φ, is assumed to be given by: $\sin\varphi = \pi/4$ which corresponds to the case of a system of randomly orientated airways, Heyder (1975).

II. The settling velocity U_g of the particle is:

$$U_g = C_c\,\rho g d_p^2 / 18\mu \quad (92)$$

where:

C_c = slip correction factor given by:

$$C_c = 1 + \frac{\lambda}{d_p}\left[2.514 + 0.8\exp\left[\frac{-0.55\,d_p}{\lambda}\right]\right] \quad (93)$$

in which:

λ is the mean free path of air molecules

($\lambda \approx 0.069 \times 10^{-4}$cm at body temperature 37°C)

3. Diffusion

(i) For turbulent flow, Landahl (1963) gives:

$$\eta_{Dj} = 4\Delta^{\frac{1}{2}} (1 - 0.444\Delta^{\frac{1}{2}} + \ldots) \tag{94}$$

(ii) For laminar flow, Ingham (1975) gives:

$$\eta_{Dj} = 1 - 0.819 \exp(-14.63\Delta) - 0.0976 \exp(-89.22\Delta) - 0.0325 \exp(-228\Delta) - 0.0509 \exp(-125.9\Delta^{2/3}) \tag{95}$$

where

$$\Delta = \frac{DL_j}{d_j^2 U_j}$$

in which D is the Brownian diffusion coefficient of an aerosol particle, given by Einstein (1905) as:

$$D = \frac{C_c kT}{3\pi\mu d_p}$$

where:

k = Boltzmann constant ($k \approx 1.38 \times 10^{18}$ erg K^{-1})

T = absolute temperature (T = 310 K for the human body)

4. Electrostatic deposition

There are two types of electrostatic force due to image effects and space charge.

(i) The space charge force: is due to the mutual repulsion of aerosol particles of like charge. The deposition efficiency, η_{spj}, due to the space charge force, was derived by Yu (1977) and is:

$$\eta_{spj} = \frac{C_o R_j^3 \tau_j}{1 + C_o R_j^3 \tau_j} \tag{96}$$

where:

$$\tau_j = \frac{C_c\, q^2 t_j}{3\pi\mu R_j^3 dp} \qquad (96.A)$$

in which:

c_o = the concentration of aerosol particles at the entrance of j^{th} airway generation

q = the amount of charge on the particle

R_j = radius of the j^{th} generation airway

t_j = residence time for aerosol in j^{th} generation airway ($t_j \sim L_j/U_j$)

For small deposition efficiency $\eta_i \ll 1$, this equation can be reduced to:

$$\eta_S P_j = c_o R_j^3 \tau_j \qquad (97)$$

(ii) The image force: is due to the interaction of charged particles with the conducting respiratory walls. For a unipolar aerosol, under *slug flow* conditions, Yu (1977) derived the following deposition efficiency:

$$\eta_{imj} = 1 - x^2 \qquad (98)$$

where x parameter is a solution of the following equation:

$$4\left[\frac{1}{x} + 2\,\ell n\, x - x\right] = \tau_j \qquad (99)$$

where:

τ_j is a dimensionless time defined in equation (96.A). It is impossible to obtain an exact, analytical inverse function $\eta_{imj} = \eta(\tau_j)$ corresponding to equations (98) and (99), Pich (1978), and so numerical techniques are required. Simplified analytical results were obtained, by Pich, for the two extreme cases as follows:

(1) In the limit as $\eta_{imj} \to 0$ $\quad \eta_{imj} = (6\tau_j)^{1/3}$ (100)

(2) In the limit as $\eta_{imj} \to 1$ $\quad \eta_{imj} = 1 - (4/\tau_j)^2$ (101)

The deposition of charged particles also depends on the conventional mechanisms. The image force contributes significantly to deposition only when the particle charge reaches an appreciable level q_c. Thus, for $q < q_c$, the particle charge has a minor effect on deposition.

The following expression for deposition efficiency was developed by Yu (1985) and gives good agreement with experimental results:

$$\eta_{imj} = \left[\frac{4\, C_c\, L_j}{3\pi\mu d_p R_j^3 U_j} \right]^{\frac{1}{2}} (q - q_c) \qquad (102)$$

Equation (102) differs from equation (100) because of the use of a parabolic velocity profile for the aerosol flow. The parabolic velocity profile is a better description of the flow field in the small airways where the effect of the image force is expected to be important. For *parabolic flow*, Yu and Chandra (1978) derived:

$$\eta_{imj} = (1 - x^2)^2 \qquad (103)$$

where x parameter is a solution of the following equation:

$$8\left[\frac{1}{x} + 2\ell nx - x^2 + (x-1)/3 \right] = \tau_j \qquad (104)$$

As before, numerical techniques (eg. Newton–Raphson iteration) are required to obtain η_{imj} as a function of τ_j.

6.7.1 Deposition efficiencies considered as probabilities

It is reasonable to think of the various deposition efficiencies as probabilities if a particle is chosen at randum from the airway entrance. The separate mechanisms can be summarized as follows:

η_I impaction efficiency (or probability)
η_S sedimentation efficiency (or probability)
η_D diffusion efficiency (or probability)
η_q electrostatic efficiency (or probability)

The probability of a particle not to be deposited in an airway by, for example, sedimentation is $(1-\eta_S)$ and so on. The probability that it is not deposited by any of the mechanisms is $(1-\eta_I)\ (1-\eta_S)\ (1-\eta_D)\ (1-\eta_q)$, and so the total probability of deposition, by any of the mechanisms, is:

$$\eta = 1 - (1-\eta_I)\ (1-\eta_S)\ (1-\eta_D)\ (1-\eta_q) \qquad (105)$$

However, the expressions for the deposition efficiencies (or probabilities) were all derived assuming particle concentration to be *uniform* at the airway entrance. This implies that for each generation, the deposition expressions are independent of the transfer taking place up-stream. Consequently, the aerosol loss in each generation can be calculated by superimposing the losses to the airway surfaces and attached alveoli as follows:

$$\eta = \eta_I + \eta_S + \eta_D + \eta_q \qquad (106)$$

Calculation shows that this assumption leads to a slightly higher deposition than equation (105). In fact, this higher deposition is desirable, since the *air-mixing effect* is not accounted for in the derivation. Consequently, this expression for the combined efficiencies has been adopted.

6.7.2 Deposition during the pause

For the pause only the sedimentation, diffusion and electrostatic deposition mechanisms are present, impaction being absent. It is assumed that the combined deposition efficiency P is:

$$P = 1 - (1-P_s)\ (1-P_D)\ (1-P_q) \qquad (107)$$

where:

P_s, P_D and P_q are respectively the deposition efficiencies due to the individual mechanisms of sedimentation, diffusion and electrostatic deposition, applicable during the pause period.

The deposition, by sedimentation, of an aerosol in randomly oriented tubes was obtained by Heyder (1975). His results may be expressed quantitatively by the following polynomials, Yu (1978):

$$P_s = 1.1094\tau_g - 0.2604\tau_g^2 \qquad \text{for } 0 < \tau_g < 1 \qquad (108)$$

and

$$P_s = 1 - 0.0069\tau_g^{-1} - 0.0859\tau_g^{-2} - 0.0582\tau_g^{-3} \qquad \text{for } \tau_g > 1 \qquad (109)$$

where:

$$\tau_g = \frac{U_g \, t_p}{d_j}$$

in which:

t_p is the pause time

The expression for diffusion, shown below, was given by Ingham (1981) and Yu (1978):

$$P_D = 1 - \sum_{i=1}^{3} \frac{4}{\alpha_i^2} \exp(-\alpha_i^2 \tau_d) - \left[1 - \sum_{i=1}^{3} \frac{4}{\alpha_i^2} \right] \exp \left[-4 \sqrt{\frac{\tau_d}{\pi}} \times \left[1 - \sum_{i=1}^{3} \frac{4}{\alpha_i^2} \right]^{-1} \right] \qquad (110)$$

where:

$$\tau_d = \frac{D t_p}{R_j}$$

in which:

α_1, α_2 and α_3 are the first three roots of the equation $J_0(\alpha) = 0$ where J_0 is the Bessel function of zeroth order.

For electrostatic deposition during the pause, the image deposition efficiency corresponds to that of the *slug flow* profile, equation (98), residence time being replaced by the pause duration in this case. [See Appendix II.B for the derivation, applicable to the conditions prevailing during the pause (zero flow rate)].

6.8 Head Deposition

Particle deposition in the *naso*– or *oro*–pharyngeal regions is referred to as head deposition. The amount of particles which enter the lung depends upon the choice of breathing mode. Normally, more particles are collected by the nasal route than the oral route, due to the presence of hairs in the nasal air passages, which are more complex airways. Since the aerosol residence time in the head

region (of the total volume ~ 50cm^3) is very short, the major deposition mechanism here is impaction. Yu et al. (1981) derived empirical formula for deposition in the human head, by nose or mouth breathing. These depend on the parameter S, as shown below, where:

$$S = \rho d_p^2 Q/(g\mu m^2 s^{-1})$$

in which:

ρ measured in gm cm^{-3}

Q in cm^{3}s^{-1} and

d_p in μm.

(S is equivalent to particle Stokes number).

For oral breathing:

$$H_{in} = -1.117 + 0.324 \log S \quad \text{for } S > 3000 \quad (111)$$

$$H_{in} = 0 \quad \text{for } S < 3000 \quad (112)$$

and

$$H_{ex} = 0 \quad (113)$$

For nasal breathing

$$H_{in} = -0.014 + 0.023 \log S \quad \text{for } S < 337 \quad (114)$$

$$H_{in} = -0.959 + 0.397 \log S \quad \text{for } S > 337 \quad (115)$$

and

$$H_{ex} = 0.003 + 0.033 \log S \quad \text{for } S < 215 \quad (116)$$

$$H_{ex} = -0.851 + 0.339 \log S \quad \text{for } S > 215 \quad (117)$$

where:

H is the deposition efficiency in the head,

the subscripts "in" and "ex" denoting inhalation and exhalation respectively.

Head deposition efficiency can be defined as follows:

$$H = \frac{M_d}{M_e} = \frac{\text{number of aerosol particles deposited in the head}}{\text{number of aerosol particles entering the head}}$$

For inhalation:

$$M_d = H_{in}\, C_{oh}\, Q_{oi}\, t_1 \qquad (118)$$

For exhalation:

$$M_d = H_{ex}\, Q_{oe} \int_{t_2}^{T_{eh}} C_e(t)\,dt \qquad (119)$$

where:

Q_{oi} is the inhalation flow rate in the head

Q_{oe} is the exhalation flow rate in the head

C_{oh} is the concentration of inhaled aerosol entering the head

$C_e(t)$ is the lung exhalation concentration as a function of time t

t_1 is the inhalation duration

t_2 is the time at which exhalation starts

T_{eh} time of one complete breathing cycle (including head residence time)

For both inhalation and exhalation, the denominator term M_e is:

$$M_e = C_{oh}\, Q_{oi}\, t_1 \qquad (120)$$

Note: The concentration entering the lung is:

$$C_o = C_{oh}\,(1 - H_{in}) \qquad (121)$$

and the concentration leaving the head (C_ℓ) after exhalation is:

$$C_\ell(t) = C_e(t)\,(1 - H_{ex})$$

The integration of equation (119) can be represented by a summation of terms obtained using the Trapezium rule.

6.9 Critique of the Presentation of Yu's Lung Model

The task of calculating concentration and deposition is made more

difficult by the uncertainty involved. For example:

1. Yu only deals with small deposition efficiency $\eta \ll 1$, but the physical situations which he tries to match are, sometimes, outside the scope of this limitation.

2. There is confusion in the scheme of numerical implementation of Yu's derivation because of the difference between a continuous system and a discrete system, specially for high η.

3. In Yu's derivation a continuous system approach was used, although the use of a discrete system could not be avoided in the numerical computation. There is uncertainty involved in the discretization and the way the discontinuity in flow rate and area, at the end of each generation, is dealt with.

4. A correction is needed should the position of the aerosol front lie between two generations to give the correct airway volume, length and number of alveoli per generation for the final generation (particularly important in the A–region)

5. The typographic errors:

   i. Expression for diffusion mechanism during pause: four different versions of the same expression exist in four different places. See references:
   - Yu, C.P., Powder Tech., 21 (1978): p. 61
   - Yu, C.P. et al., Am. Ind. Hug. Asso. J., 40 (1979): p. 1004
   - Yu, C.P. et al., J. Aerosol Sci. & Tech., 5 (1986): p. 340
   - Yu, C.P. et al., J. Aerosol Sci., 18 (1987): p. 425

   ii. Sign mistakes in the general expression for image deposition efficiency. See reference:
   - Yu, C.P., Am. Occup. Hyg., 29 (1985): p. 221

   iii Error in time τ for expression in equation (A.6) in the appendix, see reference:
   - Yu, C.P. et al., J. Aerosol Sci., 14 (1983): p. 608

6. When trying to match Yu's theoretical predictions, uncertainty was

encountered in the specification of tidal volume (i.e. tidal volume is the product of flow rate and inhalation time but only the value of tidal volume was specified).

7. Yu used an expression for image deposition efficiency (equation 102) which cannot easily be justified but which does appear to fit the experimental data very well.

These differences are thought to account for any discrepancy between Yu's results and those of the new model.

6.10 Outline of the Computer Program for Respiratory Deposition

A detailed description of the computer model for calculating respiratory deposition would be a lengthy process and, perhaps, inappropriate at present. However, a simplified description is now presented:

1. In the program, the lung is considered to be divided into 23-generations starting from the trachea, the last 7 of which are alveolated.

2. The inhalation and exhalation solution domains, defined by the aerosol front curves, are partitioned in time using characteristic curves which correspond to the airway entrances and exits at the end of inhalation. Spatial partitioning is provided by the starts and ends of the airways.

   This partitioning leads to many "diamond"-shaped regions and fewer "triangle"-shaped regions adjacent to the pause region (see Figure II.8).

3. In the "diamond"-shaped regions, the airway entrances and exits are distinct so far as the programming is concerned. However, in the case of "triangle"-shaped regions, the airway entrance is also considered to be its exit, as the aerosol does not leave via the natural airway exit in this case.

4. For any generation, the two "triangle"-shaped regions and intermediate rectangular regions are considered together (see Section 6.4.2.B and Figure II.9).

5. Deposition is calculated in terms of the difference in aerosol flux across

an airway entrance and exit. Inhalation is dealt with initially and exhalation subsequently.

6. Deposition efficiency is calculated for each generation and varies with type of solution (i.e. inhalation, pause, etc.)

7. Weibel's lung morphology is assumed and a global time average considered to account for changes in airway diameter with time.

8. The concentration solution is determined for the entire solution domain, using iterative expressions (see Section 6.4.1), before any deposition calculations are made.

9. If a pause is considered, this is accounted for between the inhalation and exhalation calculations.

10. Head deposition may be determined for either nasal or oral breathing.

11. Weibel's model is incorporated in the program as a data block.

12. Breathing conditions and particle properties are input via the computer keyboard. The output data can be presented on VDU or output to a disc for storage and subsequent analysis.

13. If necessary, the deposition data can be determined for inhalation, pause and exhalation independently, but usually the overall deposition in a generation is considered.

The program architecture is shown in Figure II.10. A listing of the program appears in Appendix II.C. The program is written in Basic and has been designed to run on a BBC personal computer. A typical execution time for a single run (i.e. one particle size and one breathing condition) is 2 minutes or less.

FIGURE II.10 FLOW CHART FOR THE ARCHITECTURE OF THE PREDICTIVE LUNG DEPOSITION COMPUTER MODEL

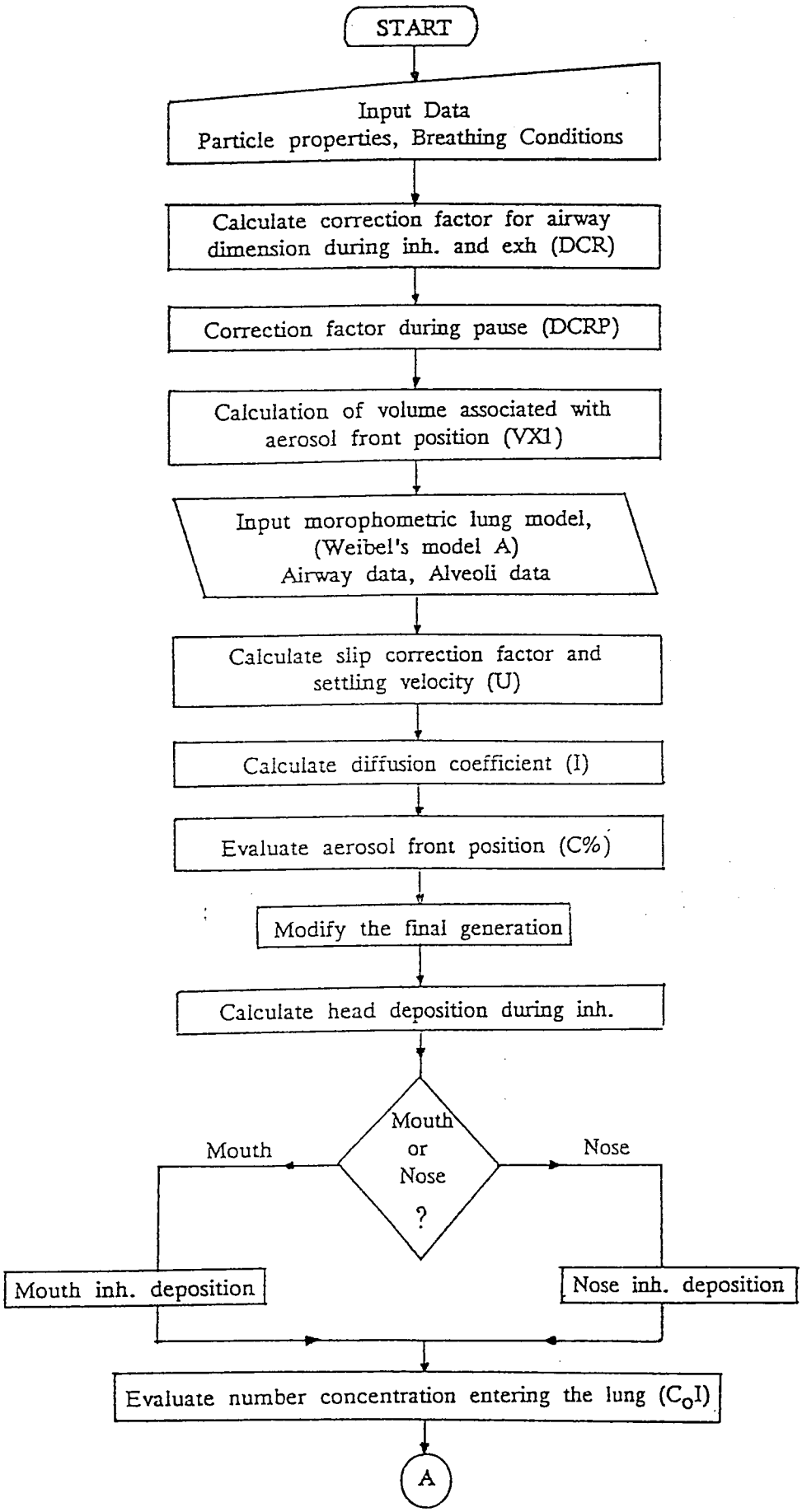

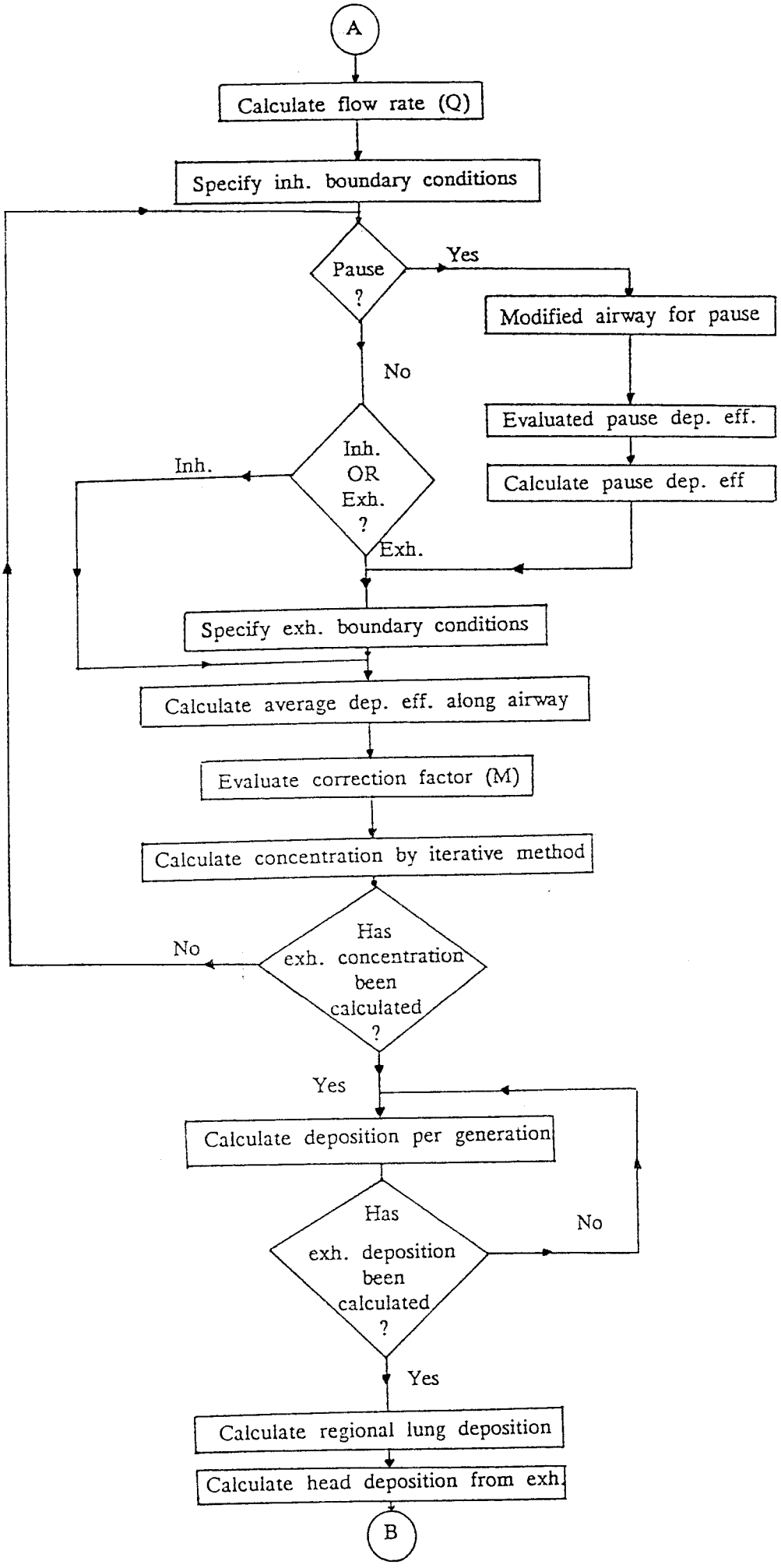
A
Calculate flow rate (Q)
Specify inh. boundary conditions
Pause ?
Yes
Modified airway for pause
Evaluated pause dep. eff.
Calculate pause dep. eff
No
Inh. OR Exh. ?
Inh.
Exh.
Specify exh. boundary conditions
Calculate average dep. eff. along airway
Evaluate correction factor (M)
Calculate concentration by iterative method
Has exh. concentration been calculated ?
No
Yes
Calculate deposition per generation
Has exh. deposition been calculated ?
No
Yes
Calculate regional lung deposition
Calculate head deposition from exh.
B

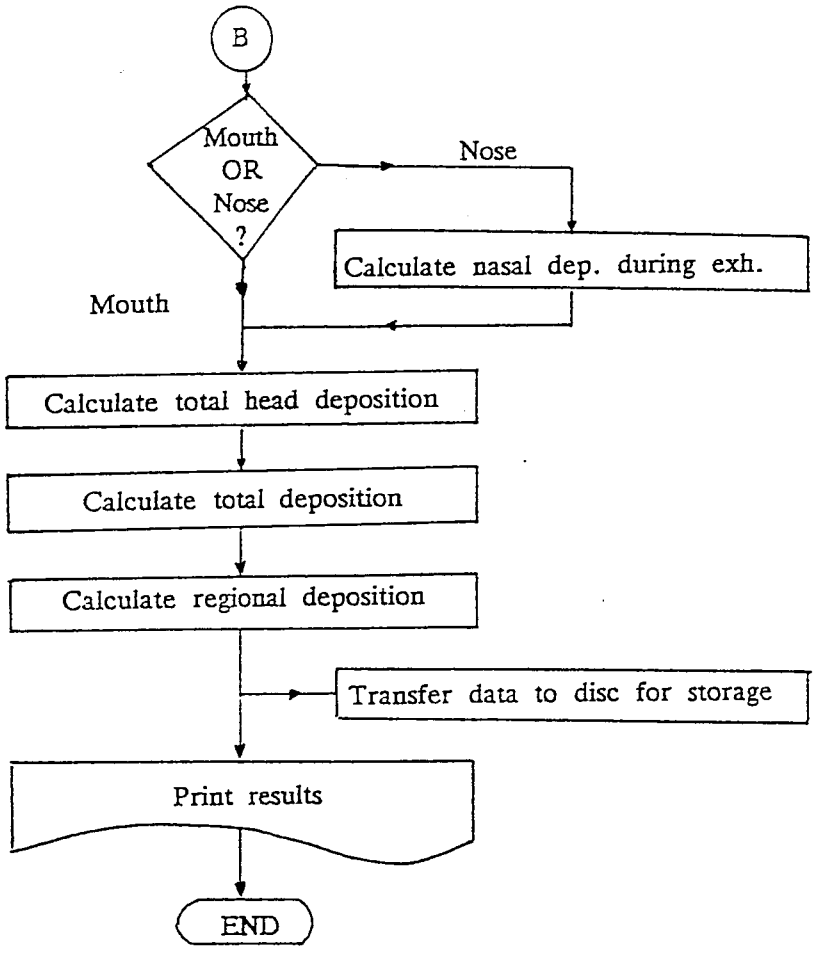
B
Mouth OR Nose ?
Nose
Calculate nasal dep. during exh.
Mouth
Calculate total head deposition
Calculate total deposition
Calculate regional deposition
Transfer data to disc for storage
Print results
END

7. RESULTS AND DISCUSSION

In order to establish a datum for charge-enhanced deposition it has been necessary to consider, firstly, conventional mechanical deposition mechanisms. This was a pre-requisite, in any case, since it was obligatory to validate the deposition model with regard to the new approach (i.e. the iterative approach which allows high deposiion efficiencies to be considered). Consistency of the results obtained using the new approach with published experimental data and accepted theoretical predictions provides the necessary validation.

Besides total deposition, it has also been possible to consider regional deposition for which little experimental data is available. This has made it possible to assess how regional deposition varies with physical factors and breathing conditions, and how this variation contributes to the observed changes in total deposition, for charged and neutral aerosols.

7.1 Respiratory Deposition of Uncharged Particles

In a given respiratory tract, the deposition of inhaled particles depends upon the particle characteristics and the pattern of breathing. The physical factors responsible for deposition, for spherical uncharged aerosols are: (1) particle diameter (d_p); (2) particle density (ρ); (3) mean air flow rate (Q); and (4) mean residence time (τ), see Appendix I. Heyder and co-workers (1975 and 1980) have reported experimental data on total deposition of spherical, uncharged aerosols of various particle diameters and mass densities, under a variety of well-controlled breathing conditions. Yu and Diu (1982 and 1983) made theoretical predictions of these data, using their model, and obtained good agreement.

7.1.A Comparison with the published data of total deposition

In the deposition calculations described here, unless otherwise stated, the breathing cycle consists of inhalation at constant flow rate, exhalation (of equal duration) at constant flow rate but no pause. This is consistent with the experimental conditions of Heyder et al. (1975, 1980).

The lung model used in most of the calculations is that of Weibel adjusted to a rest lung volume of 3000cm^3. The airway dimensions are scaled to an average lung volume of 3000cm^3 plus half the tidal volume.

7.1.A.1 Effect of particle diameter on total deposition

The effect of particle diameter on the total deposition of an aerosol is well established. Figures II.11 and II.12 compare calculated total deposition and experimental data versus particle size, for unit density spheres. The tidal volume pertaining is $1000cm^3$, mouth and nose breathing are considered. It can be seen from these figures that the predicted deposition values compare well with the experimental data. Deposition is less for mouth breathing than for nose breathing as more particles are captured in the head region. A minimum in the total deposition curve exists, close to $0.5\mu m$ diameter, due to the combined effects of sedimentation and diffusion (impaction being negligible for this size of particle).

In Figures II.13 and II.14, deposition profiles (including mouth breathing) are plotted in terms of airway generation number, for particle sizes representing the case when one of the deposition mechanisms is dominant. Figure II.13 shows the deposition profiles for diffusion-dominated deposition (particles ~ $0.01\mu m$ in diameter). It can be seen that diffusional deposition occurs predominantly in the deeper generations, mainly in the A-region. Figure II.14 shows the profiles for sedimentation-dominated (particles ~ $1\mu m$ in diameter) and impaction-dominated (particles ~ $10\mu m$ in diameter) deposition. It can be seen that sedimentation deposition predominates in the A-region, whereas impaction is important in the TB-region, mainly in the early generations. Good agreement is found with Yu's theoretical prediction (1982) calculated for the same conditions.

7.1.A.2 Effect of particle mass density on total deposition

The respiratory tract is known to collect particles according to their aerodynamic size (Task Group, 1966). Figures II.15 and II.16 show the comparison between calculated total deposition and experimental data, plotted as a function of aerodynamic particle diameter. Two particle mass densities are considered for two different breathing patterns ($Q = 250cm^3s^{-1}$, $\tau = 4s$ and $Q = 750cm^3s^{-1}$, $\tau = 2s$), and mouth breathing is assumed. For larger aerodynamic particle diameters, both calculations and measurements indicate that deposition is a function of a single aerodynamic diameter, regardless of mass density. This is because deposition is here dominated by impaction and sedimentation. Diffusion becomes increasingly important for particles of aerodynamic diameter $< 2.5\mu m$. Deposition, therefore, cannot be expressed as a function of aerodynamic diameter alone, for the total particle size range of interest, as is often done in the literature, except for particles larger than about $0.5\mu m$ in geometrical diameter.

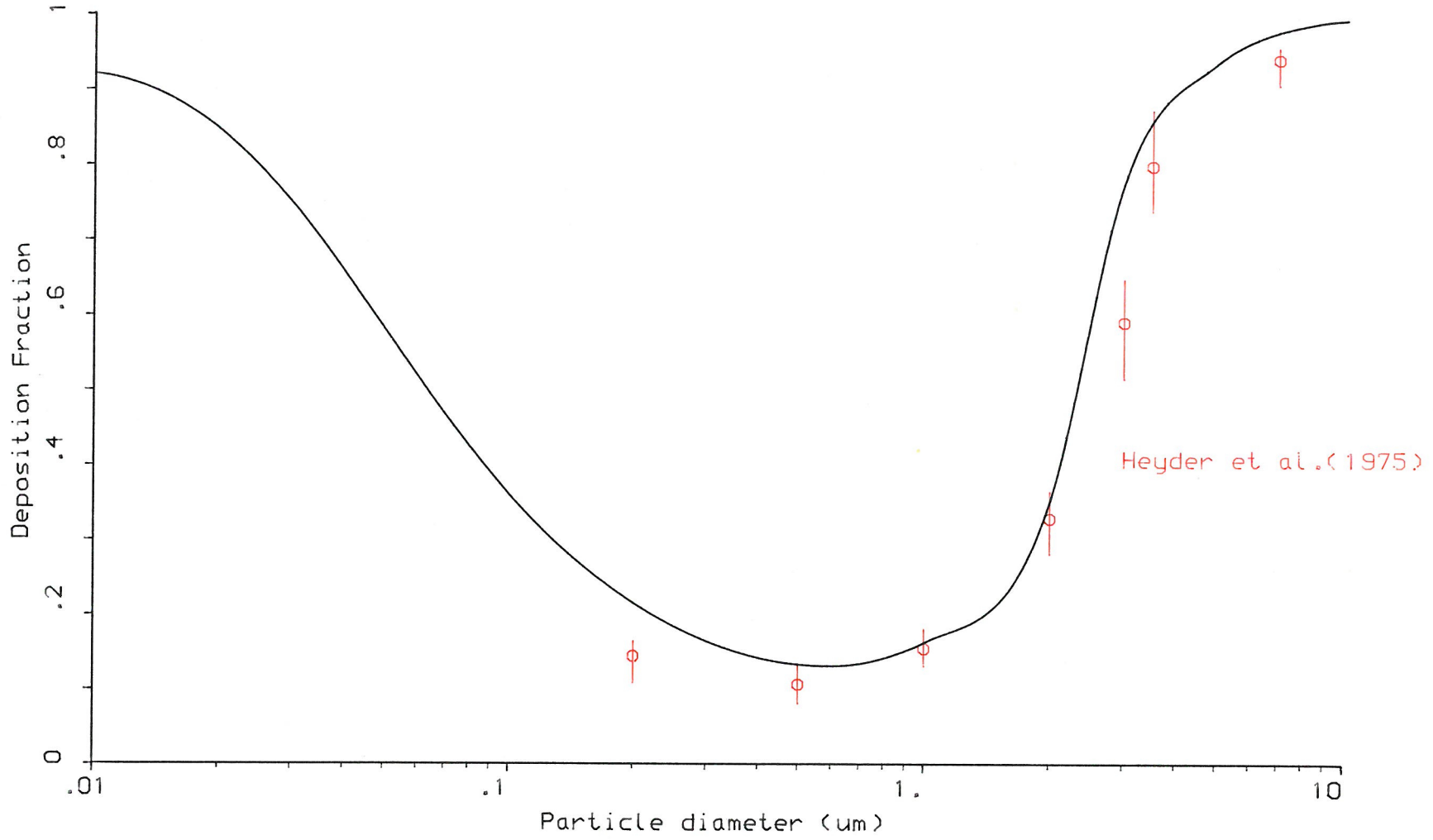

FIG.(II.11): Total deposition as a function of particle diameter at mouth breathing for Qo=500cm3/s, T=2s (p=1g/cm3, FRC=3000cm3 , no pause) .The solid line represent the predicted values.

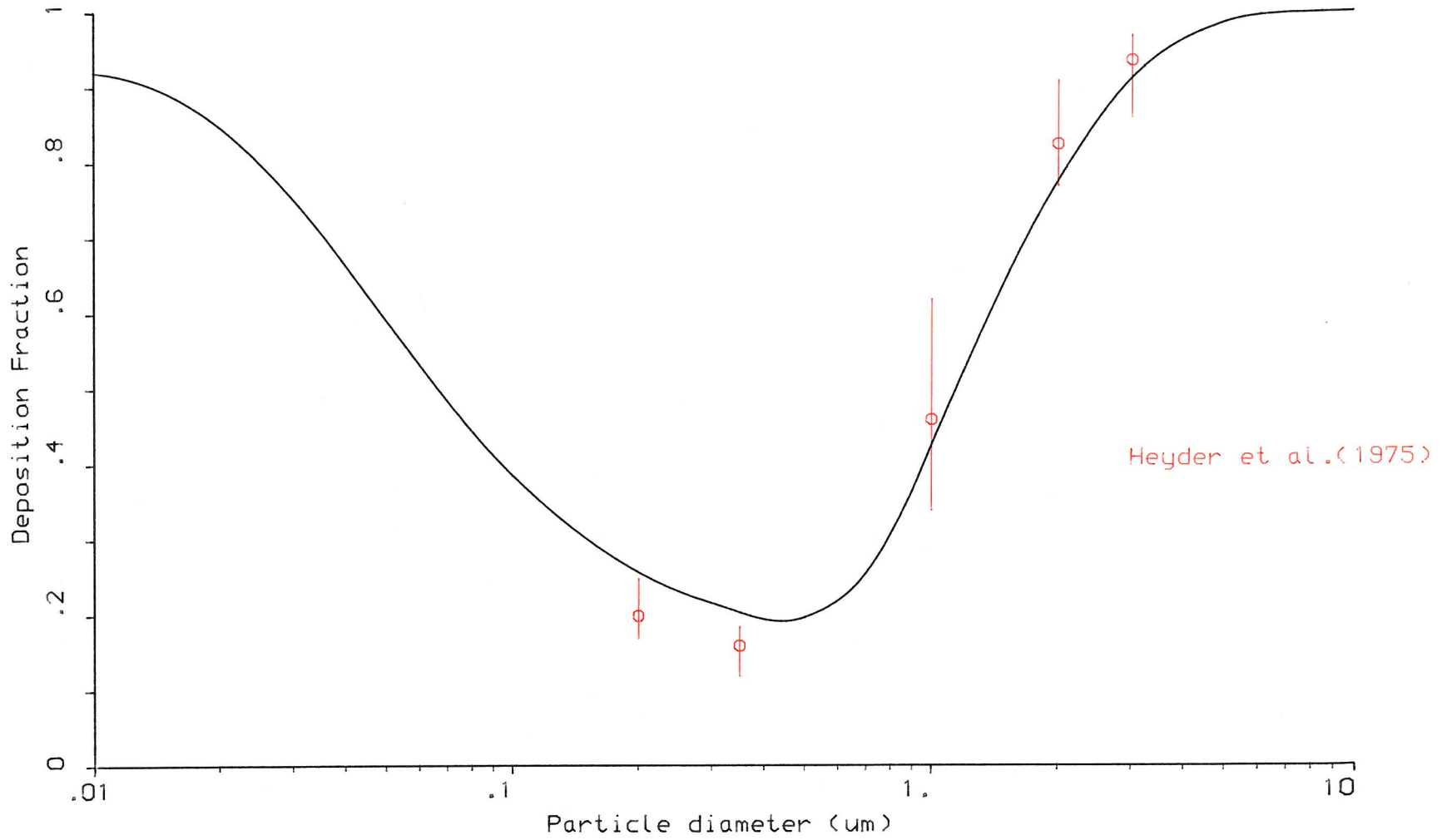

FIG.(II.12): Total deposition as a function of particle diameter at nose breathing for Qo=500cm3/s, T=2s (p=1g/cm3, FRC=3000cm3 , no pause). The solid line represent the predicted values.

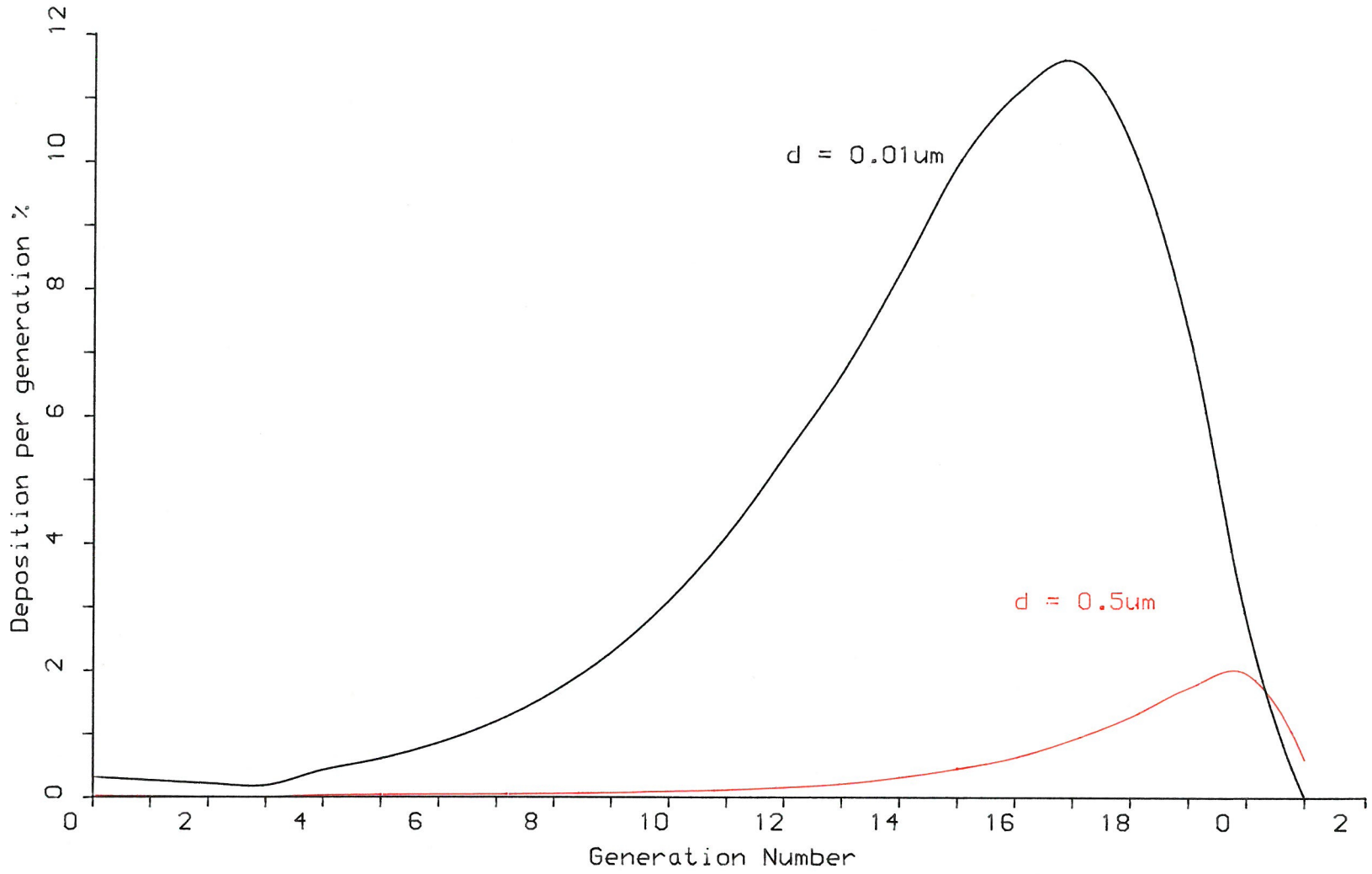

FIG.(II.13): Deposition profiles at mouth breathing along airway generation for different particle sizes representing diffusion dominated (d =0.01um) and d =0.5um particle size
(p=1g/cm3 , Q=500 cm3/s , T=2s , no pause , FRC=3000 cm3)

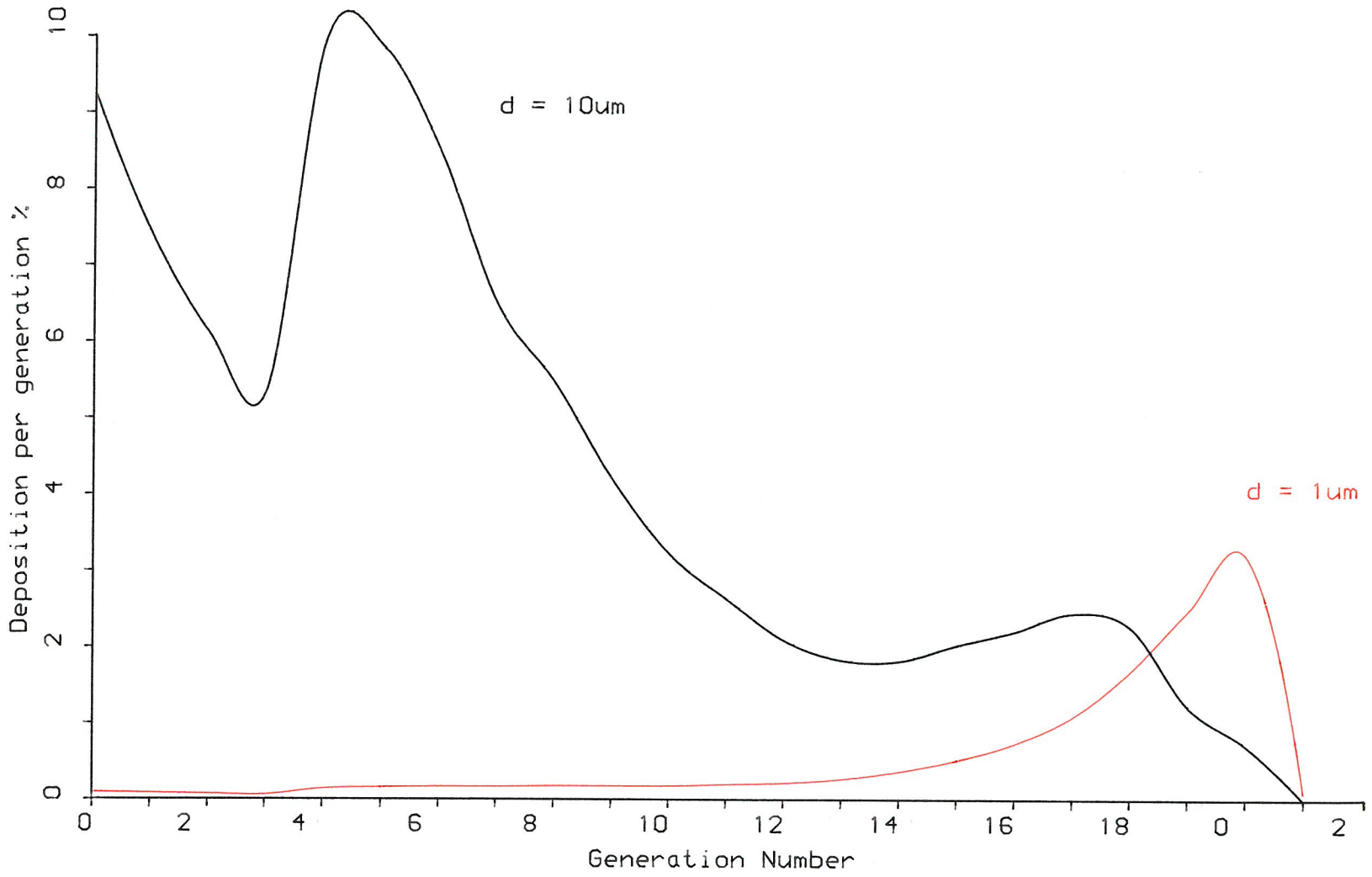

FIG.(II.14): Deposition profiles at mouth breathing along airway generation for different particle sizes representing impaction dominated (d =10 um) and sedimentation dominated (d =1 um), (p=1g/cm3 , Q=500 cm3/s , T=2s , FRC=3000 cm3 , No pause)

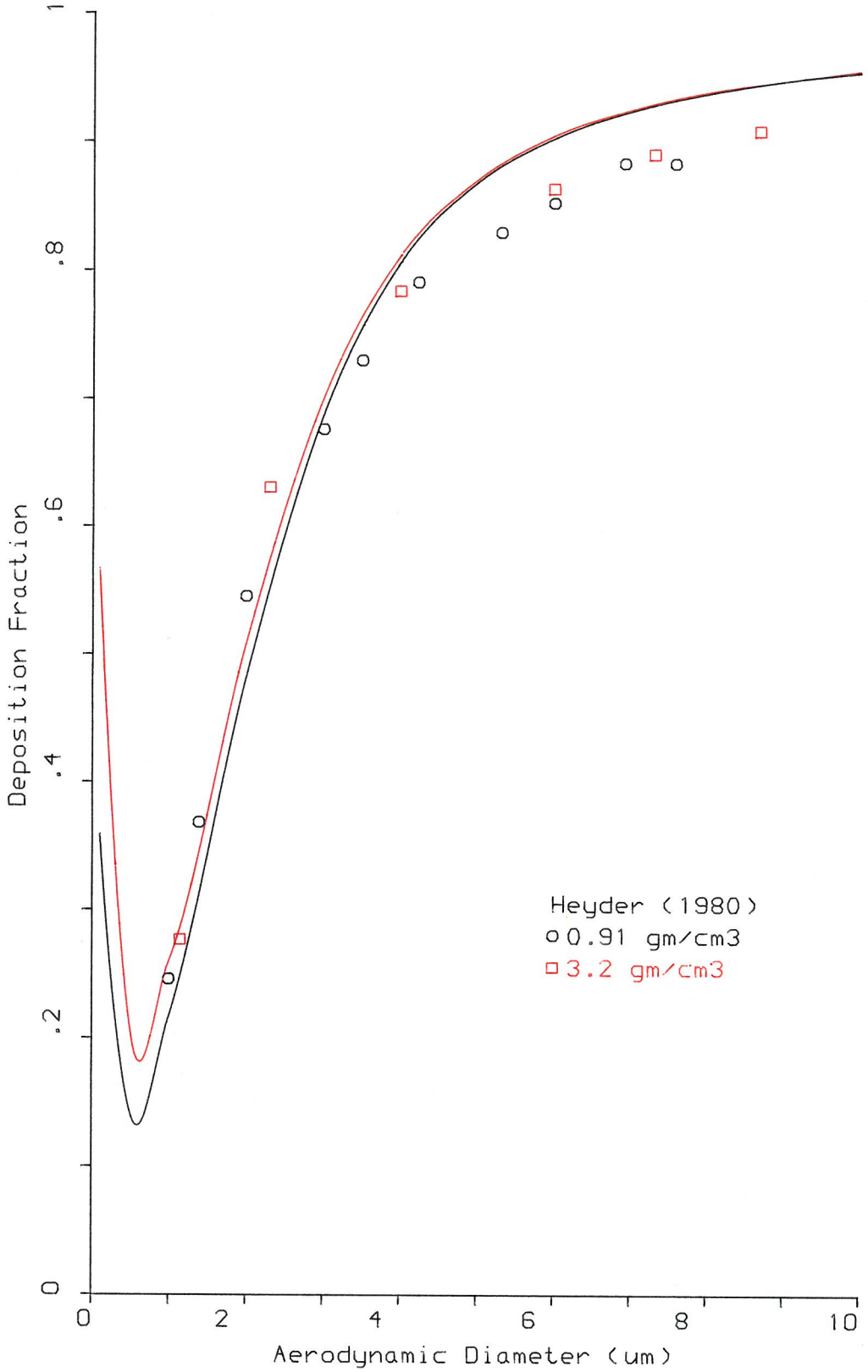

FIG.(II.15): Total deposition as a function of aerodynamic particle diameter at mouth breathing for p=0.91 & 3.2 g/cm3 (Q=250cm3/s, T=4s)
(the solid lines are the calculated values)

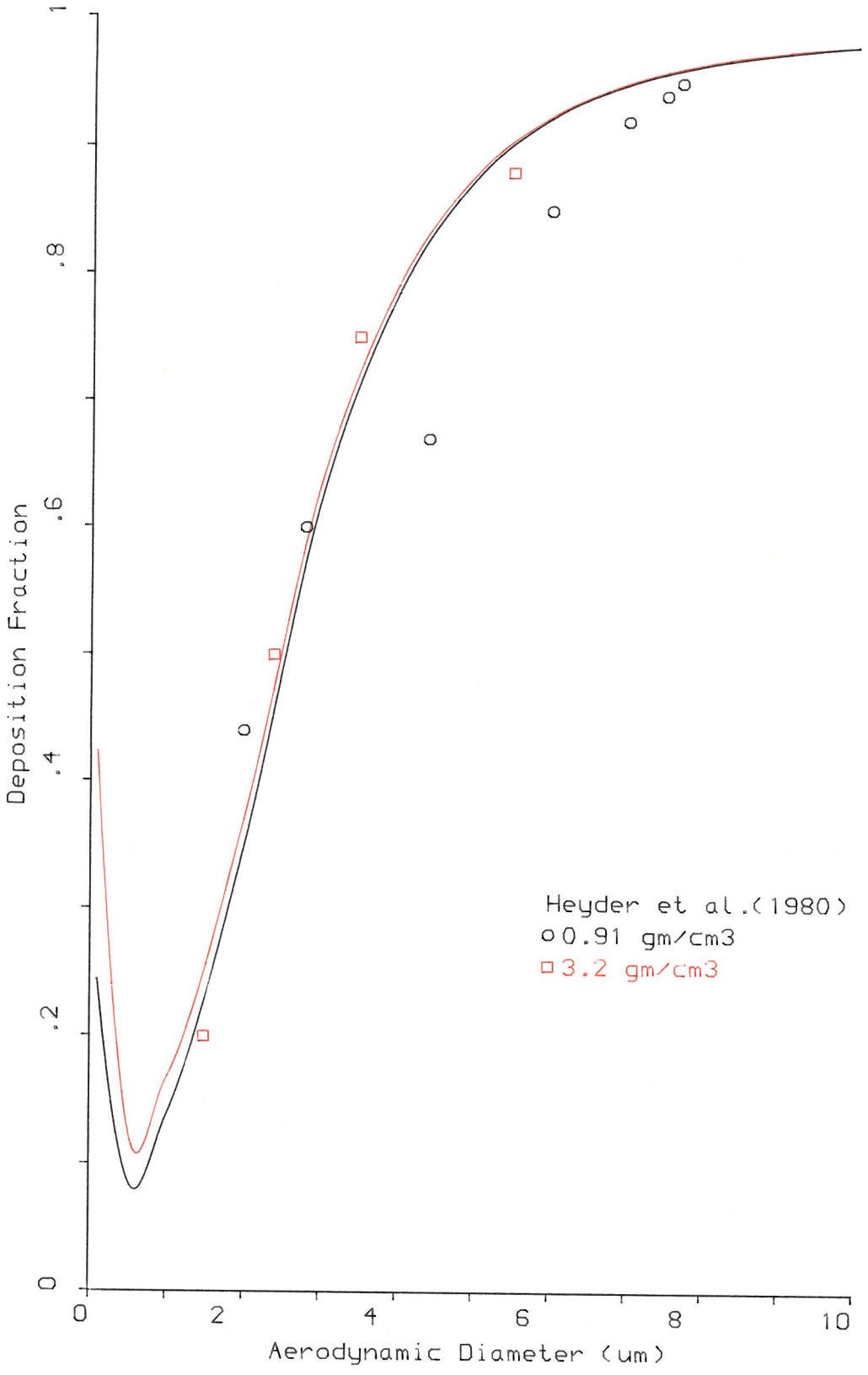

FIG.(II.16): Total deposition as a function of aerodynamic particle diameter at mouth breathing for p=0.91 & 3.2g/cm3 (Q=750cm3/s, T=2s)
(the solid lines are the calculated values)

Figure II.17 further demonstrates the importance of particle mass density with regard to the deposition of aerosol particles in the human respiratory tract. It shows the calculated and experimental data for total deposition plotted as a function of geometrical particle diameter. Increasing particle mass density causes an increase in deposition over the entire range of particle diameters. Again, very good agreement is found between the prediction of the model, and both experimental data of Heyder et al. (1975, 1980) and accepted independent theoretical predictions, Yu and Diu (1983).

7.1.A.3 Effect of mean air flow rate on total deposition

The influence of flow rate on total deposition, plotted as a function of particle diameter, is shown in Figures II.18 and II.19. In Figure II.18, the mean residence time is fixed at 1s so that the depositional effects of sedimentation and diffusion are minimal. It can be seen that total deposition increases with flow rate since deposition by impaction is then enhanced. The calculated results agree reasonably well with the experimental data except for larger particles ($> 6.5\mu m$ diameter) where they slightly overestimate deposition. When the mean residence time is increased to 2s, sedimentation and diffusion become relatively significant. Figure II.19 shows the effect of flow rate on total deposition for this case. Agreement between the calculated and experimental data is better since the flow rate has a reduced effect on deposition.

To gain further understanding of the flow rate effect, Figure II.20 has been plotted. It shows the calculated regional deposition for various flow rates and a residence time of 1s. For flow rate $Q > 500 cm^3 s^{-1}$, the increase in total deposition is due to enhanced impaction deposition in the H and TB-regions. A-deposition, for flow rates $Q < 500 cm^3 s^{-1}$, remains virtually unchanged since deposition in this region is governed by sedimentation and diffusion, and only increases as residence time increases. However, there is a dramatic increase in A-deposition when the flow rate increases from 250 to $500 cm^3 s^{-1}$. This is the tidal volume effect, due to aerosol entering the A-region rapidly.

Physical considerations dictate that A-deposition is maximised for particles of a certain diameter. Figure II.20 corresponds to a flow rate of $500 cm^3 s^{-1}$ and residence time of 1s, shows such a maximum in A-deposition for particles of $4.5\mu m$ diameter. The particle size corresponding to maximum A-deposition decreases to $3.5\mu m$ as the mean flow rate is increased to $1000 cm^3 s^{-1}$.

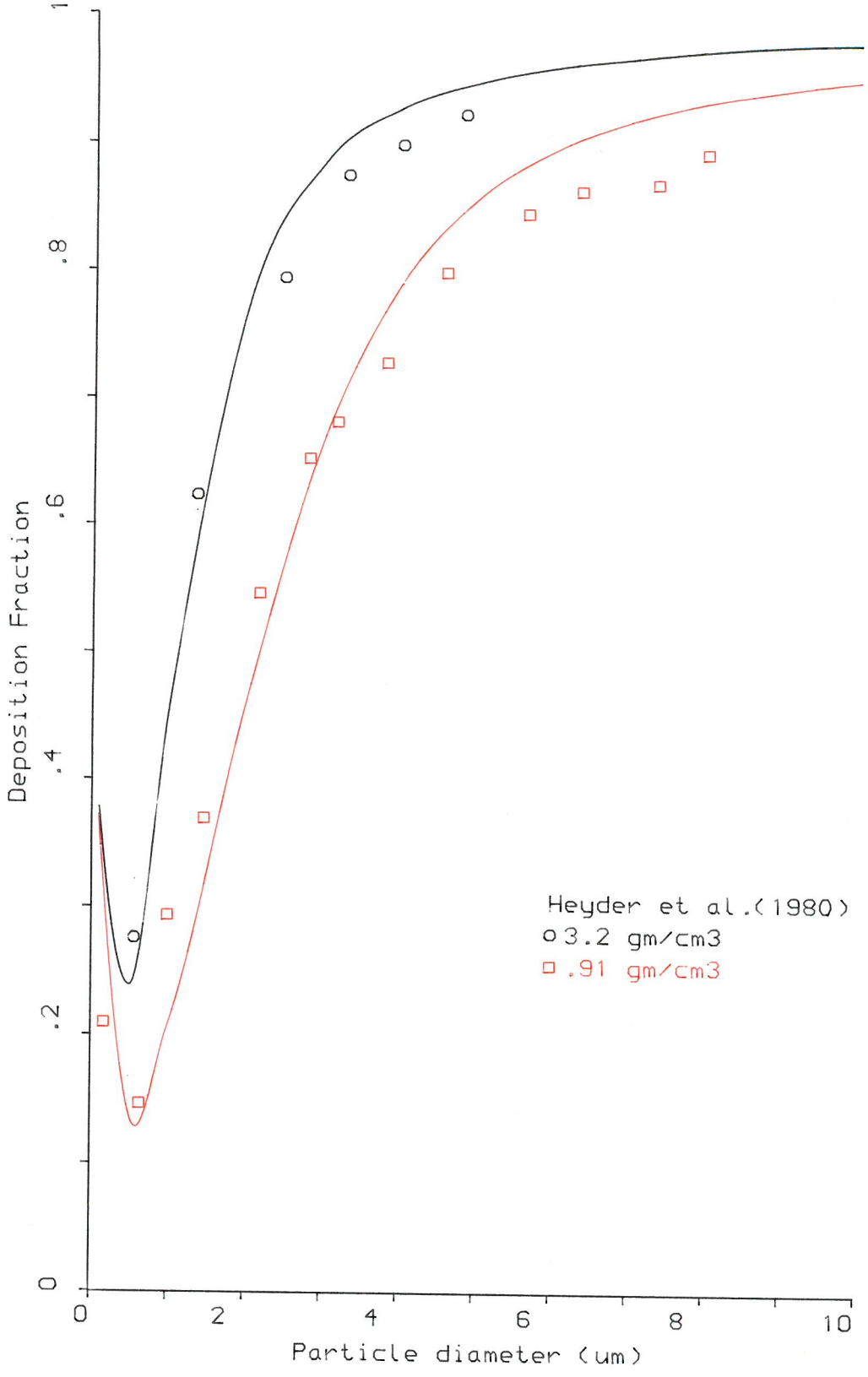

FIG.(II.17): Effect of particle size and particle density on total deposition for mouth breathing at Q=250 cm3/s and T=4s
(the solid lines are the calculated values)

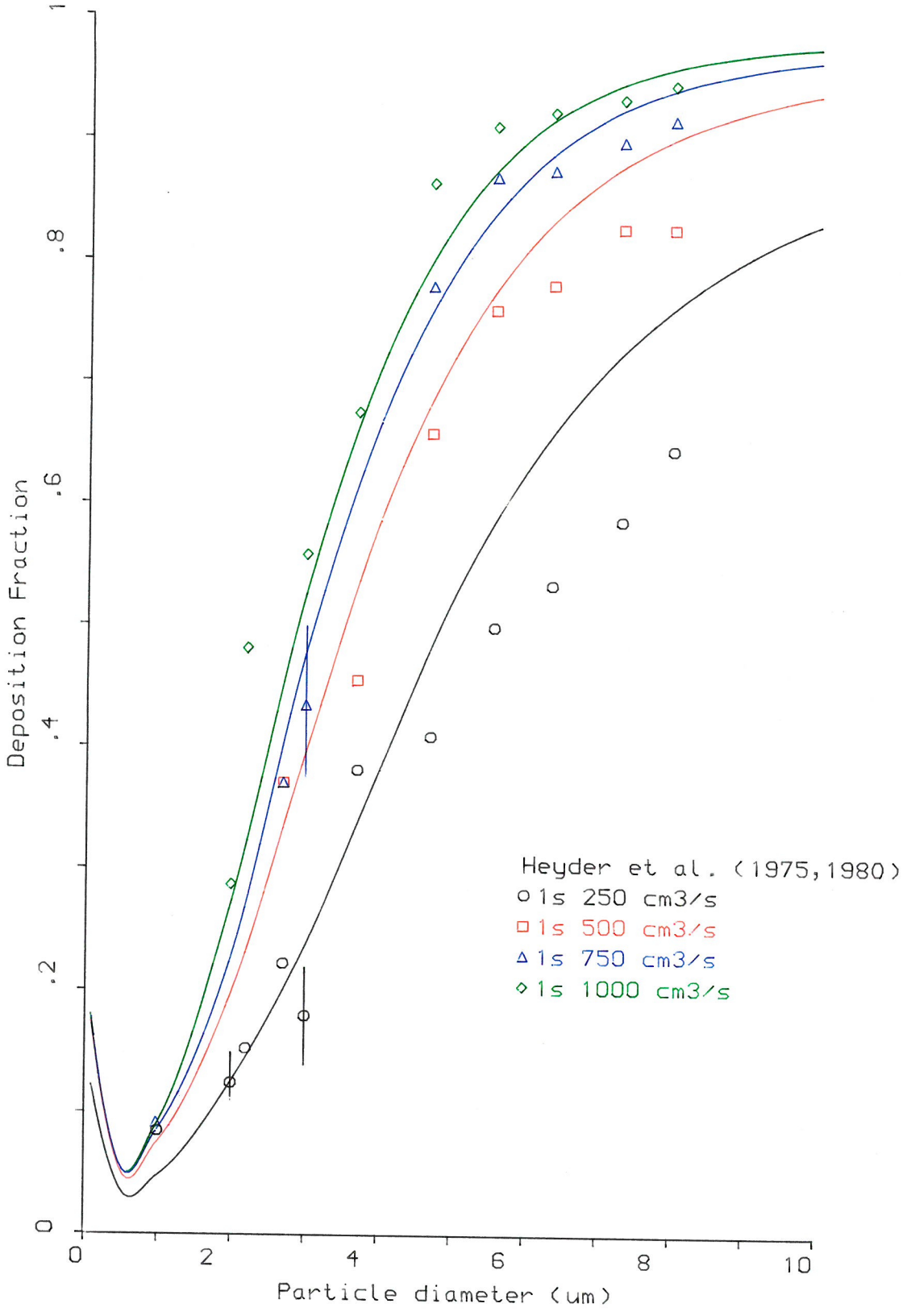

FIG.(II.18): Total deposition as a function of particle diameter at mouth breathing for various Qo at T=1s (p=0.91 g/cm3) (the solid lines are the calculated values)

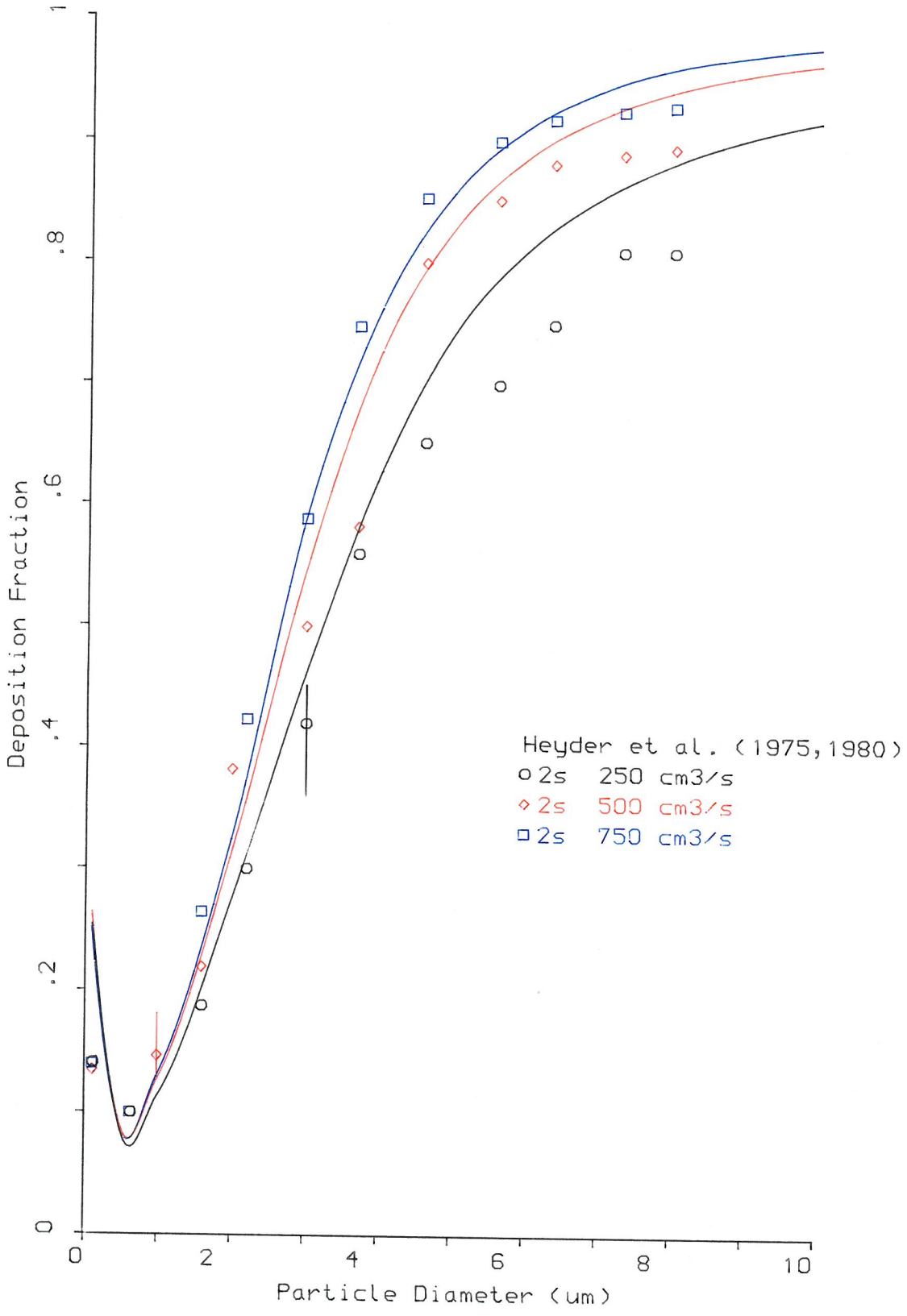

FIG.(II.19): Total deposition as a function of particle diameter at mouth breathing for various Q at T=2s (p=0.91 g/cm3)
(the solid lines are the calculated values)

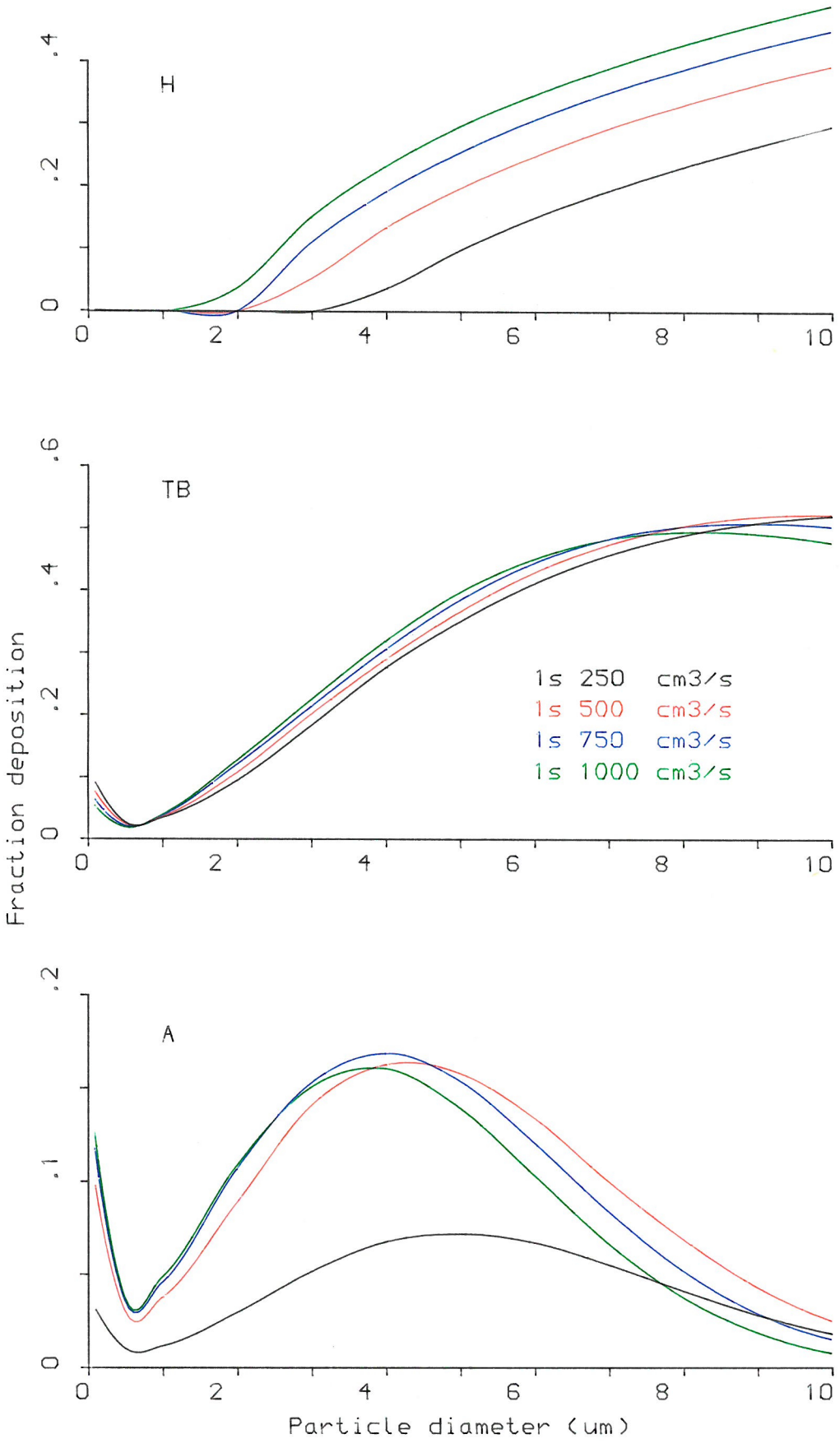

FIG(II.20): Calculated regional deposition as a function of particle diameter at mouth breathing for various Q at T=1s (p=0.91 g/cm3)

7.1.A.4 Effect of mean residence time on total deposition

The effect of mean residence time on particle deposition is caused by the mechanisms of sedimentation and diffusion. Figures II.21 and II.22 show the effect on total deposition, as a function of particle diameter, of varying the mean residence time. Mouth breathing is assumed, and in order to vary the mean residence time, two flow rates Q = 250 and 750cm^{3}s^{-1} are used. Figure II.23 illustrates the same effect but for nose breathing with a flow rate of 250cm^{3}s^{-1}.

Deposition is enhanced by increasing mean residence time, for all particle diameters, since more time is available for particles to deposit in the respiratory tract: there is more time for the diffusion of particles smaller than 0.5μm diameter and for the sedimentation of the larger particles.

The calculated regional deposition, shown in Figure II.24, illustrates that this increase occurs in the A–region, and is due to longer residence time and deeper aerosol penetration. It can also be seen that the maximum in A–deposition is reduced from 3.6μm to 3μm diameter due to the increase in aerosol flow rate.

The effect of residence time on deposition is less at the higher flow rate of 750cm^{3}s^{-1}, than at 250cm^{3}s^{-1}, because more particles are deposited by inertial impaction and, consequently, fewer particles are available for deposition by sedimentation.

Another way of examining the effects of flow rate and residence time is to vary each of them such that their product is constant. This corresponds to the tidal volume being fixed, for which the effect of aerosol penetration on deposition is no longer a factor. Figures II.25 and II.26 are the theoretically predicted depositions and experimental data for mouth and nose breathing respectively. As can be seen from Figure II.25, for 1μm particles, deposition increases with increasing mean residence time, indicating that sedimentation is the main mechanism here. For 8μm diameter particles, however, the increase in deposition with increasing aerosol flow rate is mainly due to impaction. There exists a transition particle diameter at which deposition shifts from a sedimentation dominated regime to an impaction dominated one. For mouth breathing, this was found to be about 4μm by Heyder et al. (1980), while the present model predicts a value of about 6μm. Again, this value (6μm) is in very good agreement with Yu's prediction.

For nose breathing, see Figure II.26, impaction is more important and

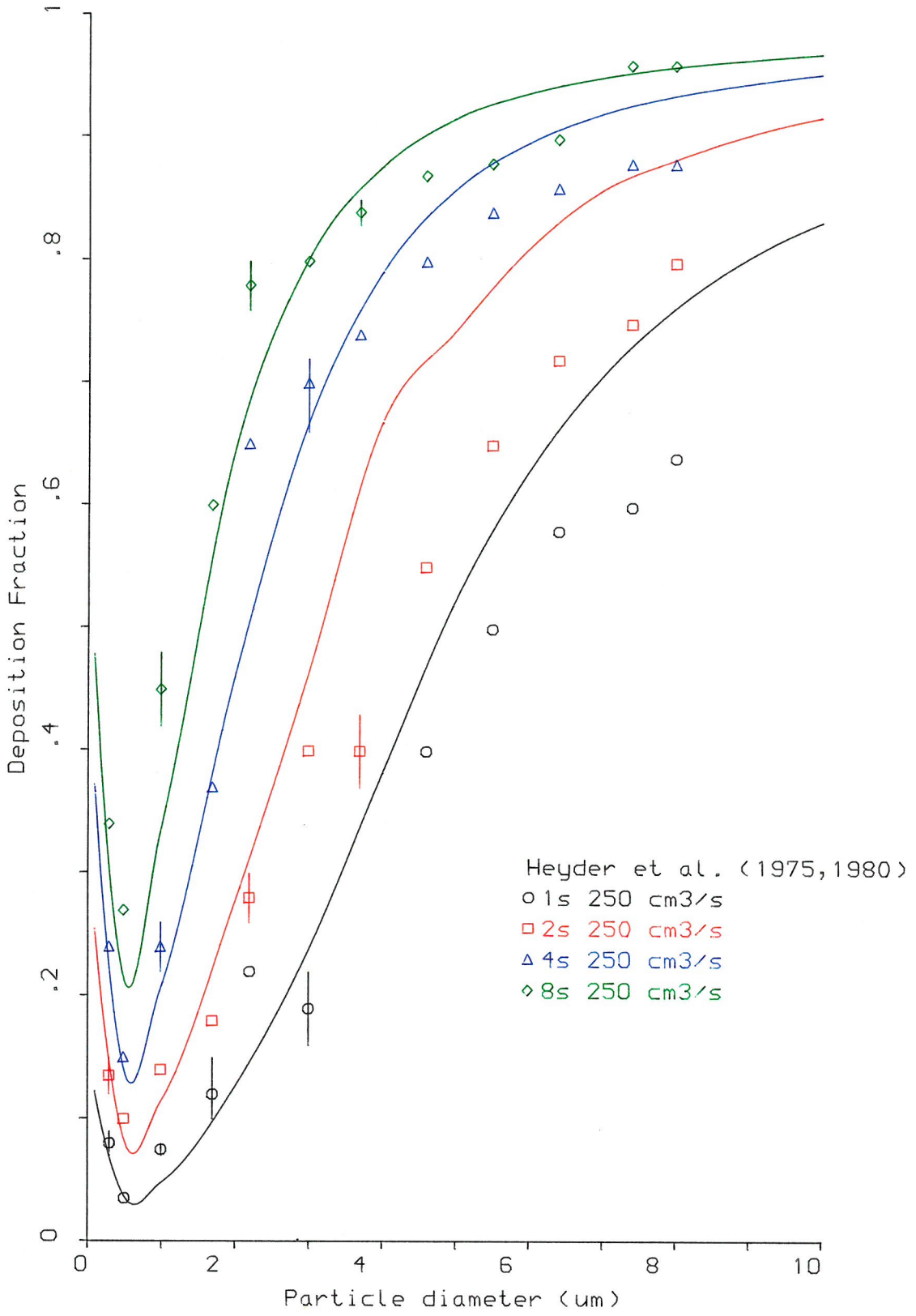

FIG.(II.21): Total deposition as a function of particle diameter at mouth breathing for various T at Q=250 cm3/s (p=0.91 g/cm3) (the solid lines are the calculated values)

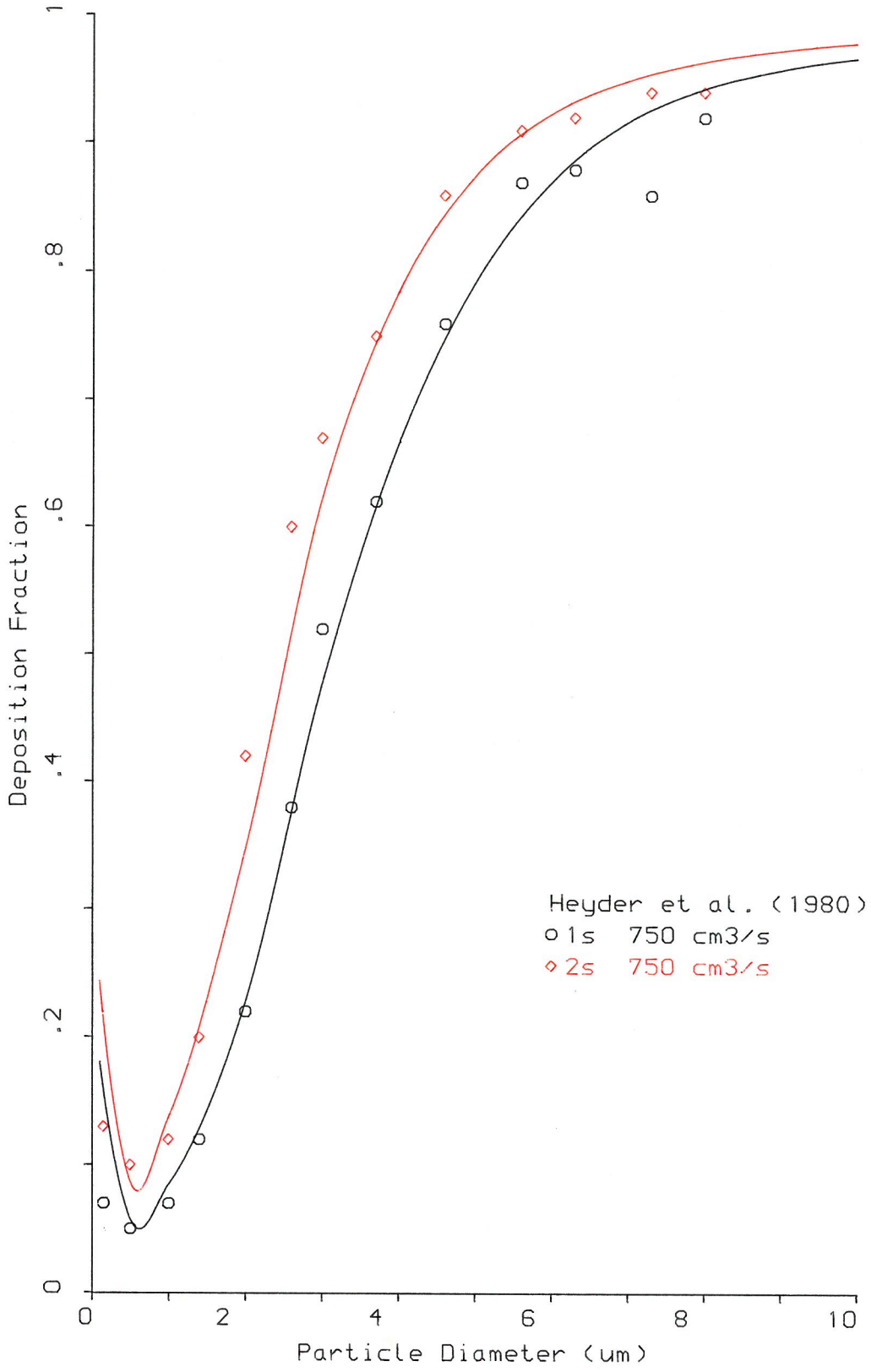

FIG.(II.22): Total deposition as a function of particle diameter at mouth breathing for various T at Qo=750 cm3/s (p=0.91 g/cm3)
(the solid lines are the calculated values)

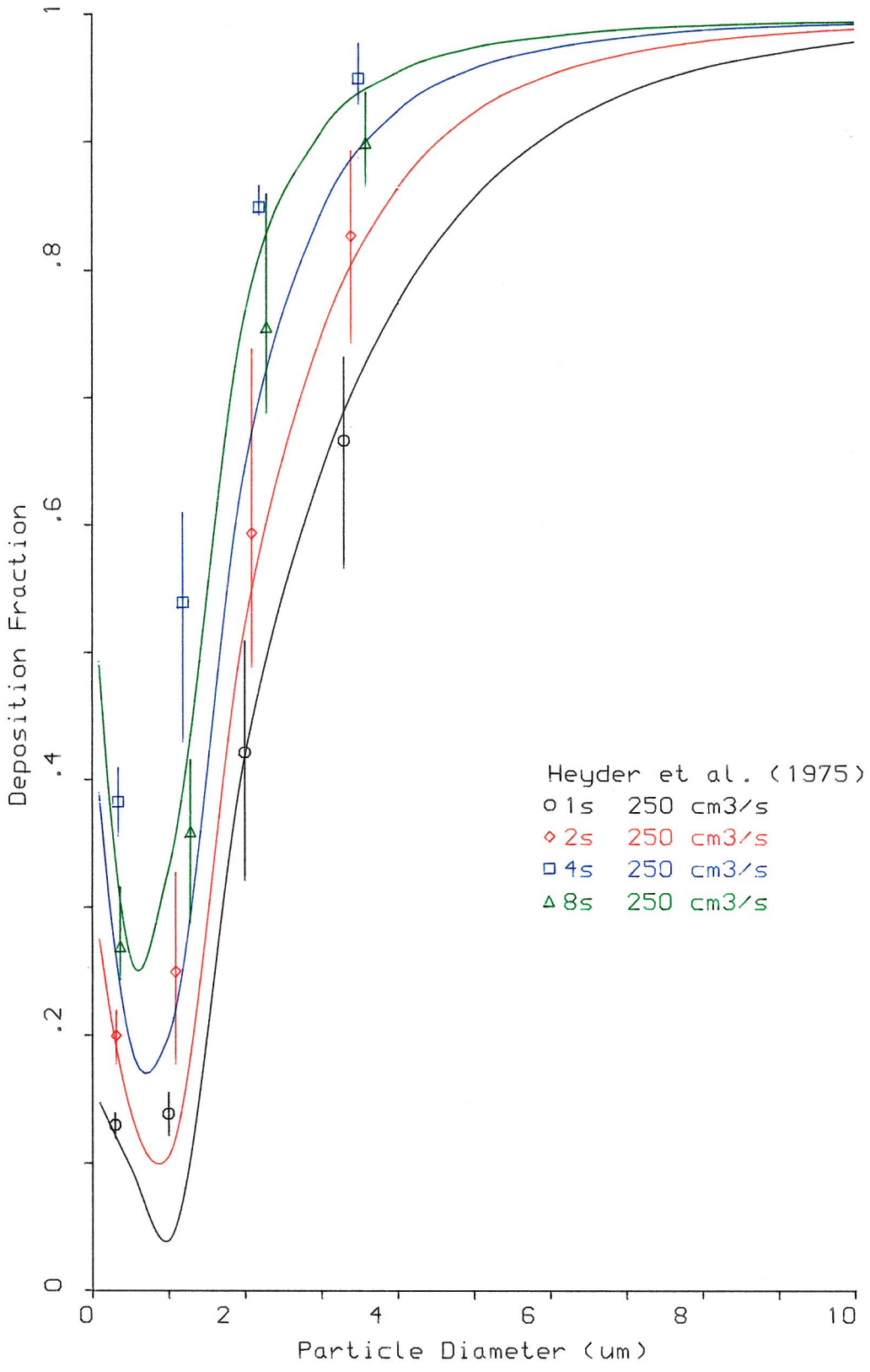

FIG.(II.23): Total deposition as a function of particle diameter at nose breathing for various T at Qo=250 cm3/s (p=0.91 g/cm3) (the solid lines are the calculated values)

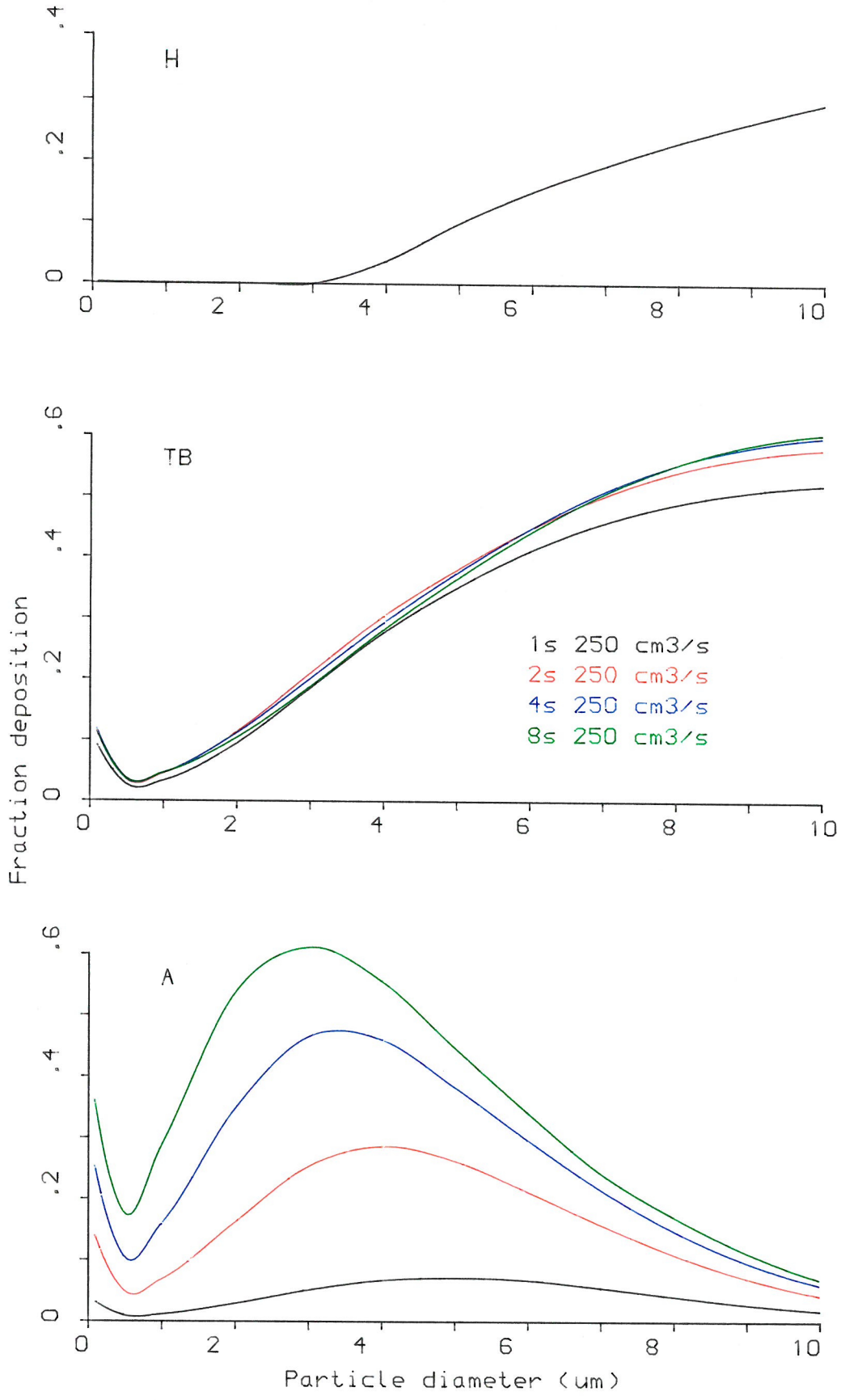

FIG(II.24): Calculated regional deposition as a function of particle diameter at mouth breathing for various T (Q=250cm3/s, p=0.91g/cm3)

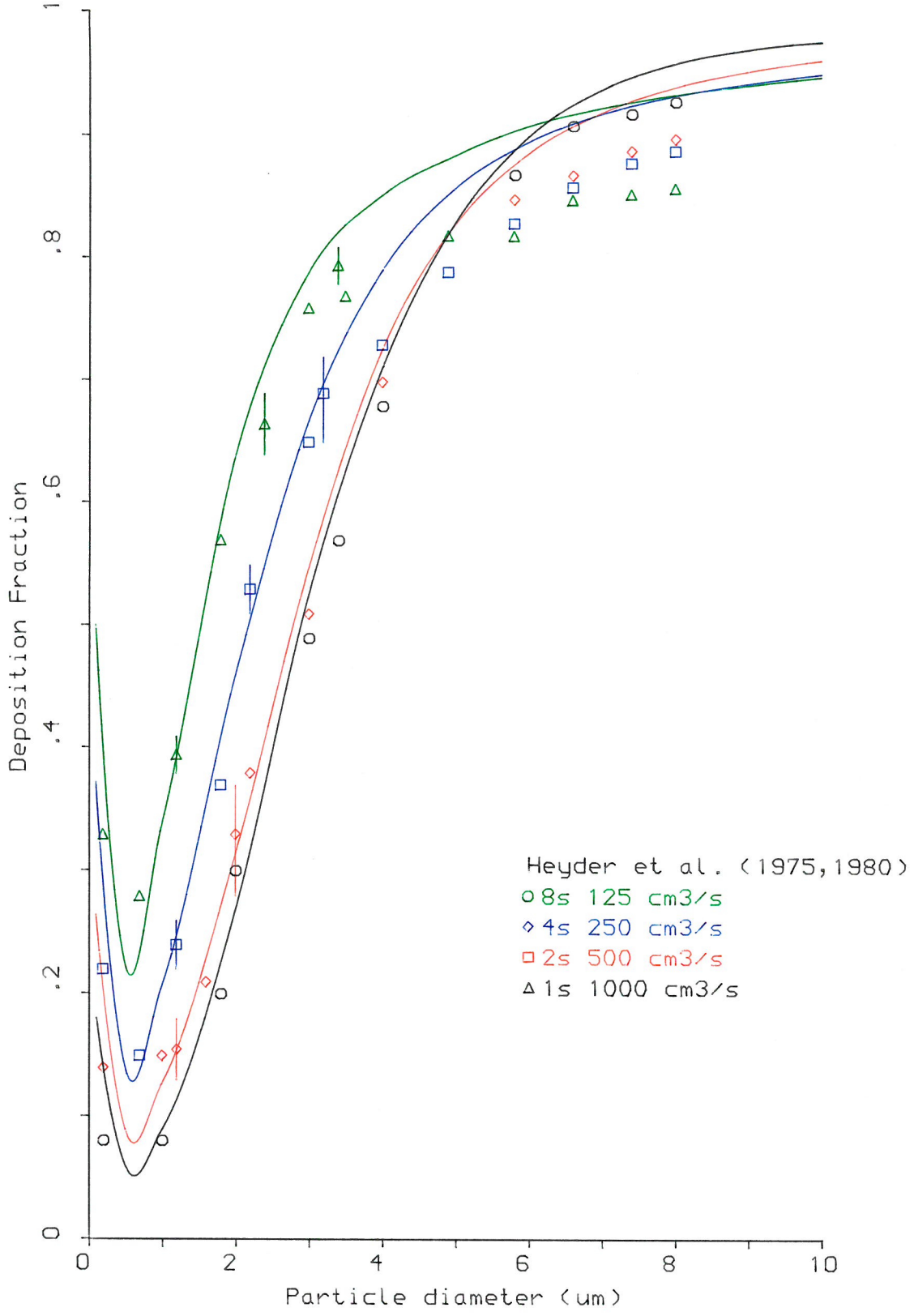

FIG.(II.25): Total deposition as a function of particle diameter at mouth breathing for QT=1000 cm3 (p=0.91 g/cm3) (the solid lines are the calculated values)

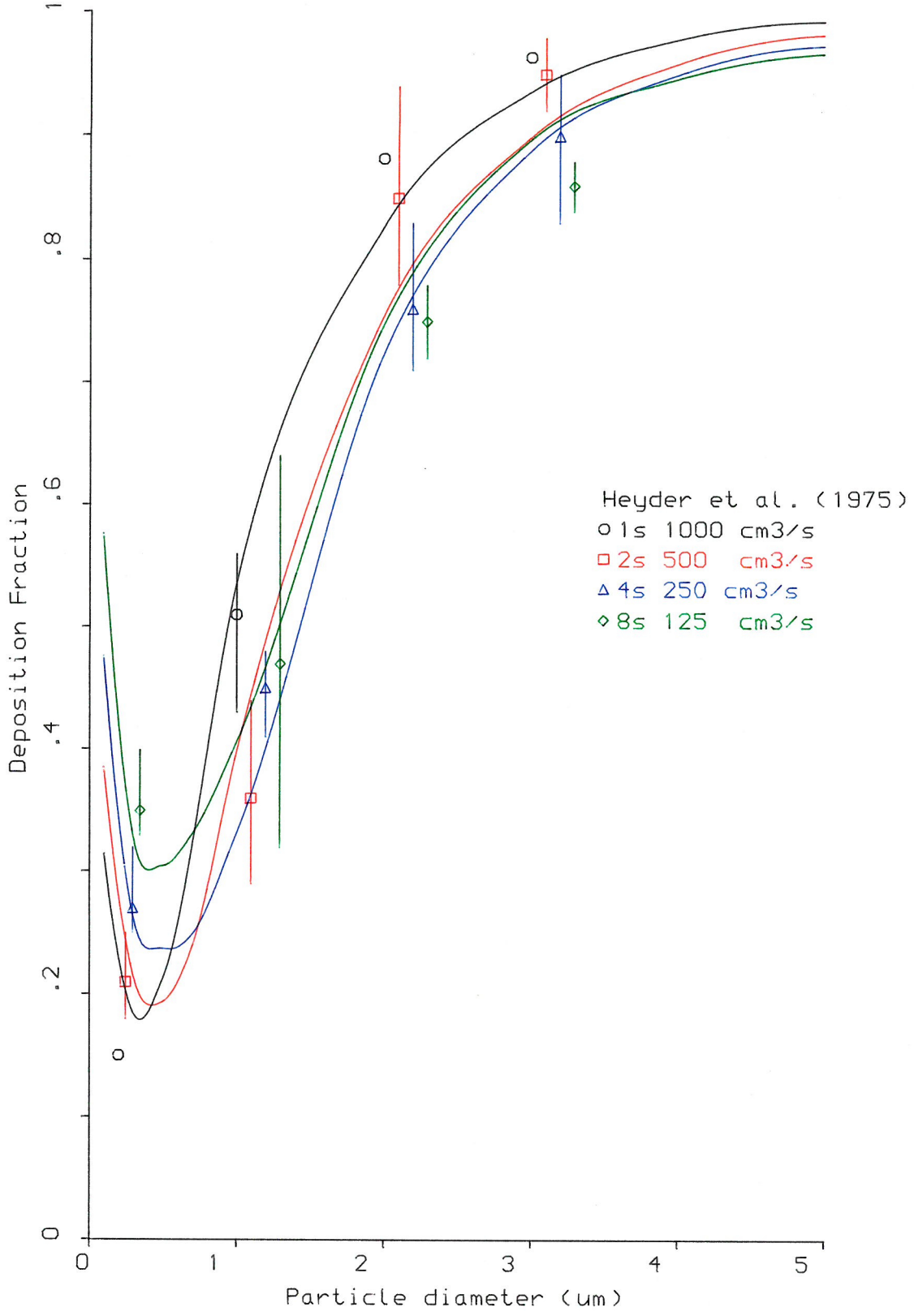

FIG.(II.26): Total deposition as a function of particle diameter at nose breathing for QT=1000 cm3 (p=0.91 g/cm3) (the solid lines are the calculated values)

the transition particle diameter decreases to a value of 1μm, as found by both calculation and experiment.

Regional deposition for constant tidal volume, mouth breathing assumed, is presented in Figure II.27. It shows that larger H–deposition is always associated with high flow rate, and that A–deposition increases with mean residence time.

7.1.A.5 Effect of intersubject variation on total deposition

Two notable causes for intersubject variation in lung deposition are differences in: (1) lung dimension; and (2) breathing pattern. For a similar lung structure, a larger functional residual capacity (FRC) yields a smaller deposition because the airway dimensions are enlarged. Figure II.28 shows the total and A–deposition in the lung (including mouth breathing) versus particle diameter for unit density spheres. Three different FRC's are considered. The tidal volume, applicable in all cases, is 1000cm^3 the cycle time being 4s without pause. It can be seen that there is a significant decrease in total deposition when the FRC increases from 2000cm^3 to 5000cm^3. This decrease takes place primarily in the A–region, except for very large particles.

Figure II.29 shows a comparison of the calculated total deposition and experimental data, plotted as a function of FRC, for different particle sizes and breathing patterns. As can be seen, good agreement is found between the predictions of the model and the experimental data of Heyder et al. (1980).

7.1.A.6 Effect of pause on total deposition

Under normal breathing conditions, variation in the pause time can arise for any given subject. The inclusion of the pause during a respiratory cycle can significantly effect particle deposition. Figure II.30 shows the total deposition of unit density spheres plotted as a function of particle size. The effect of mouth breathing has been considered, the tidal volume being 1000cm^3 and cycle time 4s (with and without pause). The pause, of duration 0.4s, is assumed to be at the end of inhalation. The increase in deposition, due to the pause, is clearly shown. It can be seen from Figure II.30 that the increased deposition occurs in the A–region, for small and medium particle sizes. Figure II.31 shows the comparison between the calculated depositions and the experimental data, compiled by Lippmann and Altshuler (1976), where mouth breathing has been considered and the pause period is one–tenth of the breathing cycle time. This corresponds to a tidal volume of 1000cm^3 and total breathing period of 4.29s. There appears to be

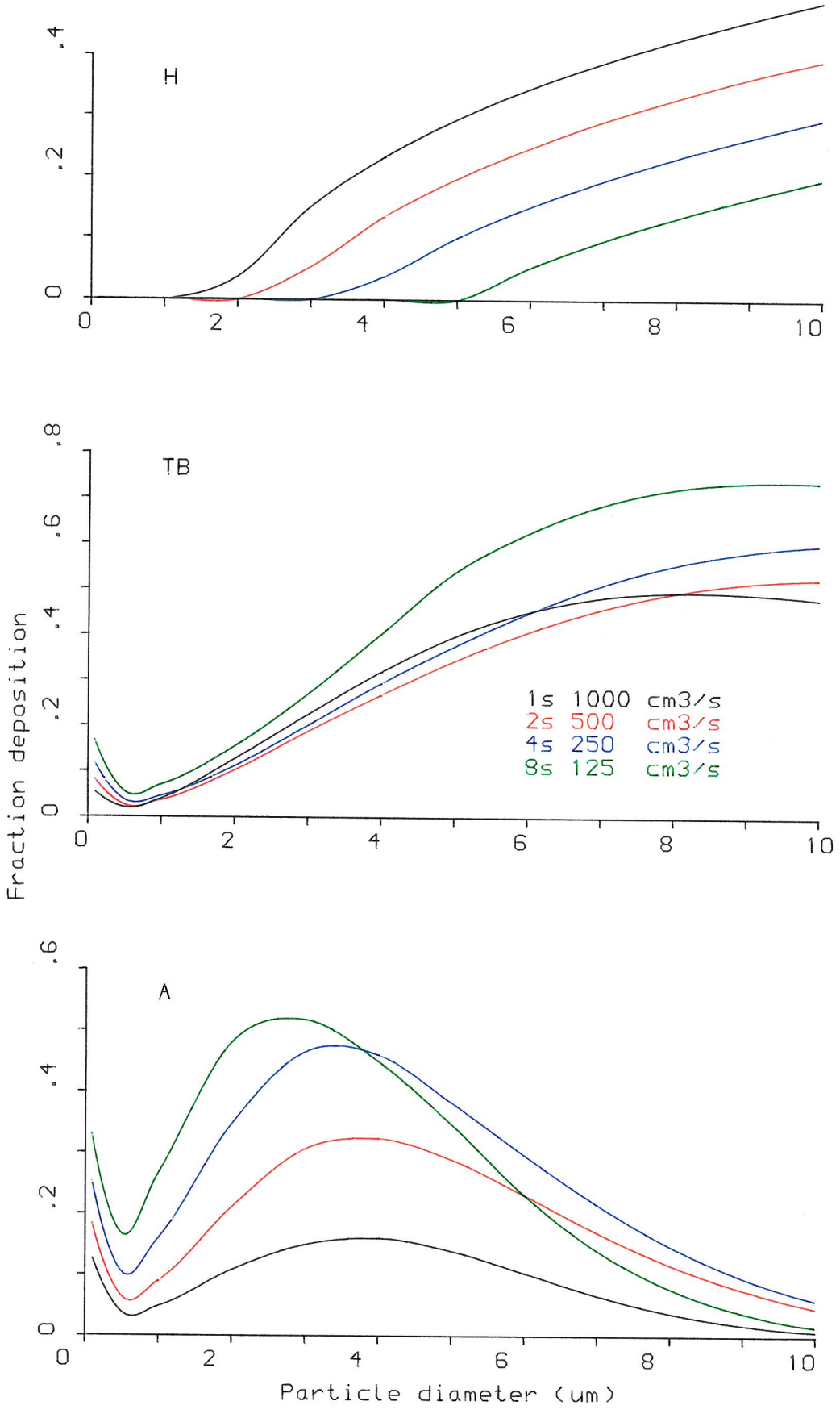

FIG(II.27): Calculated regional deposition as a function of particle diameter at mouth breathing for QT=1000 cm3 (p=0.91 g/cm3)

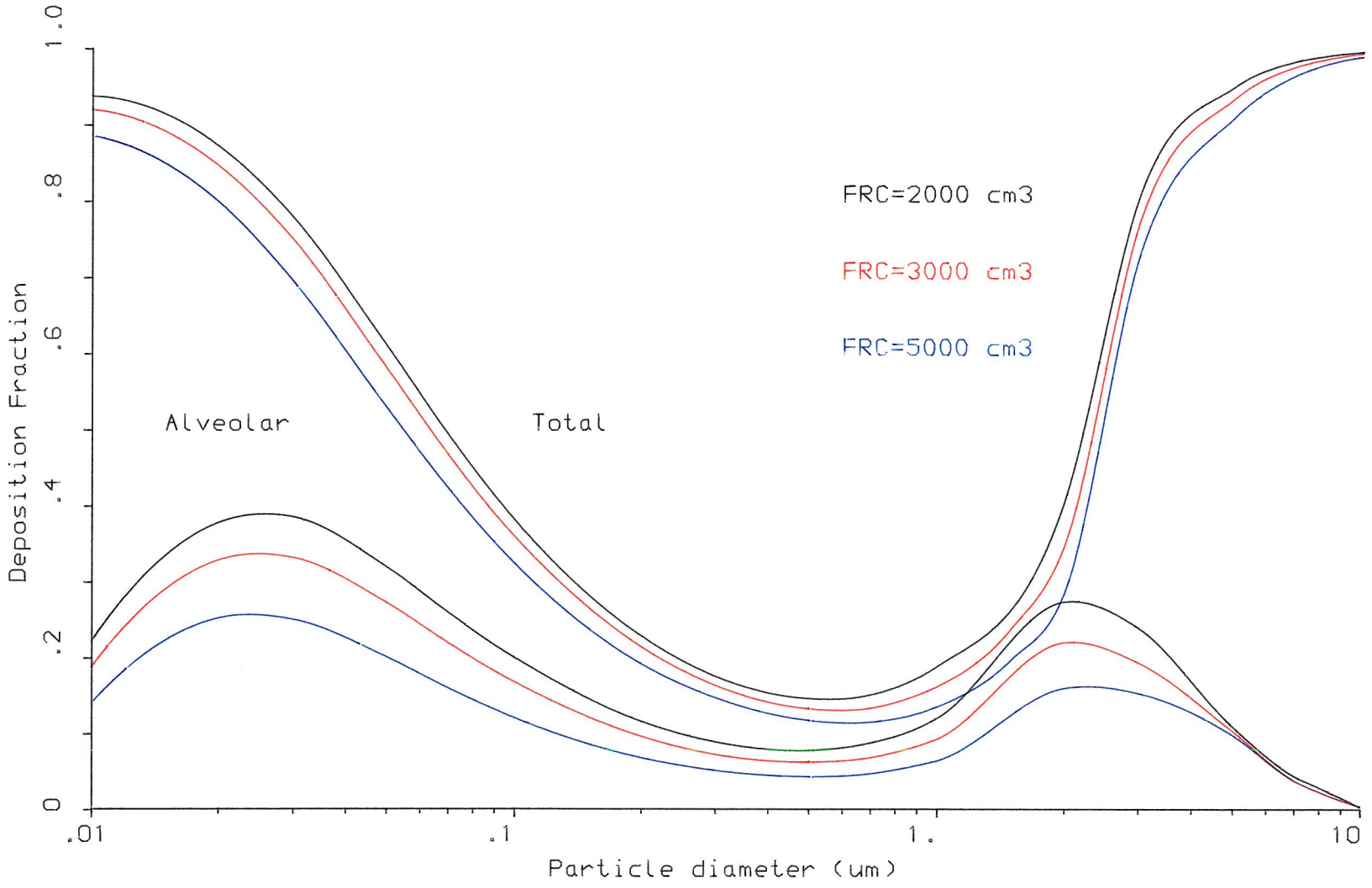

FIG.(II.28): Effect of FRC on total and A-deposition for mouth breathing at tidal volume=1000 cm3, Qo=500 cm3/s, t=2s
(p=1gm/cm3, No pause)

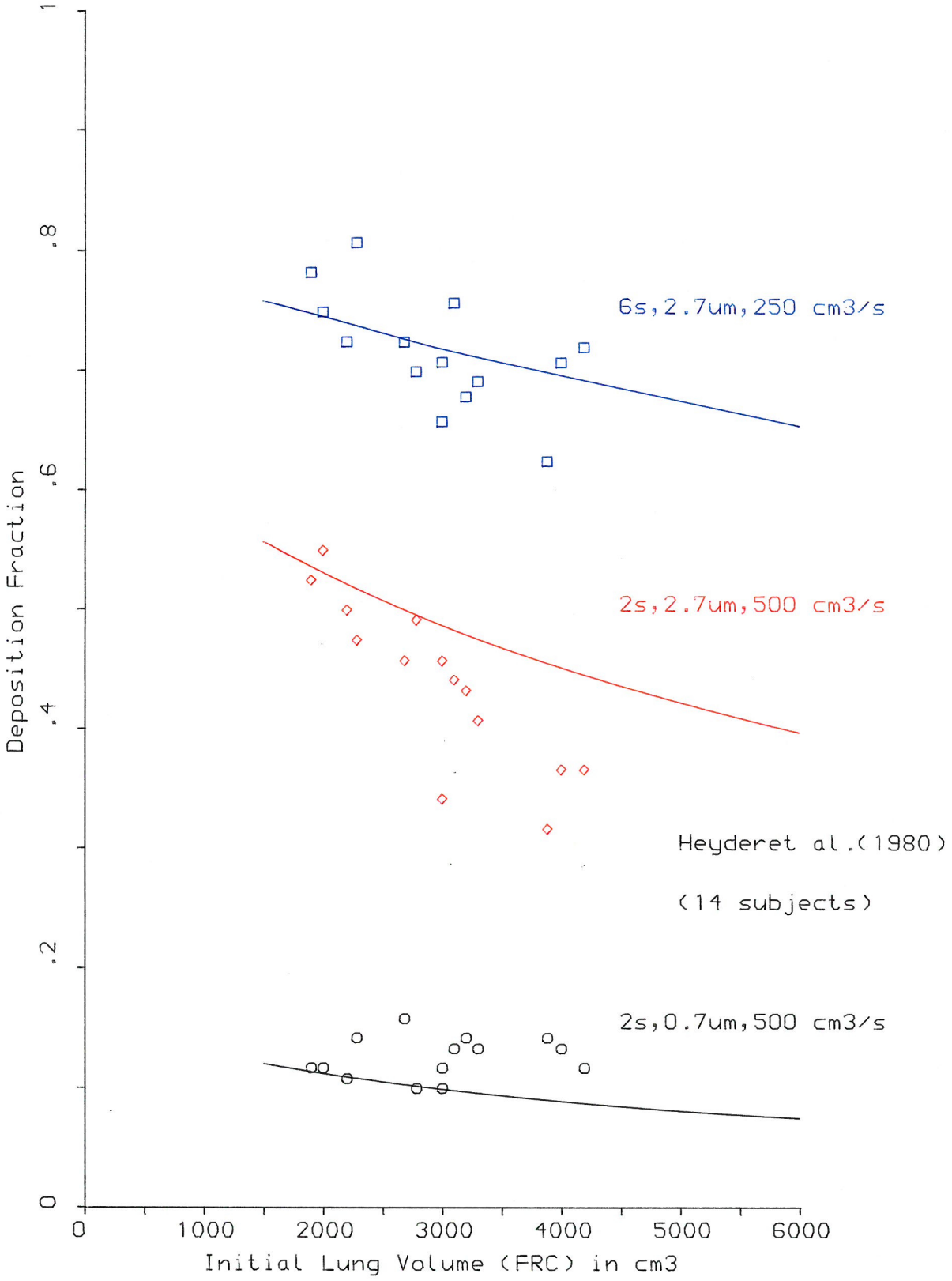

FIG.(II.29): Total deposition fraction versus initial lung volume (FRC) for different particle sizes and breathing patterns (the solid lines are the calculated values)

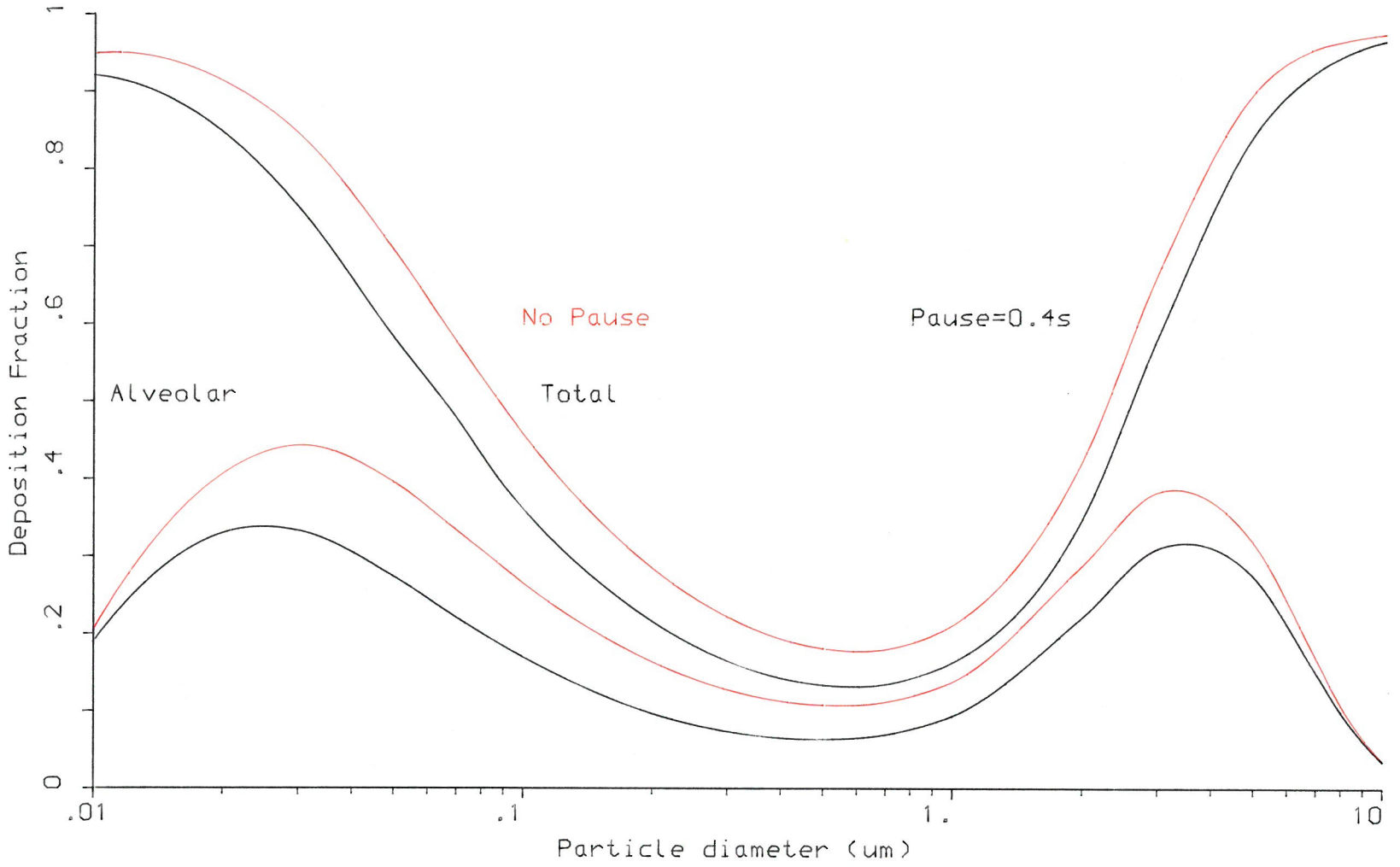

FIG.(II.30): Total and A-deposition as a function of particle diameter at mouth breathing for various Qo at T=1s (p=.91gm/cm3, FRC=3000 cm3, No pause)

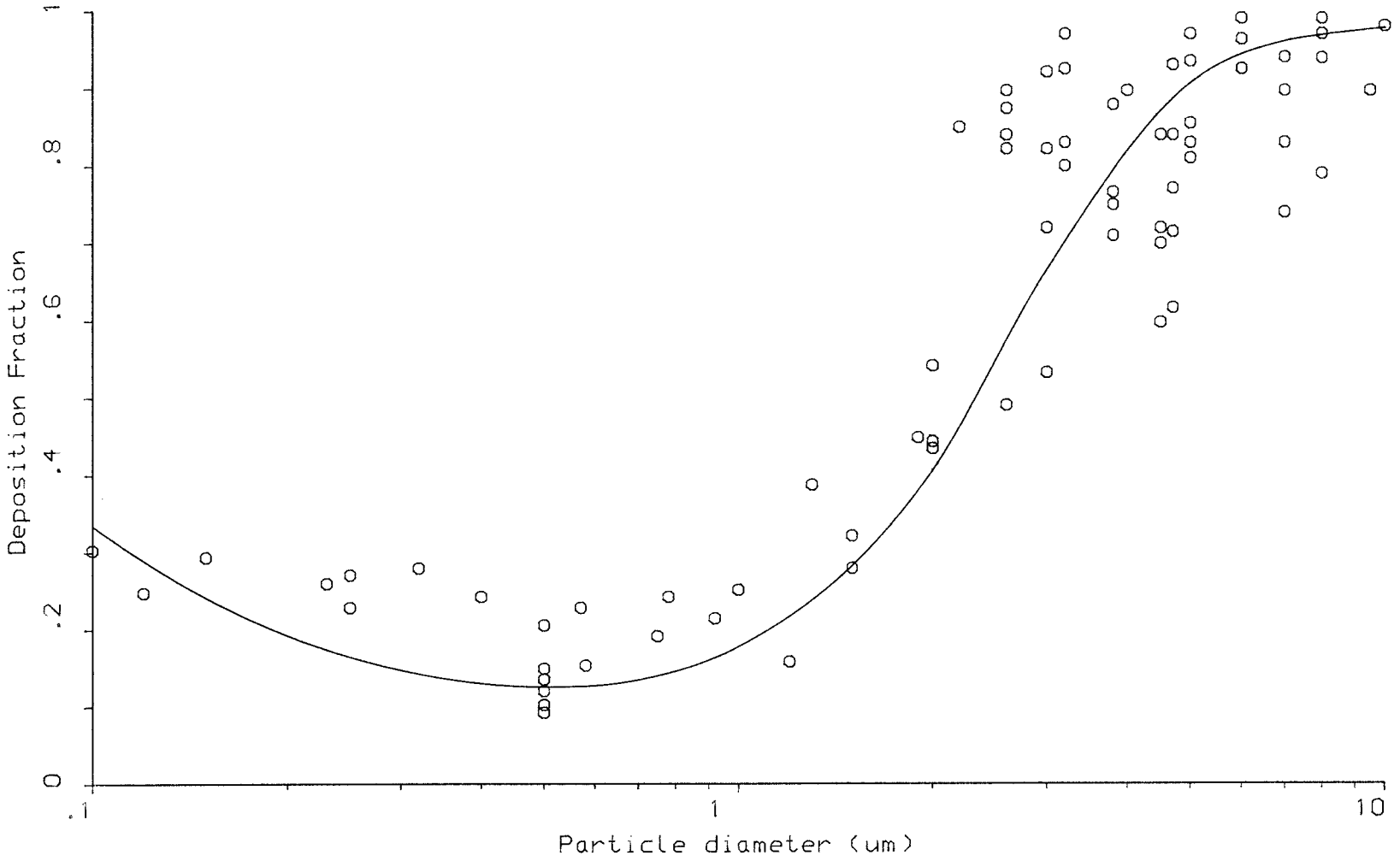

FIG.(II.31): Total deposition vs particle diameter, comparison between the predicted values (solid lines) and the exp.data compiled by Lippmann et al.(1976)

satisfactory agreement between the theoretical and experimental data (in view of the uncertainties in FRC and breathing pattern of the experimental data).

Very good agreement is also found between the predictions of the model and the theoretical predictions of Yu (1978).

7.1.B Comparison with the published data of regional deposition

There are still not enough experimental data available with regard to regional deposition under well controlled breathing conditions. Intersubject variability in A and TB-deposition is still not known. For TB-deposition, there are discrepancies between the reported data produced by different laboratories. For example, Stahlhofen et al. (1980) reported very small (insignificant) deposition in the H and TB-regions, for small particles under mouth breathing conditions, whereas, Chan and Lippmann (1980) found a significant TB-deposition.

For A-deposition, however, the data are in good agreement. The experimental data for A-deposition, produced by the two above mentioned laboratories, are used for comparison with the predictions of the new model. Chan and Lippmann (1980), reported experimental data for the A-deposition of iron oxide spheres (ρ = 3.2g/cm^3) in 26 subjects. A tidal volume of 1000cm^3 and cycle time of 4.29s (including 0.43s pause at the end of inhalation) were used and mouth breathing was considered. Figure II.32 presents these data together with the calculated A-deposition, predicted using the new model, for Weibel's lung data, adjusted to 3000cm^3 rest lung volume.

The deposition of iron oxide particles in the lung was evaluated by Stahlhofen et al. (1980) for 3 subjects using the following breathing patterns (where f is the breathing frequency):

A. V_t = 1000cm^3, f = 7.5min^{-1}, τ = 4s, Q = 250cm^{3}s^{-1}

B. V_t = 1500cm^3, f = 15min^{-1}, τ = 2s, Q = 750cm^{3}s^{-1}

In neither case was a respiratory pause considered. Figures II.33 and II.34 compare the calculated results and experimental data, for total and A-deposition, using these two breathing conditions. In this case calculations were based upon a *different* lung model, Yeh and Schum (1980), adjusted to a rest lung volume of 3000cm^3. Yeh and Shum use the same lung structure as Weibel but TB-airways have larger dimensions.

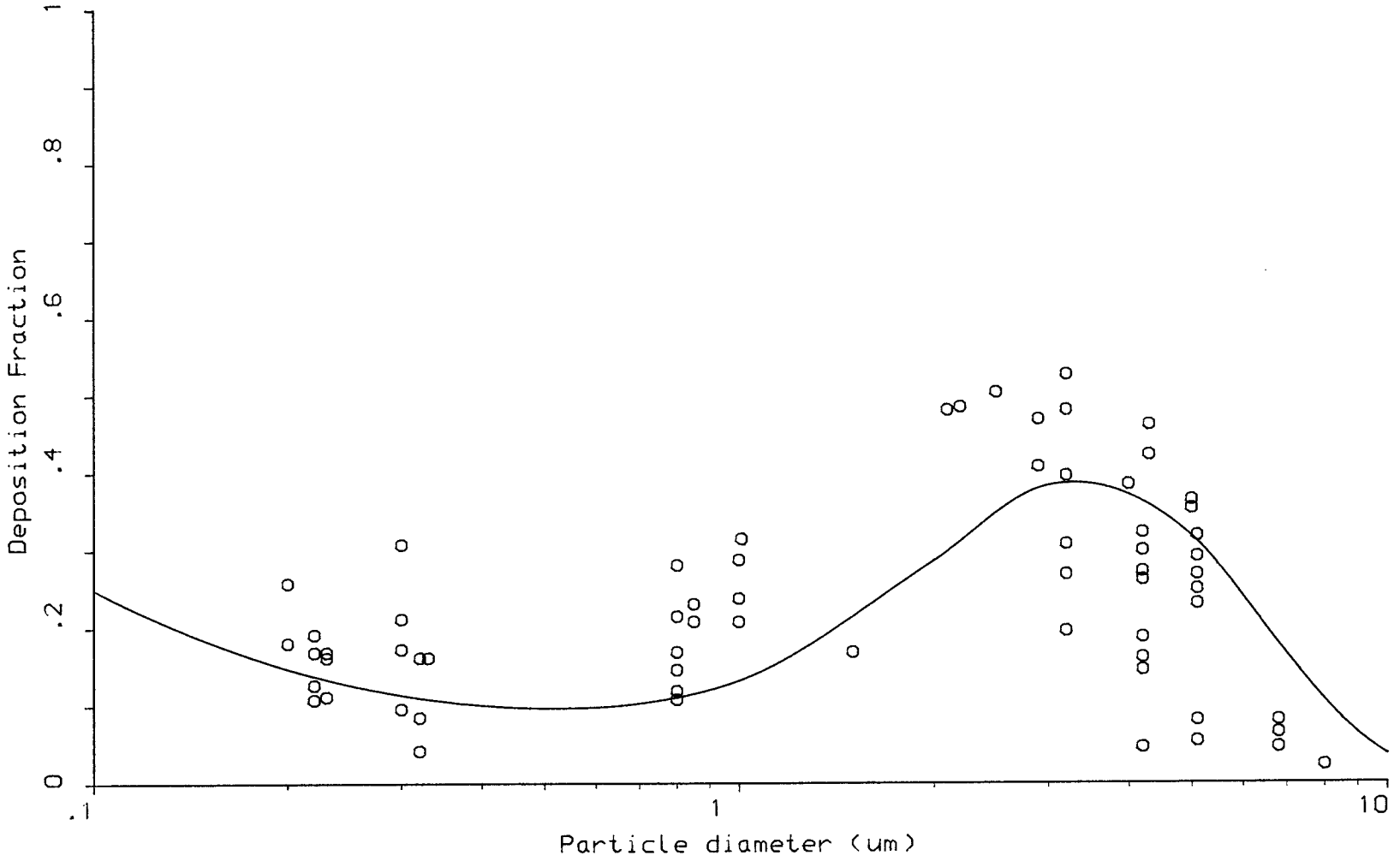

FIG.(II.32): Alveolar deposition vs particle diameter, comparison between the predicted values (solid lines) and the experimental data of 26 subjects ,Chan and Lippmann(1976) (tidal volume=1000 cm3 , T=4.3s , pause=o.423s)

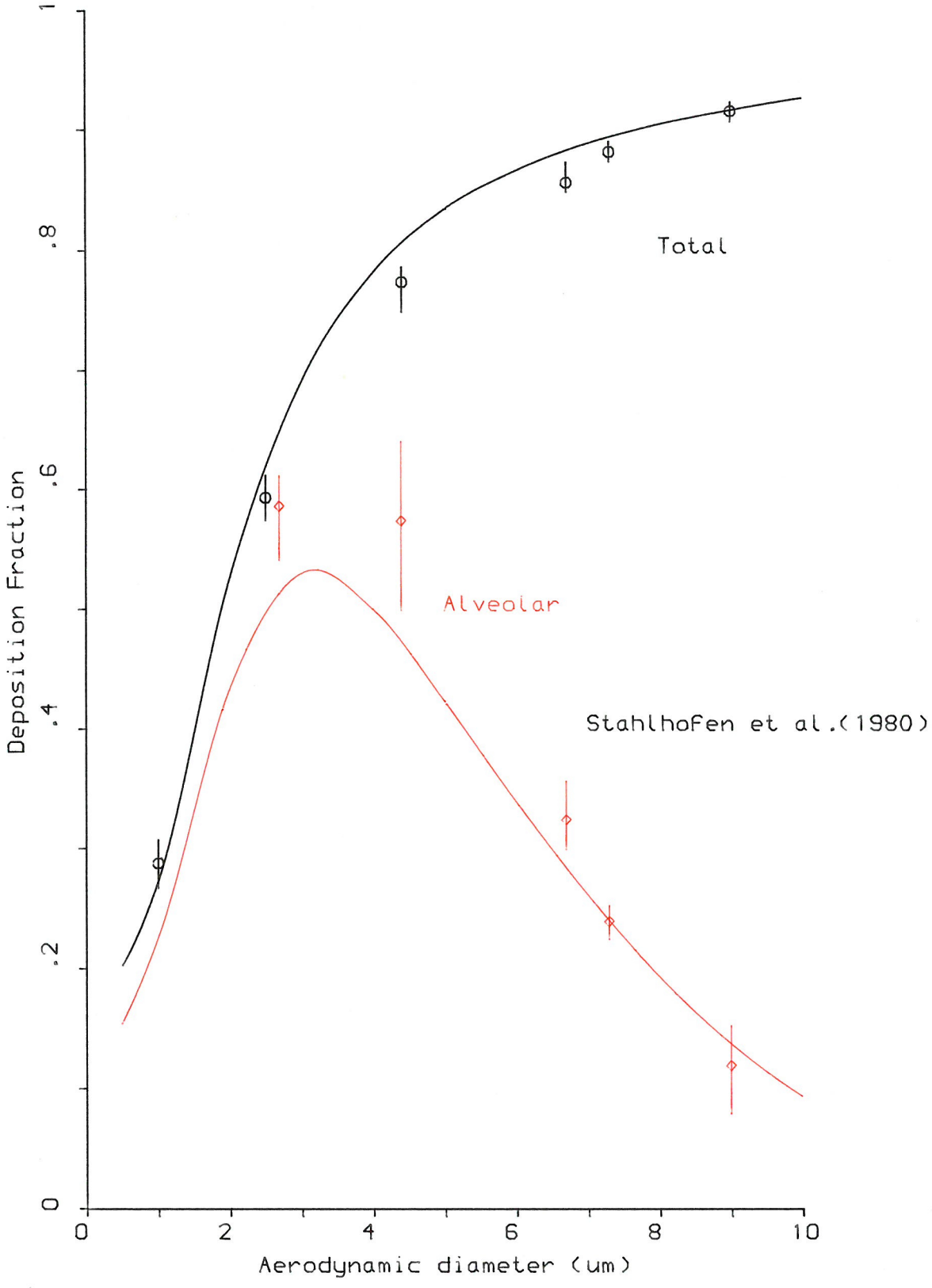

FIG.(II.33): Total and Alveolar deposition as a function of aerodynamic particle diameter at mouth breathing for Q=250 cm3/s, T=4s , p=3.2g/cm3 (the solid lines are the calculated values)

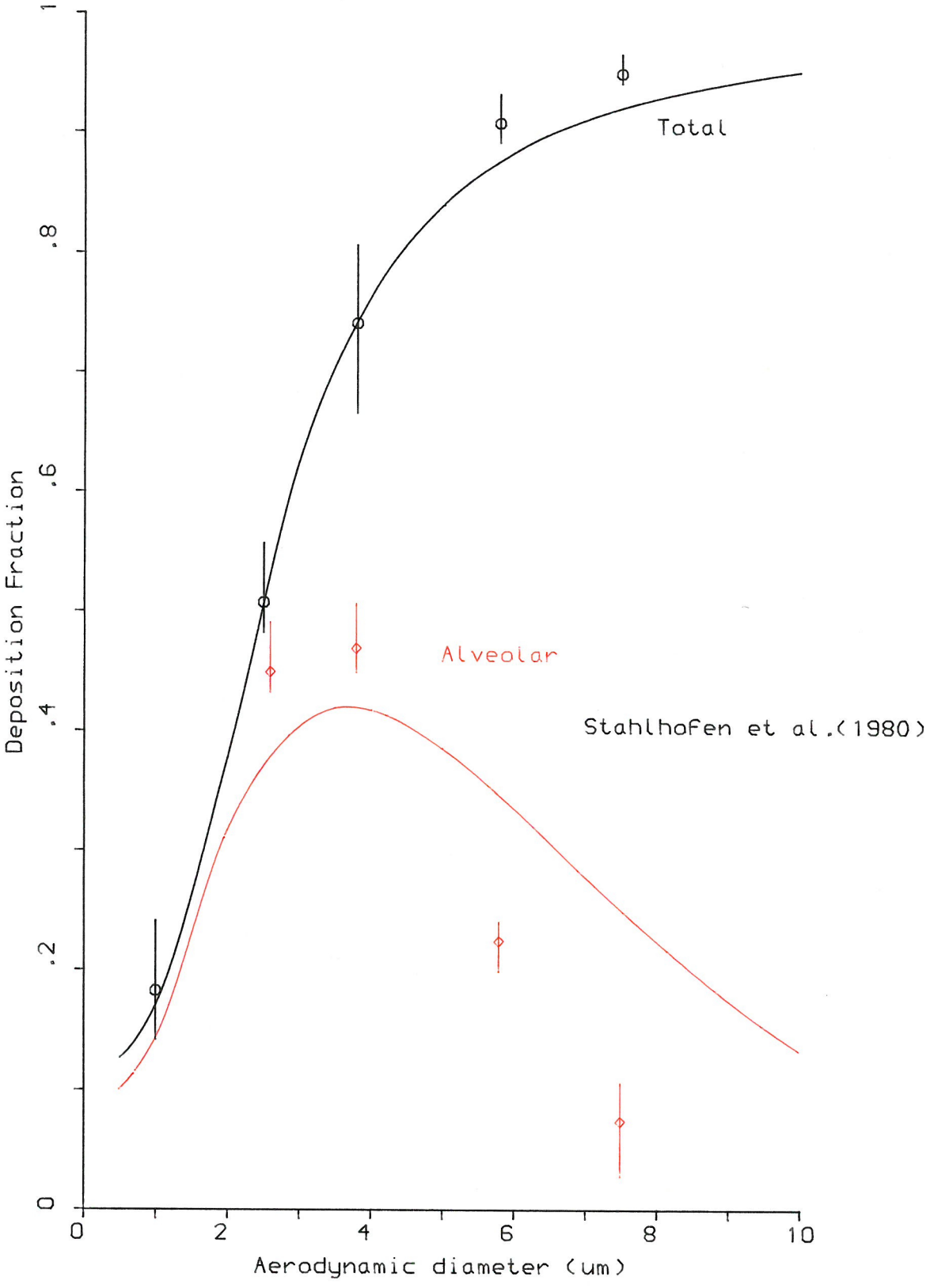

FIG.(II.34): Total and Alveolar deposition as a function of aerodynamic particle diameter at mouth breathing for Q=750 cm3/s, T=2s , p=3.2g/cm3 (the solid lines are the calculated values)

As it can be seen, the agreement between the calculated and experimental data appears to be very good.

7.2 Respiratory Deposition of Charged Particles

7.2.1 Prediction of the effect of charge on deposition

Using equation 104 (with η_q representing the image force deposition efficiency) and Weibel's lung model, inhalation deposition efficiencies were computed, for each airway generation, using two particle sizes (1 and 10μm diameters) and various charge levels, and a flow rate of 250cm^{3}s^{-1}. The results are shown in Figure II.35. For 1μm diameter particles, significant increases in deposition for a charge level of only 50 electronic units of charge per particle, are seen in all generations, the greatest effect being in the A-region. Conversely, there is negligible effect of charge on particles of dimater 10μm. The effect of charge on deposition efficiency increases as particle charge increases and particle size decreases.

There are several mechanisms by which aerosol particles acquire electrostatic charges (see Section 2.3 in Part I). The upper particle charge limits for these mechanisms have been established theoretically. The actual charge levels encountered usually lie between the RMS value at Boltzmann equilibrium and the Rayleigh limit (Chan and Mercer, 1971), see Appendix II.D.

Inhalation deposition efficiencies have been calculated for 1 and 10μm diameter particles, using a flow rate of 250cm^{3}s^{-1} and charge level corresponding to: (i) half Rayleigh limit, (ii) the maximum RMS atomization charge, Smoluchowski (1972), and (iii) the RMS charge at Boltzmann equilibrium (see Figures II.36a and b). It can be seen that aerosols whose droplets are charged to half their Rayleigh limit are subject to complete deposition in the lung.

7.2.2 Comparison of predicted results with published data for the effect of charge

Figure II.37 shows the calculated and experimental differences in total deposition between charged and uncharged particles, DD, versus $|q/e|$ for unit density particles of diameter 0.3, 0.6 and 1.0μm. In the calculations, an expression for critical charge q_c, given by Yu (1985), was used; for particles of diameter 0.3, 0.6 and 1μm the values of $|q_c/e|$ are 12, 30 and 54 respectively. In principle, q_c can have different values for the various airway generations, because of the differences in residence times and airway diameters. Such a

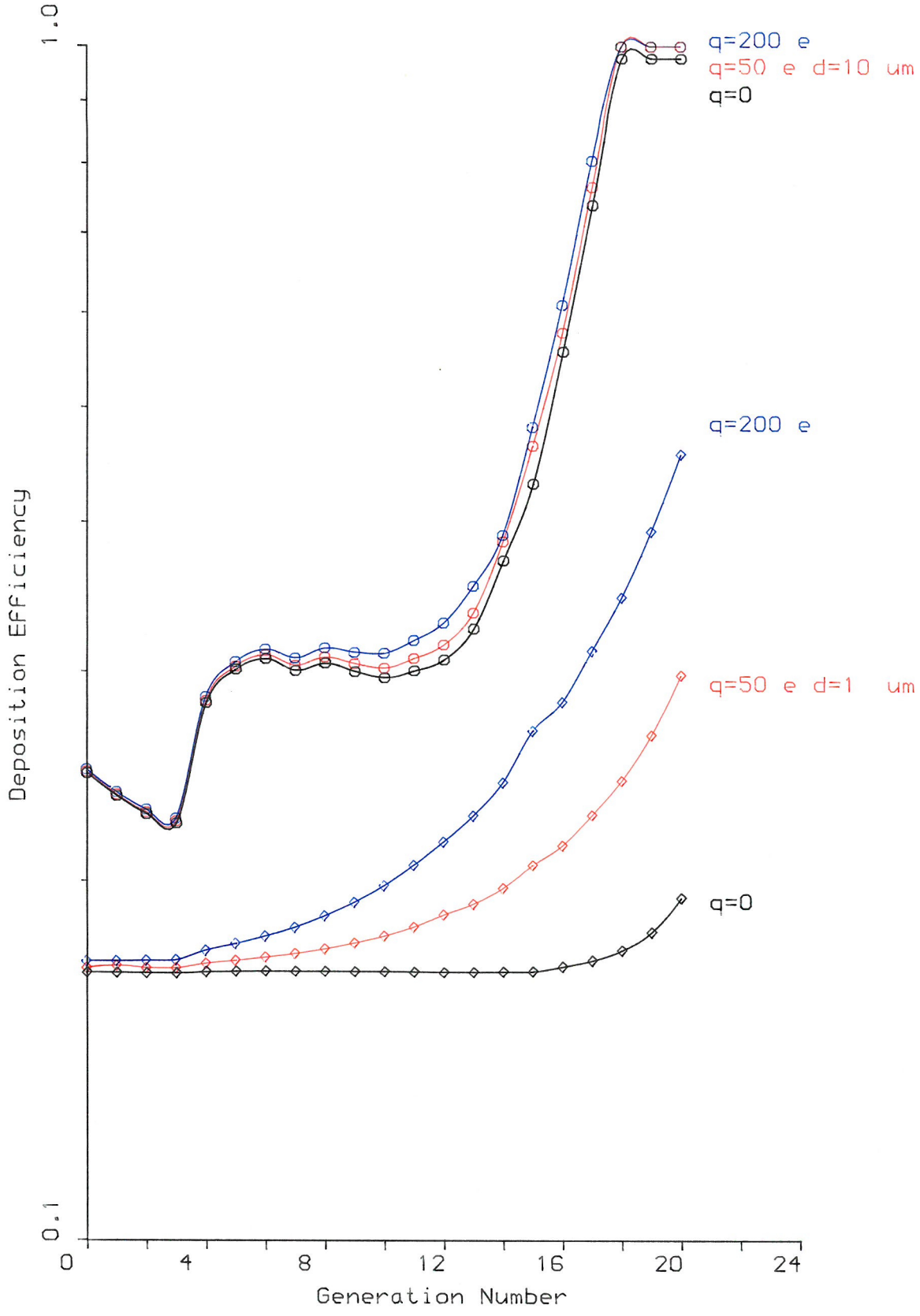

FIG.(II.35): Effect of aerosol particle charge on deposition efficiency in the human respiratory tract. (Qo=250 cm3/s, T=2s)

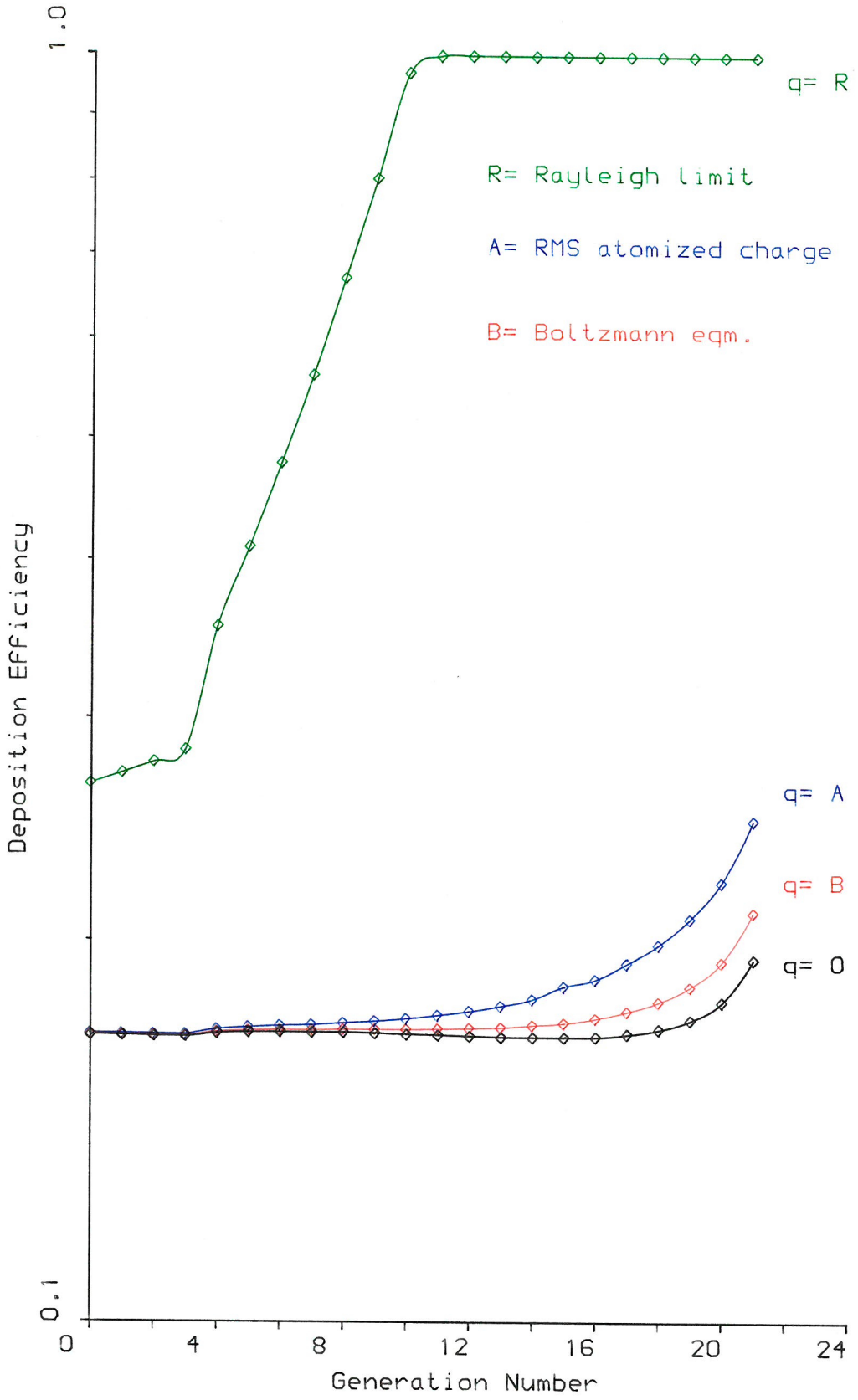

FIG.(II.36a): The effect on deposition efficiency of charging aerosol droplets to the charging limits associated with Rayleigh limit, RMS atomized charge and Boltzmann equilibrium. (d=1 um, Qo= 500 cm3/s , T= 2s)

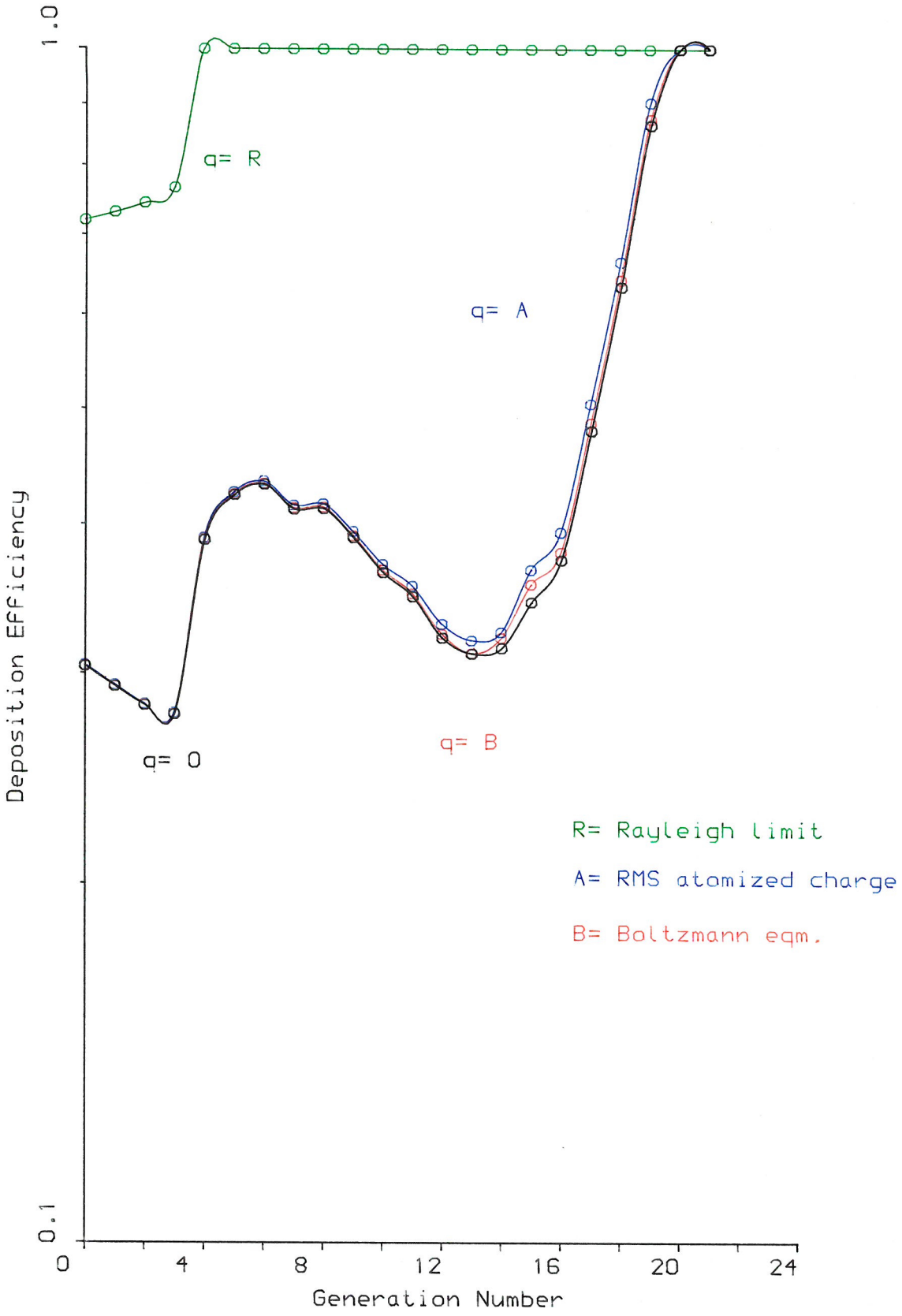

FIG.(II.36b): The effect on deposition efficiency of charging aerosol droplets to the charging limits associated with Rayleigh limit, RMS atomized charge and Boltzmann equilibrium. (d=10 um, Qo= 500 cm3/s , T= 2s)

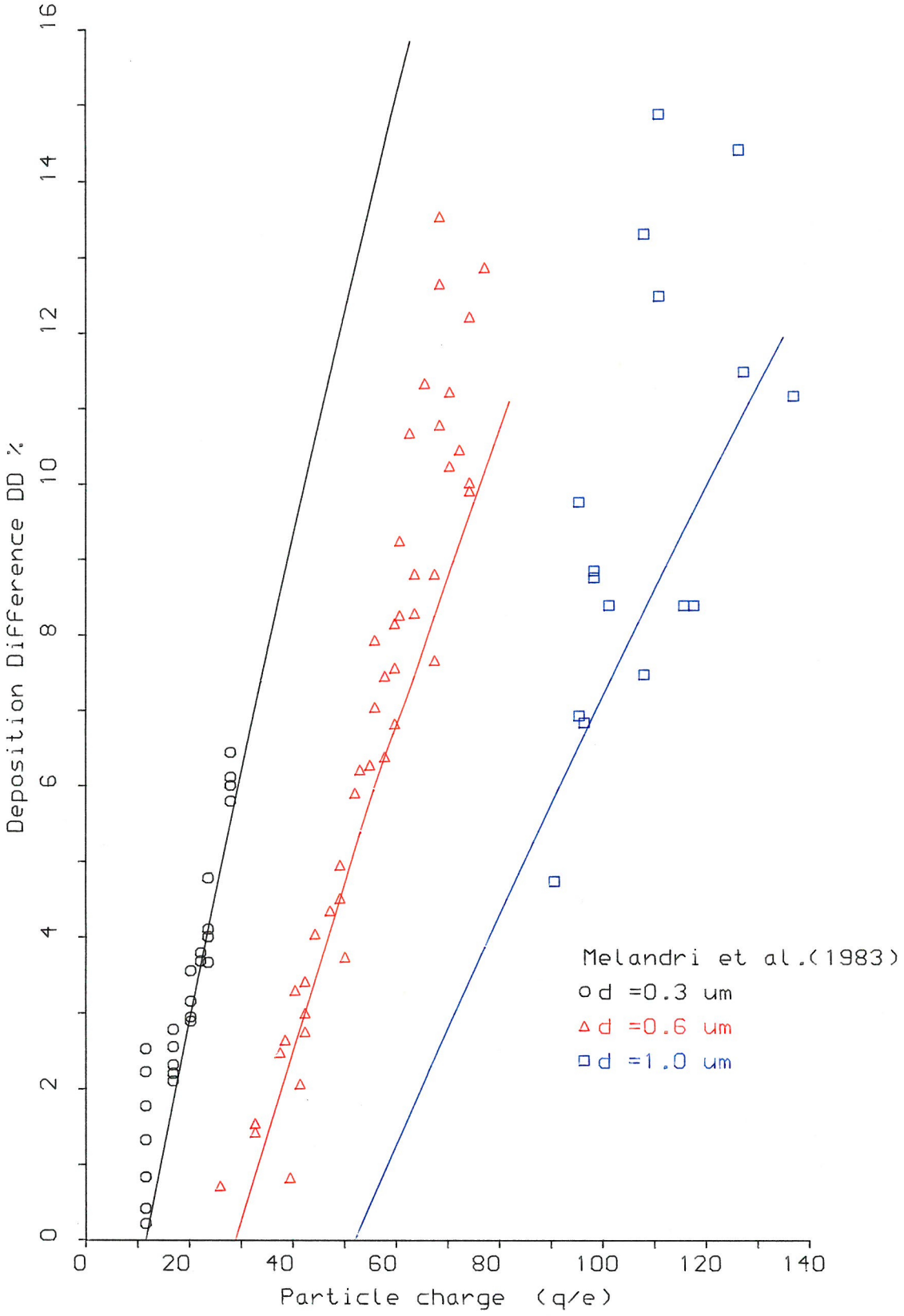

FIG.(II.37): Difference in total deposition versus normalized particle charge (q/e) for three particle diameters at 0.3,0.6 and 1um , p=1g/cm3 (the solid lines are the calculated values)

refinement has been ignored, since most deposition takes place in the A–region of the lung, for particles of this size, as explained earlier. As can be seen from Figure II.37, the calculated results are in very good agreement with the experimental data reported by Tarroni et al. (1980) and Melandri et al. (1983). In Figure II.38, deposition difference (DD) is plotted as a function of normalised $|q/e|$, for particles of diameter 0.3, 0.6 and 1.0μm, with regard to TB and A–deposition. The results show that charge–enhanced deposition is most prominent in the A–region. A more detailed illustration of the deposition site of charged particles is shown in Figure II.39, for 0.6μm diameter particles and several levels of charge.

Melandri et al. (1983), investigated the effect of FRC on charged particle deposition. If lung volume is reduced, while maintaining lung structure, the airway radii reduced, and so lower values of q_c and higher values of η_q are expected, as explained before.

Consequently, for smaller lung volumes, the effect of particle charge results in a deposition increase. The quantity ΔT, defined previously by Heyder et al. (1978) and has the form:

$$\Delta T = \frac{PD_{q=q} - PD_{q=0}}{1 - PD_{q=0}}$$

where $PD_{q=q}$ is the total deposition of charged particles
$PD_{q=0}$ is the deposition for the same particles without charge.

Figure II.40 shows the calculated values of ΔT and the experimental data of Melandri et al. (1983). Both the calculated and experimental data confirm an increase in deposition for smaller rest lung volumes.

7.3 Predictions of the deposition model as applied to aerosol therapy

The deposition model can be used to assess the performance of clinical nebulisers with regard to total and regional deposition (Hashish et al., 1988). Figure II.41 shows the Malvern size distribution for the Inspiron Mini–neb JN under typical operating conditions. Assuming that each size band consists of mono–disperse aerosol droplets, of size represented by the midpoint values, and that there is no interaction between the droplets in different size bands. It is then possible to apply the deposition model to each of the size bands independently in

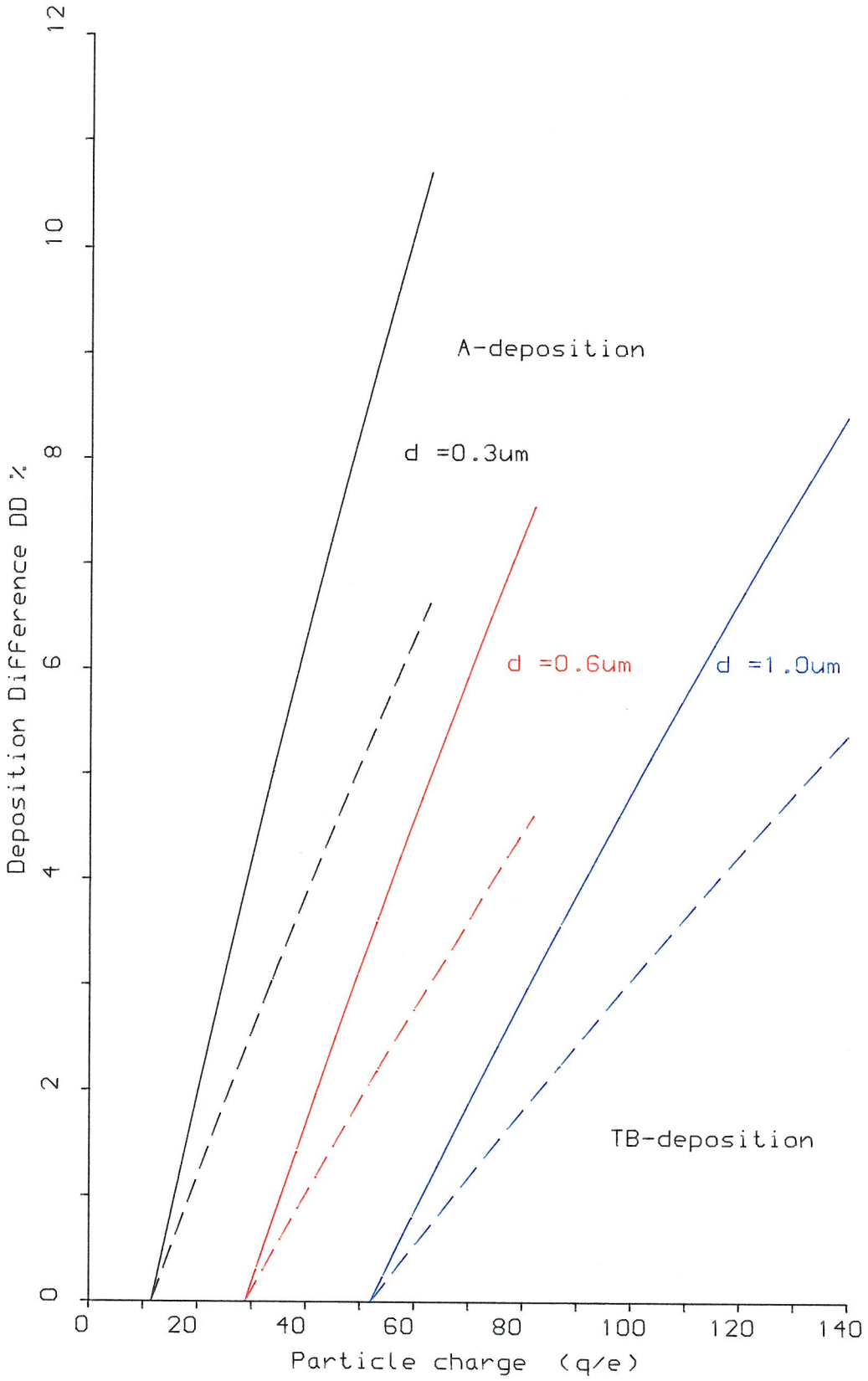

FIG.(II.38): Deposition difference DD% in the TB- and A- regions versus normalized particle charge (q/e) for three particle diameters 0.3,0.6 and 1um (p=1 g/cm3 , TV=1000 cm3, FRC=3000 cm3)

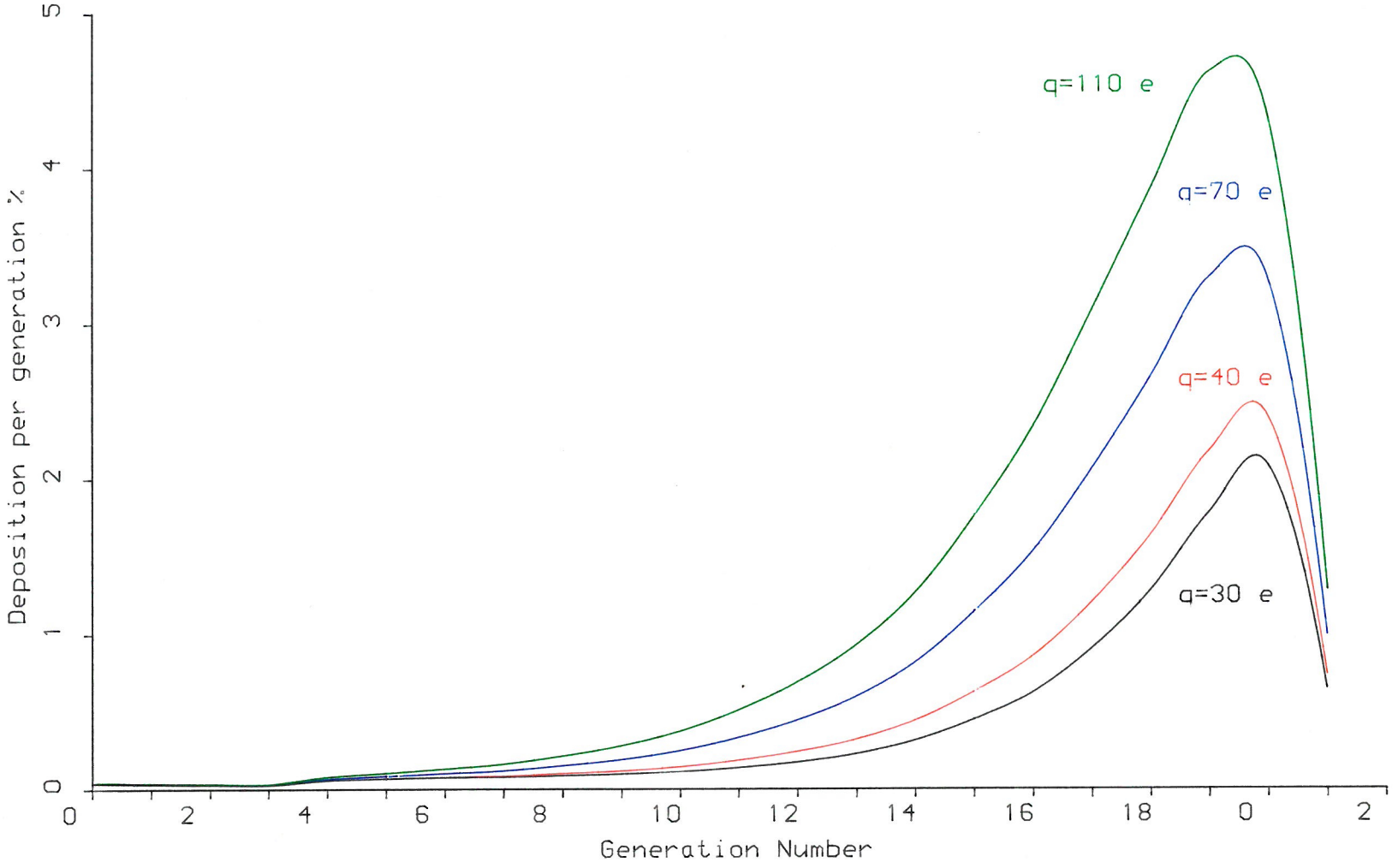

FIG.(II.39): Deposition profiles at mouth breathing along airway generation for 0.6 um diameter particles at various charge levels (p=1g/cm3 , Q=500 cm3/s , T=2s , no pause , FRC=3000 cm3)

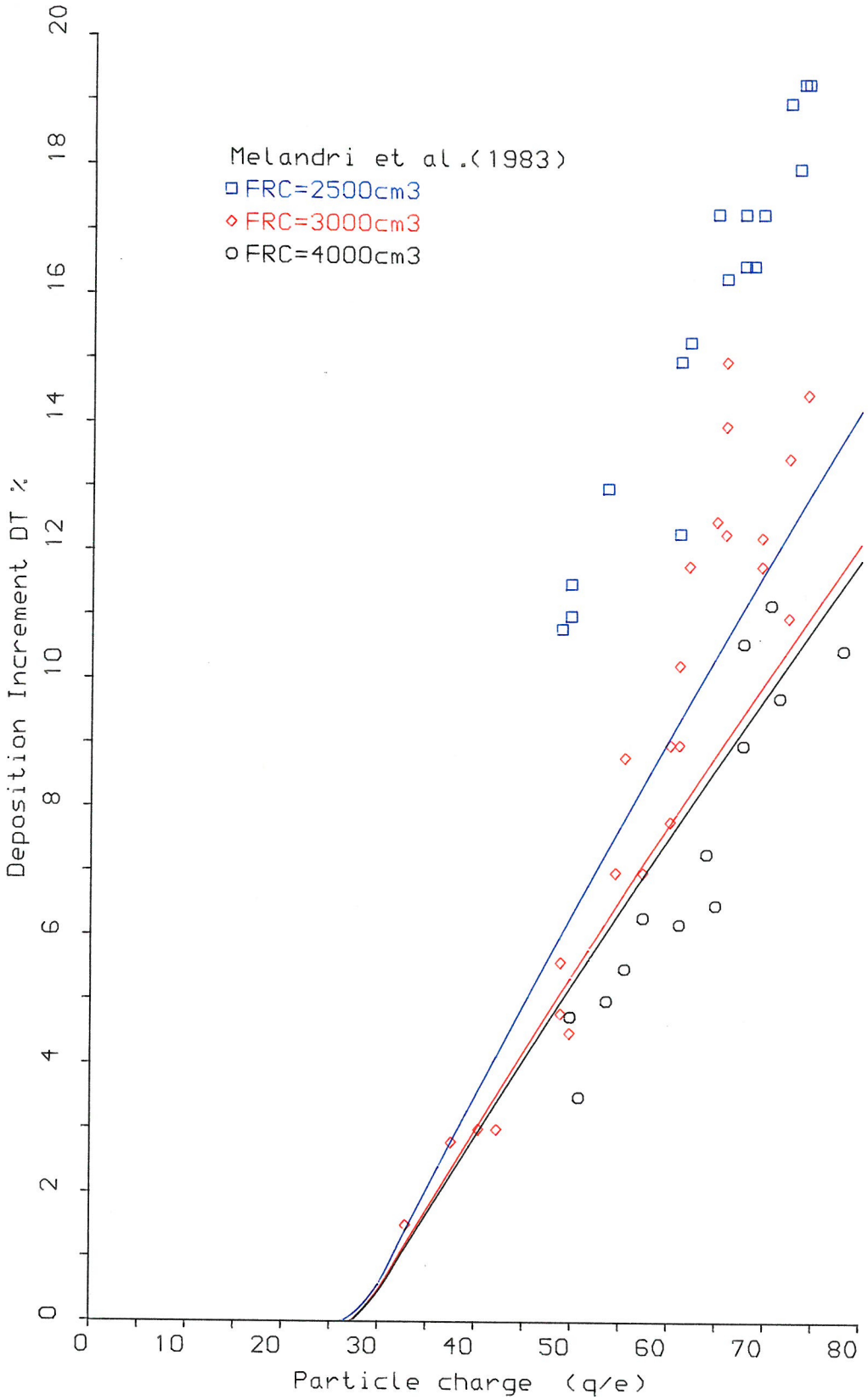

FIG.(II.40): Deposition increment DT % versus normalise particle charge (q/e) for different lung volumes (FRC) for d=0.6 um (p=1 g/cm3 ,TV=1000cm3).The solid lines are the calculated values

band no.	size range (μm)
1.	1.2 - 1.5
2.	1.5 - 1.9
3.	1.9 - 2.4
4.	2.4 - 3.0
5.	3.0 - 3.9
6.	3.9 - 5.0
7.	5.0 - 6.4
8.	6.4 - 8.2
9.	8.2 - 10.5
10.	10.5 - 13.6
11.	13.6 - 17.7
12.	17.7 - 23.7
13.	23.7 - 33.7
14.	33.7 - 54.9
15.	54.9 -118.4

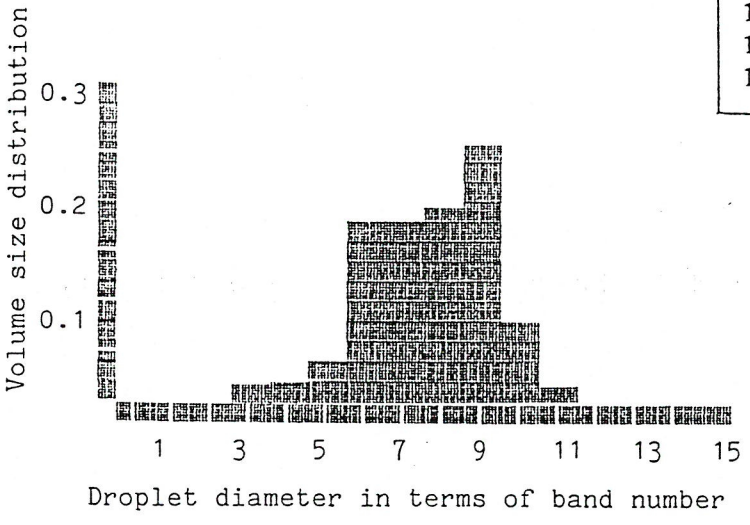

FIGURE II.41 Malvern size distribution for Inspiron Mini-neb JN (8 ℓ/min drive rate 30 ℓ/min suck rate)

order to predict total and regional deposition.

The number of droplets in each size band n_i, per unit volume of aerosol can be calculated as follows:

$$n_i = \frac{\text{fractional volume of aerosol liquid in band i}}{\text{volume of 1 droplet in band i}} \times \text{volume fraction of aerosol liquid in the aerosol}$$

where:

$$\text{Volume fraction of aerosol liquid in the aerosol} = \frac{\text{rate of flow of liquid into the aerosol}}{\text{rate of flow of air into the aerosol}}$$

The results are shown in Table II.5. Using the deposition model and Weibel's airway data, total and regional deposition fraction were computed at a flow rate of $500 cm^3 s^{-1}$, for particle sizes corresponding to the mid-point values of the histogram (see Figure II.41), and natural levels of charge. The initial lung volume, tidal volume and breathing frequency were chosen to be $3000 cm^3$, $1000 cm^3$ and 15 cycle min^{-1} respectively. The breathing cycle consisted of equal durations for inhalation and exhalation, at constant flow rate, without a respiratory pause. Mono-disperse aerosols, composed of droplets of liquid of unit density, were used in the calculations.

TABLE II.5

Inspiron JN

Band No	Size Band			Volume of one particle in band cm^3	% Volume weight in band	No. of particles in band
	Upper (μm)	Mid-Point (μm)	Lower (μm)			
1	1.5	1.35	1.2	1.29×10^{-12}	0.0	-
2	1.9	1.70	1.5	2.57×10^{-12}	0.1	15175
3	2.4	2.15	1.9	5.20×10^{-12}	1.9	142500
4	3.0	2.70	2.4	1.97×10^{-11}	2.1	41574
5	3.9	3.45	3.0	2.15×10^{-11}	4.3	7800
6	5.0	4.45	3.9	4.16×10^{-11}	18.4	155662
7	6.4	5.70	5.0	9.70×10^{-11}	18.4	73979
8	8.2	7.30	6.4	2.04×10^{-10}	19.5	37279
9	10.5	9.35	8.2	4.28×10^{-10}	25.6	23327
10	13.6	12.05	10.5	9.16×10^{-10}	8.2	3491
11	17.7	15.65	13.6	1.97×10^{-9}	1.4	277
12	23.7	20.70	17.7	4.64×10^{-9}	0.2	17
13	33.7	28.70	23.7	1.24×10^{-8}	0.0	-
14	54.9	44.30	33.7	4.55×10^{-8}	0.0	-
15	118.4	86.65	54.9	3.41×10^{-7}	0.0	-

Figure II.42 shows the histogram of Figure II.41, output of the Inspiron JN, with predicted total and regional deposition superimposed.

The calculated maximum natural aerosol charge, developed during the nebulisation process (as shown in Table I.8, Part I), is small and has negligible effect on deposition. This finding is in agreement with Yu (1985), who concluded that electrostatic deposition is negligible if the charge level is less than some critical value which depends on particle size. It is necessary, therefore, to charge an aerosol, by some external means (eg. corona charging), if it is desired to increase droplet deposition in the respiratory tract. Deposition fraction was calculated for both neutral and corona-charged droplets ($\approx$ half the Pauthenier limit, 1932). Figure II.43 shows the calculated total and regional depositions plotted as a function of droplet size of interest (0.5-10μm in diameters). It can be seen that deposition is significantly enhanced in the TB-region whereas in the A-region it is lower than the uncharged equivalent in the case of larger droplets (assuming breathing cycle of 4s without pause). With 0.2s pause at the end of inhalation, the electrostatic enhancement in deposition is shifted to the A-region, especially for smaller droplets as shown in Figure II.44.

It can be seen from these results that the presence of charge on aerosol droplets increase their probability of deposition in the lung and allows control to be exercised over their site of deposition. A more efficient delivery of therapeutic agents to the TB and A-regions can be achieved by optimizing aerosol flow rate, respiratory rate, tidal volume, paused period, particle size and particle charge.

7.4 The Predictive Model : Applicability and Sensitivity

The predictive lung model is generally quite sensitive to the choice of initial parameters. Calculation of aerosol concentration and deposition are dependent on:

1. the physical characteristics of the inhaled aerosol, especially with regard to particle size, mass density and electrical charge.

2. a realistic anatomical model which accurately represents the asymmetrical branching typical of mammalian respiratory systems.

3. the realistic estimation of breathing patterns including total lung capacity,

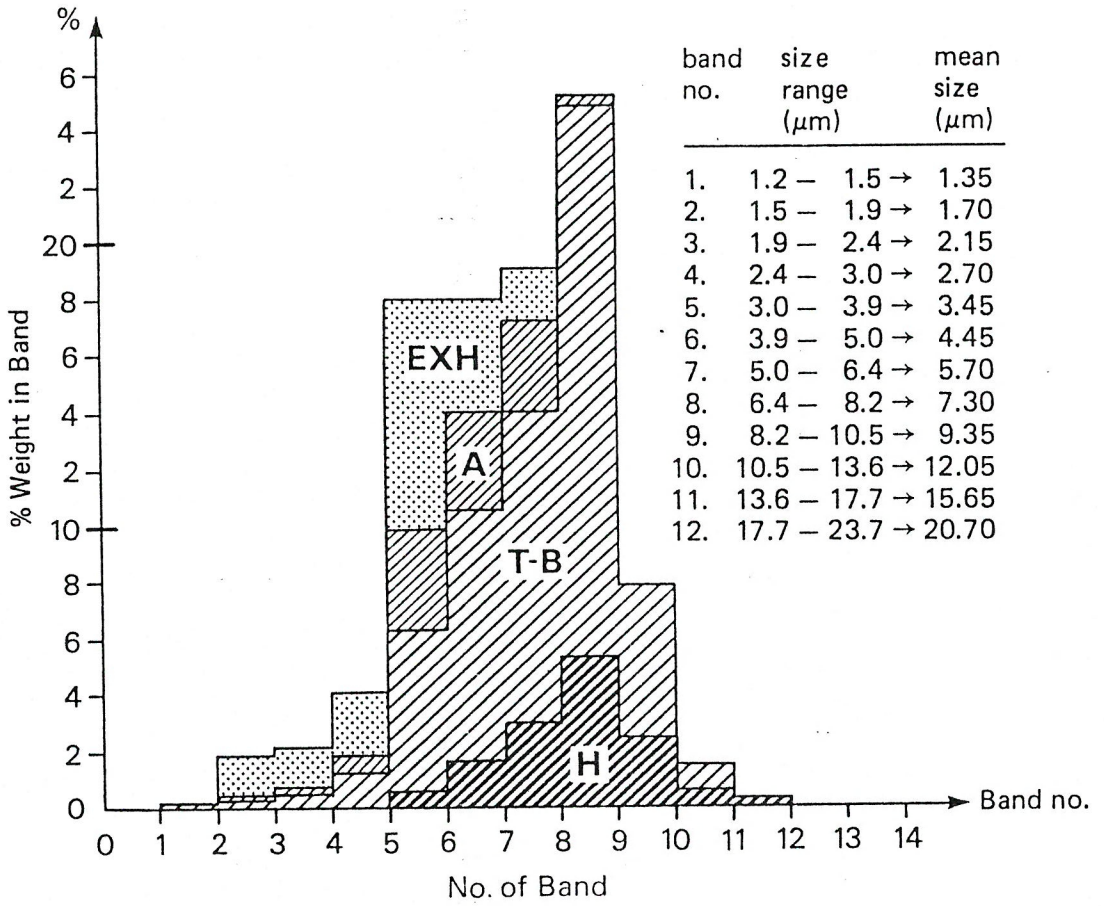

FIGURE II.42 Performance of the Inspiron Mini-neb JN

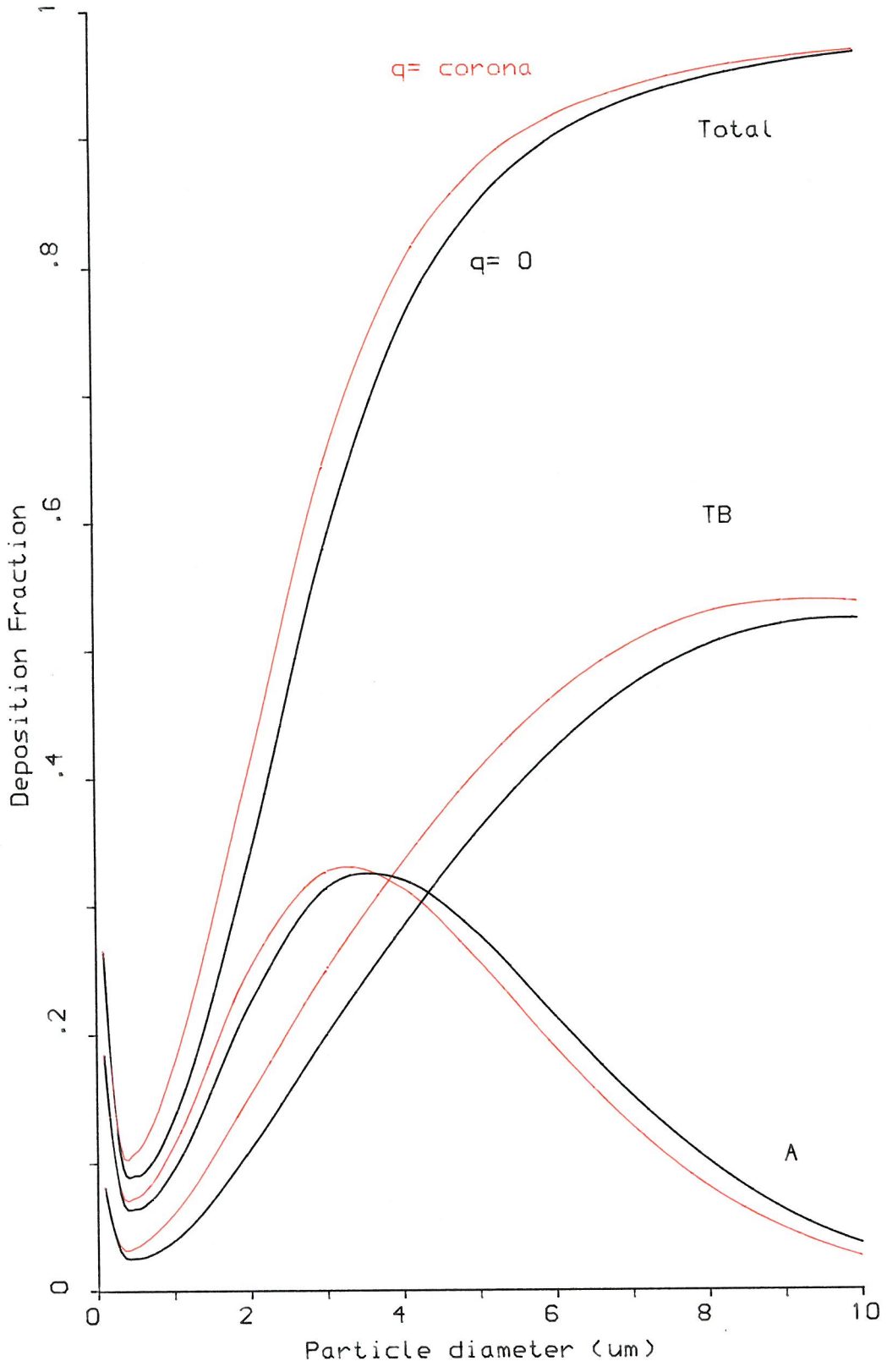

FIG.(II.43): Predicted total and regional depositions versus particle diameter for neutral and corona-charged aerosols q(corona)=1/2 Pauthenier , p=1g/cm3, Q=500cm3/s, T=2s, no pause

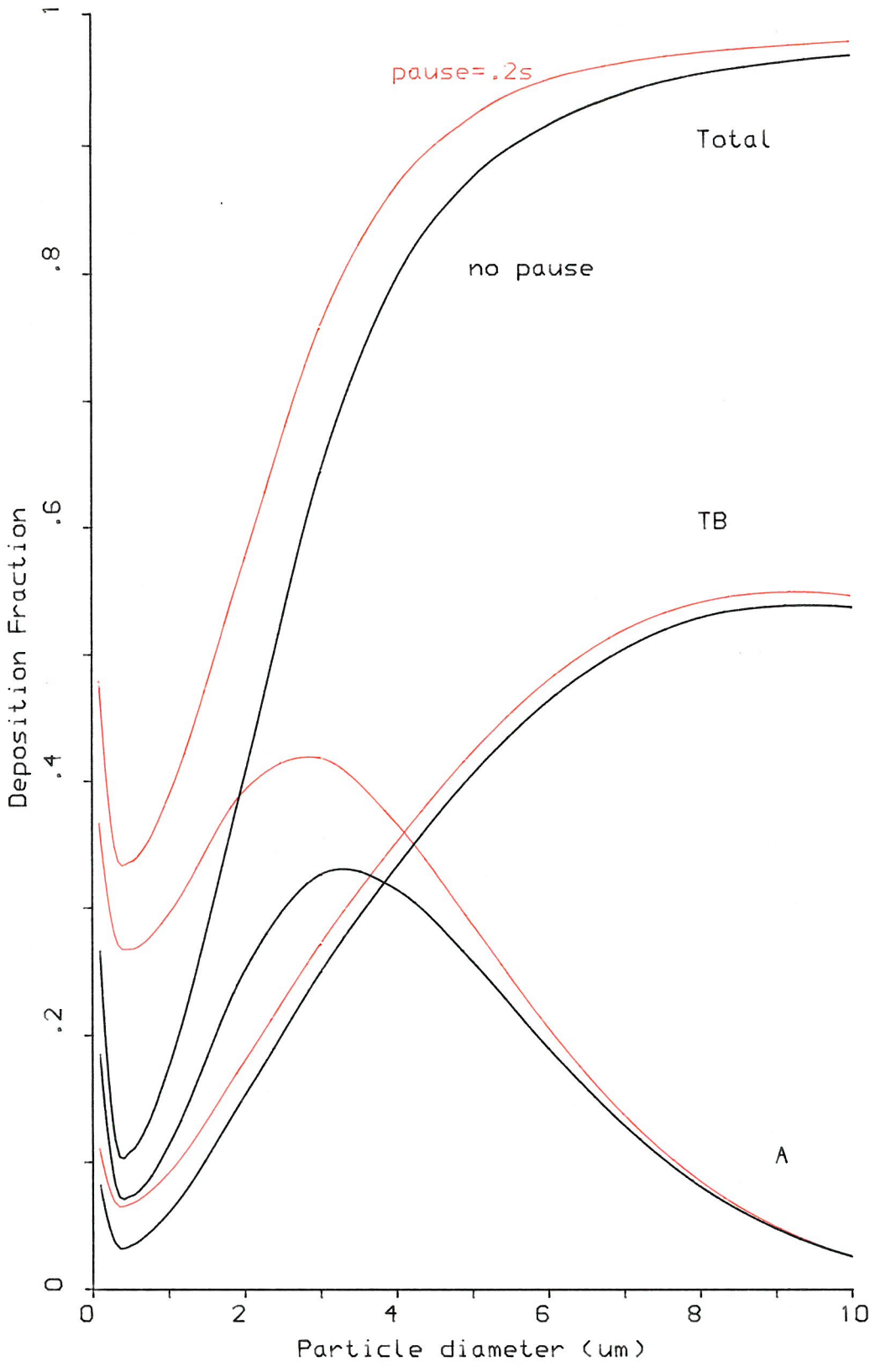

FIG.(II.44): Predicted total and regional depositions versus particle diameter for corona-charged aerosols with and without pause, q(corona)=1/2 Pauthenier , p=1g/cm3, Q=500cm3/s, T=2s

tidal volume and respiratory rate.

The model has been validated by comparing the deposition fractions predicted theoretically with the experimental data collected from controlled aerosol deposition studies. The aerosol characteristics and breathing patterns used in the model were chosen to correspond as closely as possible to these studies.

The model is found to predict accurately total and regional aerosol deposition when all the experimental parameters have been estimated with good precision. Large discrepancies can arise if the aerosol characteristics and individual breathing patterns are not well defined.

8. SUMMARY AND CONCLUSIONS OF PART II

1.(a) A lung deposition model, based on Yu's formulation, has been developed. Yu's analytical solutions have been replaced by iterative solutions which allow high deposition efficiencies to be considered.

(b) For computational purposes, the deposition double integral has been transformed into a line integral using Green's theorem. This allows the model to be implemented using a personal computer, since aerosol concentration then only needs to be considered at the start and end of each airway.

(c) It appears that the present theory gives a reasonably accurate prediction of the total and regional deposition of inhaled neutral and charged aerosol particles. Good agreement is found between the theoretical predictions and experimental data.

2.(a) The electrostatic charging of aerosol particles can lead to their increased deposition in the lung. The deposition theory described has been shown to be consistent with experimental data regarding the deposition of charged particles in the human respiratory tract and, therefore, can be used as a predictive model for respiratory depostion.

(b) The theoretical and experimental results indicate that enhancement in deposition, due to charge, may be accounted for not only in the smaller airways but also in the trachea and TB–region.

3.(a) The deposition model can be used in aerosol therapy, to assess the performance of clinical nebulisers with regard to total and regional deposition.

(b) The presence of charge on therapeutic aerosols increases their probability of deposition in the lung and allows control to be exercised over their site of deposition.

(c) Efficient delivery of therapeutic agents to the TB and A–regions can be achieved by optimizing aerosol flow–rate, respiratory rate, paused period, particle size, particle mass density and particle charge.

4.(a) The model is sensitive to the choice of parameters defining the breathing pattern and the physical characteristics of inhaled aerosol particles.

(b) The model accurately predicts regional deposition patterns when all the breathing pattern parameters and aerosol characteristics are well defined.

PART

III

THE EFFECT OF ENVIRONMENTAL POLLUTION ON THE HUMAN RESPIRATORY SYSTEM

PART III

THE EFFECT OF ENVIRONMENTAL POLLUTION ON THE HUMAN RESPIRATORY SYSTEM

1. INTRODUCTION AND AIMS

The atmospheric environment in which man lives is a thin layer about 29km thick which contains, in addition to its normal gaseous constituents, gaseous and particulate pollutants. A pollutant is defined as *a potentially harmful contaminant of the environment* (Hinds, 1980). Some of these pollutants may occur as the result of natural phenomena (eg. dust, spray, natural decay ... etc), while others arise due to human activity (eg. combustion and comminution). Particulate air pollutants, of either natural or man-made origin, can acquire electrostatic charges. Electric field forces and atmospheric ions can lead to the formation of charged particles in the atmosphere, whereas highly charged particles in the occupational environment are generated under high shear forces during grinding, sanding and similar operations. The charge carried by these particulate air pollutants may enhance their deposition in the lung. As explained earlier, the main reason for this electrostatic enhancement is the image force (space-charge forces being relatively insig nificant for the particle concentration and charging level pertaining to most aerosols found in ambient and workplace environments, Yu, 1985). The effect is dependent on the magnitude of the charge carried but not its polarity. For a given particle size, there is an effective threshold value for the magnitude of electric charge, below which enhancement is negligible. For example, this threshold charge is found to be about $50|e|$ ($|e|$ is the magnitude of charge carried by a single electron) for a particle of diameter $1\mu m$ and density $1 g/cm^3$, inhaled by a human subject breathing under "*normal*" conditions.

The static electrification (see glossary of terms) of particulate air pollutants in the workplace is an important factor in relation to occupational health, but so far it has been largely ignored. Recently, however, measurements have been conducted to evaluate the static electrification of workplace aerosols (Kosenko, 1970; Shevchenko, 1971; and Vincent et al., 1983). From such work, it is generally found that workplace aerosols are charged to levels substantially above Boltzmann equilibrium. While the individual levels of charging vary markedly from one factory to another and between processes within a given factory, the charges are invariably distributed symmetrically between positive and negative polarities. The highest charge levels tend to be associated with the more energetic dust-making processes.

There are some industrial processes (eg. crop and paint spraying, powder coating ... etc) where very high charge levels are deliberately used to assist deposition.

An estimation of the health hazard originating from particulate airborne materials requires the determination of *total* and *regional* deposition of inhaled particles in the human respiratory tract. In occupational and environmental hygiene, more information is needed with regard to the fate and biological effectiveness of particles of different materials entering the body during breathing. Particulate materials which are rapidly *soluble* in the liquids of the respiratory tract can enter the tissues and circulating blood even during the short residence time associated with the H and TB–airways. Therefore *total deposition* is the appropriate parameter for an estimation of the health risks originating from such particles. Substances which are *insoluble* or only slightly soluble in the body liquids are less dangerous if the particles are deposited in the H–region and larynx or the TB–region, because the clearance time for these sites is short. However, inert particles, which are deposited in the A–region, are removed at a very slow rate the clearance half–times being several weeks or even months, and are therefore much more dangerous, Stahlhafon et al., 1980. Since such particles are mainly produced in industrial processes, health hazard evaluation in industrial and occupational hygiene is usually based on *alveolar deposition*. From this point of view, the lung deposition model, developed earlier, can be used in the field of industrial hygiene to assess the health hazard of electrostatic lung depositon.

The aims of Part III are: (i) to review the available data regarding electrostatic charge in actual workplace aerosols including relevant laboratory studies, (ii) to investigate the health hazard associated with electrostatic crop and paint spraying, and (iii) to assess the hazards of electrostatically–enhanced lung deposition.

2. REVIEW OF ELECTROSTATIC CHARGE MEASUREMENT OF LABORATORY AND WORKPLACE AEROSOLS

Aerosols in workplace environments are generated by a wide range of industrial processes. The aerosol particles become electrically charged during their generation. For any of these processes, the level of charging increases with the amount of energy expended in generating the particles. The nature of the charge on an aerosol may be described in terms of the probability of finding an individual particle carrying a given charge. For a given dispersal process, this probability will

depend on particle size. The median magnitude of charge per particle, $|q/e|_m$ (equivalent in magnitude to the number of elementary charges e), obtained from a particular charge distribution for a particle of given diameter d, measured in μm, may be expressed as:

$$|q/e|_m = A\ d^n \qquad (1)$$

where A and n are numerical coefficients (eg. see Table III.1, for typical values).

It is more appropriate to express particle size in terms of aerodynamic diameter since most airborne particles, in workplace environments, have arbitrary shapes, ie they are *isometric particles* (see glossary of terms).

The constant A in equation (1) may be defined as the median number of charges, equivalent in magnitude to the number of elementary charges e, carried by particles of aerodynamic diameter 1 μm.

Aerosol particles having shapes with extreme aspect ratios (eg *fibres*) are considered separately, because their size cannot be adequately represented by a single dimension. The overall charge carried by a fibre may be described in terms of the median magnitude of charge per unit length of fibre, $|\sigma|_m$, which is independent of fibre diameter, Vincent, 1986. Thus, for a fibre of length ℓ:

$$|q/e|_m = \sigma_m \ell \qquad (2)$$

2.1 Electrostatic Charging of Aerosols in the Laboratory

A number of quantitative laboratory studies have been reported which are of particular relevance to workplace aerosols. Some typical results for dusts comprising isometric particles are summarised in Table III.1, together with an assessment of the electrostatic enhancement in lung deposition, see Section 2.3.

Typical states of charge for fibrous aerosols, generated in the laboratory (obtained by Vincent et al., 1981), are summarised in Table III.2 together with the estimated median magnitude of charge carried by fibres of aerodynamic diameter 1 μm.

TABLE III.1

Results of charge measurements on a range of dusts dispersed in the laboratory by a variety of means.

Type of aerosol	Method of dispersal	$\frac{\|q/e\|_m = Ad_{ae}^n}{A \quad n}$		Reference	$DD_1\%$*
Coal	Wright-type dust feeder	67	1.0	Walkenhorst (1971)	6.1
	Wright-type dust feeder	126	1.2	Stein (1972)	9.6
	Timbrell-type disperser	40	1.6	Johnston et al. (1985)	4.4
Quartz	Compressed air	14	1.0-1.4	Kunkel (1950)	2.2
	Wright-type dust feeder	26	1.0	Johnstone et al. (1985)	3.3
Sandstone	Drilling	40	1.4	Walkenhorst (1971)	4.4
Sodium Chloride	Collision nebuliser	5	1.0	Johnston et al. (1985)	1.3
Sulphur	Compressed air	14	1.0-1.4	Kunkel (1950)	2.2
Polystyrene	Wright-type dust feeder	3	1.3	Fry (1970)	0.8

* Electrostatic enhancements of lung deposition in human at working condition for aerosol particles with 1μm aerodynamic diameter, see Section 2.3

TABLE III.2

Results of charge measurements on clouds of amosite and chryostile asbestos fibres generated by UICC (Union International Centre de Cancer) reference samples.

Type of aerosols	Method of dispersal	Median charge per unit length of fibre $\|\sigma/e\|_m$	Median charge on a fibre of d_{ae} = 1μm $\|q/e\|$
UICC amosite	Timbrell-type dispersal	16	112
	Timbrell-type dispersal (neutralisation by ions from a sonic-jet ioniser)	8	56
UICC chrysatile	Timbrell-type dispersal	20	140
	Timbrell-type dispersal (neutralisation by ions from a TI-204 source)	1	7

2.2 Electrostatic Charging of Aerosols in the Workplace

There appears to be very little published information about electrostatic charge carried by actual workplace aerosols. The only major studies, of the charge levels of airborne dusts arising from industrial operations, have been carried out in the Soviet Union. Some of the results are summarised in Table III.3.

TABLE III.3

Results of charge measurements or airborne dusts (isometric particles) carried out in a range of workplaces in the Soviet Union.

Workplace	Average or median charge per particle |q/e|	Reference
Ceramic tiles	20 - 30	Kasenko (1970)
Gypsum work	10 - 65	"
Foundry	45 - 90	"
Manganese mine	15 - 30	Chubutiya (1970)
Dry drilling		
Mine No. 1	< 40	Shevchenko (1971)
Mine No. 2	120 - 160	"
Wet drilling	40 - 80	"
Quarry	< 40	"
Iron Foundry	A = 20 n = 2.1	Walkenhorst (1983)
Coal mine	>Boltzmann equilibrium	Stein (1972)

More recently, Vincent et al. (1983) and Johnston et al. (1985), have reported comprehensive data for 48 workplace locations in 16 industrial plants including textile, extraction and manufacturing industries in the UK. A summary of their results for dusts of isometric and fibrous particles is presented in Table III.4, together with an assessment of electrostatic enhancement of lung deposition, see Section 2.3.

TABLE III.4

Results for charge measurements on airborne dusts carried out in a range of workplaces in the UK.

Factory	Workplace	$\frac{\|q/e\|_m}{A} = \frac{Ad_{ae}^n}{n}$		$DD_1\%$
- Isometric particles				
Chemical	: Silica gel production	29	0.72	3.6
Cotton	: Weaving	50	1.25	5.1
Colliery	: Return roadway	28	1.20	3.5
Flax	: Hackling/drawing	38	1.77	4.3
	Carding	69	1.12	6.3
	Weaving	41	1.23	4.5
	Spinning	18	1.84	2.6
	Winding	24	1.84	3.1
Jute	: Batching	30	1.03	3.6
	Spreading	35	0.80	4.0
	Carding	40	1.19	4.4
	Drawing	29	1.18	3.6
	Spinning	21	1.44	2.9
	Winding	18	1.16	2.6
Quarry A	: Primary Crusher	22	1.50	2.9
	Secondary Crusher	4	1.39	0.9
Quarry B	: Primary Crusher	52	0.75	5.2
Rubber	: Mixing	6	1.69	1.3
	Rolling	5	1.91	1.1
- Asbestos Fibres		$\|\sigma/e\|_m$		$\|q/e\|_1$
Textile A:	Carding	8		56
	Spinning (dry)	11		77
	Spinning (damp)	5		35
	Weaving	6		42
Textile B:	Carding	13		91
	Spinning	10		70
	Weaving	10		70

2.3 An Assessment of Hazards Due to Electrostatically-Enhanced Lung Deposition

The hazard caused by inhaled particulate air pollutants in the workplace depends on their *chemical composition* and their *site of deposition* within the respiratory system. Usually the particulate matter is composed of soluble and insoluble components. To evaluate properly their health hazards, a knowledge of the total and regional deposition is required. Charge carried by these particles may represent an additional hazard due to the enhancement of deposition in the A-region by the action of the electrical image force.

The lung deposition model can be used to assess the practical significance of deposition in the respiratory tract of charged laboratory and workplace aerosols. With regard to the present calculations, total and A-deposition data were determined for mouth breathing under steady-state conditions using the following breathing patterns:

$$\text{A} : V_t = 1000\text{cm}^3; \quad T = 4\text{s}, \quad Q = 250\text{cm}^3\text{s}^{-1}$$
$$\text{B} : V_t = 1500\text{cm}^3; \quad T = 2\text{s}, \quad Q = 750\text{cm}^3\text{s}^{-1}$$

where V_t is the tidal volume, T is the breathing time and Q is the mean volumetric flow rate. Both patterns with a period of pause at the end of inhalation equal to one-tenth of the breathing period.

Pattern A can be considered as typical for a subject *at rest*, whereas pattern B corresponds to the *working condition*, Stahlhofen, 1980. Weibel's airway morphometery (adjusted to a rest lung volume of 3000cm^3) has been taken used as the "*average*" human lung. The calculations were performed for two particle sizes, of aerodynamic diameter 0.6 and 1 μm respectively, for which the effect of charge is expected to be important, see Part II, Section 7.2.2.

Figures III.1 to III.4 show the calculated fraction of total and A-deposition verses charge, $|q/e|$, typical of the states of charge found in workplace aerosols, for particles of aerodynamic diameter of 0.6 and 1 μm and the breathing conditions corresponding to patterns A and B. It can be seen from these figures and the calculated difference in total and A-deposition between charged and uncharged 1 μm particles (presented in the last column in Tables III.1 and III.4, alongside the laboratory and workplace data on aerosol charge levels) that there is no significant electrostatic enhancement in lung deposition for such

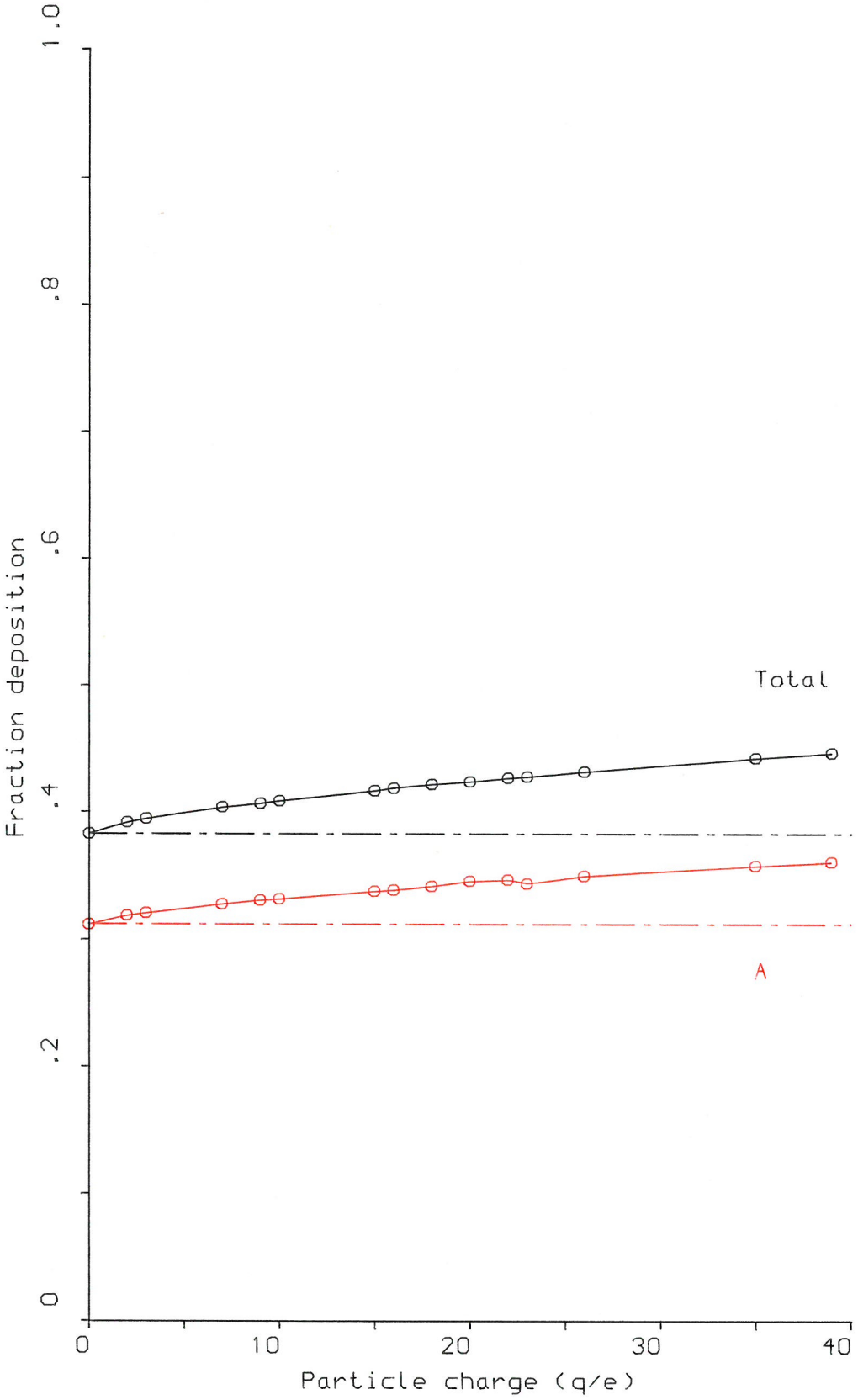

FIG.(III.1): Total and A-deposition versus normalized workplace particle charge (q/e) for dae=0.6 for a man at rest
(the dotted lines represent the deposition of neutral particles)

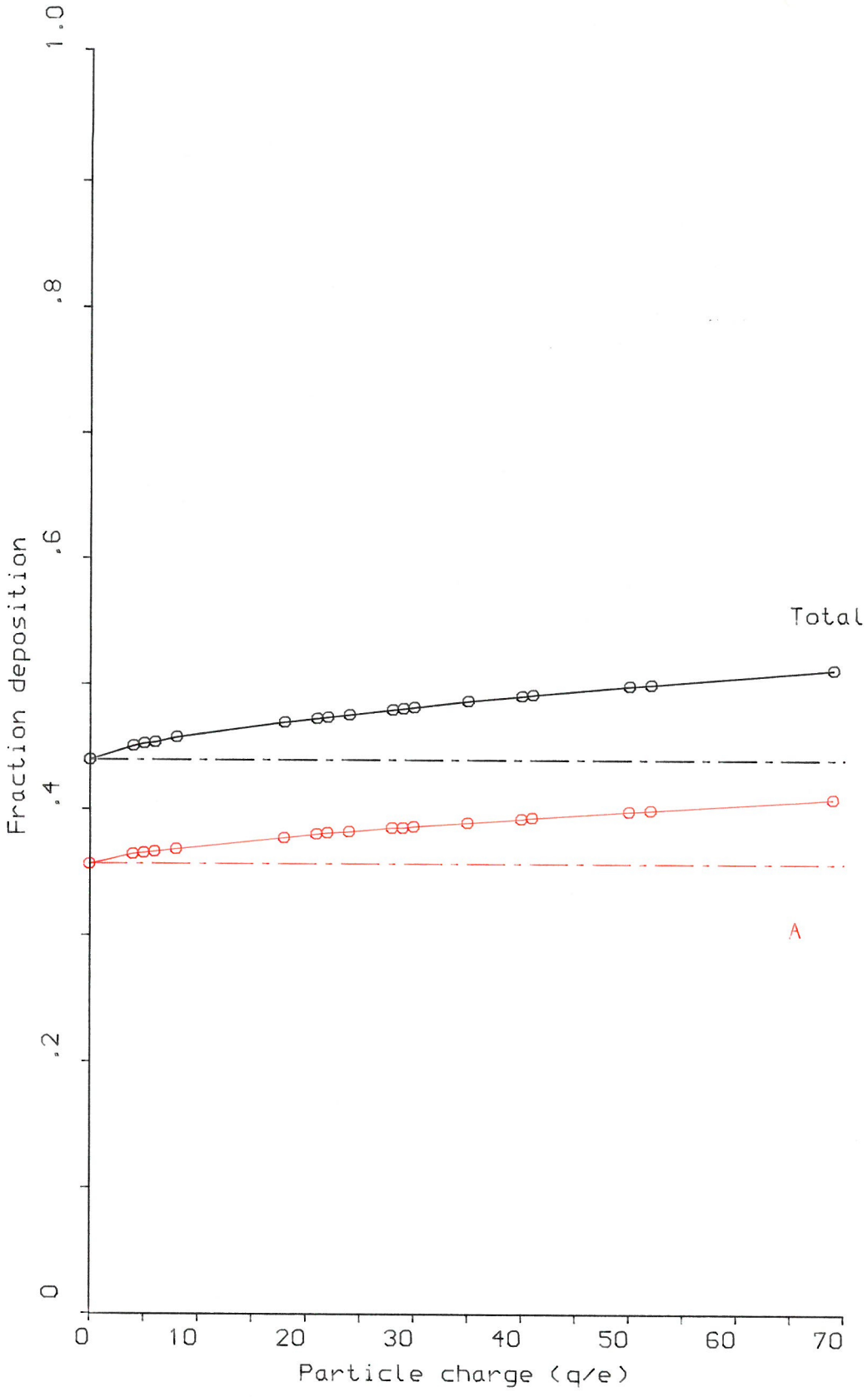

FIG.(III.2): Total and A-deposition versus normalized workplace particle charge (q/e) for dae=1.0 for a man at rest
(the dotted lines represent the deposition of neutral particles)

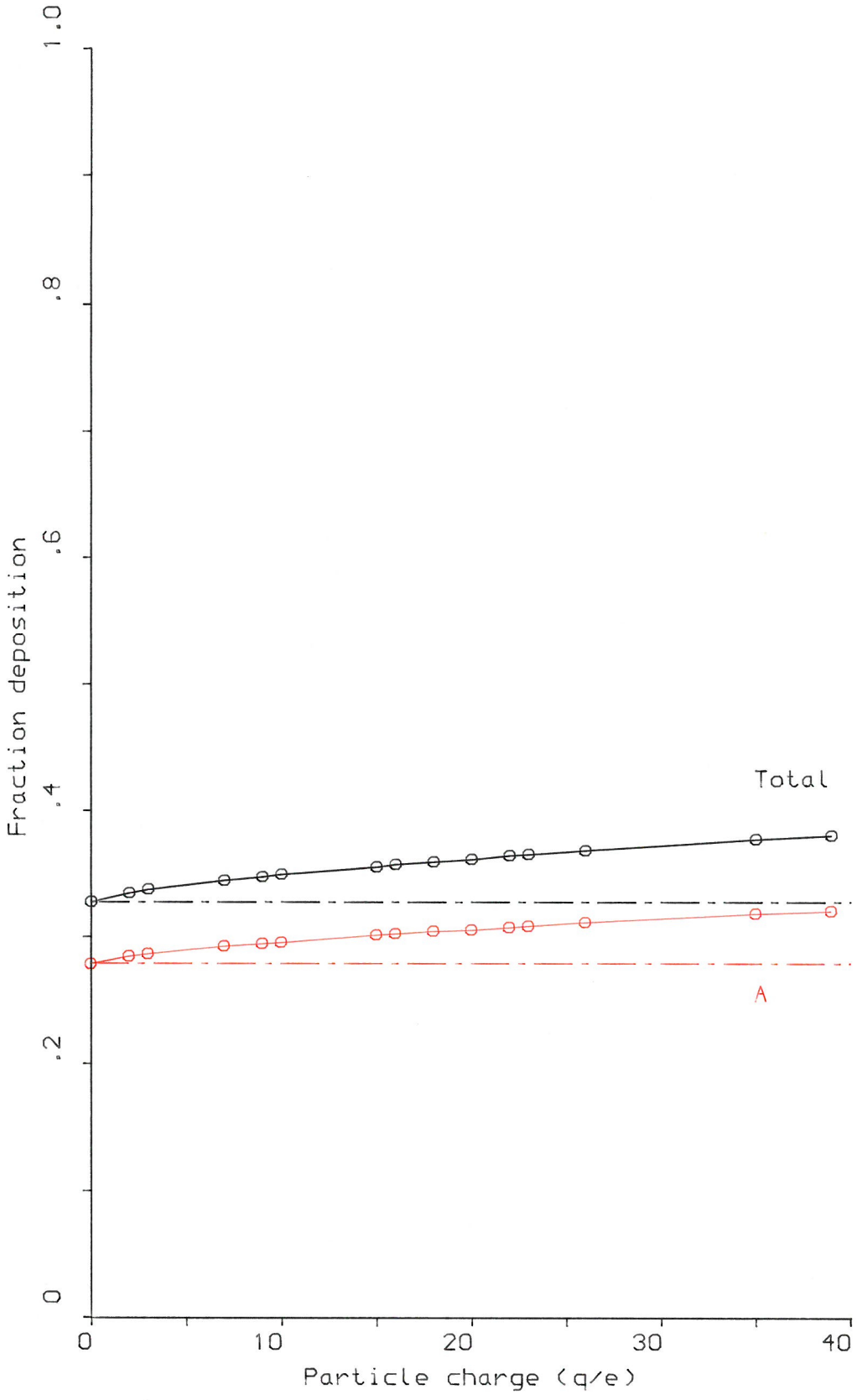

FIG.(III.3): Total and A-deposition versus normalized workplace particle charge (q/e) for dae=0.6 for a man under working conditions (the dotted lines represent the deposition of neutral particles)

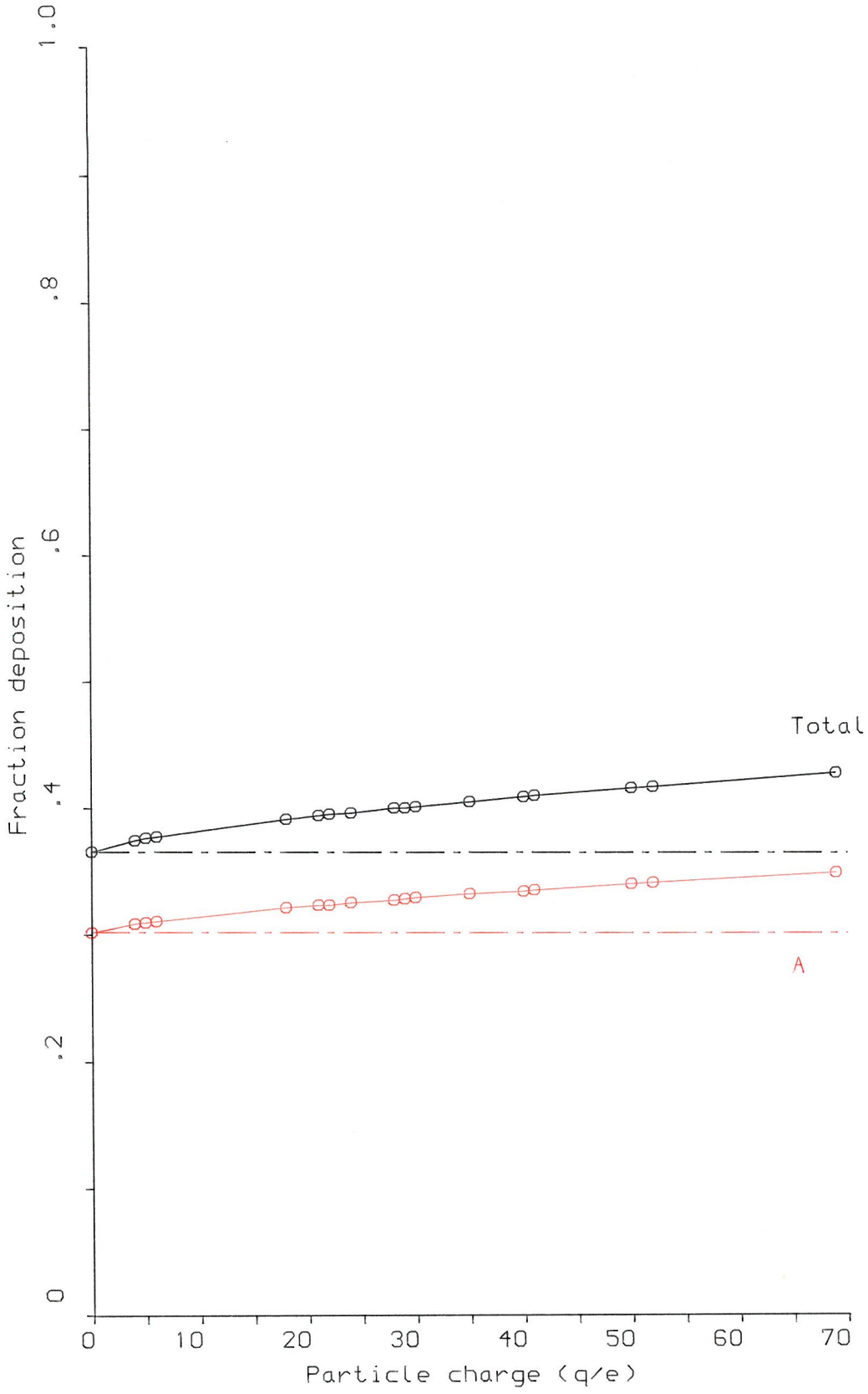

FIG.(III.4): Total and A-deposition versus normalized workplace particle charge (q/e) for dae=1.0 for a man under working conditions (the dotted lines represent the deposition of neutral particles)

particles. However, for fibrous particles, with an aerodynamic diameter corresponding to the isometric particles, the levels of charge are relatively high (even greater than the critical value q_c for each size) and a significant electrostatic contribution to lung deposition may occur. At present, there is no adequate equivalent theory for charge fibres or other particles of non-uniform aspect ratio.

The actual magnitude of any effect, in terms of the electrostatic enhancement of the mass of material deposited in the lung (i.e. *lung dose*), could be obtained if a detailed knowledge existed of both particle charge and size distribution, for each and every case examined. This is an area for future work.

There are some industrial processes (eg. crop and paint spraying) where very high particle charge levels are deliberately used to assist deposition. In this case highly charged aerosols could be produced, leading to a significant enhancement in lung deposition.

In the next section an attempt is made to assess the health hazard associated with electrostatic crop spraying.

3. HEALTH HAZARDS ASSOCIATED WITH ELECTROSTATIC CROP SPRAYING

3.1 Electrostatic Crop Spraying : A Brief Overview

Employing electrostatic technology to crop spraying may improve the efficiency of pesticide application (eg. increased deposition, improved uniformity of cover and even the "*wrap-around*" effect can be obtained when using electrostatic crop sprayers), Bailey, 1986. Production of a charged spray cloud can be achieved utilising corona charging (Arnold and Pye, 1980), induction charging (Law, 1980 and Inculet et al., 1981) and electrostatic atomization (Coffee, 1979). Usually pesticides have a water or oil based formulation. The electrostatic sprayers used for pesticide application are various in form, using different types of machinery, powered or hand-operated, and may even be carried by an aircraft.

The droplet size range of interest, in chemical pesticide application, is from 1μm to 1000μm diameter, Law, 1975. Figure III.5 shows typical size distributions for an induction charging nozzle of Law and Table III.5, shows the volume median diameters (VMD's) for several hand-operated electrostatic atomisers produced by ICI, Coffee, 1981. The charged droplets issuing from the Law nozzle are water based and charged to about 20% of the Rayleigh limit under typical

band no.	size range (μm)
1.	5.9 - 7.2
2.	7.2 - 9.1
3.	9.1 - 11.4
4.	11.4 - 14.5
5.	14.5 - 18.5
6.	18.5 - 23.7
7.	23.7 - 30.3
8.	30.3 - 39.0
9.	39.0 - 50.2
10.	50.2 - 64.6
11.	64.6 - 84.3
12.	84.3 - 112.8
13.	112.3 - 160.4
14.	160.4 - 261.6
15.	261.6 - 564.0

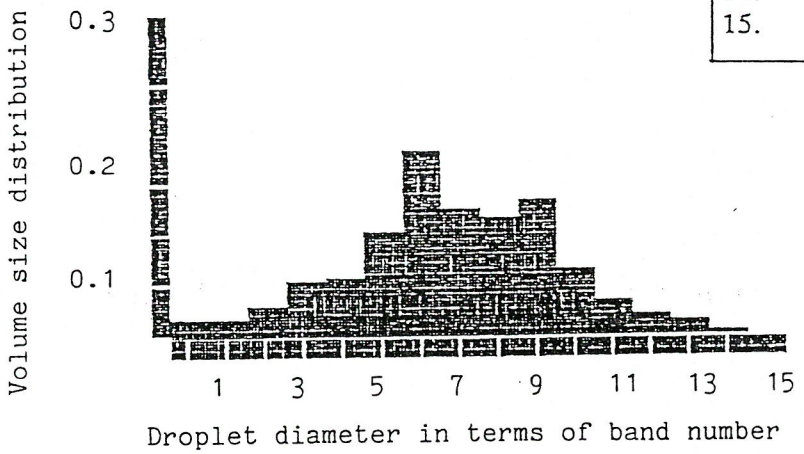

FIGURE III.5 A typical computer output from the Malvern Particle Size Analyser for Law's nozzle under typical operating conditions.

TABLE III.5

VMD and NMD measurements for several hand-operated sprayers.

Nozzle type	Formulation	VMD	NMD	$\frac{V}{N}$ MD
Prototype Electrodyn	Blank oil	25.1	23.4	1.08*
		39.5	36.5	1.08*
		89.3	76.6	1.17*
Prototype Electrodyn	Pirimicarb (oil-base)	62.9	61.7	1.02†
Mini-Ulva	Pirimicarb (oil-base)	59.0	12.6	4.65†
	Water	78.4	47.6	1.74†
Knapsack (15 psi) (hydraulic)	Water	310	60	5.63†
Herbi (1.0 mℓ/sec)	Water	230	195	1.18‡
(1.7 mℓ/sec)		250	104	2.40‡
Commercial Electrodyn and Bozzle	Crypermethrin (oil-base)	44.0	37.6	1.17‡

Analysis methods: *Coulter counter, †Malvern laser, ‡Mn0 film.

Source: Coffee (1981)

operating conditions, Bailey, 1986. Measurements of the charge-to-mass ratio of droplets produced by the ICI atomiser, of oil based type, show a value corresponding to 50-70% of the Rayleigh limit, Coffee, 1980.

Typically the particles used in electrostatic crop spraying are large and, therefore, not regarded as a respirable hazard. However, it is possible for particle size to reduce, due to the effects of evaporation. As evaporation proceeds, *mass is lost but charge is conserved*, Bailey 1986. When the relationship between drop charge q and diameter d becomes consistent with the Rayleigh stability criterion the drop disintegrates, ejecting about 25% of its mass (Abbas and Latham, 1987) and 30% of its initial charge (Doyle et al., 1964) in the form of one or more highly-charged satellite droplets. Following such charge and mass losses, the residual drop becomes stable and evaporation proceeds towards another instability. By the time it reaches average head height, due to being blown up by the wind during hand-held , tractor spraying or by falling during aerial spraying, multiple disintegrations will have occurred and many satellite droplets may form from the initial drop, all of which are respirable. Since the level of charge they carry is very high, it is likely that complete deposition will occur in the respiratory system, since the deposition efficiency is high due to the presence of high levels of aerosol charge on the aerosol droplets, see Part II Section 7.2.1. This, of course, is hazardous because the entire mass of toxic material present in the original droplet may be deposited in the lung.

3.2 Droplet Evaporation

The rate of charge of particle size with time is given by, Hinds, 1982c:

$$\frac{d}{dt}(d_p) = \frac{4\, I_v\, M}{R\, \rho_p\, d_p} \left[\frac{P_\infty}{T_\infty} - \frac{P_d}{T_d} \right] \quad \text{for } d_p > \lambda \qquad (3)$$

Equation (3) can be re-written as:

$$d_p \frac{d}{dt}(d_p) = -\alpha \qquad (4)$$

where

$$\alpha = \frac{4\, I_v\, M}{R\, \rho_p} \left[\frac{P_d}{T_d} - \frac{P_\infty}{T_\infty} \right] \qquad (5)$$

in which:

λ = mean free path between water vapour molecules

I_v = diffusion coefficient of vapour in air in cm^2s^{-1}

M = molecular weight of evaporation vapour, g/mole

R = universal gas constant

d_p = droplet diameter

ρ_p = density of liquid

P_∞ = partial pressure of vapour away from droplet

P_d = partial pressure of vapour at droplet surface

T_∞ = ambient temperature

T_d = droplet surface temperature

When the partial pressure of vapour well away from the droplet, P_∞ , is less than the vapour pressure at the droplet surface, P_d, the right hand side of equation (3) will decrease with time, that is, net evaporation occurs.

The ratio of the actual partial pressure of vapour, P_∞, to saturation vapour pressure, P_s, at the temperature of the system is defined as "*saturation ratio*". The more familiar term for saturation ratio, in case of water vapour is relative humidity, RH, which can be defined as:

$$RH = P_\infty / P_s \qquad (6)$$

The saturation vapour pressure of water in mm Hg, at temperature, T, measured in °C, can be calculated using the following empirical expression, Hinds, 1982c,

$$\log_{10} P_s = 8.11 - \frac{1750}{T + 235} \qquad (7)$$

For droplet diameters $>0.01\,\mu m$ the partial pressure of water vapour at the surface of droplet, P_d, is approximately equal to the saturation vapour pressure P_s.

It can be seen from equation (3) that droplet evaporation rate depends on the material properties, $I_v M P_s/\rho_p$, a quantity that varies widely for different pesticide liquids. Equation (4) can be integrated to obtain the time, t, required for a droplet of a given diameter d_o to evaporate to some smaller diameter d_1.

$$\int_{d_o}^{d_1} d_p \, dd_p = \int_{o}^{t} -\alpha \, dt$$

$$\therefore \quad d_1^2 = d_o^2 - 2\alpha t \qquad (8)$$

Equation (8) gives droplet diameter d_1 as a function of time and initial diameter d_o. Of particular interest is the case when $d_1 = 0$, since this gives the time required for complete evaporation (the droplet life time or *drying time*, t_L). Equation (8) becomes:

$$t_L = d_o^2/2\alpha \qquad (9)$$

Equations (3) and (9) are accurate for calculating the rate of evaporation and drying time of large droplets (>10μm) of *low-volatility* liquid (eg oil-based pesticide droplets). For *volatile* liquids, which includes aqueous formulations, an additional correction must be applied to account for the *cooling effect* associated with the latent heat of evaporation. An equilibrium droplet temperature is established by balancing the heat lost due to evaporation with the heat gained by conduction from the warmer surrounding air. The resulting *steady-state temperature depression*, $(T_\infty - T_d)$, is given by, Davies, 1978:

$$T_\infty - T_d = \frac{I_v \, M \, H}{R \, K_v} \left[\frac{P_d}{T_d} - \frac{P_\infty}{T_\infty} \right] \qquad (10)$$

where

H = the latent heat of evaporation

K_v = thermal conductivity of the gas.

To account for the self-cooling of a volatile liquid, it is necessary to solve equation (10), but this requires numerical techniques. Graphical data, Figure III.6, (Hinds, 1982c) shows temperature depression as a function of relative humidity for different amibent temperatures. For the larger droplets (>50μm), an additional correction must be applied to compensate for the effect of settling velocity on evaporation rate, i.e. the "*wind*" factor. For example, for water droplets of dimaters 50μm and 100μm the evaporation rates are increased by 10% and 31% respectively over the rates predicted by equation (5).

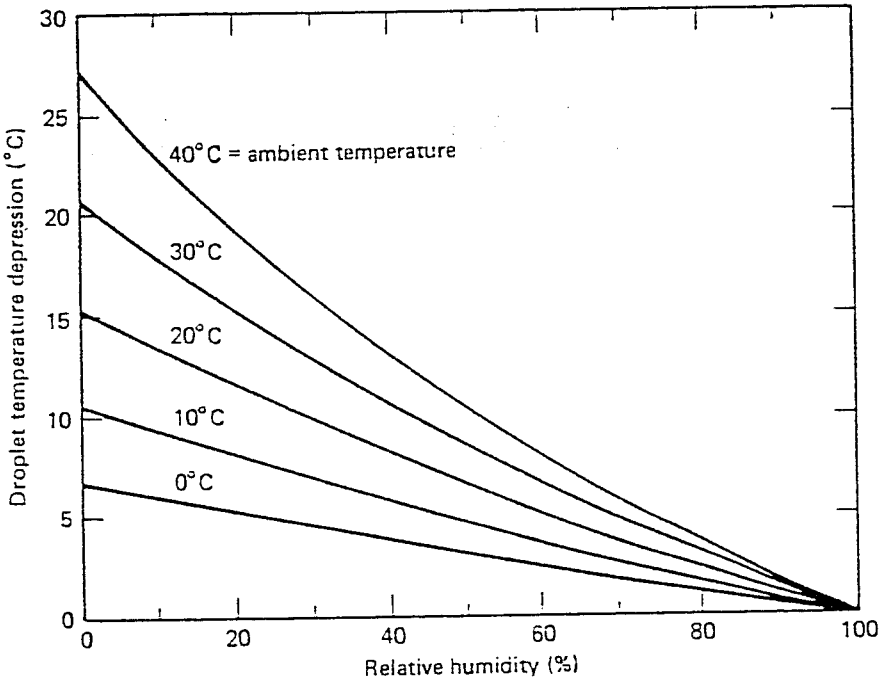

FIGURE III.6 Water droplet temperature depression as a function of relative humidity for ambient temperatures 0-40°C

Source: Hinds (1982)

When a pesticide droplet, of initial diameter d_o, is released in air at height h (due to being blown up by the wind during hand-held or tractor spraying or by falling during aerial spraying), it quickly reaches its terminal settling velocity, v_{ts}, and travels at that velocity towards the target plant. For a man standing in this area, the droplet will take time, t_c, to reach head height. After this critical time, t_c, (assuming no droplet disintegration) the man will be susceptible to inhaled toxic materials (assuming the drying time t_L is greater than the critical time t_c). To calculate the critical time, t_c, the following procedure may be followed:

The settling velocity, in the *Stokes's regime*, for a droplet of diameter d_p is:

$$U_{t_s} = \frac{\rho_p \, g}{18\mu} \, d_p^2$$

OR

$$- \frac{dz}{dt} = \beta \, d_p^2 \qquad (11)$$

where

$$\beta = \rho_p g/18\mu \qquad (12)$$

in which

g = acceleration of gravity

μ = viscosity of air

From equations (8) and (11)

$$- \frac{dz}{dt} = \beta \left[\, d_o^2 - 2\alpha t \, \right] \qquad (13)$$

By integration

$$\int_h^{h_c} dz = \int_o^{t_c} - \beta \left[\, d_o^2 - 2\alpha t \, \right] dt$$

$$h_c - h = -\beta \, d_o^2 t_c + \alpha\beta t_c^2 \qquad (14)$$

Equation (14) has the solution:

$$t_c = \frac{1}{2\alpha}\left[d_o^2 \pm \sqrt{d_o^4 - 4\alpha(h-h_c)/\beta} \right]$$

The negative root must be taken since $2\alpha t \leq d_1^2$ for all values of t.

$$t_c = \frac{d_o^2}{2\alpha}\left[1 - \sqrt{1 - 4\alpha(h-h_c)/\beta d_o^4} \right] \qquad (15)$$

Thus a particle of diameter d_o, released at height h will take time t_c to reach the average head height of a human subject. If droplet disintegration occurs, the critical time must be derived from the consideration of the time elapsed before disintegration, using equation (8), and the previous process has to be repeated for the new droplets.

To analyse the trajectories of larger droplets, where Stokes's law does not apply, numerical techniques are required. In a small time increment, it can be assumed that droplet diameter does not change significantly. The terminal speed and distance travelled by the droplet in that time can then be calculated. A reduction in droplet size during that time due to evaporation is then considered (assuming no disintegration), and the process repeated.

3.3 Theoretical Estimate of the State of Charge on Respirable Pesticide Particles

In electrostatic pesticide spray applicatons, especially aerial, droplet transit distance can be quite large. Also, for the temperature and relative humidities encountered in field work, evaporation of water-based pesticide spray is usually significant. To further compound the following predicted problem, many spray formulations include surface-active agents which drastically reduce droplet surface tension, Law, 1975. For an evaporating charged droplet, in transit from the nozzle to the target plants, rupture may occur if the critical surface charge density is reached (Rayleigh limit). The disintegration rate increases with initial droplet charge, transit distance and the increased evaporation due to *wind effects*. It decreases with increasing surface tension, relative humidity and droplet velocity. At the first disintegration a droplet will eject a small portion of its mass (according to Abbas and Latham, 1967, ~ 20-30% of original mass) and approximately 30%

of its initial charge q_o. The ejected mass may depart as a number of newly-formed smaller droplets. The primary droplet then attains another stable state. The process acting on the primary droplet is repetitive so long as evaporation continues and the droplet charge is not lost by other means (eg charge neutralisation due to ambient ions of opposite sign, photo emission, .. etc., Robertson, 1969). In addition, the ejected droplets are subjected to this same phenomenon as they evaporate. Thus, when charged droplets of a volatile liquid are subject to evaporation, an exponential growth in the number of respirable, highly-charged satellite droplets may be expected, the level of charge carried ranging from 30% to 70% of the Rayleigh limit.

3.3.1 Case history of an individual evaporation droplet

If an aerosol is generated using a Law nozzle, with a water-based pesticide formulation, the droplets will be charged to about 20% of the Rayleigh limit under typical operating conditions. Assume the volatile water-based droplets to be released 0.5 meter above head height, the temperature to be 20°C and the RH = 50%. For a large drop, of initial diameter d_o = 100μm, the initial charge will be Q_o approx. 4.10^{-3}stC. Evaporation will reduce the size of the droplet until it reaches the critical diameter (corresponding to the Rayleigh limit) d_{Ro} = 34.2μm after time t = 0.94s and transient distance D = 25.88cm. The single 34.2μm diameter drop will then eject about 25% of its mass as a newly formed smaller droplet with diameter 21.54μm charged to 1.276×10^{-3}stC, corresponding to 30% of the initial charge. The residual drop then assumes a new diameter of 31.07μm and charge 2.978×10^{-3}stC. As the droplets evaporate further instabilities and subdivisions occur as illustrated in Figure III.7.

3.4 An Assessment of the Health Hazard Associated with Electrostatic Crop Spraying

Although aerosol droplets may be relatively large initially, and therefore not be a health hazard, by the time they fall to head height, multiple disintegrations may have occurred. The case history shows that many satellite droplets are formed from the initial droplet, all of which are respirable (see glossary of terms) and therefore a health hazard.

A computer program could be developed to account for the change in size distribution of the nascent aerosol as a function of reduction in height. The final size distribution (at average head height) could be used as input data for the

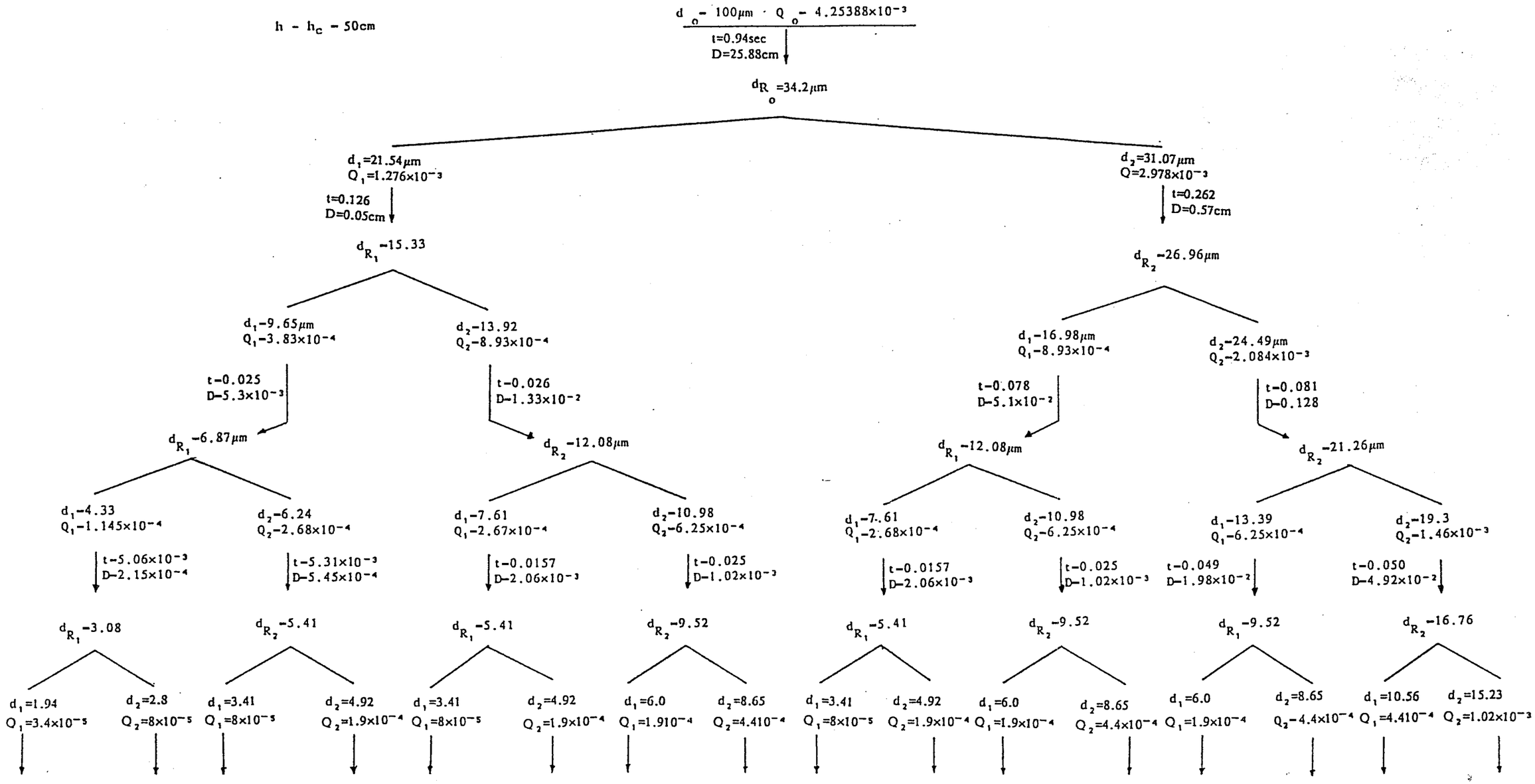

FIGURE III.7

CASE HISTORY OF A WATER DROPLET OF INITIAL DIAMETER 100μm FALLING FROM A HEIGHT OF 50cm ABOVE THE HEAD AT TEMPERATURE OF 20°C AND 50%RH"

d = droplet diameter (μm)
d_R = critical diameter (μm)
t = evaporation time (s)
D = distance travelled between two disintegrations (cm)
Q = charge (stC)

lung deposition model in order to evaluate aerosol deposition. Since the deposition model only accounts for monodisperse aerosols it would be necessary to divide the aerosol size distribution into bands and to compute the deposition for each band separately (as done in Part II, Section 7.3). This procedure assumes that there is no interaction between particles in different bands and that the combined deposition is just the summation of the depositions corresponding to the different bands. In this way it should be possible to evaluate the *dose* of toxic material deposited in the lung for different crop spraying scenarios. This would allow the nature of the hazard to be properly assessed.

4. HEALTH HAZARD OF CHARGED AEROSOL: DISCUSSION AND RECOMMENDATION FOR FUTURE WORK

Some aerosol manufacturers are now considering using triboelectrification techniques to improve the effectiveness of their aerosol products (which it is understood can be achieved by careful nozzle design). The implications with regard to health hazards may be serious, since charge is known to enhance particle deposition in the lung and volatile droplets will disintegrate on reaching the Rayleigh limit producing respirable droples from droplets which were, perhaps, harmless initially.

This aspect of health hazard should be assesed in view of the toxic material present in some commercially available aerosols (aerosol spray paint, insecticide, etc.). Similar hazards can arise in industrial liquid paint spraying operations where the aerosols are charged.

Potentially charged particles in cigarette smoke (Kingdon, 1961), mining atmospheres (Stein, 1973) and automobile emission (Westermark, 1961) should be studied, and the biological response to electrostatic charge (Andersen, 1971) established.

5. SUMMARY AND CONCLUSIONS OF PART III

1.(a) Measurement of electric charge on workplace aerosols shows that invariably aerosols are electrostatically charged to levels substantially above Boltzmann equilibrium.

(b) Effective charge levels are higher for fibrous aerosols (eg. asbestos) than for most similarly dispersed non-fibrous aerosols.

(c) The lung deposition model may be used, in the field of industrial hygiene, to assess the practical significance of the static electrification of airborne dust in the workplace.

(d) For most workplace aerosols, the proportion of A-deposition fraction due to electric charge is small. However, this might not necessarily apply to fibrous dusts.

2.(a) For electrostatic crop spraying applications, a mathematical model has been developed to account for the change in size and charge distributions of the nascent pesticide aerosol as a function of reduction in spraying height.

(b) Although the initial droplet sizes, typical of crop spraying, are relatively large and not a health risk, by the time droplets reach human head height, multiple disintegrations may have occurred, leading to respirable droplets of high charge-to-mass ratio (i.e. a health risk).

(c) To assess properly the nature of the hazard in electrostatic crop-spraying the lung model could be used to evaluate the dose of toxic material deposited in the lung for different crop spraying scenarios.

OVERALL SUMMARY AND CONCLUSIONS

OVERALL SUMMARY AND CONCLUSIONS

I. A Critical Comparison of the Operating Characteristics of Jet and Ultrasonic Nebulisers

I.1.1 Nebulisers come in two types, namely compressed-air (JN) and ultrasonic (UN) nebulisers. They generate aerosols by completely different mechanisms from one another.

I.1.2 The spray produced by both types often consist of particles covering a wide range of size, i.e. they are polydisperse.

I.1.3 For the JN particle size is inversely proportional to the driving gas flow rate while for the UN, the MMD of particles produced correlates with the excitation sound frequency of the piezoelectric transducer.

I.1.4 For the two types of nebuliser, particle size is influenced by the inhalation rate, large particles being pulled up into the aerosol cloud at high suction rates. Thus, for optimal operation, in which the number of respirable particles is maximised, a JN should be driven at a high gas drive flow rate and the subject should inhale at a low inspiratory flow rate.

I.1.5 The volume of solution placed within the nebuliser reservoir is not critical so far as aerosol MMD is concerned.

I.1.6 The MMD of aerosol generated by JN decreases with decreasing humidity and increasing temperature of the solution.

I.2.1 Neutral particles, charged particles and free ions are present in the aerosols generated by both JN and UN.

I.2.2 For the JN, the ratio between negative and positive ion concentrations was found to be dependent on the violence with which the liquid surface is disrupted.

I.2.3 The addition of electrolyte to the pure solution reduced the concentration of charged ions.

I.2.4 No reproducable current could be measured using aerosols generated by

the UN.

I.2.5 Both types of nebuliser can be modified using an auxiliary corona electrode so that the aerosol generated can be charged in a controlled manner.

I.2.6 For the JN, the charge-to-mass ratio increased with gas-drive flow rate. For the UN, the charge-to-mass ratio varied in a random fashion.

I.3.1 As the gas-drive flow rate increased, the mass output rate increased.

I.3.2 During jet nebulisation there is a rapid fall in the temperature of the reservoir solution. This fall is proportional to the flow rate of driving gas, and inversely proportional to the volume of solution placed in the nebuliser.

This cooling is believed to be caused by heat loss due to the latent heat of evaporation, the formation of new droplet surface area and adiabatic expansion of the gas jet.

I.4.1 The irritant effects (cough and subjective sensation) of ultrasonically nebulised distilled water can be significantly reduced when the same aerosol is unipolarly charged.

I.4.2 It was found that the irritation effects are related to the fluctuating electrical charge carried by the aerosol particles.

II. Predictive Lung and Respiratory Deposition Model

II.1.1 A computational lung deposition model, based on Yu's formulation, has been developed. Yu's analytical solutions have been replaced by iterative solutions which allows high deposition efficiencies to be considered.

II.1.2 Green's theorem has been used to transform the deposition double integral into a line integral. This formulation is advantageous since it is only necessary to evaluate the concentration at the airway entrances and exits, which allows the model to be implemented using a personal computer.

II.1.3 The model has been validated by comparing the theoretically predicted deposition fractions with experimental data, collected from various controlled inhalation aerosol deposition studies, for both total and regional deposition.

The breathing patterns and the aerosol characteristics used in the model calculations were chosen to correspond, as closely as possible, to these studies.

II.2.1 If the level of charge is sufficiently high, deposition is enhanced and regional deposition is influenced. The deposition theory, described here, has been shown to be consistent with experimental data regarding the deposition of charged particles in the human respiratory tract and, therefore, can be used for predicting respiratory deposition.

II.2.2 The deposition model can be used in aerosol therapy, to assess the performance of clinical nebulisers with regard to total and regional deposition.

II.2.3 The presence of charge on therapeutic aerosols increases their probability of deposition in the lung and allows control to be exercised over their site of deposition.

II.2.4 A more efficient delivery of therapeutic agents, to different parts of the lung, can be achieved by optimising aerosol flow rate, respiratory rate, tidal volume, pause period, particle size, particle density and particle charge.

II.3.1 The model is sensitive to the choice of parameters defining the breathing pattern and the physical characteristics of the inhaled aerosol particles.

II.3.2 The model accurately predicts regional deposition patterns when all the breathing pattern parameters and aerosol characteristics are well defined.

III. The Effect of Environmental Pollution on the Human Respiratory System

III.1.1 The static electrification of particulate air pollutants in the workplace is an important factor in relation to occupational health.

Measurements of electrical charge on workplace aerosols show that, substantially above Boltzmann equilibrium.

III.1.2 Effective charge levels are higher for fibrous aerosols than for most similarly-dispersed non-fibrous aerosols.

III.1.3 The lung deposition model could be used, in the field of industrial hygiene, to assess the practical significance of the static electrification of airborne dust in the workplace.

III.1.4 For most workplace aerosols, the proportion of alveolar deposition fraction due to electric charge is small. However, this might not necessarily apply in the case of fibrous dusts.

III.2.1 A mathematical model, applicable to electrostatic crop spraying, has been developed to account for the changes in the size and charge distribution of the nascent pesticide aerosols as the droplets fall and disintegrate.

III.2.2 Although the initial size of a droplet, typical of crop spraying, is relatively large, and therefore not a health risk, by the time it reaches a respirable position, multiple disintegration are likely to have occurred, leading to respirable droplets of large charge-to-mas ratio (i.e. health risk).

III.2.3 To assess properly the nature of the health hazard in electrostatic crop spraying and of inhaling charged particles in general, the lung deposition model could be used to evaluate the dose of toxic material deposited in the lung.

REFERENCES

REFERENCES

Abbas M.A., and Latham J., (1967), 'The instability of evaporating charged drops', J. Fuel Mech., 30 : 663–670.

Adams F., (1844), 'Commentary on the seven books of Paulus Aeginatur', (Trans.) London, Sydenham Society, 1 : 475–478.

Arnold A.J., and Pye B.J. (1980), 'Spray application with charged rotary atomisers', Br. Crop Protection Conf. Application Symposium – Spraying Systems for the 1980's, (Walker J.O., Ed.), BCPC Publications, Croydon, UK : 109–118.

Bailey A.G., (1974), 'Review: the generation and measurement of aerosols', J. Materials Sci., 9 : 1344–1362.

Bailey A.G., (1986), 'The theory and practice of electrostatic spraying', Atomization and Spray Tech., 2 : 95–134.

Beeckmans J.M., (1965), 'The deposition of aerosols in the respiratory tract', Can. J. Physiol. Pharmacol., 43 : 157.

Brain J.D., and Valberg P.A., (1979), 'State of the art : Deposition of aerosol in the respiratory tract', Am. Rev. Res. Dis., 120 : 1325–1372.

Cameron J.R., and Skofronick J.G., (1978), 'The physics of the lungs and breathing' : In 'Medical Physics', J. Wiley, N.Y. : 119–150.

Chain T.L., and Lippmann M., (1980), 'Experimental measurements and empirical modelling of the regional deposition of inhaled particles in humans', Am. Ind. Hyg. Assoc. J, 41 : 399–409.

Chan T.L., Lippmann M., Cohen V.R., and Schilesinger R.B., (1978), 'Effect of electrostatic charges on particle deposition in a hollow cast of human larynx – tracheobronchial tree', J. Aerosol Sci., 9 : 463–468.

Chan T.L., and Yu C.P., (1982), 'Charge effects on particle deposition in the human tracheobronchial tree', Ann. Occup, Hyg., 26 : 65–75.

Cheney F.W., and Butler J., (1968), 'The effects of ultrasonically–produced aerosols on airway resistance in man', Anesthesiology, 29 : 1099–1106.

Chubutija V.A., (1970), 'Electrical properties of industrial dusts and their influence on respiratory organs', Presented at the Int. Conf. on Harmful Dust in Mines, Gattwaldov, Conference Paper A2.

Coffee R.A., (1979), 'Electrodynamic spraying - a new approach to pesticide application', Proc. 1979 Br. Crop Protection Conf., 'Pests and Diseases', : 777-789.

Coffee R.A., (1980), 'Electrodynamic spraying', Br. Crop Protection Conf. Application Symposium - Spraying Systems for the 1980's, (Walker J.O., Ed.), BCPC Publications, Croydon, UK : 95-107.

Coffee R.A., (1981), 'Electrodynamic crop spraying', Outlook on Agriculture, 10 : 350-356.

Davies C.N., Heyder J., and Ramu C.S., (1972), 'Breathing of half-micron aerosols: 1. Experimental', J. Appl. Physiol., 32 : 591-600

Doyle A., Moffett D.R., and Vonnegut B., (1964), 'Behaviour of evaporating electrically charged droplets', J. Colloid Sci., 19 : 136-143.

Einstein A., (1905), 'Uber die van der molecular kinetischen theri der wörmer gefaorderite bewegun van in ruhenden flussigkeiten suspendierten teilchen', Annalen der Physik, 17 : 549-560.

Ferin J., Mercer T.T., and Leach L.J., (1983), 'The effect of aerosol charge on the deposition and clearance of T_iO_2 particles in rats', Environ, Res., 31 : 148-151.

Findeisen W., (1935), 'Uher das obsetzen kleiner, in der luft suspendiertan teilchen in der menschlichen lung bei der atmung', Arch. Ges. Physical, 236 : 367.

Fraser D.A., (1966), 'The deposition of unipolar charged particles in the lungs of animals', Arch. Environ. Health, 2 : 535-543.

Fry F.A. (1970), 'Charge distribution of aerosols and deposition in the human nose', J. Aerosol Sci., 1 : 135.

Fuchs N.A., (1964), 'The mechanics of aerosols', Pergamon, N.Y. : 112

Guyton A., (1986), 'Textbook of medical physiology', 7th Edition, W.B. Saunders Co., Philadelphia : 466-478.

Handbook of Air Pollution (1969), USPHS 999-AP-44.

Hashish A.H., and Bailey A.G., (1987), 'Administration of drugs using nebulisers : effect of electrostatic charge on aerosols', Inst. Phys. Conf. Ser. No.(85), Section 1 : 81-86. Paper presented at Electrostatic '87, Oxford.

Hashish A.H., Bailey A.G., and Williams T.J.., (1988), 'A mathematical model of the human lung which accounts for the depositional effect of charge on aerosol particles', Proc. of 2nd Conf. of Aerosol Soc., Bournemouth, UK, : 121-126.

Heyder J., (1975), 'Gravitational deposition of aerosol particles within a system of randomly oriented tubes', J. Aerosol Sci., 6 : 133-137.

Heyder J., and Rudolf G., (1984), 'Mathematical models of particle deposition in the human respiratory tract', J. Aerosol Sci., 15 : 697-707.

Hinds W.C., (1980), 'The lung and the environment', Sem. Res. Med., 1 : 197-210.

Hinds W.C., (1982a), 'Aerosol technology', J. Wiley - Interscience Publication, N.Y. : 292-300.

Hinds W.C., (1982b), 'Aerosol technology', J. Wiley - Interscience Publication, N.Y., : 211-232.

Hinds W.C., (1982c), 'Aerosol technology', J. Wiley - Interscience Publication, N.Y. : 265-273

Hughes J.M., Happin F.G. Jr., and Mead J., (1972), 'Effect of lung inflation on bronchial length and diameter in exercised lungs', J. App. Physiol., 32 : 25-35.

Hughes J.F., (1984), 'Electrostatic powder coating', Research Studies Press Ltd., England.

Inculet I.I., (1978), 'Electrostatic in Industry', J. Electrostatics, 4 : 175–192.

Inculet I.I., Castle G.S.P., Menzies D.R., and Frank R., (1981), 'Deposition studies with a novel form of electrostatic crop sprayer', J. Electrostatics, 10 : 65–72.

Ingham D.B., (1975), 'Diffusion of aerosols from a stream flowing through a cylindrical tube', J. Aerosol Sci., 6 : 125–132.

Ingham D.B., (1981), 'Precipitation of charged particles in human airways', J. Aerosol Sci., 12 : 131–135.

International Standards Organisation, (1981), 'Size definitions of particle sampling : Recommendations of ad hoc working group appointed by Committee TC 146 of the International Standards Organisation', Am. Ind. Hyg. Assoc. J., 42 : A64–A68.

James M.L., Smith G.M., and Walford J.C., (1967), 'Applied numerical methods for digital computation with Fortran', International Textbook Company, Pennsylvania : 139–145.

Johnston M.M., Vincent J.H., and Jones A.D., (1985), 'Measurement of electric charge for workplace aerosols', Ann. Occup. Hyg., 19 : 271–284

Kingdon K.H., (1961), 'Possible biological effects of electrically charged particles in tobacco smoke', Nature, London, 189, : 180.

Kosenko A.I., (1970), 'Electrostatic charges on airborne dusts originating in some industrial operations', Presented at the Int. Conf. on Harmful Dust in Mines, Gattwaldov, Conference Paper A1.

Kunkel W.B., (1954), 'The static electrification of dust particles on dispersion into a cloud', J. Appl. Phys., 21 : 826.

Landahl H.D., (1950), 'On the removal of airborne droplets by the human respiratory tract: I. The lung', Bull. Math. Biol., 12 : 43–56.

Landahl H.D., (1963), 'Particle removal by the respiratory system. Notes on the removal of airborne particulates by the human respiratory tract with particular reference to the role of diffusion', Bull. Math. Biophys., 25 : 29–39.

Lang R.J., (1962), 'Ultrasonic atomization of liquids', J. Acoust. Soc. Am., 34 : 6–8.

Law S.E., and Bowen H.D., (1975), 'Theoretically predicted interactions of surface charge and evaporation on airborne pesticide droplets', Trans. of the ASAE, 18 : 35–39 & 45.

Law S.E., (1980), 'Droplet charging and electrostatic deposition of pesticide sprays', Br. Crop Protection Conf. Application Symposium – Spraying Systems for the 1980's, (Walker J.O., Ed.), BCPC Publications, Croydon, UK : 85–94.

Law S.E., (1980), 'Electrostatic deposition of pesticide sprays onto ionizing targets : charge and mass transfer analysis', Conference record of the 1980 IAS Annual Meeting, IEEE Ind. Apl. Soc., 105(6) : 774–777.

Ledermann W., (1966), 'Multiple Integrals', Library of Mathematics (Ed. W. Ledermann), Rautlege and Kegon Paul Ltd., London, : 36–41.

Lewis R.A., Ellis C.J., Bailey A.G., Hashish A.H., and Balachandran W., (1985), 'Cough induced by ultrasonically nebulised water is related to aerosol particle charge', Br. Thoracic Soc., Summer meeting.

Lippmann M., (1977), 'Regional deposition of particles in the human respiratory tract', In: Handbook of Physiology, (Lee D.H.K., Ed.), Belhesda.Md., Am. Physiology Soc. : 213–232.

Loeb L.B., (1958), 'Static electrification', Springer–Verloog, Heidelberg : 1

Longley M.Y., (1960), 'Pulmonary deposition of dust as affected by electric charges on the body', Am. Ind. Hyg. Assoc. J., 21 : 187–194.

Lui B.Y., and Pui D.Y., (1974), 'Electrical neutralization of aerosols', J. Aerosol Sci., 5 : 465–472.

Lui B.Y., and Kapadia H., (1978), 'Combined field and diffusion charging of aerosol particles in the continuum regime', J. Aerosol Sci., 9 : 227–242.

Luke G.D., Asgharion B., and Yu C.P., (1985), 'Sedimentation of charged particles inside cylinders and spheres', Paper presented at the 16th Ann. Meeting of the 'Fine Particles Society', Miami Beach : 61–63.

Melandri C., Prodi V., Tarroni G., Formignani M., De Zalacomo T., Bompane G.F., and Maestri G., (1977), 'On the deposition of unipolar charged particles in the human respiratory tract', In : Inhaled particles IV (Walton W.H., Ed.), Pergamon Press, Oxford : 193–200.

Melandri C., Tarroni G., Prodi V., De Zalacomo T., Formignani M., and Lombardi C.C., (1983), 'Deposition of charged particles in the human airways', J. Aerosol Sci., 14 : 657–669.

Mercer T.T., Millery M.I., and Chow H.Y., (1968), 'Operating characteristics of some compressed air nebulizers', Am. Ind. Hyg. Ass. J., 29 : 66–78.

Mercer T.T., (1973), 'Production and characterization of aerosols', Arch. Intern. Med., 131 : 39–50.

Mercer T.T., (1975), 'The deposition model of the Task Group on lung dynamics : A comparison with recent experimental data'. Health Phys., 29 : 673–680.

Nakiyama S., and Tanasawa Y., (1939) 'An experiment on the atomization of liquid', Trans. Soc. Mech. Eng. (Japan), 5 : 62–68.

Newman S.P., and Clark S.W., (1983), 'Therapeutic aerosols 1 – Physical and practical considerations', Thorax, 38 : 881–886.

Newman S.P., Pellow P.G., and Clark S.W., (1987), 'Dropsizes from medical atomisers (nebulisers) for drug solutions with different viscosities and surface tensions', Atomisation and Spray Tech., 3 : 1–11.

Pauthenier M., and Moreau-Hanot M., (1932), 'Charging of spherical particles in an ionizing field', J. Phys. Radium, 3 : 590–613.

Pich J., (1972), 'Theory of gravitational deposition of particles from laminar flows

in channels', J. Aerosol Sci., 3 : 351-361.

Pich J., (1978), 'Comments on the paper C.P. Yu's precipitation of unipolarly charged particles in cylindrical and spherical vessels', J. Aerosol Sci., 9 : 275-278.

Rayleigh, Lord, (1882), 'On the equilibrium conductnig masses charged with electricity', Phil. Mag., 14 : 184-185.

Ruch-Patton (1974), 'Respiration', In: Textbook of Physiology and Biophysics II, W.B. Saunlers Co., : 355-370.

Scherer P.W., Shendalmon L.H., and Green N.M., (1972), 'Simultaneous diffusion and convection in single breath lung washout', Bull. Math. Biophys., 34 : 393-412.

Schlesinger R.B., and Lippmann M., (1972), 'Particle deposition in casts of the human tracheobronchial tree', Am. Ind. Hyg. Ass. J., 33 : 237-261.

Schlesinger R.B., Bahning D.E., Chan T.L., and Lippmann M., (1977), 'Particle deposition in a hollow cast of the human tracheobronchial tree', J. Aerosol Sci., 8 : 429-445.

Shevchenko A.M., (1971), 'The role of some physical and chemical properties of mine dust in the development of pneumaconiosis', In: Inhaled Particles II (Walton W.H., Ed.), Unwin Bros., Old Woking : 561-568.

Smoluchowski M.V., (1912), 'Experimentally demonstratable molecular phenomena which contradict conventional thermodynamics', Phys. Z, 13 : 1069.

Stainforth J.N., Lewis R.A., Tattersfield A.E., (1983), 'Dosage and delivery of nebulised Beta Agonists in hospital', Thorax, 38 : 751-754.

Stein R.L., (1972), 'Deposition of aerosols on a charged polystyrene surface', Am. Ind. Hyg. Ass. J., 33 : 775.

Stein R.L., Ryback W.H., and Sparks A.W., (1973), 'Deposition of aerosol in a plastic chamber', J. Colloid Interface Sci., 42 : 441.

Steventon R.D., and Wilson R.S., (1979), 'Nebuliser units', Br. J. Cli. Equip. :

153-155.

Struss W., (1971), 'Air pollution control', Part 1, J. Wilely, Interscience Publication, N.Y., : 227.

Swift D.L., (1980), 'Aerosol and humidity therapy : Generation and respiratory deposition of therapeutic aerosols', Am. Rev. Res. Dis., 122 : 71-77.

Swithenbank J., Beer J.M., Taylor D.S., Abbot D., and McCreath G.C., (1977), 'A laser diagnostic technique for measurement of droplet and particle size distribution', Progress in Astronautics and Aeronautics, 53 : 421-437.

Tarroni G., Melandri C., Prodi V., De Zaiacoma T., Farmignoni M., and Bassi P., (1980), 'An indication on the biological variability of aerosol total deposition in humans', Am. Ind. Hyg. Assoc. J., 41 : 826-831.

Task Group on Lung Dynamics, (1966), 'Deposition and retention models for internal dosimetry of the human respiratory tract', Health Phys., 12 : 173-207.

Taulbee D.B., and Yu C.P., (1975), 'A theory of aerosol deposition in the human respiratory tract', J. Appl. Physiol., 38 : 77-85

Testone R., (1986), 'Effects of air ionization', Evaluation Engineering, June, : 78-89.

Timbrell V., (1965), 'The inhalation of fibrous dusts', Ann. N.Y. Acad. Sci., 132 : 255-273.

Topp M.N., and Eisenklam P., (1972), 'Industrial and medical uses of ultrasonic atomizers', Ultrasonics, 127-133.

Vincent J.H., Johnston W.B., Jones A.D., and Johnston A.M., (1981), 'Static electrification of airborne asbestos : a study of its cause, assessments and effect of airborne asbestos: a study of its cause, assessment and effects on deposition in the lungs of rats', Am. Ind. Hyg. Assoc. J., 42 : 711-721.

Vincent J.H., Johnson A.M., Jones A.D., and McLachlan C.Q., (1983),

'Measurements of the static electrification of airborne dusts in workplaces', Inst. of Occup. Med. (Edinburgh), Report No. TM/83/15.

Vincent J.H., (1986), 'Review: Industrial hygiene implications of the static electrification of workplace aerosols', J. Electrostatic, 18 : 113-145.

Walkenhoist W., (1971), 'Charge measurement of dust particles', Staub Reinhalt-Luft (English translation), 31 : 8.

Wehner A.P., (1969), 'Special Review: Electro-aerosols, air ions and physical medicine', Am. J. Phys. Med.; 48 : 119-149.

Weibel E.R., (1963), 'Morphometry of the human lung', Academic Press, N.Y. : 136-140.

Westermark T., (1961), 'Detection of free charges from motor-car exhaust gases', Nature, London, 189 : 910.

White H.J., (1963), 'Industrial electrostatic precipitation', Addison-Wesley, Reading, Massachusetts.

Wilson I.B., (1947), 'The deposition of charged particles in tubes with reference to the retention of therapeutic aerosol in the human lung', J. Coll. Sci., 2 : 271-276.

Yu C.P., and Chandra K., (1977), 'Precipitation of submicron charged particles in human lung airway', Bull. Math. Biol., 39 : 471-478.

Yu C.P., (1977), 'Precipitation of unipolar charged particles in cylindrical and spherical vessels', J. Aerosol Sci., 8 : 237-241.

Yu C.P., (1978), 'Exact analysis of aerosol deposition during steady breathing', Powder Tech., 21 : 55-62.

Yu C.P., and Chandra K., (1978), 'Deposition of charged particles from laminar flows in rectangular and cylindrical channels by image force', J. Aerosol Sci., 9 : 175-180.

Yu C.P., Nicaloides P., and Soong T.T., (1979), 'Effect of random airway sizes on aerosol deposition', Am. Ind. Hyg. Ass. J., 40 : 999-1005.

Yu C.P., Diu C.K., and Soong T.T., (1981), 'Statistical analysis of aerosol deposition in nose and mouth', Am. Ind. Hyg. Ass. J., 42 : 726–733.

Yu C.P., and Diu C.K., (1982), 'A comparative study of aerosol deposition in different lung models', Am. Ind. Hyg. Assoc. J., 43 : 54–65.

Yu C.P., and Diu C.K., (1983), 'Total and regional deposition of inhaled aerosols in humans', J. Aerosol Sci., 14 : 599–609.

Yu C.P., (1985), 'Theories of electrostatic lung deposition of inhaled aerosols', Ann. Occup. Hyg., 29 : 219–227.

Yu C.P., and Xu G.B., (1986), 'Predictive models for deposition of diesel exhaust particulates in human and rat lungs', Aerosol Sci. and Tech., 5 : 337–347.

Yu C.P., (1987), Personal Communication.

Yu C.P., and Xu G.B., (1987), 'Predicted deposition of diesel particles in young humans', J. Aerosol Sci., 18 : 419–429.

APPENDICES

APPENDIX (I)

Glossary of Terms

Air Pollution:

The World Health Organisation has defined *air pollution* as: a situation in which the outdoor ambient atmosphere contains material in concentration that is harmful to man or his environment.

Inhalable Aerosol:

An *inhalable aerosol* is an aerosol that is capable of being deposited in the respiratory tract beyond the larynx. The upper size limit for such aerosol particles is 15μm diameter, International Standards Organisation, 1981.

Isometric Particles:

An *isometric particle* is one of arbitrary shape but which has no prominent dimension. Fibrous and plate-like particles, for example, are not isometric since they do not conform to the above definition, Vincent, 1986.

Mean Flow Rate (Q):

The *mean flow rate* is defined as the time average, for a single cycle, of the volumetric flow rate at the entrance to the respiratory tract, and is given by:

$$Q = \frac{1}{T} \int_0^T |\dot{V}| \, dt$$

where

$\dot{V}$ = the instantaneous volumetric flow rate of air.

T = the inhalation duration of a single breathing cycle (assuming the inhalation and exhalation durations to be identical).

Mean Residence Time (τ):

An undeposited particle inhaled at the beginning of a breath stays

longer in the respiratory tract than one inhaled at the end of the inhalation period. The associated *mean residence time* can be defined as:

$$\tau = \frac{1}{2Q} \int_0^T |\dot{V}| \, dt$$

where

$\dot{V}$ = the instantaneous volumetric flow rate

Q = the mean flow rate

(assuming the inhalation and exhalation duration to be identical)

Respirable Aerosols:

Respirable aerosols are those capable of being deposited in the alveolar sacs at the lung periphery, in the alveolar region of the lung.

The upper size limits for these aerosol particles is 7μm diameter, International Standards Organisation, 1981.

Regional Deposition:

Regional deposition is the average probability of an inspired particle touching a surface of the respiratory tract, in the region considered, and thereby being deposited.

Total deposition is, therefore, the sum of the regional depositions. Usually, it is confined to steady-state breathing and will be considered so in this thesis.

Static Electrification:

Static electrification covers all processes for producing segregation of positive and negative electrical charges by mechanical actions which operate by contact or impact. These involve such processes as frictional, contact, or tribo-electrification, spray electrification and electrification in dust, Loeb, 1958.

Total Deposition:

Total deposition is the average probability of an inspired particle touching a surface of the respiratory tract and thereby being deposited.

APPENDIX II

APPENDIX II.A

The Relationships Between Airway Dimensions and the Lung Volume (Scaling Factor)

Consider the dimensions of n^{th} airways at rest are d_{on} and ℓ_{on} for the diameter and the length respectively. The initial n^{th} airway volume:

$$V_{on} = \frac{\pi}{4} d_{on}^2 \ell_{on} \qquad (A.1)$$

Then expanded $d_{en} = \alpha d_{on}$ and $\ell_{en} = \alpha \ell_{on}$. The expanded n^{th} airway volume:

$$V_{en} = \frac{\pi}{4} d_{en}^2 \ell_{en}$$

$$\therefore \quad V_{en} = \alpha^3 \frac{\pi}{4} d_{on}^2 \ell_{on} \qquad (A.2)$$

From (A.1) and (A.2),

$$\therefore \quad V_{en} = \alpha^3 V_{on} \qquad (A.3)$$

Accordingly, for the whole lung, we have

$$\sum_{n=1}^{24} V_{en} = \alpha^3 \sum_{n=1}^{24} V_{on}$$

i.e. $$V_{eT} = \alpha^3 V_{oT} \qquad (A.4)$$

From (A.4) we have scaling factor α as follows:

$$\alpha = (V_{eT}/V_{oT})^{1/3}$$

APPENDIX II.B

The Deposition Efficiency of Charged Particles During the Pause

There are two mechanisms by which the presence of charge on aerosol particles can enhance their deposition, namely image force deposition and space charge deposition. Initially, the effects of image force will be considered. Consider a mono-disperse aerosol of unipolar charged particles, each of which carries a charge q, suspended in a cylindrical conducting airway of radius R.

During the pause, the axial aerosol flow rate is zero and the image force takes the following form (Yu, 1977):

$$F = \frac{q^2 r^2}{16\pi\epsilon_o R^2 (R-r)^2} \qquad (B.1)$$

This electrostatic image force causes the particles to migrate radially towards the wall where deposition occurs. The equation of motion for the particle is shown below, where B is the mechanical mobility of the particle.

$$\frac{dr}{dt} = BF = \frac{B\, q^2 r^2}{16\pi\epsilon_o R^2 (R-r)^2} \qquad (B.2)$$

Integrating equation (B.2) gives:

$$\int_{r_c}^{R} \frac{(R-r)^2}{r^2}\, dr = \frac{B\, q^2}{16\pi\epsilon_o R^2} \int_{o}^{t_p} dt \qquad (B.3)$$

where r_c is the collection radius, defined such that all particles situated at a radius $r \geq r_c$ are deposited during the pause time (see Figure B).

$$\int_{r_c}^{R} \left[\frac{R^2}{r^2} - \frac{2R}{r} + 1 \right] dr = \frac{B\, q^2 t_p}{16\pi\epsilon_o R^2} \qquad (B.4)$$

$$\therefore \quad 2\ell n \left[\frac{r_c}{R} \right] + \frac{R}{r_c} - \frac{r_c}{R} = \frac{Bq^2\, t_p}{16\pi\epsilon_o R^3} = \frac{\tau}{4} \qquad (B.5)$$

where τ is a dimensionless time parameter.

$$\because \text{deposition efficiency} = \frac{\text{amount of aerosol deposited during pause}}{\text{initial amount of aerosol in the airway}}$$

$$\therefore \quad \eta = \frac{\pi R^2 Lc - \pi r_c^2 Lc}{\pi R^2 Lc}$$

where: c is the number concentration

$$\eta = 1 - \left[\frac{r_c}{R} \right]^2 \qquad (B.6)$$

Since stationary conditions are applicable (Q=0), the *slug flow* deposition efficiency expression, equation (98) may be used, where τ_j is the dimensionaless time defined in equation (B.5) and stated expressly below:

$$\tau = \frac{Bq^2 t_p}{4\pi\epsilon_o}$$

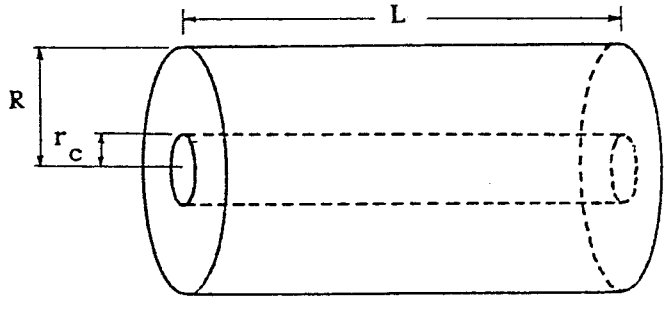

Figure B

APPENDIX II.C

Listing of the Computer Program for the Predictive Lung Model

```
10 REM HASSAN Program .
20 CLS
30 DIMC(3,23,23),PDP(23),F(3,23),Y(5,23),NH(3),NALPA(23)
40 REM Predictive Lung Deposition
50 REM model cpu program.
60 *TV250,1
70 REM Input Particle Characteristics.
80 PRINT"Particle Diameter in cm =";
90 INPUT D
100 PRINT"Particle Density in g/cm3 =";
110 INPUT K
120 PRINT"Particle Charge in elmentary units =";
130 INPUT Q
140 PRINT"Particle Concentration, n/cm3=";
150 INPUT C0
160 REM Input Breathing Characteristics.
170 PRINT"Inhalation flow rate in cm3/sec=";
180 INPUT F0I
190 PRINT"Exhalation flow rate in cm3/sec=";
200 INPUT F0E
210 PRINT"Inhalation Time in sec=";
220 INPUT T0I
230 PRINT"Pause Time in sec=";
240 INPUT T0P
250 PRINT"Exhalation Time in sec=";
260 INPUT T0E
270 REM HEAD=1 for mouth breathing
280 REM HEAD=2 for nasal breathing
290 PRINT"Breathing Mode:Mouth(1),Nasal(2),=";
300 INPUT HEAD
310 IF HEAD=1 THEN PRINT"Mouth breathing mode"
320 IF HEAD=2 THEN PRINT"Nasal breathing mode"
330 REM Calculate time spend in the
340 REM head (head volume=50 cm3).
350 HT= 50/F0I
360 REM Calculate inhalation time for
370 REM the lung.
380 T0I=T0I-HT
390 REM Correction factor to readjust
400 REM WEIBLE's data to the mean
410 REM value of lung volume (corres-
420 REM ponding to rest lung volume
430 REM of 3000+half tidal volume).
440 REM tidal volume).
450 VLR=3000:DCR=SQR(1+(F0I*T0I)/(2*VLR))
    :PRINT"VLR in cm3=";VLR
460 REM Diameter correction for pause
470 DCRP=SQR(1+(F0I*T0I)/VLR)
480 REM Calculate the position of
490 REM aerosol front VX1
500 VX1=((VLR*T0I)/(T0I+(VLR/F0I))) :PRINT"VX1=";VX1
510 REM Data for No.of alveolar sacs
520 REM per airway.
530 NALPA(18)=5
540 NALPA(19)=8
550 NALPA(20)=12
560 NALPA(21)=20
```

```
570 NALPA(22)=20
580 NALPA(23)=20
590 REM Volume of alveolar sac
600 REM defined as VAS=6.707E-6
610 VAS=6.707E-6
620 REM Data of WEIBLE'S model for
630 REM lung morphology (adjusted for
640 REM 3000cm3 rest lung volume)
650 REM 5*23 array
660 DATA 1,1,1.539,10.26,19.06
670 DATA 2,2,1.043,4.07,25.63
680 DATA 3,4,.71,1.624,28.63
690 DATA 4,8,.479,.65,29.5
700 DATA 5,16,.385,1.086,31.69
710 DATA 6,32,.299,.915,33.75
720 DATA 7,64,.239,.769,35.94
730 DATA 8,128,.197,.65,38.38
740 DATA 9,256,.159,.547,41.13
750 DATA 10,512,.132,.462,44.38
760 DATA 11,1024,.111,.393,48.25
770 DATA 12,2048,.093,.333,53
780 DATA 13,4096,.081,.282,59.13
790 DATA 14,8192,.07,.231,66.25
800 DATA 15,16384,.063,.197,77.13
810 DATA 16,32768,.056,.171,90.69
820 DATA 17,65536,.051,.141,109.25
830 DATA 18,131072,.046,.121,139.31
840 DATA 19,262144,.043,.1,190.6
850 DATA 20,524288,.04,.085,288.16
860 DATA 21,1048578,.038,.071,512.94
870 DATA 22,2097152,.037,.06,925.04
880 DATA 23,4194304,.035,.05,1694.16
890 FOR ROW=1 TO 23
900 FOR COLUMN=1 TO 5
910 READ Y(COLUMN,ROW)
920 NEXT COLUMN
930 NEXT ROW
940 TAI=VLR/F0I:TAE=VLR/F0E:TT=T0E+T0I*(TAE/TAI)
950 TIME1=TAI+T0I:TIME2=TAE+TT-T0E
960 REM Slip correction factor CR
970 CR=1+(0.069E-4/D)*(2.514+0.8*EXP(-0.55*D/0.069E-4))
980 REM Calculation of settling
990 REM velocity U
1000 U=CR*K*D*D*981/(18*1.89E-4)
1010 REM Diffusion coefficient I at
1020 REM body temp.37c
1030 I=CR*1.38E-16*310.15/(3*PI*1.89E-4*D)
1040 REM To establish aerosol front
1050 REM postion C%
1060 B%=0
1070 B%=B%+1
1080 V1=Y(5,B%) :IF V1<VX1 GOTO1070
1090 C%=B% :PRINT "C%=";C%
1100 REM Head deposition for inh.
1110 HCI=K*D^2*F0I/1E-8:HCE=K*D^2*F0E/1E-8
1120 IF HEAD=2 GOTO 1140
1130 IF HCI>3000 THEN NH(1)=-1.117+0.324*LOGHCI ELSE
     NH(1)=0:GOTO 1170
```

```
1140 IF HCI< 337 THEN NH(1)=-0.014+0.023*LOGHCI ELSE
     NH(1)=-0.959+0.397*LOGHCI
1150 IF HCE< 215 THEN NH(3)= 0.033+0.003*LOGHCE ELSE
     NH(3)=-0.851+0.339*LOGHCE
1160 IF NH(3)>1 THEN NH(3)=1
1170 IF NH(1)>1 THEN NH(1)=1
1180 REM No. conc. entering lung C0I
1190 C0I=C0*(1-NH(1))
1200 REM Normalisation const.for dep.
1210 NORM=C0I*F0I*T0I
1220 REM Adjust airway volume,no.of
1230 REM alveoli per gen.and airway
1240 REM length of final generation
1250 REM (C%) to account for aerosol
1260 REM front position.
1270 Y(5,C%)=VX1 :V0=Y(5,C%-1)
1280 AF=(VX1-V0)/(V1-V0)
1290 NALPA(C%)=NALPA(C%)*AF
1300 Y(4,C%)=Y(4,C%)*AF
1310 REM To calculate flow rate array
1320 FOR K%=1 TO 3 STEP 2
1330 FOR B%=0 TO C%
1340 IF K%=1 THEN F0=F0I
1350 IF K%=3 THEN F0=F0E
1360 F(K%,B%)=F0*(1-(Y(5,B%)/VLR))
1370 NEXT B%
1380 NEXT K%
1390 REM Inhalation boundary condition
1400 FOR J%=0 TO C%
1410 C(1,0,J%)=C0I
1420 NEXT J%
1430 REM To calculate conc.throughout
1440 REM the solution domain.
1450 FOR K%=1 TO 3 STEP2
1460 IF K%=1 THEN LS=1:LE=C%:LST=1
1470 IF K%<>3 THEN GOTO 1550
1480 LS=C% :LE=1 :LST=-1
1490 REM Exhalation boundary condition
1500 REM No need to correct DA since
1510 REM first gen.is not in A-region
1520 DA=Y(3,1)
1530 C(3,0,0)=C(1,0,0)*(1-FNpause)
1540 PRINT"FNpause=";FNpause
1550 FOR B%=LS TO LE STEP LST
1560 BM%=B%-1
1570 NA=Y(2,B%):DA=Y(3,B%):L=Y(4,B%)
1580 DA=SQR(DA*DA+(4*NALPA(B%)*VAS/(PI*L)))
1590 IF K%=1 THEN DUM1%=BM%:DUM2%=B%:F0=F0I
1600 IF K%<>3 GOTO 1650
1610 DUM1%=B% :DUM2%=BM% :F0=F0E
1620 REM General Exhalation
1630 REM boundary condition
1640 C(3,B%,B%)=C(1,B%,B%)*(1-FNpause)
1650 VS=Y(5,BM%):VE=Y(5,B%)
1660 F1=F0*(1-(VS/VLR)):NS=FNdepeff
1670 F1=F0*(1-(VE/VLR)):NE=FNdepeff
1680 REM Average value of dep.eff.(N)
1690 REM to account for flow rate
```

```
1700 REM along airway.
1710 N=(NS+NE)/2 1720 FOR J%=B% TO C%
1730 REM Calculate correction factor M
1740 M=(VLR-Y(5,B%-1))/(VLR-((Y(5,B%-1)+Y(5,B%))/2))
1750 REM Concentration by iteration
1760 C(K%,DUM2%,J%)=C(K%,DUM1%,J%)*(1-M*N)
1770 NEXT J%
1780 NEXT B%
1790 NEXT K%
1800 REM Calculation of particle dep.
1810 PD=0
1820 FOR B%=1 TO C%
1830 PDP(B%)=0
1840 FOR K%= 1 TO 3 STEP2
1850 IF K%=1 THEN LSJ=C%:LEJ=B%:LSTJ=-1
1860 IF K%=3 THEN LSJ=B%:LEJ=C%:LSTJ=1
1870 BM%=B%-1
1880 FOR J%=LSJ TO LEJ STEP LSTJ
1890 JM=J%-1
1900 PROCtime
1910 IF K%=1 THEN DUM1%=BM%:DUM2%=B%
1920 IF K%=3 THEN DUM1%=B%:DUM2%=BM%
1930 REM Use average value OF conc.
1940 REM during Exhalation
1950 C1=(C(K%,DUM1%,JM%)+C(K%,DUM1%,J%))/2
1960 C2=(C(K%,DUM2%,JM%)+C(K%,DUM2%,J%))/2
1970 PDP(B%)=PDP(B%)+(F(K%,DUM1%)*C1*TS-F(K%,DUM2%)*C2*TF)
     /NORM
1980 NEXT J%
1990 NEXT K%
2000 PD=PD+PDP(B%)
2010 IF B%=17 THEN TB=PD
2020 NEXT B%
2030 IF HEAD=1 THEN HDE=0 :GOTO2180
2040 REM Calculate integral Cdt from
2050 REM t2 to T by TRAPEZIUM rule
2060 ICDT=0
2070 K%=3:B%=1
2080 FOR J%=1 TO C%
2090 PROCtime
2100 ICDT=ICDT+(C(3,0,J%)+C(3,0,J%-1))*TF/2
2110 NEXT J%
2120 REM Head dep.for exh.(Nasal only)
2130 HDE=NH(3)*F0E*ICDT/(C0*F0I*T0I)
2140 REM Fraction of aerosol available
2150 REM for exh depostion in the head
2160 LIMIT=1-PD*(1-NH(1))-NH(1)
2170 IF HDE>LIMIT THEN HDE=LIMIT
2180 PRINT"Head dep.=";NH(1)+HDE
2190 PRINT"NH(1)=";NH(1),"HDE=";HDE
2200 PRINT"TB-DEP.=";TB*(1-NH(1))
2210 PRINT"A-DEP.=";(PD-TB)*(1-NH(1))
2220 PRINT"TOTAL DEP.=";PD*(1-NH(1))+NH(1)+HDE
2230 END
2240 REM FN to calc. Dep.efficiencies.
2250 DEF FNdepeff
2260 REM Calc. cross-sectional area
2270 REM of each generation
```

```
2280 F=F1
2290 DA=DA*DCR
2300 A=PI*DA*(DA/4)*NA
2310 REM Calc. Impaction efficiency N1
2320 S=K*D*D*(F/A)/(9*1.89E-4*DA)
2330 H=L/(4*DA)
2340 N1=0.768*S*H
2350 IF B%>17 OR K%>1 THEN N1=0
2360 REM Calc.sedimentation
2370 REM efficiency N2
2380 E=(3*PI*U*L)/(16*(F/A)*DA):IFE>1 THEN N=1: GOTO2590
2390 X=E^(1/3)
2400 N2=(2/PI)*((2*E-X)*(1-X*X)^0.5+ASN X)
2410 REM Calc. Diffusion efficiency N3
2420 J=(I*L)/(DA*DA*(F/A))
2430 YY=0.0325*EXP(-228*J)+0.0509*EXP(-125*(J^(2/3)))
2440 N3=1-0.819*EXP(-14.63*J)-0.0976*EXP(-89.22*J)-YY
2450 REM Calc. electrostatic dep.
2460 REM efficiency (using e.s.u).
2470 IF Q=0 THEN N4=0 :GOTO 2580
2480 Q1=Q*4.80325E-10
2490 TAUE=(CR*Q1*Q1*L)/(3*PI*(F/A)*((DA/2)^3)*1.89E-4)
2500 REM For small TAUE use PICH-sol.
2510 IF TAUE<1E-2 THEN N4=(6*TAUE)^(1/3):GOTO 2580
2520 REM YU's-eqn.for parabolic flow
2530 REM solved using NEWTEN-RAPHSON.
2540 XI=FNNR
2550 N4=(1-XI*XI)^2
2560 REM Combiend depostion efficiency
2570 REM for charged particles N.
2580 N=N1+N2+N3+N4  :IF N>1 THEN N=1
2590 =N
2600 REM Procedure to calculate time
2610 DEF PROCtime
2620 JM%=J%-1 :BM%=B%-1
2630 VXI=Y(5,J%) :VXIP=Y(5,JM%):V1=Y(5,B%):V0=Y(5,BM%)
2640 V0L=VXI-VXIP:CONST1=TIME1*V0L:CONST2=TIME2*V0L
2650 IF K%=3 GOTO 2690
2660 TS=CONST1/(VLR-V0)
2670 IF B%=J% THEN TF=0 ELSE TF=CONST1/(VLR-V1)
2680 GOTO 2710
2690 TF=CONST2/(VLR-V0)
2700 IF B%=J% THEN TS=0 ELSE TS=CONST2/(VLR-V1)
2710 ENDPROC
2720 REM NEWTON-RAPHSON solution to
2730 REM establish XI in YU's eq.
2740 DEFFNNR
2750 W=TAUE/8
2760 REM Initial sol. obtained by
2770 REM assuming X0=.5
2780 X0=0.5
2790 REM NEWTON-RAPHSON iterative
2800 REM expression
2810
XIT=X0+((3-X0)*(1-X0^3)*(X0/3)+(X0^2)*(2*(LNX0)-W))
     /((1+X0)*((1-X0)^3))
2820 IF ABS(XIT-X0)<1E-4 THEN =XIT
2830 X0=XIT
```

```
2840 GOTO 2810
2850 REM FNAscale gives airway area
2860 REM scaling factor as fn(t)
2870 DEF FNAscale
2880 VXI=Y(5,J%):V1=Y(5,B%):V0=Y(5,B%-1)
2890 IF K%=3 GOTO 2930
2900 T1P=TIME1*(VLR-VXI)/(VLR-V0)-TAI
2910 T2P=TIME1*(VLR-VXI)/(VLR-V1)-TAI
2920 =1+(T1P+T2P)/(2*TAI)
2930 T1P=TAE+TT-TIME2*(VLR-VXI)/(VLR-V1)
2940 T2P=TAE+TT-TIME2*(VLR-VXI)/(VLR-V0)
2950 =1+(TT-(T1P+T2P)/2)/TAE
2960 REM FNpause to account for pause
2970 REM depostion.
2980 DEF FNpause
2990 IF T0P=0 THEN =0
3000 DA=DA*DCRP
3010 IF Q=0 THEN EQ=0:GOTO 3090
3020 REM Image charge efficiency for
3030 REM pause with YU's slug flow.
3040 Q1=Q*4.80325E-10
3050 TAUE=(CR*Q1*Q1*T0P)/(3*PI*(DA/2)^3*D*1.89E-4)
3060 IF TAUE<1E-2 THEN EQ=(6*TAUE)^(1/3):GOTO 3090
3070 XI1=FNNR1
3080 EQ=1-XI1*XI1
3090 TAUS=U*T0P/DA
3100 IF TAUS>1 GOTO 3120
3110 ES=(1.1094-0.2604*TAUS)*TAUS :GOTO3130
3120 ES=1-(0.0069+(0.0859/TAUS)+(0.0582/(TAUS*TAUS)))/TAUS
3130 TAUD=4*I*T0P/(DA*DA)
3140 KL=0.1238
3150 VL1=-(2.405^2)*TAUD
3160 VL2=-(5.52^2)*TAUD
3170 VL3=-(8.654^2)*TAUD
3180 ED=1-4*((EXPVL1)/2.405^2)+((EXPVL2)/5.52^2)
+((EXPVL3)/8.654^2)
3190 ED=ED-KL*EXP(-4*SQR(TAUD/PI)/KL)
3200 =1-(1-ES)*(1-ED)*(1-EQ)
3210 REM NEWTEN-RAPHSON sol.for XI1
3220 DEFFNNR1
3230 W=TAUE/8
3240 X0=0.5
3250 Z1=(1/X0)-1
3260 REM N-R iterative expression.
3270 XIT1=2*(Z1+LNX0-W)/(Z1*Z1)
3280 IF ABS(XIT1-X0)<1E-4 THEN =XIT1
3290 X0=XIT1
3300 GOTO 3250
```

APPENDIX II.D

Charging Limits

1. Rayleigh Limit

When the mutual repulsion of electric charge within droplets exceeds the binding force of surface tension, the droplet shatters into smaller droplets. The limiting charge is given by:

$$n = \frac{(2\pi \gamma \, dp^3)^{\frac{1}{2}}}{e} \qquad \text{(in e.s.u)}$$

where γ is the surface tension of the droplet liquid.

N.B. A moderately charged droplet will become highly charged as it evaporates to smaller size. It will eventually reach the Rayleigh limit and disintegrate. When the droplet disintegrates, the fragments are below the Rayleigh limit because the same amount of charge is now distributed over a large surface.

2. Boltzmann Equilibrium

In a gaseous medium containing bipolar ions and aerosol particles, an equilibrium bipolar charge will eventually appear on the aerosol as a result of the random thermal motion of the ions and the frequent collisions of ions with particles. The charge distribution at equilibrium is described by Boltzmann's law:

$$f = \frac{\exp(-n^2/2\sigma^2)}{\sum_{n=-\infty}^{\infty} \exp(-n^2/2\sigma^2)}$$

where $$\sigma = \frac{\left[\frac{dp}{2} kT\right]^{\frac{1}{2}}}{e} \qquad \text{(in e.s.u.)}$$

σe	is the characteristics of the Boltzmann's charge
f	is the fraction of particle carrying n elementary units of charge
e	(= 4.8×10^{-10} e.s.u.) is the elementary unit of charge
dp	is the particle diameter
k	(= 1.381×10^{-16}dyn.cm/k) is Boltzmann's constant

T(K) is the absolute temperature

This low level, bipolar charge represents the residual charge remaining on an aerosol after the charge neutralization process is completed in a bipolar atmosphere.

For large particles, σ can be interpreted as the root-mean-square (r.m.s.) particle charge or the standard deviation of charge, since Boltzmann's law then becomes identical to the normal, Gaussian distribution,

$$f = \frac{1}{\sqrt{2\pi}\ \sigma} \exp\ (-n^2/2\sigma^2)$$

3. Ionic Fluctuation Theory of Smoluchowski

According to Smoluchowski (1912), the droplet charge depends upon the number of +ve and −ve ions which happened to be in that volume of liquid when it is released. There is thus a random distribution of charges, but on the average

$$\sigma^2 = 2NV$$

where σ^2 is the mean square value of the charge expressed in terms of the number of elementary charge

N is the concentration of ions of the same sign

V is the volume of the droplet

Figure D shows the level of particle charge to be expected from various charging limits as illustrated by Liu et al. (1974). Included in Figure D are the charging of sprayed droplets according to the ionic fluctuation theory of Smoluchowski, the maximum charge at the Rayleigh limit and the r.m.s. charge for water droplets at Boltzmann's equilibrium. According to Figure D, Table D1 shows the distribution of charge on aerosol particles as expected from various charging limits and mechanisms.

TABLE D1

Droplet diameter (μm)	Rayleigh Limit (in elementary units)	Max RMS charge on atomized droplet (in elementary units)	RMS charge at Boltzmann's Equ'm (in elementary units)
1	3.80×10^4	19	3.3
2	1.03×10^5	28	4.9
3	2.30×10^5	34	5.8
4	3.80×10^5	38	7.0
5	5.00×10^5	44	7.6
6	6.15×10^5	49	8.0
7	8.00×10^5	54	8.6
8	1.00×10^6	58	8.8
9	1.20×10^6	61	9.2
10	1.50×10^6	68	9.6

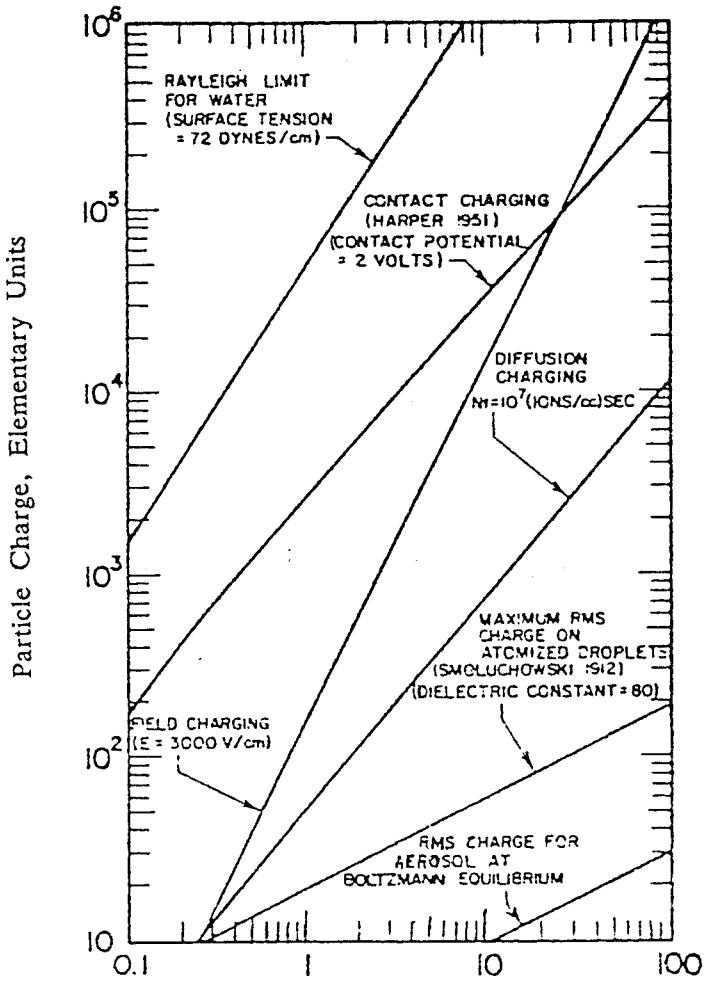

FIGURE D ILLUSTRATION OF THE LEVEL OF PARTICLE CHARGE TO BE EXPECTED FROM VARIOUS CHARGING LIMITS LIU ET AL., 1974